Untersuchungen zur Synthese und Reaktivität von Chalkogenidomerkuraten in ionischen Flüssigkeiten

Kumulative Dissertation

Zur Erlangung des akademischen Grades eines

Doktors der Naturwissenschaften

(Dr. rer. nat.)

dem Fachbereich Chemie der Philipps-Universität Marburg

vorgelegt von

Carsten Donsbach

aus Biedenkopf (Lahn)

Erstgutachterin: Prof. Dr. Stefanie Dehnen

Zweitgutachter: Prof. Dr. Bernhard Neumüller

Einreichungstermin: 27. Juni 2018

Prüfungstermin: 24. Juli 2018

Marburg (Lahn) 2018

Hochschulkennziffer 1180

Erklärung

Ich erkläre, dass eine Promotion noch an keiner anderen Hochschule als der Philipps-Universität Marburg, Fachbereich Chemie, versucht wurde. Weiterhin versichere ich, dass ich meine vorgelegte Dissertation "Untersuchungen zur Synthese und Reaktivität von Chalkogenidomerkuraten in ionischen Flüssigkeiten" selbst und ohne fremde Hilfe verfasst, nicht andere als die in ihr angegebenen Quellen oder Hilfsmittel benutzt, alle vollständig oder sinngemäß übernommenen Zitate als solche gekennzeichnet sowie die Dissertation in der vorliegenden oder einer ähnlichen Form noch bei keiner anderen in- oder ausländischen Hochschule anlässlich eines Promotionsgesuchs oder zu anderen Prüfungszwecken eingereicht habe.

Marburg, den 25. Juni 2018   Carsten Donsbach

Einreichungsdatum: 27. Juni 2018

Annahme der Promotion: 20. Juli 2018

Prüfungstermin: 24. Juli 2018

Die vorliegende Arbeit wurde in der Zeit von Juli 2014 bis Juni 2018 unter der Leitung von Frau Prof. Dr. Stefanie Dehnen am Fachbereich Chemie der Philipps-Universität Marburg angefertigt.

„Was wir heute tun,

entscheidet,

wie die Welt morgen aussieht.“

BORIS PASTERNAK

Inhalt

Abbildungsverzeichnis

Tabellenverzeichnis

Danksagung

hast sie –, und für noch viel mehr schöne Stunden im Lehramtspraktikum als sonst jemandem.

Darüber hinaus danke ich allen meinen Freunden, sowohl denen in der nicht ganz so fernen Heimat, die mich in letzter Zeit aber trotzdem kaum gesehen haben, als auch denen, die ich während meiner Zeit hier in Marburg kennen gelernt habe und teilweise noch immer kennen darf – einigen davon ganz besonders –, für so manche wunderbare Stunde, für die vielen helfenden Hände oder aufbauenden Worte… Ich denke, Ihr wisst, dass Ihr gemeint seid!

Und zu guter Letzt geht mein Dank nach Hause, an meine Eltern und an meine Oma, die Ihr in Eurer unnachahmlichen Art immer für mich da gewesen sind, seitdem ich denken kann, und wahrscheinlich sogar schon ein bisschen länger – DANKE!

1.   Einleitung

1.1   Chalkogenidometallate

Chalkogenidometallate sind ionische Verbindungen, deren Anionenstrukturen formell als Komplexe positiv geladener Metallkationen mit negativ geladenen Anionen der Chalkogenelemente (O, S, Se, Te) als Liganden aufgefasst werden können. Die Klasse der (Poly-)Oxometallate zeichnet sich durch eine große strukturelle Vielfalt aus. Ihre Vertreter finden vor allem in katalytischen Prozessen, als Trägermaterialien, Ionenaustauscher oder Sorptionsmittel Anwendung.[1] Deren höheren Homologe, also die Sulfido-, Selenido- und Telluridometallate, unterscheiden sich von den Oxometallaten vor allem durch eine höhere Polarisierbarkeit der Chalkogenatome, wodurch eine größere Flexibilität der Bindungen und eine bessere Ladungsverteilung erreicht werden, so dass neue Strukturmotive und höhere Anionenladungen möglich werden. Die Chalkogenidometallat-Materialien zeichnen sich in erster Linie durch ihre optoelektronischen, elektrochemischen und strukturellen Eigenschaften aus. Dabei ist eine feine Abstimmung der gewünschten Halbleitereigenschaften durch Variation der Strukturmotive und Elementkombinationen möglich.[2] Vor allem Verbindungen mit offenen und porösen Strukturen eignen sich aufgrund ihrer großen inneren Oberfläche als Photokatalysatoren,[3-8] Ionenleiter in Elektrodenmaterialien oder Festkörperelektrolyten,[9-11] Ionenaustauscher,[12-16] oder oder zur Verwendung in opto-elektronischen Bauteilen.[17-18] Speziell schwere Chalkogenidometallate haben zudem Potential im Bereich der Thermoelektrika und für die Detektion harter Strahlung.[19-22]

1.2   Strukturen von Chalkogenidomerkuraten

Die Klasse der Chalkogenidomerkurate weist eine große strukturelle Vielfalt von binären und ternären Anionenstrukturen auf. Die wiederkehrenden Koordinationsgeometrien am Quecksilber sind dabei die lineare, trigonal-planare und tetraedrische Koordination, wobei durch Verzerrung leicht davon abweichende Geometrien beobachtet werden. Neben molekularen Anionen sind auch komplexere Anionenstrukturen in Form von Strängen, Schichten oder Netzwerken bekannt, die jedoch allesamt aus linearen, trigonal-planaren oder tetraedrischen Merkurat-Bausteinen aufgebaut sind. In Abbildung 1 werden die bislang bekannten Anionenstrukturen zusammengefasst.

0D-Anionen (molekular):

a)

$[HgE_2]^{2-}$
E = S Se **Te**

b)

$[HgE_3]^{4-}$
E = Se **Te**

c)

$[HgE_4]^{6-}$
E = S Se **Te**

1D-Anionen (Stränge):

d)

$[HgE_2]^{2-}$
E = Se

e)

$[HgE_2]^{2-}$
E = S

f)

$[HgE_3]^{4-}$
E = S

g)
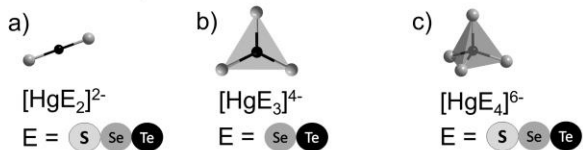
$[Hg_3E_4]^{2-}$
E = S Se **Te**

2D-Anionen (Schichten):

h)

$[Hg_3E_4]^{2-}$
E = S

i)

$[Hg_7E_9]^{4-}$
E = Se

3D-Anionen (Netzwerke):

j)

$[Hg_6E_7]^{2-}$
E = S Se

k)
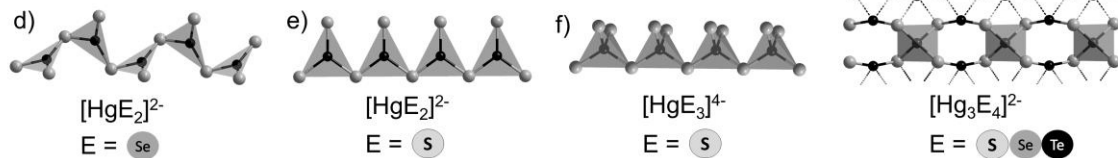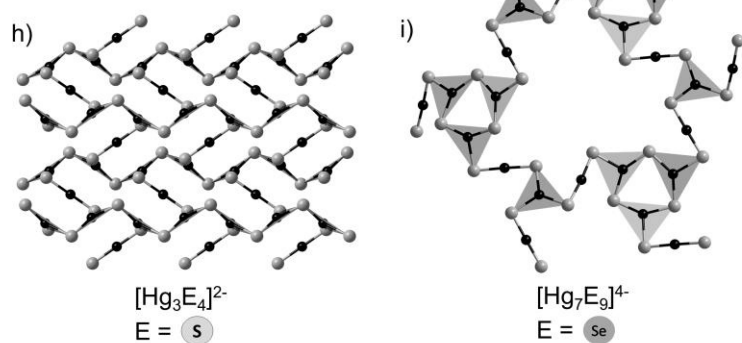
$[Hg_2E_3]^{2-}$
E = Se
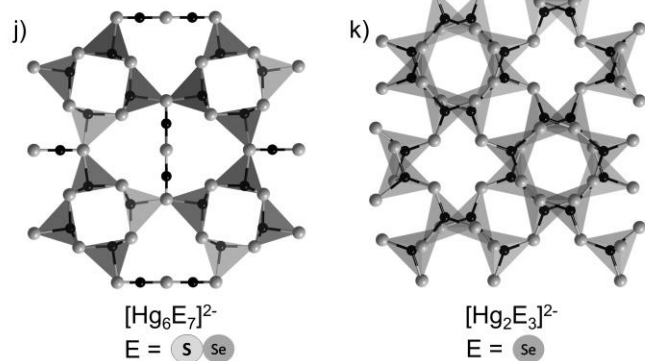
Abbildung 1: Strukturen binärer Chalkogenidomerkurat-Anionen unterschiedlicher Ausdehnungen: a) $[HgS_2]^{2-}$,[23,24] $[HgSe_2]^{2-}$,[25] $[HgTe_2]^{2-}$;[26,27] b) $[HgSe_3]^{4-}$,[28] $[HgTe_3]^{4-}$;[28,29] c) $[HgS_4]^{6-}$,[30] $[HgSe_4]^{6-}$;[30] d) $[HgSe_2]^{2-}$;[28] e) $[HgS_2]^{2-}$;[31] f) $[HgS_2]^{2-}$;[31] g) $[Hg_3S_4]^{2-}$,[20,32-34] $[Hg_3Se_4]^{2-}$,[33-34] $[Hg_3Te_4]^{2-}$;[33] h) $[Hg_3S_4]^{2-}$;[35] i) $[Hg_7Se_9]^{4-}$;[36] j) $[Hg_6S_7]^{2-}$,[33] $[Hg_6Se_7]^{2-}$;[33] k) $[Hg_2Se_3]^{2-}$.[37] Hg Atome werden als scharze Kugeln dargestellt, Chalkogen-Atome als graue. Die Koordinationspolygone bzw. Polyeder sind nur für Hg-Atome werden dargestellt. Gestrichelte Linien deuten nahe Hg…Te-Kontakte ~2.9 Å an.

Besonders die schweren Homologe der Chalkogenide sind sehr empfindlich gegenüber Oxidation, wobei Polychalkogenid-Anionen gebildet werden. Auch diese sind in der Lage, Metallkationen zu koordinieren. Die in der Regel kettenförmigen Polychalkogenide fungieren dabei fast immer als zweizähnige Liganden. Chalkogenidomerkurate, die mindestens ein Polychalkogenid-Fragment enthalten, sind in Abbildung 2 dargestellt.

0D-Anionen (molekular):

a) $[Hg(E_6)_2]^{2-}$ E = S
b) $[Hg_2(E_4)_3]^{2-}$ E = Se
c) $[Hg_7E_8(E_2)]^{4-}$ E = Se
d) $[Hg(E_4)_2]^{2-}$ E = S Se Te
e) $[Hg(E_7)]^{2-}$ E = Te
f) $[Hg_2E(E_2)(E_3)_2]^{4-}$ E = Te
g) $[Hg_4E_2(E_2)_2(E_3)_2]^{4-}$ E = Te

1D-Anionen (Stränge):
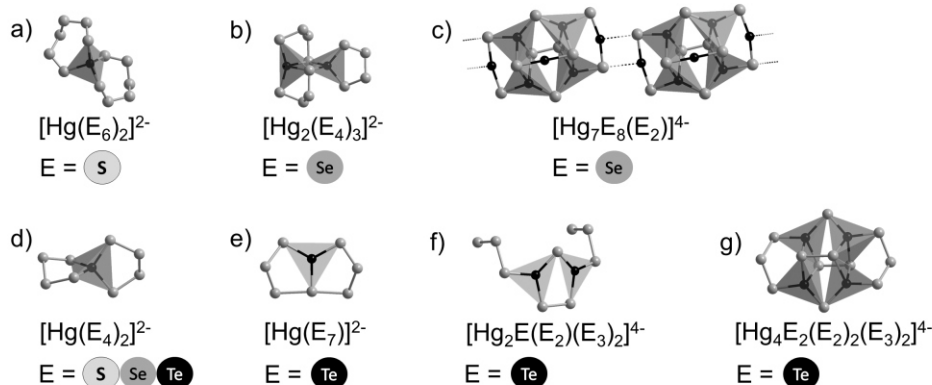
h) $[Hg_2E_2(E_2)]^{2-}$ E = Te
i) $[Hg_2E(E_2)_2]^{2-}$ E = Te
j) $[Hg_3E_3(E_2)_2]^{4-}$ E = Te
k) $[Hg_5(E_2)_2(E_4)E_4]^{2-}$ E = Te
l) $[Hg_5(E_2)_2(E_4)E_4]^{2-}$ E = Te
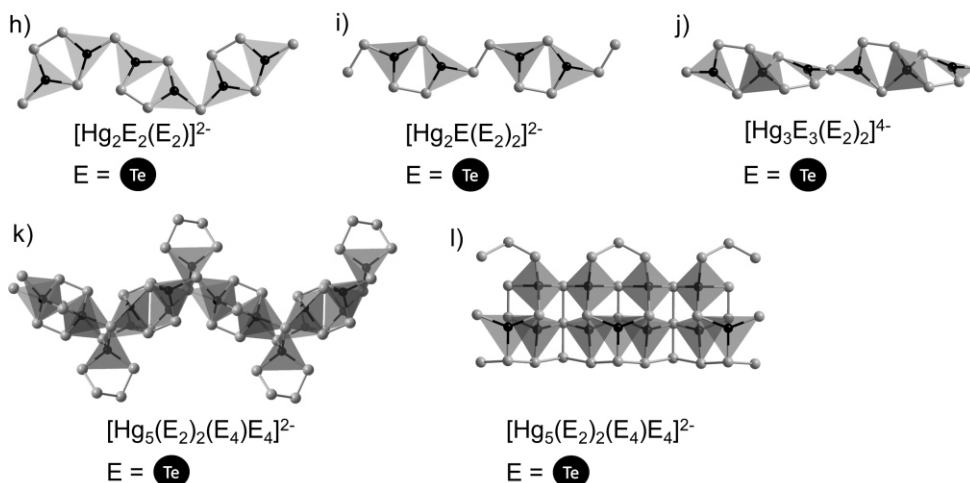
Abbildung 2: Strukturen binärer (Poly-)Calkogenidomerkurat-Anionen unterschiedlicher Ausdehnungen: a) $[Hg(S_6)_2]^{2-}$;[38,39] b) $[Hg_2(Se_4)_3]^{2-}$; c) $[Hg_7Se_8(Se_2)]^{4-}$;[36] d) $[Hg(S_4)_2]^{2-}$,[39-40] $[Hg(Se_4)_2]^{2-}$,[25,41-50] $[Hg(Te_4)_2]^{2-}$;[51] e) $[Hg(Te_7)]^{2-}$;[52-54] f) $[Hg_2Te(Te_2)(Te_3)_2]^{4-}$;[55,56] g) $[Hg_4Te_2(Te_2)_2(Te_3)_2]^{4-}$,[57-59] h) $[Hg_2Te_2(Te_2)]^{2-}$;[55,59,60] i) $[Hg_2Te(Te_2)_2]^{2-}$;[57] j) $[Hg_3Te_3(Te_2)_2]^{4-}$;[60] k) $[Hg_5(Te_2)_2(Te_4)Te_4]^{2-}$;[59] l) $[Hg_5(Te_2)_2(Te_4)Te_4]^{2-}$.[33] Die Koordinationspolygone bzw. -polyeder sind nur für Hg-Atome werden dargestellt.

Neben den binären Anionen sind eine ganze Reihe Strukturen aus ternären Systemen Elementen der Gruppen 13 (In), 14 (Ge, Sn) und 15 (As, Sb) bekannt, wobei hauptsächlich anionische Schichtstrukturen auftreten. Auch in diesen ternären Anionenstrukturen sind die Hg-Atome stets linear, trigonal-planar oder tetraedrisch koordiniert. Durch den Einbau anderer Metallatome in unterschiedlichen Verhältnissen lässt sich so eine Vielzahl neuer Strukturen realisieren. Eine Auswahl dieser wird in Abbildung 3 gezeigt.

a) 0D-[Hg$_4$Sn$_4$E$_{17}$]$^{10-}$ E= Se, Te

b) 1D-[HgSnE$_4$]$^{2-}$ E= Se, Te

c) 1D-[HgSnS$_4$]$^{2-}$

d) 1D-[HgAsSe$_3$]$^-$

e) 2D-[HgAs$_3$S$_6$]$^-$

f) 2D-[Hg$_3$Sn$_2$S$_8$]$^{2-}$

g) 2D-[Hg$_3$Ge$_2$S$_8$]$^{2-}$

h) 2D-[HgSbSe$_3$]$^-$

i) 2D-[HgSbS$_3$]$^-$

j) 2D-[HgInS$_3$]$^-$
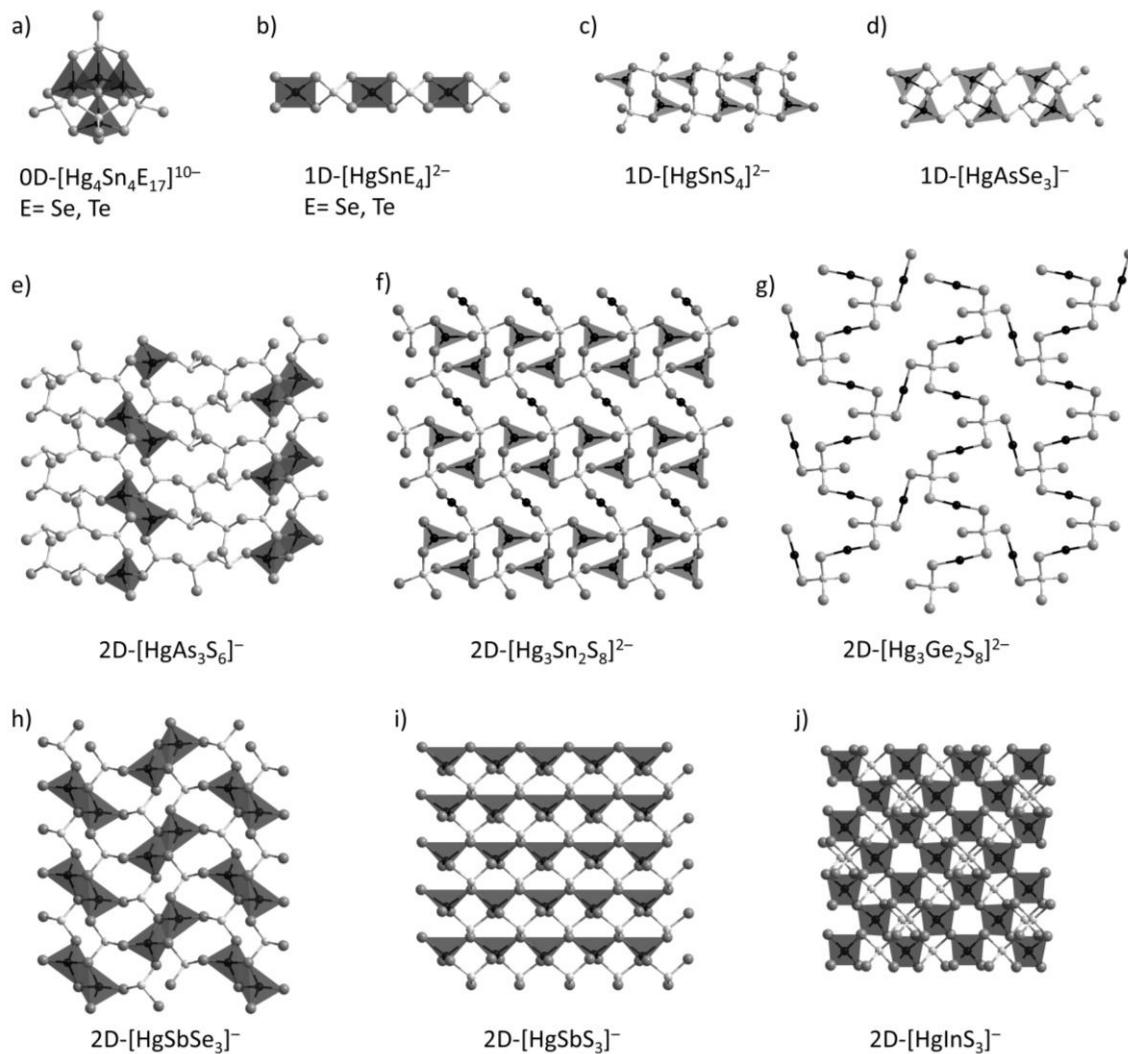
Abbildung 3: Beispiele für Strukturen ternärer Calkogenidomerkurat-Anionen unterschiedlicher Ausdehnungen: a) 0D-[Hg$_4$Sn$_4$Se$_{17}$]$^{10-}$,[61] 0D-[Hg$_4$Sn$_4$Te$_{17}$]$^{10-}$;[62] b) 1D-[HgSnSe$_4$]$^{2-}$;[61,62] 1D-[HgSnTe$_4$]$^{2-}$;[62,63] c) 1D-[HgSnS$_4$]$^{2-}$;[64] d)1D-[HgAsSe$_3$]$^{2-}$;[65] e) 2D-[HgAs$_3$S$_6$]$^{2-}$;[66] f) 2D-[Hg$_3$Sn$_2$S$_8$]$^{2-}$;[67] g) 2D-[HgAs$_3$S$_6$]$^{2-}$;[68] h) 2D-[HgAs$_3$S$_6$]$^{2-}$;[69] i) 2D-[HgAs$_3$S$_6$]$^{2-}$;[70] j) 2D-[HgAs$_3$S$_6$]$^{2-}$.[71] Hg Atome werden als scharze Kugeln dargestellt, Chalkogen-Atome als graue und alle übrigen Elemente als weiße Kugeln. Die Koordinationspolygone bzw. -polyeder sind nur für Hg-Atome werden dargestellt.

1.3 Synthese von Chalkogenidometallaten

Klassiche Syntheserouten von Chalkogenidometallaten bedienen sich unter anderem löungmittelfreier Methoden wie den Hochtemperatur-Festkörperreaktionen. Auf diese Weise werden allgemein eher ausgedehnte und dichte gepackte Netzwerkstrukturen wie das Kaliumelenidostannat $K_2[Sn_2Se_5]$ erhalten.[72] Zur Reaktionsführung bei etwas niedrigeren Temperaturen von 200–600 °C können auch Flussmittelschmelzen eingesetzt werden, um die Edukte zu lösen und so schon bei Temperaturen weit unter ihrem Schmelzpunkt zur Reaktion zu bringen. Bei diesen sogenannten Flux-Synthesen können die Reaktionsbedingungen über die Stöchiometrie der eingesetzten Salzschmelze und die Reaktionstemperatur variabel anpasst werden. In der Arbeitsgruppe von KANATZIDIS wurde diese Methode erfolgreich zur Synthese einer Vielzahl von ternären und quarternären Chalkogenidometallaten und insbesondere auch Merkuraten eingesetzt.[33,73] Als Flussmittel dienen dabei Alkalimetallpolychalkogenid-Schmelzen. Im Gegensatz zu den Festkörperreaktionen sind über die Flux-Route auch Verbindungen mit offeneren Anionennetzwerken oder Schichtstrukturen zugänglich, wie beispielsweise $K_6Sn[Zn_4Sn_4S_{17}]$ oder $A_2[Sn_4S_9]$ (A = K, Rb, Cs).[15,74] Ein Nachteil der Synthesemethode sind die Möglichkeit des unerwünschten Einbaus von Polychalkogenid-Anionen und vor allem die vergleichsweise unökonomische Reaktionsführung, da das Flussmittel nach der Reaktion nicht wiederverwendet werden kann.

Lösungsmittelfreie Synthesemethoden

Hochtemperatur-Festkörper-Reaktionen

Synthesen im Polychalkogenid-*Flux*

Lösungsmittelbasierte Synthesemethoden

Solvothermal-Synthesen

Reaktionen in Lösungen

$K_2[Sn_2Se_5]$ $K_2[Hg_6S_7]$ $[Zn_{25}In_{31}S_{84}]^{25-}$ $[K_{10}(H_2O)_{20}][Hg_4Sn_3Te_{17}]$
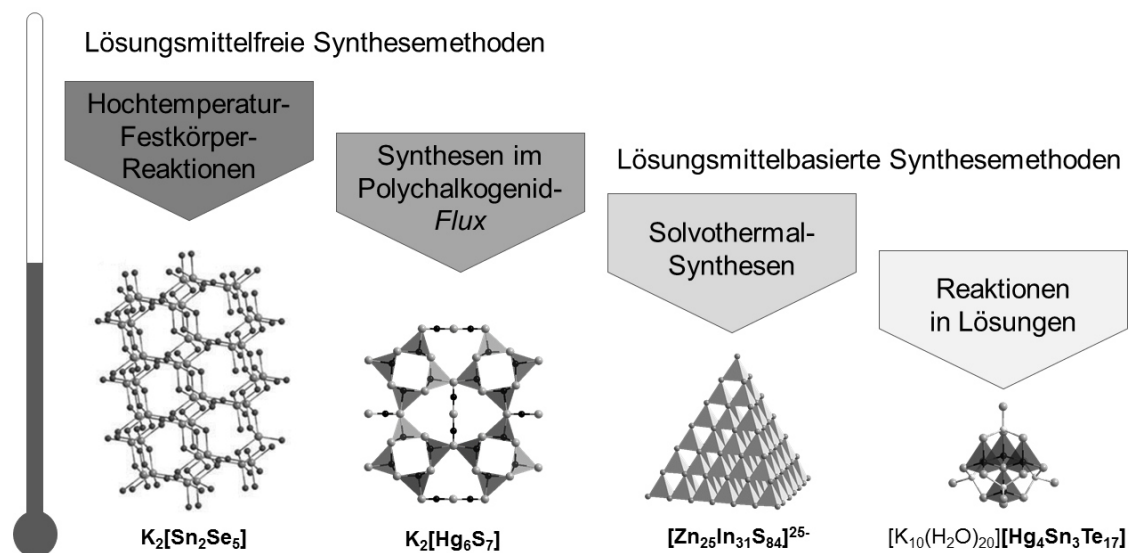
Abbildung 4: Übersicht über die klasssichen Methoden bei der Synthese von Chalkogenidometallaten.

Im Temperaturbereich unterhalb 400 °C lassen sich auch lösungsmittelbasierte Verfahren wie Solvothermalreaktionen anwenden.[75-78] Man unterscheidet hierbei je nach Art des verwendeten Lösungsmittels unter anderem zwischen hydrothermalen (Wasser),

methanolothermalen (Methanol), aminothermalen (Amine) und ammonothermalen (Ammoniak) Reaktionen.[79] Die Edukte werden hierbei zusammen mit einem geeigneten Lösungsmittel in einem Autoklaven erhitzt. Dabei ist auch die Zugabe unterschiedlicher Auxiliare und Template möglich. Die damit verbundene Druckerhöhung, teilweise bis in überkritische Bereiche, führt zu einer Verbesserung der Löslichkeiten der eingesetzten Stoffe. Vor kurzem konnte das größte supertetraedrische Chalkogenidometallat-Clusteranion $[Zn_{25}In_{31}S_{84}]^{25-}$ (T6) durch hydrothermale Synthese erhalten werden.[80-82] Solvothermale Verfahren werden teilweise auch als ein nachgeschalteter zweiter Reaktionsschritt mit Hochtemperatur-Festkörper-Reaktionen oder Flux-Synthesen kombiniert.[83,84] Bei der Variante der Hydrazin-Solvothermalsynthesen werden Mischungen von Hydrazin und einem herkömmlichen Lösungsmittel wie Wasser oder Aminen zusammen mit elementaren Chalkogenen als Edukten eingesetzt, die dabei *in-situ* zu den entsprechenden Chalkogeniden reduziert werden.[5,59,77,85]

Eine weitere Variante, die sich aus den klassischen Solvothermalsynthesen entwickelt hat, ist die Tensidothermalsynthese. Hierbei werden oberflächenaktive Substanzen wie Polyethylenglykol als Lösungsmittel eingesetzt.[86-91]

Die mildeste Reaktionsmethode stellen die Synthesen in Lösung bei Raumtemperatur dar. Hierbei werden entsprechende Chalkogenidometallat-Vorläufer mit Übergangsmetallsalzen zur Reaktion gebracht, Auf diese Weise sind vielfältige ternäre Chalkogenidometallat-Anionen zugänglich. Im Gegensatz zu den übrigen Methoden werden hierbei bereits Chalkogenidometallat-Verbindungen als Edukte benötigt. Zudem werden bei Reaktionen aus Lösung häufig Solvate erhalten.[92-96]

1.4 Ionothermalsynthese

Als ionische Flüssigkeiten („ILs", Einzahl „IL", vom englischen Begriff "ionic liquid") werden Salze mit besonders niedrigem Schmelzpunkt (unter 100 °C) bezeichnet. Diese bestehen in der Regel aus schwach koordinierenden Anionen wie Halogeniden (Cl^- oder Br^-), Tetrafluoroborat ($[BF_4]^-$), Tetracyanoborat ($[B(CN)_4]^-$), Hexafluorophosphat ($[PF_6]^-$), Trifluormethylsulfonat ($(F_3CSO_3)^-$) oder Bis(trifluormethylsulfonyl)-imid ($(F_3CSO_3)_2N^-$) und großen organischen Gegenionen mit langen Seitenketten wie Tetraalkylammonium-, 1,(2,)3- Tri(Di)alkylimidazolium-, Alkylpyrrolidinium-, Alkylpyridinium- oder Tetra-alkylphosphonium-Kationen (siehe Abbildung).

Beispiele langkettiger organischer IL-Kationen:
(k, l, m, n = 0, 1, 2, ...)

| Tetraalkyl-ammonium | 1,(2,)3-Trialkyl imidazolium | N,N-Dialkyl-pyrrolidinium | N-Alkyl-pyridinium | Tetraalkyl-phosphonium |
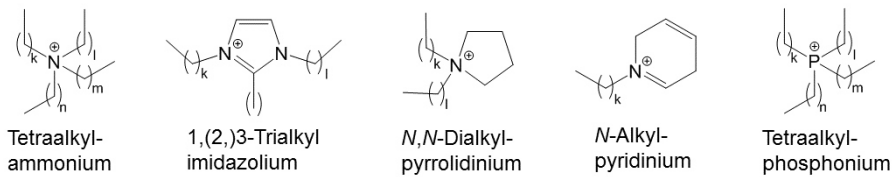
Beispiele (schwach koordinierender) IL-Anionen:

| Halogenid | Tetrafluoro-borat | Hexafluoro-phosphat | Trifluormethyl-sulfonat (OTf) | Bis(trifluormethan)-sulfonimid (TFSI) |
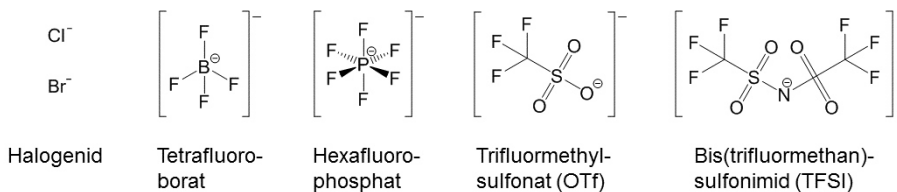
Abbildung 5: Beispiele von Kationen und Anionen von ionischen Flüssigkeiten.

ILs weisen allgemein einen vernachlässigbaren Dampdruck, hohe thermische Stabilität und durch ihren ionischen Charakter naturgemäß eine hohe elektrische Leitfähigkeit sowie gute Lösungseigenschaften für Salze auf. Ihre chemische Stabilität hängt dabei stark von ihren Bestandteilen ab. Die Kombination dieser Eigenschaften macht sie zu einem interessanten Lösungsmittel für die Synthese von ionischen Verbindungen wie Chalkogenidometallaten. Erfolgt ein Erhitzen der Reaktionsmischungen, wird analog zur solvothermalen Methode von Ionothermal-Reaktionen gesprochen. Aufgrund des niedrigen Dampfdrucks der ILs werden dabei jedoch keine überkritischen Bedingungen erreicht, so dass ohne Druckgefäße gearbeitet werden kann. Wie bei Solvothermalreaktionen ist die Zugabe von Auxiliaren möglich, allerdings besitzen die organischen Kationen bereits selbst auch strukturdirigierende Effekte.[18,97-99]

Ionothermale Synthese im Bereich der Chalkogenidometallate beschränkten sich bislang hauptsächlich auf Selenidotetrelate. Hierbei konnten dreidimensional ausgedehnten Netzwerkstrukturen zu Verbindungen mit anionischen Schicht- oder Strangstrukturen abgebaut werden.[100-103] Diese Syntheseroute wird als „Top-down"-Ansatz bezeichnet. Der Aufbau ternärer Anionenstrukturen gelang auch ausgehend von molekularen Präkursoren, Elementen und Metallsalzen,[104] was als „Bottom-up"-Ansatz bezeichnet wird. In der Arbeitsgruppe DEHNEN wurde auf diesem Weg das bis dahin größte diskrete sphärische Polyanion, der sogenannte „Zeoball" erhalten.[105,106] Ein beispielhafter Überblick über die genannten Reaktionswege ist in Abbildung 6 dargestellt. Allen bisher genannten Verbindungen gemein ist die Präsenz von IL-Kationen zum Ladungsausgleich. Nur in seltenen Fällen, beispielsweise bei Verwendung von $([B(CN)_4]^-$ -basierten ILs, wird kein Kationenaustausch beobachtet.[107] Auf dem Gebiet der

Chalkogenidotrielate konnten in der Arbeitsgruppe HUANG auch Salze mit supertetraedrischen ternären Clusteranionen dargestellt werden.[8,108]
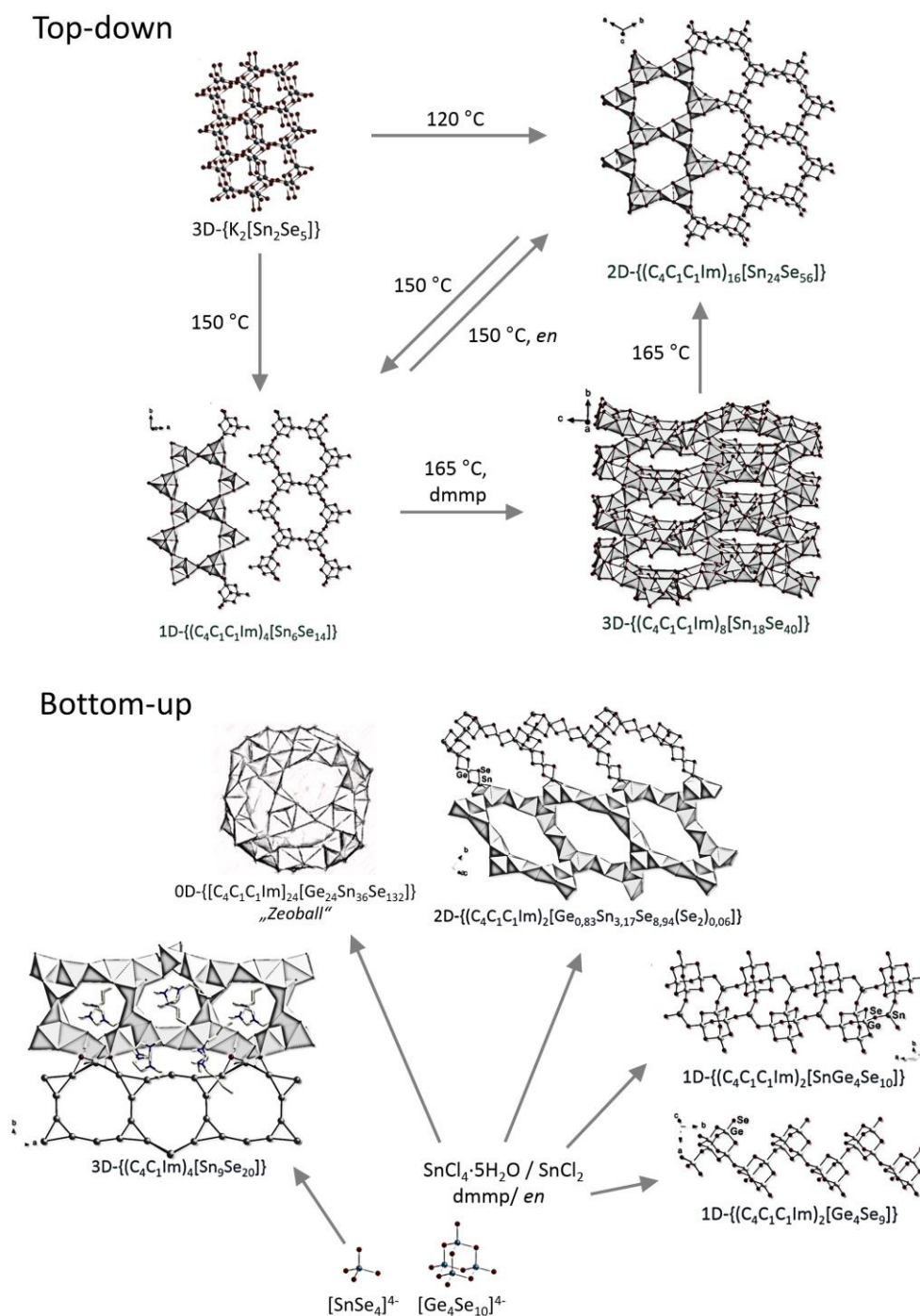
Abbildung 6: Reaktionsschema ionothermaler Synthesestrategien zur Synthese von Chalkogenidotetrelaten aus der Arbeitsgruppe DEHNEN. ($C_k(C_l)C_m$Im): 1,(2,)3-Tri/Di-Alkylimidazolium, wobei die Variablen k, l, m die Anzahl der Kohlenstoffatome der entsprechenden Alkylsubstituenten beschreiben; dmmp: 2,6-Dimethylmorpholin; en: 1,2-Diaminoethan.

Nicht nur bei der Synthese anionischer Chalkogenidometellate finden ILs Verwendung, sondern auch kationische Metallchalkogenid-Verbindungen können auf ionothermalem Weg synthetisiert werden. In den Arbeitsgruppen RUCK und KANATZIDIS wurden durch Zusatz von Trielhalogeniden zu Halogenid-basierten ionischen Flüssigkeiten Lewis-azide Reaktionsmedien erzeugt, in denen ausgehend von den Elementen eine Reihe von Salzen kationischer Pentelchalkogenidcluster synthetisiert wurden.[109-115]

2. Aufgabenstellung und Motivation

Verbindungen aus der Klasse der Chalkogenidometallate besitzen vielversprechende opto-elektronische Eigenschaften. Ein großer praktischer Vorteil auf der Suche nach neuen Materialien sind ihre strukturelle Vielfalt und die breite Elementauswahl, was eine feine Abstimmung der physikalischen Eigenschaften für verschiedene Anwendungsbereiche ermöglicht. Aufgrund ihrer besonderen Lösungseigenschaften für ionische Verbindungen, des vernachlässigbaren Dampfdrucks und dementsprechend hoher möglicher Reaktionstemperaturen sowie ihrer allgemein guten chemischen Inertheit bieten sich ionische Flüssigkeiten als Reaktionsmedium für die Synthese von Chalkogenidometallat-Materialien an.

Ionothermale Reaktionsmethoden werden in der Arbeitsgruppe DEHNEN bereits seit mehreren Jahren auf dem Gebiet der Synthese von Chalkogenidotetrelaten angewendet. Dabei wurden unter anderen der strukturdirigierende Einfluss verschiedener Amine auf den Abbau und die Umwandlung ausgehnter anionischer Netzwerkstrukturen sowie der Aufbau komplexer ternärer Chalkogenidotetrelate unter Einsatz molekularer Vorläuferverbindungen oder einfacher Metallsalze untersucht. Bei Synthesen, in denen Verbindungen mit ausgehnten Anionenstrukturen als Edukte eingesetzt werden, spricht man von einer Top-down-Strategie, während Synthesen, in denen ausschließlich Verbindungen mit molekularen Anionen, einfache Salze oder Elemente eingesetzt werden, als Bottom-up-Strategie bezeichnet werden.

Neben den Chalkogenidotetrelaten wurden auch Untersuchungen zur Synthese und Reaktivität von Chalkogenidometallaten schwerer d^{10}-Metalle wir Hg, Tl, und Bi durchgeführt, bislang jedoch nur unter aminothermalen Bedingungen.

Ziel dieser Arbeit waren die Weiterentwicklung der ionothermalen Synthesemethoden, ihre Übertragung auf neue Chalkogenidometallate, sowie die Erweiterung des Verständnisses ionothermaler Reaktionen.

Aufbauend auf den bisherigen Studien in der Arbeitsgruppe DEHNEN sollte die Übertragbarkeit der ionothermalen Synthesestrategien aus dem Bereich der Chalkogenidotetrelate auf die Metallate der schweren d^{10}-Metalle geprüft und diese entsprechend angepasst und weiterentwickelt werden. Der primäre Fokus sollte hierbei auf den Merkuraten liegen, da diese Substanzklasse bereits eine große strukturelle Vielfalt aufwies und vielversprechende Reaktivitäten unter aminothermalen Bedingungen gezeigt hatte. Dabei sollte auch die ionothermale Darstellung ternärer Anionenstruktukturen durch Kombination bekannter Stannate mit anderen Metallaten untersucht werden. Auf der

Suche nach weiteren potentiellen Präkursoren für ionothermale Reaktionen und zum Vergleich der Reaktivitäten der verschiedenen solvothermalen Methoden wurden auch weiterhin aminothermale Reaktionen durchzuführen.

Darüber hinaus galt es, genauere Einblicke in die Abläufe ionothermaler Reaktionen, insbesondere die Löslichkeiten und Reaktivitäten verschiedener Edukte, sowie den Einfluss unterschiedlicher Parameter, zu gewinnen. Zu diesen Parametern zählen der Zusatz von Aminen oder Salzen mit Fremdionen, die Reaktionstemperatur und –dauer – vor allem vor dem Hintergrund der kinetischen oder thermodynamischen Kontrolle der Reaktionsführung – und der Einfluss unterschiedlicher IL-Kationen. Außerdem sollte die Reaktivität spezieller Hydrogenchalkogenid-basierter ionischer Flüssigkeiten wie 1-Ethyl-3-Methylimidazoliumhydrogensulfid und –selenid in Reaktivitäten mit Chalkogenido-metallaten untersucht werden.
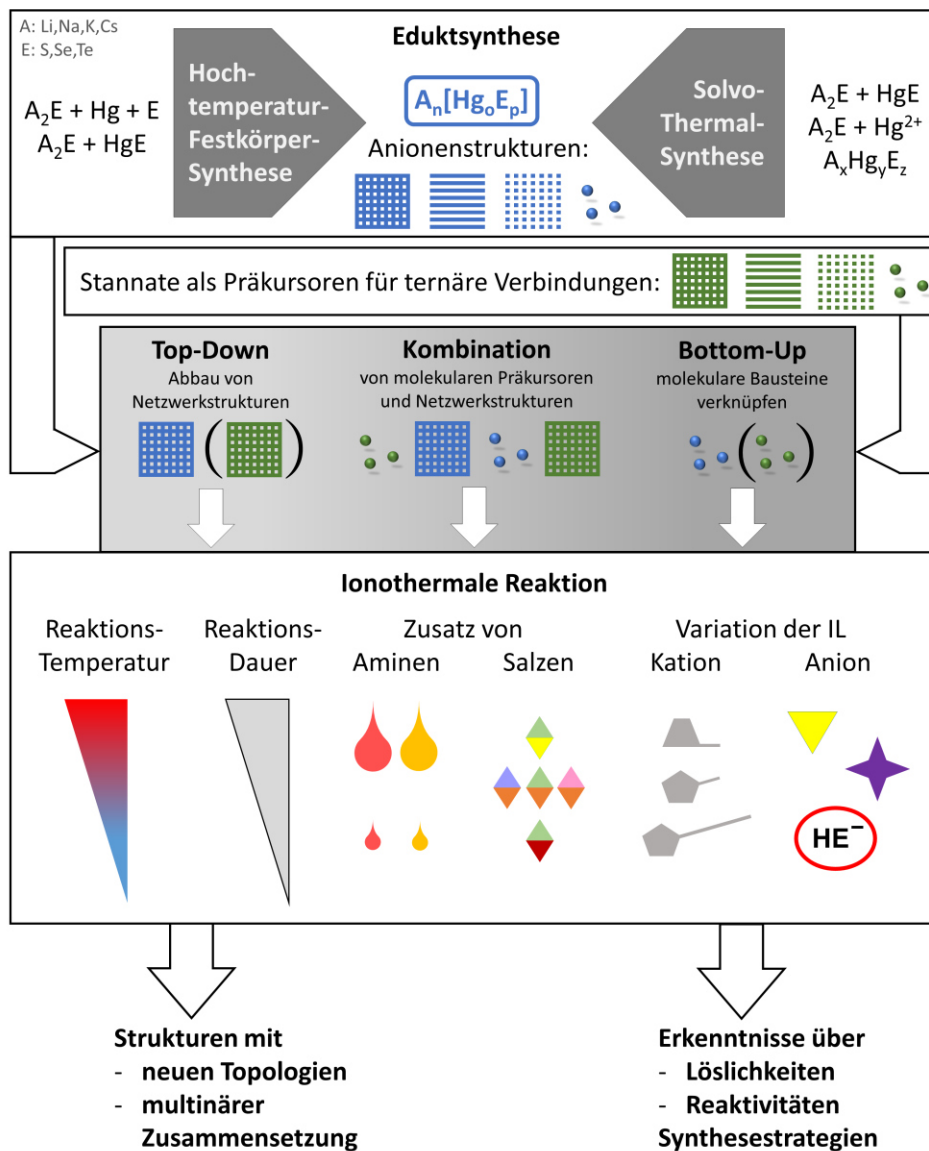
Abbildung 7. Vorgehen und zu untersuchende Parameter bei der ionothermalen Synthese von binären und ternären Chalkogenidomerkuraten.

3. Kumulativer Teil

Diese kumulative Dissertation besteht aus sechs Publikationen, die im Rahmen meiner Forschungsarbeiten entstanden sind und zu denen ich jeweils den größten Teil beigetragen habe. Außerdem bin ich Coautor des Manuskripts „Not so innocent after all? The role of ionic liquid cations as methylation agent" (3.8), in dem unter anderem die Bildung und Struktur zweier neuer Verbindungen präsentiert werden, die von mir synthesiert und charakterisiert wurden. Darüber hinaus bin ich Coautor der Publikation „Combining Solid-state and Solution-based Techniques: Synthesis and Reactivity of Chalcogenidoplumbates(II or IV)" (3.2), in der Arbeitstechniken und Methoden meines Forschungsgebietes im Videoformat präsentiert werden. Im folgenden Kapitel werden diese acht Publikationen in der nachstehend aufgeführten chronologischen Reihenfolge ihrer Veröffentlichung vorgestellt. Zusatzinformationen zu Synthesen und Analytik, die bei manchen Publikationen nicht im Hauptmanuskript enthalten sind, sondern als „Supporting Information" angehängt wurden, sind im Appendix zu finden.

3.1 Mercurates from a Revised Ionothermal Synthesis Route: The Pseudo-Flux Approach

C. Donsbach, G. Thiele, L. H. Finger, J. Sundermeyer, S. Dehnen, *Inorg. Chem.* **2016**, *55*, 6725–6730.

3.2 Combining Solid-state and Solution-based Techniques: Synthesis and Reactivity of Chalcogenidoplumbates(II or IV)

G. Thiele, C. Donsbach, I. Nußbruch, S. Dehnen, *J. Vis. Exp.* **2016**, *118*, e54789.

3.3 Formation of Crystalline Telluridomercurates from Ionic Liquids Near Room Temperature

C. Donsbach, S. Dehnen, *Z. Anorg. Allg. Chem.* **2017**, *643*, 14–19.

3.4 Syntheses and properties of selenido mercurates with $[HgSe_2]^{2-}$ anions in diverse chemical environments

C. Donsbach, S. Dehnen, *Inorg. Chem. Front.* **2017**, *4*, 336–342.

3.5 $[Hg_4Te_8(Te_2)_4]^{8-}$: A Heavy Metal Porphyrinoid Embedded in a Lamellar Structure

C. Donsbach, K. Reiter, D. Sundholm, F. Weigend, S. Dehnen, *Angew. Chem. Int. Ed.* **2018**, *57*, DOI: 10.1002/anie.201803233, *im Druck*; *Angew. Chem.* **2018**, *129*, DOI: 10.1002/ange.201803233, *im Druck*.

3.6 Formation of $[(C_nC_1imTe)_4Hg]^{2+}$ (n = 6, 8) upon In-Situ Generation of Dialkylimidazole-2-Tellurones in Ionic Liquids at Room Temperature

C. Donsbach, S. Dehnen, **2018**, *Manuskript eingereicht*.

3.8 $(C_4C_1Im)_6[Hg_7Se_{10}]$: The Salt of a Molecular Selenido Mercurate Anion Obtained from Ionic Liquids

C. Donsbach, S. Dehnen, **2018**, *Manuskript eingereicht*.

3.7 Not so innocent after all? The role of ionic liquid cations as methylation agent

B. Peters, S. Santner, C. Donsbach, S. Dehnen, **2018**, *Manuskript in Vorbereitung*.

3.1 Mercurates from a Revised Ionothermal Synthesis Route: The Pseudo-Flux Approach

C. Donsbach, G. Thiele, L. H. Finger, J. Sundermeyer, S. Dehnen, *Inorg. Chem.* **2016**, *55*, 6725–6730.

Abstract: $K_2Hg_6Se_7$, $Na_2Hg_3S_{2.51}Se_{1.49}$, $K_2Hg_3S_{1.03}Se_{2.97}$, and $K_2Hg_3S_{2.69}Se_{1.31}$ were prepared by ionothermal treatment of $K_2Hg_2Se_3$, Na_2HgSe_2, and $K_2Hg_3Se_4$, respectively, in a nonclassical hydrosulfide ionic liquid (EMIm)(SH). In contrast to their lighter congeners, the title compounds could so far not be synthesized by inorganic polychalcogenide salt flux techniques. The applied method hence mimics polychalcogenide flux conditions, while operating at much lower temperatures below the decomposition temperature of the ionic liquid. It might thus be viewed as a *pseudo*-flux approach.

Inhalt: Die Synthese von vier neuen Chalkogenidomercuraten, $K_2Hg_6Se_7$ (**1**), $Na_2Hg_3S_{2.51}Se_{1.49}$ (**2**), $K_2Hg_3S_{1.03}Se_{2.97}$ (**3**) und $K_2Hg_3S_{2.69}Se_{1.31}$ (**4**) in einer neuartigen ionischen Flüssigkeit basierend auf Hydrogensulfid-Anionen wird präsentiert. Alle Verbindungen wurden mittels Einkristall-Röntgenstrukturanalyse charakterisiert. Sie sind isostrukturell zu den bereits bekannten Schwefelanaloga. Zuästzlich wurden bei den Verbindungen **2** – **4**, welche Mischbesetzungen der Chalkogenpositionen mit Schwefel- und Selen-Atomen aufweisen, die Elementzusammensetzung mittels energiedisperser Röntgenspektroskopie (EDX) bestimmt und ihre optischen Absorptionseigenschaften mittels UV-Vis-Spektroskopie untersucht.

Zur Synthese aller vier Verbindungen wurden entsprechende ternäre Selenidomerkurat-Verbindungen in unter Vakuum abgeschmolzenen Glasampullen in der ionischen Flüssigkeit 1-Ethyl-3-Methylimidazoliumhydrogensulfid für wenige Tage auf Temperaturen von 100–120 °C erhitzt. Die kristallinen Produkte wurden nach dem Abkühlen auf Raumtemperatur erhalten. Diese Reaktionsbedingungen sind deshalb bemerkenswert, da analoge Schwefel-Verbindungen bislang nur bei höhreren Temperaturen in einer Polychalkogenidsalz-Schmelze, unter sogenannten *Flux*-Bedingungen, erhalten werden konnten. Unter Verwendung dieser speziellen ionischen Flüssigkeit können vergleichbare Reaktionsbedingungen bei deutlich niedrigeren Temperaturen realisiert werden. Darüber hinaus ist der bei den Verbindungen **2** – **4** beobachtete, temperaturabhängig steuerbare, teilweise Chalkogenidaustausch interessant, da sich auf diese Weise die Bandlücke der Produkte fein einstellen lässt, was

einen vielversprechenden Syntheseweg für chalkogenhaltige optoelektronische Materialien darstellen könnte.

Eigener Anteil: Die Synthese der Verbindungen **2 – 4** wurde von mir geplant und durchgeführt. Die Analyse der Verbindungen mittels Einkristall-Strukturanalyse und spektroskopischer Methoden (*EDX* und UV-Vis-Spektroskopie) inklusive Auswertung erfolgte durch mich. Die Synthese von Verbindung **1** wurde von Günther Thiele geplant und unter seiner Anleitung von Hendrik Borkowski durchgeführt. Die Charakterisierung von Verbindung **1** erfolgte ebenfalls durch Günther Thiele. Das Manuskript wurde von mir in Zusammenarbeit mit Günther Thiele und Stefanie Dehnen verfasst. Die übrigen Co-Autoren waren dabei an der Überarbeitung des Manuskripts beteiligt.

Mercurates from a Revised Ionothermal Synthesis Route: The *Pseudo*-Flux Approach

Carsten Donsbach, Günther Thiele, Lars H. Finger, Jörg Sundermeyer, and Stefanie Dehnen*

Fachbereich Chemie and Wissenschaftliches Zentrum für Materialwissenschaften, Philipps-Universität Marburg, Hans-Meerwein-Straße 4, 35043 Marburg, Germany

S *Supporting Information*

ABSTRACT: $K_2Hg_6Se_7$, $Na_2Hg_3S_{2.51}Se_{1.49}$, $K_2Hg_3S_{1.03}Se_{2.97}$, and $K_2Hg_3S_{2.69}Se_{1.31}$ were prepared by ionothermal treatment of $K_2Hg_2Se_3$, Na_2HgSe_2, and $K_2Hg_3Se_4$, respectively, in a nonclassical hydrosulfide ionic liquid (EMIm)(SH). In contrast to their lighter congeners, the title compounds could so far not be synthesized by inorganic polychalcogenide salt flux techniques. The applied method hence mimics polychalcogenide flux conditions, while operating at much lower temperatures below the decomposition temperature of the ionic liquid. It might thus be viewed as a *pseudo*-flux approach.

INTRODUCTION

Ionothermal reactions—that is, syntheses in ionic liquids (ILs) at moderately elevated temperatures in closed systems—have attracted considerable attention in recent times.[1−3] Among a variety of different peculiarities of this technique are the reusability of solvent, comparably low reaction temperatures, and new structural motifs of product compounds, which are not accessible via traditional solid-state or solution routes.[4,5] Most activities so far were focused on oxidic materials, whereas chalcogenides were addressed to a much smaller extent.[6−14]

We investigated phase formation and phase transitions of chalcogenido stannates and chalcogenido germanates in ILs to gain profound experience considering reaction pathways and equilibria in the still-young area of low-temperature materials synthesis,[15−19] and we recently extended this work to chalcogenido mercurates.[20] Such compounds are promising materials, for instance, regarding thermoelectric applications or hard radiation detection.[21]

Most of the ionothermal reactions, which have been reported to date, made use of ILs with organic cations and halide or halidoborate anions. Our previous investigations[21,22] revealed the salt metathesis of starting metalates (MET) with the IL to be dominant (see eqs 1 and 2 for a general reaction scheme and an example, respectively; BMIm = 1-butyl-3-methylimidazo-lium). Thereby the efficiency of new reaction conditions is reduced, as it rules out the reuse of the IL.

$$(Cat^{MET})(An^{MET}) + (Cat^{IL})(An^{IL})$$
$$\rightarrow (Cat^{IL})(An^{MET}) + (Cat^{MET})(An^{IL}) \qquad (1)$$

$$K_4[SnSe_4] + 4(BMIm)[BF_4]$$
$$\rightarrow 4K[BF_4] + (BMIm)_4[SnSe_4] \qquad (2)$$
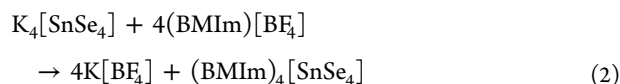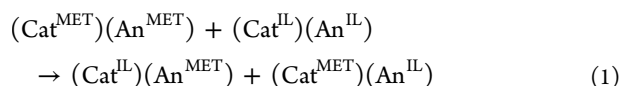
Therefore, we are currently exploring the use of ILs with hydrosulfide, $(SH)^−$, and hydroselenide, $(SeH)^−$, anions for phase transformation reactions,[23−25] and report on our first results upon treatment of chalcogenido metalate phases.

EXPERIMENTAL SECTION

General. All manipulations were performed under strict exclusion of air, moisture, and light using standard Schlenk and glovebox techniques. 1,3-Dimethylmorpholine (dmmp) and ethane-1,2-diamine (en) were freshly distilled from CaH_2. (EMIm)(SH) and (EMIm)(SeH) were synthesized according to literature procedures and purified by recrystallization from acetonitrile/diethyl ether.[23]

Synthesis of $K_2Hg_6Se_7$.[20] 200 mg of $K_2Hg_2Se_3$[20] (0.109 mmol) were added to 0.5 g of (EMIm)(SH) (2.62 mmol) beside traces of dmmp (one droplet) in a pyrex tube. The latter was sealed under vacuum and placed in an oven. The ampule was heated to 100 °C for 5 d, then the heating was turned off for slow cooling of the reaction mixture to room temperature. **1** was obtained as black sticks in ∼90% crystalline yield.

Synthesis of $Na_2Hg_3S_{2.51}Se_{1.49}$. In a similar procedure as performed for the synthesis of **1**, 100 mg of Na_2HgSe_2 (0.247 mmol), which was used as-prepared by fusion of Na_2Se and HgSe (1:1) at 700 °C, and 0.3 g of (EMIm)(SH) (1.57 mmol) were treated at 100 °C for 3 d before cooling to room temperature. **2** crystallized as red blocks in almost quantitative yield.

Synthesis of $K_2Hg_3S_{1.03}Se_{2.97}$. According to the synthesis of **2**, 100 mg of $K_2Hg_3Se_4$ (0.100 mmol) and 0.3 g of (EMIm)(SH) (2.62 mmol) were treated at 100 °C for 3 d before cooling to room temperature. **3** crystallized nearly quantitatively as orange plates. $K_2Hg_3Se_4$ was prepared by fusion of K_2Se and HgSe (1:2) at 700 °C, then pestled and washed with en.

Synthesis of $K_2Hg_3S_{2.69}Se_{1.31}$ (4). Compound **4** was synthesized in the same way as **3**; 100 mg of $K_2Hg_3Se_4$ (0.100 mmol) was heated in 0.3 g of (EMIm)(SH) (2.62 mmol) at 120 °C for 3 d prior to cooling

Table 1. Results of the Elemental Analyses of the Mixed-Chalcogen Compounds 2, 3, and 4

element	atom % measured [calc] in 2		atom % measured [calc] in 3		atom % measured [calc] in 4	
Na	22.1(13)	[22.2]				
K			22.1(2)	[22.2]	22.8(6)	[22.2]
S	30.3(104)	[27.9]	11.9(13)	[11.4]	29.3(49)	[29.8]
Se	16.0(5)	[16.6]	33.0(3)	[33.0]	15.0(6)	[14.6]
Hg	31.6(21)	[33.3]	33.1(6)	[33.1]	32.9(23)	[33.3]

Table 2. Basic Crystallographic Data at 273 K (1) or 100 K (2−4), Respectively

compound	1	2	3	4
empirical formula	$Hg_6 K_2 Se_7$	$Hg_3 Na_2 S_{2.51} Se_{1.49}$	$Hg_3 K_2 S_{1.03} Se_{2.97}$	$Hg_3 K_2 S_{2.69} Se_{1.31}$
formula weight/g·mol^{-1}	1834.46	845.87	947.39	869.88
crystal color and shape	black needle	red block	orange plate	yellow plate
crystal size/mm^3	0.10 × 0.05 × 0.05	0.18 × 0.14 × 0.10	0.06 × 0.03 × 0.01	0.09 × 0.04 × 0.01
crystal system	tetragonal	orthorhombic	orthorhombic	orthorhombic
space group	$P4_2/mnm$	$Pbca$	$Pbcn$	$Pbcn$
a/Å	14.2252(16)	8.3188(17)	10.712(2)	10.605(2)
b/Å		7.3873(15)	6.7488(14)	6.6515(13)
c/Å	4.2075(5)	14.104(3)	13.917(3)	13.788(3)
V/Å^3	851.4(2)	866.7(3)	1006.1(4)	972.6(3)
Z	2	4	4	4
ρ_{calc} /g·cm^{-3}	7.156	6.482	6.255	5.941
$\mu(Mo_{K\alpha})$ /mm^{-1}	69.313	59.877	57.364	53.510
absorption correction type	numerical (STOE X-area)	numerical (STOE X-area)	numerical (STOE X-area)	numerical (STOE X-area)
min/max transmission	0.0926/0.1320	0.0104/0.0518	0.1340/0.5548	0.14976/0.5469
θ range /deg	2.025−25.316	2.889−27.829	2.927−27.104	2.955−25.025
no. of measured reflections	5604	3518	5027	2418
no. of independent reflections	459	1033	1114	854
R(int)	0.0700	0.0884	0.0935	0.1345
no. of indep. reflections ($I > 2\sigma(I)$)	420	874	724	389
no. of parameters	31	45	44	44
R_1 ($I > 2\theta(I)$)	0.0503	0.0404	0.0410	0.0586
wR_2 (all data)	0.1171	0.1006	0.0872	0.1514
S (all data)	1.255	1.050	0.914	0.877
$\Delta\rho_{max}$, $\Delta\rho_{min}$/e·Å^{-3}	1.775/−2.274	3.968/−4.067	1.921/−1.702	2.16/−3.1
	CCDC 1473364	CCDC 1473365	CCDC 1473366	CCDC 1473367

to room temperature. The product crystallized as yellow plates in almost quantitative yield.

Elemental Analyses. The identity of the mixed-chalcogen compounds 2−4 was confirmed in a semiquantitative manner by means of energy-dispersive X-ray (EDX) analyses, performed using the EDX device Voyager 4.0 of Noran Instruments coupled with the electron microscope CamScan CS 4DV. Data acquisition was performed with an acceleration voltage of 20 kV and 100 s of accumulation time. The radiation emitted by the atoms was analyzed: Na−K, K−K, S−K, Se−K, Hg−L. Table 1 summarizes the results.

Optical Absorption Spectroscopy. UV−visible spectra were measured on a Varian Cary 5000 dual-beam spectrometer equipped with a Praying Mantis sample holder from Harrik. The diffuse reflection of powdered samples was analyzed.

Single-Crystal X-ray Diffraction and Structure Refinement. Suitable crystals for analysis were measured on a STOE IPDS (1) or IPDSII (2, 3, and 4) at 273 K (1) or 100 K (2, 3, and 4) using Mo K$_\alpha$ radiation and a graphite monochromator (λ = 0.710 73 Å). Upon numerical absorption correction (STOE X-AREA), the structure solution was performed by direct methods, followed by full-matrix-least-squares refinement against F^2, using SHELXS15, SHELXT15, SHELXL15, and OLEX2 software.[26−28] Table 2 summarizes the crystallographic data for 1, 2, 3, and 4. Additional crystallographic information is available in the Supporting Information.

■ DISCUSSION

Syntheses. The ILs (EMIm)(SH) and (EMIm)(SeH), containing hydrosulfide, (SH)$^-$, and hydroselenide, (SeH)$^-$, anions, respectively (EMIm = 1-ethyl-3-methylimidazolium),[23−25] were used to treat several A/Hg/E phases with A = Na, K and E = S, Se. Upon use of (EMIm)(SH), single crystals of $K_2Hg_6Se_7$ (1), $Na_2Hg_3S_{2.51}Se_{1.49}$ (2), $K_2Hg_3S_{1.03}Se_{2.97}$ (3), and $K_2Hg_3S_{2.69}Se_{1.31}$ (4) were obtained in 90% or almost quantitative crystalline yield, respectively (see eqs 3 to 5).

$$6K_2Hg_2Se_3 \text{ in } (EMIm)(SH) \rightarrow 2K_2Hg_6Se_7 \text{ (1)} + 4K_2Se \tag{3}$$

$$3Na_2HgSe_2 \text{ in } (EMIm)(SH)$$
$$\rightarrow Na_2Hg_3S_{2.51}Se_{1.49} \text{ (2)} + 2Na_2Ch \tag{4}$$

$$K_2Hg_3Se_4 \text{ in } (EMIm)(SH) \rightarrow K_2Hg_3S_xSe_{4-x}$$
$$+ (EMIm)(SeH); x = 1.03 \text{ (3)}, 2.69 \text{ (4)} \tag{5}$$
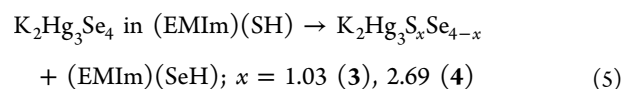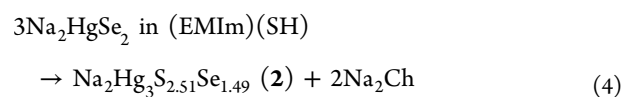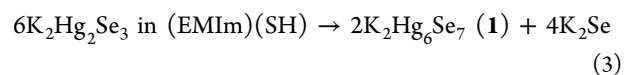
The second and third reactions (4 and 5) present a rare example of low-temperature anion exchange in metal polychalcogenide synthesis. We suppose that traces of (EMIm) (SeH) were also formed during the processes

described in eqs 3 and 4, which could, however, not be observed.

For the synthesis of compound **1**, $K_2Hg_2Se_3$[20] was heated in (EMIm)(SH) in the presence of traces of 1,3-dimethylmorpholine (dmmp) at 100 °C and subsequently cooled slowly to room temperature. It crystallized as black sticks in ~90% crystalline yield. Compound **2** was prepared in a similar way, by treatment of Na_2HgSe_2 in (EMIm)(SH) at 120 °C and subsequent slow cooling to room temperature. It crystallized as red blocks in almost quantitative yield (see Experimental Section). Compounds **3** and **4** were obtained accordingly as orange and yellow platelets upon treatment of $K_2Hg_3Se_4$ at 100 and 120 °C, respectively.

The results suggest that the method might be viewed as a *pseudo*-flux approach, as we provoke transformations of chalcogenides as typical for a treatment in polychalcogenide fluxes. However, we are operating at much lower temperatures, as the added chalcogenide source has a much lower melting point than any metal chalcogenide: (EMIm)(SH) has a melting point of 93 °C, it decomposes at 163 °C.[25] Note that the new approach is not simply exchangeable for a common flux synthesis, though: while such were used for the synthesis of ternary selenidometalates, for example, the recent synthesis of $NaCu_6Se_4$,[29] the title compounds did not emerge from any flux reaction tested to date. This is in contrast to the sulfur homologue of **1**, $K_2Hg_6S_7$, which was prepared via classical flux reactions of K_2S_3 and Hg (or HgS) at 210 °C.[30] In turn, we did so far not obtain $K_2Hg_6S_7$ by our new method. The exact reasons for the different product spectra under the different synthesis conditions are not understood yet. However, we ascribe this in part to the different temperatures not only in sulfidic versus selenidic inorganic fluxes but also versus organic IL *pseudo*fluxes, which only enable reactions with relatively low energy barriers in the latter. Furthermore, the different basicity of sulfide versus selenide anions, is expected to be an important parameter in the hydrochalcogenide ILs. In line with this, treatment of $K_2Hg_6S_7$ in (EMIm) (SeH) at temperatures between 80 and 140 °C did not lead to any visible reaction. Higher temperatures initiate decomposition into HgSe and Se, as confirmed by single-crystal X-ray diffraction. The same applies for reactions of $K_2Hg_6S_7$ in common ILs, such as (BMIm)Br or (BMIm)[BF_4]. Attempts to generate any of the $A_2Hg_6Ch_7$ phases (A = alkali metal, Ch = chalcogen) via solvothermal routes failed so far, as well; instead various selenidomercurates were obtained this way.[20,31] Nevertheless, it is possible to recrystallize crude samples of $K_2Hg_6S_7$ under solvothermal conditions in en at 130−150 °C or by the *pseudo*-flux method in (EMIm)(SH) at 80−140 °C.

Ionothermal treatment of Na_2HgSe_2 in (EMIm)(SH) provokes a partial exchange of the chalcogenide ligand. In case of $K_2Hg_3Se_4$, the metalate phase is recrystallized, and different amounts of selenium are replaced by sulfur, dependent on the temperature. The products **3** and **4** indicate that higher reaction temperatures increase the amount of chalcogen exchange, hence leading to a greater sulfur content.

No further chalcogen exchange could be observed for reaction temperatures above 120 °C. Ionothermal treatment of Na_2HgSe_2 and $K_2Hg_3Se_4$, both in (EMIm)(SH) and (EMIm) (SeH), at temperatures above 120 °C with or without addition of amines, led to decomposition under formation of HgSe besides elemental Se, as confirmed by single-crystal X-ray diffraction measurements of the crystalline products. Similar results were observed for other ternary phases $Na_xHg_yCh_z$ (Ch = Se, Te), which did only yield binary mercury chalcogenide and elemental chalcogens. Decomposition of the metalate phases starts above 120 °C for selenium phases and 100 °C for their tellurium analogues.

Crystal Structures. 1 possesses a close structural relationship to its lighter congener $K_2Hg_6S_7$ (see Figure 1).[30] However,
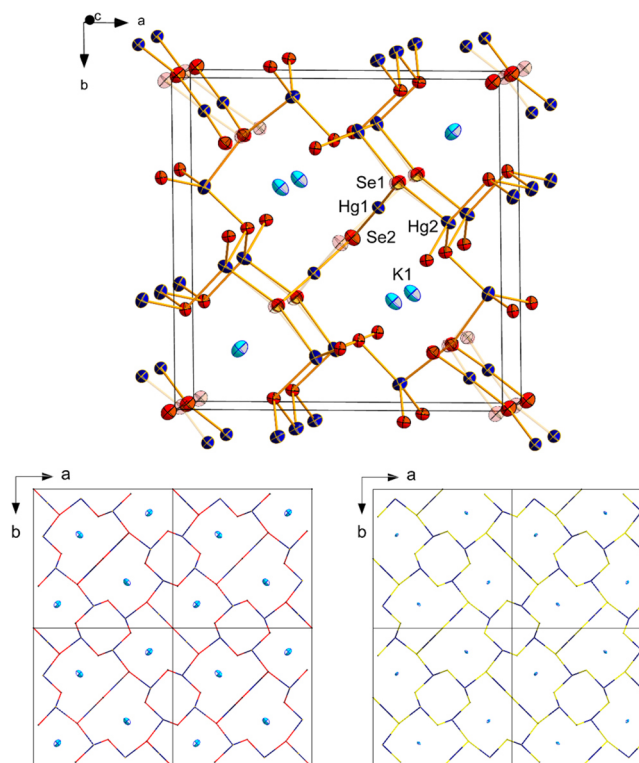
Figure 1. Crystal structure of **1** (top) and comparison of the structure with that of $K_2Hg_6S_7$ (bottom; Hg/Se and Hg/S networks shown as blue/red and blue/yellow wires, respectively).[30] Ellipsoids are drawn at 50% probability. Selected structural parameters for **1** [Å, deg]: Hg−Se 2.434(6)−2.7917(18), 3.006(7); K···Se 3.371(13)−3.775(12); Se−Hg−Se 69.6(4)−169.6(3); Hg−Se−Hg 88.71(14)−159.1(3).

the structure of **1** differs from that of the sulfide, as it crystallizes in another tetragonal space group, $P4_2/mnm$, with a = 14.2241(16) Å, c = 4.2075(5) Å (cf. $K_2Hg_6S_7$: $P\bar{4}2_1m$, with a = 13.805(8) Å, c = 4.080(3) Å). It further exhibits a disorder of two of the three crystallographically independent Se atoms. However, if neglecting the disorder both structures can be brought to congruence upon normalization of the unit cell. As reported for its lighter congener, the structure of **1** is rather particular. Two types of one-dimensional tunnels are extending along the crystallographic c axis, with the narrower ones comprising eight-membered Hg_8Se_8 rings being empty, and the larger ones being based on 12-membered rings being filled with the potassium counterions. In the eight-membered rings, tetrahedral Hg^{2+} ions alternate with pyramidal μ_3-Se atoms. In addition to these atoms, the 12-membered rings comprise seven atoms that are not shared with the eight-membered rings, two linearly coordinated Hg^{2+} atoms, one μ-Se atom, and four T-shaped μ_3-Se atoms. Respective interatomic distances and angles are Hg−Se 2.434(6)-2.7917(18) Å, 3.006(7) Å; K···Se 3.371(13)-3.775(12) Å; Se−Hg−Se 69.6(4)−169.6(3)°; Hg−Se−Hg 88.71(14)−159.1(3)°. As expected, He−Se distances are longer than in the according sulfide, by ca. 0.1 Å for the shorter Hg−Se bonds and by nearly 0.3 Å for the longest

contact. The coordination environment around the T-shaped μ_3-S atom is closer to an actual T shape than reported for the sulfide (100.9−158.1°).

Compound **2** crystallizes in orthorhombic space group *Pbca* ($a = 8.3188(17)$ Å, $b = 7.3873(15)$ Å, $c = 14.104(3)$ Å), as its isostructural homologue $Na_2Hg_3S_4$ ($a = 7.308$ Å, $b = 14.011$ Å, $c = 8.231$ Å),[32] which only differs by another cell setting being applied to the structural model (see Figure 2). The pure
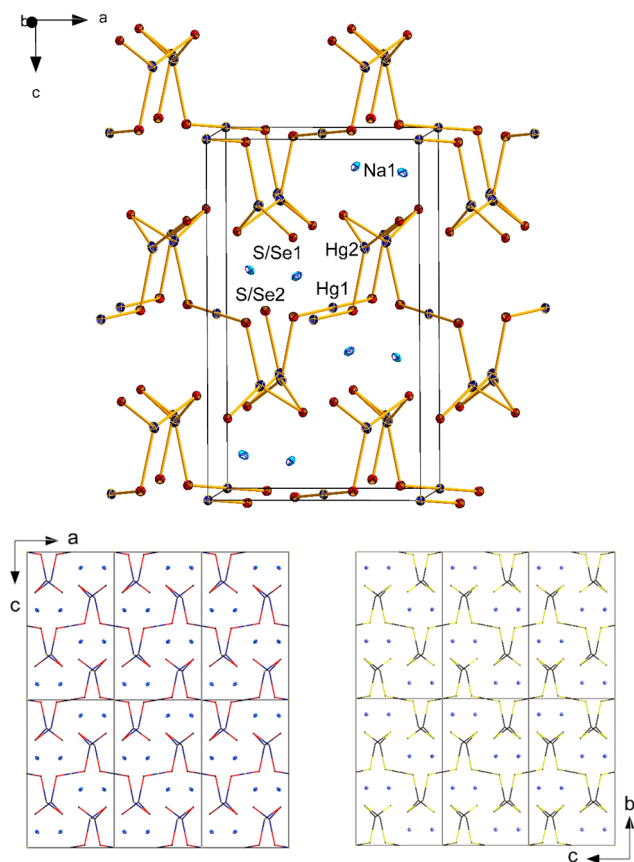
Figure 2. Crystal structure of **2** (top) and comparison of the structure with that of $Na_2Hg_3S_4$ (bottom; Se/S mixture given as Se only in the structure of **2**; Hg/Se and Hg/S networks shown as blue/red and blue/yellow wires, respectively).[32] Ellipsoids are drawn at 50% probability. Selected structural parameters [Å, deg]: Hg−Se/S 2.376(2)−2.6019(17), 3.1357(17); Na···Se/S 2.850(6)−3.002(5); Se/S−Hg−Se/S 89.97(3)−128.87(7), 180.0; Hg−Se/S−Hg 94.04(6)−104.72(6).

selenide $Na_2Hg_3Se_4$, in contrast, has not been reported. The anionic substructure of compound **2** is a two-dimensional layered chalcogenido mercurate network staggered along [001]. Two-thirds of the mercury atoms are coordinated in a trigonal planar manner by chalcogen atoms (Hg−Se/S 2.484(2)−2.602(2) Å; Se/S−Hg−Se/S 105.96(6)−128.87(7)°), forming chains of $[HgSe_2]^{2−}$ that are interconnected by mercury atoms in linear coordination (Hg−Se/S 2.376(2) Å; Se/S−Hg−Se/S 180°). The wave-shaped layers display a short Hg−S/Se interlayer contact of 3.136(2) Å. They are separated by the sodium cations (Na···S/Se 2.850(6)−3.002(5) Å). The Hg···Ch contacts are elongated by ca. 0.3−0.5 Å as compared to the sulfur analogue, giving rise for the slight overall extension of the structure, in agreement with the mixed occupation of the chalcogen positions.

Compounds **3** and **4** also crystallize in the orthorhombic crystal system, but in space group *Pbcn* ($a = 10.712(2)$ Å, $b = 6.7488(14)$ Å, $c = 13.917(3)$ Å (**3**); $a = 10.605(2)$ Å, $b = 6.6515(13)$ Å, $c = 13.788(3)$ Å (**4**)). They are isostructural to their homologues $K_2Hg_3S_4$ ($a = 10.561(5)$ Å, $b = 6.6534(14)$ Å, $c = 13.706(2)$ Å) and $K_2Hg_3Se_4$ ($a = 10.820(2)$ Å, $c = 14.042(2)$ Å).[30] The structure is shown on the example of compound **4** in Figure 3. The anionic substructures of compounds **3** and **4** are based on one-dimensional chains of edge-sharing eight-membered rings formed by alternating Hg and Se/S atoms. The chains proceed along [010], and they are arranged parallel in layers parallel to (001), with a short Hg−Se/S contact of 3.133(2) Å (**3**) and 3.099(4) Å (**4**). These are separated by layers of potassium cations, which show a distorted octahedral coordination by six chalcogen atoms (K···Se/S 3.264(4)−3.358(5) Å (**3**); K···Se/S 3.217(12)−3.347(10) Å (**4**)). Two-thirds of the mercury atoms are almost linearly coordinated by chalcogen atoms (Hg−Se/S 2.453(2)−2.461(2) Å, Se/S−Hg−Se/S 165.11(6)° (**3**); Hg−Se/S 2.414(6)−2.423(6) Å, Se/S−Hg−Se/S 165.75(21)° (**4**)), while the remaining third of the mercury atoms is found in a slightly distorted tetrahedral coordination environment (Hg−Se/S 2.646(2)−2.663(2) Å, Se/S−Hg−Se/S 104.87(19)−115.39(18)° (**3**); Hg−Se/S 2.619(6)−2.624(6) Å, Se/S−Hg−Se/S 104.64(5)−115.72(5)° (**4**)). As expected, the Hg···Ch contacts within compound **4** are elongated by 0.3−0.4 Å as compared to those of compound **3** due to the increased Se/S ratio. This trend is also approved in comparison to the pure sulfide and selenide analogues.

No other homologue with a mixed chalcogen situation as it is found in **2**, **3**, and **4** has been known to date. The atomic site occupation factors in **2**, **3**, and **4** were obtained from second free-variable refinement of the respective positions (applying EADP and EXYZ constraints) and were verified by EDX measurements (see Table 1).

Optical Absorption Properties. The band gap of the mixed-chalcogen compounds **2**−**4** was determined experimentally by optical absorption spectroscopy (see Figure 4), showing a significant blue shift for compound **4** (2.28 eV), in agreement with its larger sulfur content as compared to its slightly heavier congener **3** (2.11 eV). The band gap of **2** was determined as 2.03 eV, which cannot be compared to **3** and **4** directly because of its different morphology. The band gap and color of the compounds strongly depends on the morphology, which is determined by the alkali metal cation. This becomes obvious upon comparison of the title compounds with known sulfides: $Na_2Hg_3S_4$, which is isostructural and isotypic to compound **2**, is red,[32] whereas a $K_2Hg_3S_4$ phase, which is isostructural to compounds **3** or **4**, is yellow.[30] All measured band gaps correlate well with the visible colors of the compounds.

CONCLUSION

Four new ternary chalcogenides, namely, $K_2Hg_6Se_7$, $Na_2Hg_3S_{2.51}Se_{1.49}$, $K_2Hg_3S_{1.03}Se_{2.97}$, and $K_2Hg_3S_{2.69}Se_{1.31}$, were synthesized via ionothermal reactions in a nonclassic hydrosulfide IL (EMIm)(SH). Neither of the compounds could so far be obtained by classical synthesis techniques, but exclusively by application of $(SH)^−$ containing ILs as solvent in the nearly room-temperature regime, representing a *pseudo*-flux approach. The method provides access to materials with finely tunable electronic properties via chalcogen exchange that is controllable by the reaction temperature.
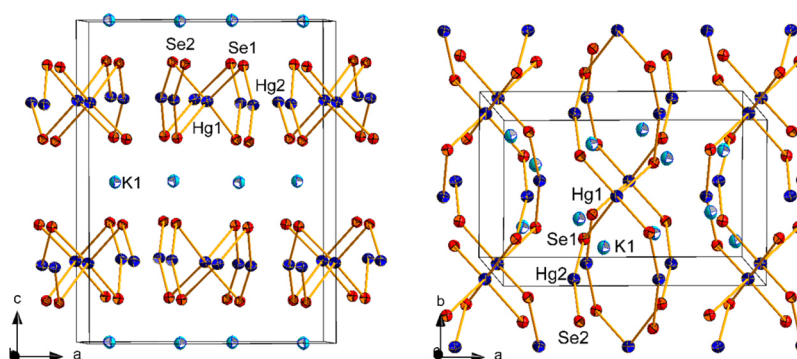
Figure 3. Crystal structure of **4**, as an example for isostructural compounds **3** and **4**, viewed approximately along crystallographic axes *b* (left) and *c* (right). The Se/S mixture is given as Se only. Ellipsoids are drawn at 50% probability. Selected structural parameters [Å, deg]: Hg−Se/S 2.4527(18)−2.6629(18), 3.133(2)−3.197(2); K⋯Se/S 3.264(4)−3.358(5); Se/S−Hg−Se/S 98.59(6)−115.39(18), 165.11(6); Hg−Se/S−Hg 77.55(5)−95.63(6) (**3**). Hg−Se/S 2.414(6)−2.625(6), 3.099(6)−3.165(6); K⋯Se/S 3.217(12)−3.347(10); Se/S−Hg−Se/S 94.49(19)−115.72(5), 165.75(21); Hg−Se/S−Hg 76.62(14)−95.5(2) (**4**).
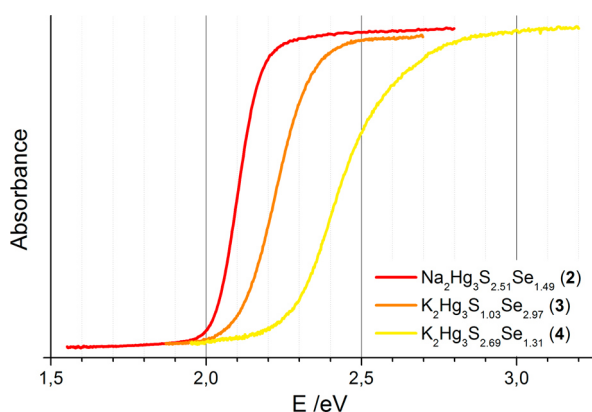
Figure 4. UV−visible spectra of compounds **2**−**4**.

ASSOCIATED CONTENT

ⓢ Supporting Information

The Supporting Information is available free of charge on the ACS Publications website at DOI: 10.1021/acs.inorg-chem.6b00974. CCDC 1473364 (**1**), CCDC 1473365 (**2**), CCDC 1473366 (**3**), CCDC 1473367 (**4**) contain the supplementary crystallographic data for this paper. These data can be obtained free of charge via www.ccdc.cam.ac.uk/data_request/cif.

  X-ray crystallographic information (CIF)
  X-ray crystallographic information (CIF)
  X-ray crystallographic information (CIF)
  X-ray crystallographic information (CIF)

AUTHOR INFORMATION

Corresponding Author

*E-mail: dehnen@chemie.uni-marburg.de. Fax: +49 6421 28-25751.

Author Contributions

The manuscript was written through contributions of all authors. All authors have given approval to the final version of the manuscript.

Notes

The authors declare no competing financial interest.

REFERENCES

(1) Cooper, E. R.; Andrews, C. D.; Wheatley, P. S.; Webb, P. B.; Wormald, P.; Morris, R. E. *Nature* **2004**, *430*, 1012−1016.

(2) Morris, R. E. *Chem. Commun.* **2009**, 2990−2998.

(3) Morris, R. E. *Dalton Trans.* **2012**, *41*, 3867−3868.

(4) Santner, S.; Heine, J.; Dehnen, S. *Angew. Chem.* **2016**, *128*, 886−904.

(5) Ahmed, E.; Ruck, M. *Coord. Chem. Rev.* **2011**, *255*, 2892−2903.

(6) Zhang, Q.; Chung, I.; Jang, J. I.; Ketterson, J. B.; Kanatzidis, M. G. *J. Am. Chem. Soc.* **2009**, *131*, 9896−9897.

(7) Biswas, K.; Zhang, Q.; Chung, I.; Song, J.-H.; Androulakis, J.; Freeman, A. J.; Kanatzidis, M. G. *J. Am. Chem. Soc.* **2010**, *132*, 14760−14762.

(8) Li, J. R.; Xie, Z.-L.; He, X.-W.; Li, L.-H.; Huang, X.-Y. *Angew. Chem., Int. Ed.* **2011**, *50*, 11395−11399.

(9) Xiong, W.-W.; Li, J.-R.; Hu, B.; Tan, B.; Li, R.-F.; Huang, X.-Y. *Chem. Sci.* **2012**, *3*, 1200−1204.

(10) Li, J.-R.; Xiong, W.-W.; Xie, Z.-L.; Du, C.-F.; Zou, G.-D.; Huang, X.-Y. *Chem. Commun.* **2013**, *49*, 181−183.

(11) Du, C.-F.; Li, J.-R.; Feng, M.-L.; Zou, G.-D.; Shen, N.-N.; Huang, X.-Y. *Dalton Trans.* **2015**, *44*, 7364−7372.

(12) Sakamoto, H.; Watanabe, Y.; Saito, T. *Inorg. Chem.* **2006**, *45*, 4578−4579.

(13) Cody, J. A.; Finch, K. B.; Reynders, G. J., III; Alexander, G. C. B.; Lim, H. G.; Näther, C.; Bensch, W. *Inorg. Chem.* **2012**, *51*, 13357−13362.

(14) Ahmed, E.; Breternitz, J.; Groh, M. F.; Isaeva, A.; Ruck, M. *Eur. J. Inorg. Chem.* **2014**, *2014*, 3037−3042.

(15) Lin, Y.; Dehnen, S. *Inorg. Chem.* **2011**, *50*, 7913−7915.

(16) Lin, Y.; Massa, W.; Dehnen, S. *J. Am. Chem. Soc.* **2012**, *134*, 4497−4500.

(17) Lin, Y.; Massa, W.; Dehnen, S. *Chem. - Eur. J.* **2012**, *18*, 13427−13434.

(18) Lin, Y.; Xie, D.; Massa, W.; Mayrhofer, L.; Lippert, S.; Ewers, B.; Chernikov, A.; Koch, M.; Dehnen, S. *Chem. - Eur. J.* **2013**, *19*, 8806−8813.

(19) Santner, S.; Dehnen, S. *Inorg. Chem.* **2015**, *54*, 1188−1190.

(20) Thiele, G.; Lippert, S.; Fahrnbauer, F.; Bron, P.; Oeckler, O.; Rahimi-Iman, A.; Koch, M.; Roling, B.; Dehnen, S. *Chem. Mater.* **2015**, *27*, 4114−4118.

(21) Li, H.; Malliakas, C. D.; Liu, Z.; Peters, J. A.; Sebastian, M.; Zhao, L.; Chung, D. Y.; Wessels, B. W.; Kanatzidis, M. G. *Cryst. Growth Des.* **2014**, *14*, 5949−5956.

(22) Thiele, G.; Santner, S.; Donsbach, C.; Assmann, M.; Müller, M.; Dehnen, S. *Z. Kristallogr. - Cryst. Mater.* **2014**, *0*, 489−495.

(23) Finger, L. H.; Wohde, F.; Grigoryev, E. I.; Hansmann, A.-K.; Berger, R.; Roling, B.; Sundermeyer, J. *Chem. Commun.* **2015**, *51*, 16169−16172.

(24) Finger, L. H.; Scheibe, B.; Sundermeyer, J. *Inorg. Chem.* **2015**, *54*, 9568−9575.

(25) Finger, L. H.; Sundermeyer, J. *Chem. - Eur. J.* **2016**, *22*, 4218−4230.

(26) Sheldrick, G. M. *Acta Crystallogr.* **2015**, *A71*, 3−8.

(27) Sheldrick, G. M. *Acta Crystallogr.* **2015**, *C71*, 3−8.

(28) Dolomanov, O. V.; Bourhis, L. J.; Gildea, R. J.; Howard, J. A. K.; Puschmann, H. *J. Appl. Crystallogr.* **2009**, *42*, 339−341.

(29) Sturza, M.; Malliakas, C. D.; Bugaris, D. E.; Han, F.; Chung, D. Y.; Kanatzidis, M. G. *Inorg. Chem.* **2014**, *53*, 12191−12198.

(30) Kanatzidis, M. G.; Park, Y. *Chem. Mater.* **1990**, *2*, 99−101.

(31) Thiele, G.; Donsbach, C.; Riedel, R.; Marsch, M.; Harms, K.; Dehnen, S. *Dalton Trans.* **2016**, *45*, 5958−5967.

(32) Klepp, K. O. *J. Alloys Compd.* **1992**, *182*, 281−288.

3.2 Combining Solid-state and Solution-based Techniques: Synthesis and Reactivity of Chalcogenidoplumbates(II or IV)

G. Thiele, C. Donsbach, I. Nußbruch, S. Dehnen, *J. Vis. Exp.* **2016**, *118*, e54789.

Abstract: The phases of "PbCh$_2$" (Ch = Se, Te) are obtained from solid-state syntheses (*i.e.*, by the fusion of the elements under inert conditions in silica glass ampules). Reduction of such phases by elemental alkaline metals in amines affords crystalline chalcogenidoplumbate(II) salts comprised of [PbTe$_3$]$^{2-}$ or [Pb$_2$Ch$_3$]$^{2-}$ anions, depending upon which sequestering agent for the cations is present: crown ethers, like 18-crown-6, or cryptands, like [2.2.2]crypt. Reactions of solutions of such anions with transition-metal compounds yield (poly-)chalcogenide anions or transition-metal chalcogenide clusters, including one with a μ-PbSe ligand (*i.e.*, the heaviest-known CO homolog).

In contrast, the solid-state synthesis of a phase of the nominal composition "K$_2$PbSe$_2$" by successive reactions of the elements and by the subsequent solvothermal treatment in amines yields the first non-oxide/halide inorganic lead(IV) compound: a salt of the *ortho*-selenidoplumbate(IV) anion [PbSe$_4$]$^{4-}$. This was unexpected due to the redox potentials of Pb(IV) and Se(-II). Such methods can further be applied to other elemental combinations, leading to the formation of solutions with binary [HgTe$_2$]$^{2-}$ or [BiSe$_3$]$^{3-}$ anions, or to large-scale syntheses of K$_2$Hg$_2$Se$_3$ or K$_3$BiSe$_3$ via the solid-state route.

All compounds are characterized by single-crystal X-ray diffraction and elemental analysis; solutions of plumbate salts can be investigated by [205]Pb and ^{77}Se or [127]Te NMR techniques. Quantum chemical calculations using density functional theory methods enable energy comparisons. They further allow for insights into the electronic configuration and thus, the bonding situation. Molecular Rh-containing Chevrel-type compounds were found to exhibit delocalized mixed valence, whereas similar telluridopalladate anions are electron-precise; the cluster with the μ-PbSe ligand is energetically favored over a hypothetical CO analog, in line with the unsuccessful attempt at its synthesis. The stability of formal Pb(IV) within the [PbSe$_4$]$^{4-}$ anion is mainly due to a suitable stabilization within the crystal lattice.

Inhalt: Im Video sowie dem zugehörigen Manuskript (siehe Appendix) werden verschiedene Synthesemethoden vorgestellt, die Anwendung im Bereich der Synthese von Chalcogenidometallat-Verbindungen finden. Die Reaktionen werden an Beispielen aus der Selenidoplumbat-Chemie präsentiert. Im Detail sind dies das Arbeiten unter Schutzgasatmosphäre (SCHLENK-Technik, Handschuhbox), die Trocknung von

Lösungsmitteln (Destillation von 1,2-Diaminoethan (en) über Calciumhydrid), Hochtemperatur-Festkörperreaktionen (Synthese von $PbSe_2$ und K_2PbSe_2), *in-situ*-Reduktion von Metall(poly-)chalkogeniden durch Alkalimetalle in Lösung (Synthese von K(18c6)]$_2$[Pb$_2$Se$_3$]) (18c6 = 1,4,7,10,13,16-Hexaoxacyclooctadecan), solvothermale Reaktionen (Synthese von K_4[PbSe$_4$]•en•NH$_3$), reaktive Überschichtungen (Synthese von [(RhPPh$_3$)$_6$(µ$_3$-Se)$_8$]•0.5en) und Überschichtung als Kristallisationsmethode ({[K(18c6)]-[K(en)$_2$]K[Rh$_3$(CN)$_2$(PPh$_3$)$_4$(µ$_3$-Se)$_2$(µ-PbSe)]}$_2$•1.3en). Außerdem werden die optische Begutachtung der kristallinen Produkte am Lichtmikroskop sowie Analysemethoden (Röntgen-Kristallstrukturanalyse, NMR-Spektroskopie und quantenchemische Untersuchungen) kurz thematisiert.

Eigener Anteil: Das Manuskript wurde von Günther Thiele und Stefanie Dehnen verfasst. Das Drehbuch wurde in Zusammenarbeit aller Autoren mit der Redaktion des Journal of Visualized Experiments (JoVE) verfasst und überarbeitet. Das Audio- und Videomaterial wurde von mir in Zusammenarbeit mit Isabell Nußbruch, Stefanie Dehnen und JoVE aufgenommen und von JoVE geschnitten.

Das Video ist über folgende Links abrufbar:

https://www.jove.com/video/54789

doi: 10.3791/54789

Video Article

Combining Solid-state and Solution-based Techniques: Synthesis and Reactivity of Chalcogenidoplumbates(II or IV)

Günther Thiele[1], Carsten Donsbach[2], Isabell Nußbruch[2], Stefanie Dehnen[2]

[1]Department of Chemistry, University of California, Berkeley

[2]Fachbereich Chemie, Philipps-Universität Marburg and Wissenschaftliches Zentrum für Materialwissenschaften

Correspondence to: Stefanie Dehnen at dehnen@chemie.uni-marburg.de

Abstract

The phases of "PbCh$_2$" (Ch = Se, Te) are obtained from solid-state syntheses (*i.e.*, by the fusion of the elements under inert conditions in silica glass ampules). Reduction of such phases by elemental alkaline metals in amines affords crystalline chalcogenidoplumbate(II) salts comprised of [PbTe$_3$]$^{2-}$ or [Pb$_2$Ch$_3$]$^{2-}$ anions, depending upon which sequestering agent for the cations is present: crown ethers, like 18-crown-6, or cryptands, like [2.2.2]crypt. Reactions of solutions of such anions with transition-metal compounds yield (poly-)chalcogenide anions or transition-metal chalcogenide clusters, including one with a µ-PbSe ligand (*i.e.*, the heaviest-known CO homolog).

In contrast, the solid-state synthesis of a phase of the nominal composition "K$_2$PbSe$_2$" by successive reactions of the elements and by the subsequent solvothermal treatment in amines yields the first non-oxide/halide inorganic lead(IV) compound: a salt of the *ortho*-selenidoplumbate(IV) anion [PbSe$_4$]$^{4-}$. This was unexpected due to the redox potentials of Pb(IV) and Se(-II). Such methods can further be applied to other elemental combinations, leading to the formation of solutions with binary [HgTe$_2$]$^{2-}$ or [BiSe$_3$]$^{3-}$ anions, or to large-scale syntheses of K$_2$Hg$_2$Se$_3$ or K$_3$BiSe$_3$ via the solid-state route.

All compounds are characterized by single-crystal X-ray diffraction and elemental analysis; solutions of plumbate salts can be investigated by ^{205}Pb and ^{77}Se or ^{127}Te NMR techniques. Quantum chemical calculations using density functional theory methods enable energy comparisons. They further allow for insights into the electronic configuration and thus, the bonding situation. Molecular Rh-containing Chevrel-type compounds were found to exhibit delocalized mixed valence, whereas similar telluridopalladate anions are electron-precise; the cluster with the µ-PbSe ligand is energetically favored over a hypothetical CO analog, in line with the unsuccessful attempt at its synthesis. The stability of formal Pb(IV) within the [PbSe$_4$]$^{4-}$ anion is mainly due to a suitable stabilization within the crystal lattice.

Video Link

The video component of this article can be found at https://www.jove.com/video/54789/

Introduction

Metal chalcogenides, such as SnSe or CuInSe, are versatile materials with a wide range of applications, for instance, as semiconductor, thermoelectric, or nonlinear optic materials[1-6]. Similar elemental compositions are found within chalcogenidometalates, where the metal is in a formally positive oxidation state and coordinated by negative (poly-)chalcogenide ligands to yield an overall anionic species. Different from the abovementioned materials, such metalates are additionally comprised of counter-ions, which are well separated from the anionic substructure. Typical cations are (solvated) alkali or alkaline earth metals, ammonium, or phosphonium ions. Most often, such salts with chalcogenidometalate anions have physical properties that are similar to their parental binary or ternary compounds, such as similar band gaps or photo- and semiconductivity properties. However, due to the broad range of possible anionic architectures within each elemental combination, ranging from isolated molecular species through strands and sheets of interconnected anions to extended three-dimensional frameworks, an even finer tuning of various properties can be achieved, ultimately aiming at the designed synthesis of compounds with the desired properties. Within the concept of dimensional reduction, it has been shown that a relative increase of counter ions per formula unit, which accompanies a reduction from 3D via 2D and 1D to 0D anionic architectures (0D representing molecular species), decreases the observed band gap[7]. Moreover, by the utilization of different (or mixtures of) chalcogenide ligands, it is even possible to achieve an ultra-fine adjustment of the band gap[8,9].

Apart from these practical applications and visionary relevancies, chalcogenidometalates are still investigated for fundamental understanding, such as for the generation of novel anionic structure types or the discovery and interpretation of an unusual bonding, as well as for their unprecedented properties. Whereas the lighter congeners (*i.e.*, oxidometalates, commonly referred to as oxometalates) have been extensively studied, in particular for potential catalytic applications, the heavier chalcogenidometalates are far less explored.

Our own interest has been focused on the synthesis, properties, and further reactivity of chalcogenidotetrelates (*i.e.,* the heavier homologs of silicates)[10,11]. There is a broad variety of such compounds, ranging from water-stable and soluble binary anions, such as the $[SnTe_4]^{4-}$ anion[12]; to organic, functionalized, and multinary cluster compounds, such as $\{[Ir_3(cod)_3(\mu_3-S)_2](\mu_3-S)SnCl\}_2$ (cod = cycloocta-1,5-diene)[13]. Our most recent studies deal with chalcogenidoplumbates, with lead as the central metal atom(s). In line with the inert-pair concept for heavy atoms, addressing the stabilization of the 6s orbital due to relativistic effects, lead is usually observed in the formal +II oxidation state. Exceptions like PbO_2 are strong oxidizing agents, and the heavier lead(IV) chalcogenides, "$PbCh_2$," have not been discovered to date[14]. The same holds for the chalcogenidoplumbate(IV) anions, of which only $[PbO_4]^{4-}$ has been reported[15] until recently (see below).

Apart from a diverse group of structurally investigated oxidoplumbates(II,IV), there have been only few examples of chalcogenidoplumbates(II), namely $[PbTe_3]^{4-}$, with a trigonal pyramidal anion[16]; and $[Pb_2Ch_3]^{2-}$, where Ch = Se or Te, with a trigonal bipyramidal anion[17]. These are synthesized by a route that has also been applied for the generation of Zintl ions[18]. Upon preparation of multinary intermetallic phases by fusion of the elements at high temperatures, subsequent extraction by solvents in the presence of a sequestering agent affords the desired products in (single-)crystalline form. In the case of the $[Pb_2Ch_3]^{2-}$ anions, for instance, a phase of the nominal composition "KPbCh" has been extracted with 1,2-diaminoethane (en) in the presence of 4,7,13,16,21,24-Hexaoxa-1,10-diazabicyclo[8.8.8]hexacosane ([2.2.2]crypt). The cryptand is necessary both for crystallization upon increase of the effective cation radius in the $\{K[2.2.2]crypt\}^+$ complex counter ion, to better match the anionic size, and for a shielding of the positive charge that suppresses an electron back-donation from the anion in solution. Such salts with encapsulated cations usually reveal high tendencies for crystallization and thus, fairly good yields when compared to the corresponding salts without sequestration agents. However, a rather cumbersome synthesis or the high prices of cryptands prevent the excessive scaling of such approaches.

In contrast, $K_4[PbTe_3]\cdot2en$ is synthesized via *in situ* reduction in solution, as has already been used as early as 1891 for the generation of the famous Pb_9^{4-} anion[19,20]. For the latter, elemental alkaline metals were added to suspensions of lead in liquid ammonia at low temperatures, whereas for the telluridoplumbate, an alloy of the nominal composition "$PbTe_2$" was reduced at room temperature, again by the addition of elemental potassium.

Our first approach towards such metalate species to be presented herein is a combination of both pathways. Here, solid-state synthesis is followed by either reduction in solution in the presence of inexpensive sequestering agents, such as 1,4,7,10,13,16-hexaoxacyclooctadecane (18-crown-6), or via reduction with alkaline metals that are chelated by the solvent itself, without the need for additional sequestering agents, similar to the synthesis of $[Na_4(en)_7][Sn_9]$[21]. Our second approach also starts with high-temperature synthesis, but it is followed by solvothermal extraction of the resulting phases (*i.e.,* extraction at elevated temperatures and pressures)[22]. In the following, we will present both synthetic approaches and some of our recent results upon application of these reaction pathways.

Protocol

Caution: Always be cautious when working with chemicals. Apply common safety precautions, including the appropriate utilization of gloves, goggles, and a lab coat at all times. In particular, be aware that all discussed compounds containing heavy elements, as well as their elemental sources, are of high toxicity. 1,2-diaminoethane is a corrosive liquid. Alkaline metals and ternary solid-state products may react pyrophorically with air and moisture.

Note: All manipulations are performed in an argon atmosphere using standard Schlenk or glovebox techniques under strict exclusion of air and external moisture. Solids or solutions containing heavy element metalate species or precursors are stored under the exclusion of light by wrapping the respective containers with aluminum foil for inhibition of a light-induced decomposition.

1. Preparation of Solvents and Solutions

1. Add 1 L of freshly purchased 1,2-diaminoethane to 25 g of CaH_2 and stir overnight. Reflux (T_b = 116 °C) until no H_2 is generated (approximately 12 h).
   1. Distill at ambient pressure.
2. Add 1 L of oxolane (THF) to 10 g of NaK alloy and stir overnight. Reflux (T_b = 66 °C) for at least 12 h. Distill at ambient pressure.
3. Make a saturated solution of $[Rh(PPh_3)_3Cl]$ by adding 150 mg of $[Rh(PPh_3)_3Cl]$ to 10 mL of THF. Stir overnight at room temperature (RT) and filtrate with an inert gas filter frit of low porosity.

2. High-temperature Solid-state Reactions

1. **Synthesis of PbSe₂**
   1. Place 3.81 g of elemental Se in a borosilicate ampule and add 5 g of elemental Pb on top. Heat it with an oxygen/methane burner until optical homogeneity of the melt is achieved (approximately 10 min). Knock the ampule gently with a cork ring throughout the synthesis to detach sublimed Se from the ampule wall, which will then drop back into the reaction mixture.
   2. Allow the ampule to cool down to room temperature. Break the ampule with a pestle in a mortar and manually remove all remaining splinters of the ampule. Pestle the crude $PbSe_2$ thoroughly.

2. **Synthesis of K₂PbSe₂**
   1. Place 0.95 g of elemental K and 5 g of elemental Pb in a thick-walled borosilicate ampule. Slowly increase the heat with an oxygen/methane burner until optical homogeneity of the melt is achieved (approximately 20 min).
   2. Carefully add 1.9 g of elemental Se pellets to the molten alloy. Upon the complete addition, increase the temperature until the reaction mixture emits bright yellow/white radiation (approximately 10 min) and hold the temperature for 10 min. Decrease the reaction temperature slightly if the radiation color turns to pure, bright white (a temperature close to the melting point of the ampule).

3. Allow the reaction mixture to cool down to RT. Break the ampule and manually remove all remaining splinters of the ampule and a regulus of elemental lead. Pestle the crude K_2PbSe_2 thoroughly.

3. *In Situ* Reduction

1. **Synthesis of a solution of [K(18-crown-6)]$_2$[Pb$_2$Se$_3$]**
   1. Place 2 g of PbSe$_2$, 3.1 g of 18-crown-6, 250 mL of 1,2-diaminoethane, and a large stir bar in a round-bottom N$_2$-flask on a stir plate. Stir rigorously at RT and slowly add 0.45 g of elemental K.
   2. Stir overnight at RT and filter the solution with an inert gas filter frit of low porosity (pore diameters: D3, 16-40 μm or D4, 10-16 μm).

4. Solvothermal Reactions

1. **Synthesis of K$_4$[PbSe$_4$]·en·NH$_3$**
   1. Place 0.5 g of K$_2$PbSe$_2$ and 2 mL of 1,2-diaminoethane in a 10-mL glass vial in a 15-mL polytetrafluorethylene vial in a standard stainless-steel autoclave. Close the autoclave tightly and it heat in an oven to 150 °C for 5 days.
   2. Turn off the oven and leave it for 1 d to slowly cool to RT. Transfer the reaction mixture into paratone oil and manually select crystals of K$_4$[PbSe$_4$]·en·NH$_3$ under a standard light microscope at 15-40X magnification.

5. Reactive Layering

1. **Synthesis of [(RhPPh$_3$)$_6$(μ$_3$-Se)$_8$]·0.5en**
   1. Place 10 mL of a solution of [K(18-crown-6)]$_2$[Pb$_2$Se$_3$] in a 50-mL flask, add 10 mL of a saturated solution of [Rh(PPh$_3$)$_3$Cl] in THF, and stir overnight.
   2. Filter the reaction solution with an inert gas filter frit of low porosity and remove the solvent under dynamic vacuum slowly during 24 h. Transfer the crude reaction product into paratone oil and manually select crystals of [(RhPPh$_3$)$_6$(μ$_3$-Se)$_8$]·0.5en under a standard light microscope at 15-40X magnification.

2. **Synthesis of {[K(18-crown-6)]-[K(en)$_2$]K[Rh$_3$(CN)$_2$(PPh$_3$)$_4$(μ$_3$-Se)$_2$(μ-PbSe)]}$_2$·1.3en**
   1. Place 10 mL of a solution of [K(18-crown-6)]$_2$[Pb$_2$Se$_3$] in a Schlenk tube and carefully layer it with 10 mL of a saturated solution of [Rh(PPh$_3$)$_3$Cl] in THF. Cover the Schlenk tube completely in aluminum foil and leave it undisturbed for 4 weeks.
   2. Transfer the resulting solid into paratone oil and select single crystals quickly under a light microscope.

6. Analysis of the Solutions and Compounds

1. Place 50 mg of "K$_2$PbSe$_2$" onto an acrylic glass sample carrier (the compound reacts with elemental Si) and cover it with tape. Place it under ambient conditions in a powder X-ray diffractometer (PXRD) and record the diffraction data within 1 h[23].
2. Place 0.6 mL of a solution of [K(18-crown-6)]$_2$[Pb$_2$Se$_3$] in a nuclear magnetic resonance (NMR) tube and thoroughly seal the latter with protective tape. Transfer it quickly into the NMR probe and record ^{77}Se and [205]Pb NMR with at least 2,000 and 5,000 pulses, respectively[25].
3. Select a single crystal under a light microscope and mount it on the goniometer head of the diffractometer. Measure it with high redundancy to enable the adequate absorption corrections[23-33].
4. Perform a simultaneous optimization of the electronic and geometric structure of [Rh$_3$(CN)$_2$(PPh$_3$)$_4$(μ$_3$Se)$_2$(μPbSe)][3-]. Apply the conductor-like screening model (COSMO) with a 10% increase of the default radii to account for charge compensation[28].
   1. Calculate the vibrational frequencies to ensure the energetic minimum[28].
   2. Perform Mulliken and/or natural bond orbital (NBO) analyses based on the density functional theory (DFT) wave function to obtain the atomic charges[28].
   3. Calculate in-orbital contributions to the "relaxed" and the original structures of a) the complete cluster, b) the CO/PbSe-free cluster, and c) the CO/PbSe ligand, and compare the results[28].

Representative Results

The existence of an *ortho*-selenidoplumbate anion [PbSe$_4$][4-23] (see **Figure 1**, top right) has been confirmed by single crystal diffraction experiments, elemental analysis, and quantum chemical calculations. The crystal structure refinement confirms the almost-perfect tetrahedral coordination geometry, as would be expected for a lead(IV) ion, whereas DFT calculations rationalize the energetically stabilized a_1 representation, which contributes to the overall stability of the anion (see **Figure 1**, bottom right). The isolation of the anion as its potassium salt was possibly caused by the unexpected stability of the anion itself, but it was mainly due to the incorporation within a reasonable crystal structure. This is rationalized by similar measures of the anion as compared to its homolog, the well-known [SnTe$_4$][4-]. K$_4$[PbSe$_4$]·en·NH$_3$ represents the first inorganic lead(IV) compound without highly electronegative ligands, such as oxygen or fluorine atoms.
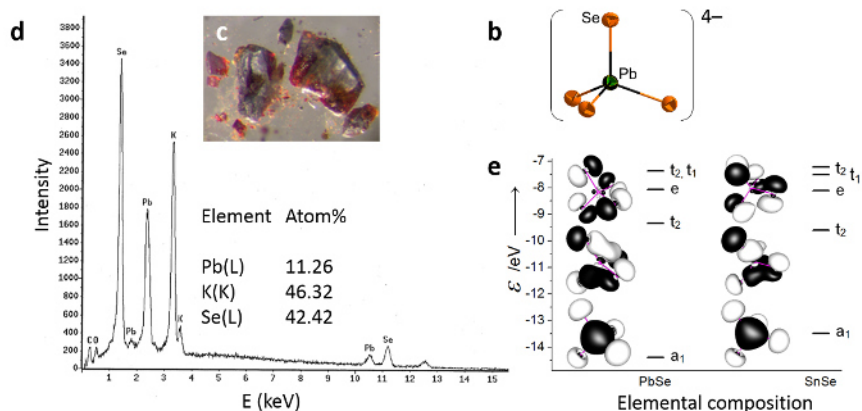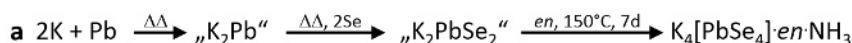
Figure 1: K$_4$[PbSe$_4$]·en·NH$_3$. Reaction pathway for the synthesis of K$_4$[PbSe$_4$]·en·NH$_3$ (**a**). Representation of the [PbSe$_4$]$^{4-}$ anion, as determined by means of single crystal X-ray diffraction with thermal ellipsoids at 50% probability (**b**). Macroscopic appearance (**c**). Results of the elemental analysis via energy dispersive X-ray spectroscopy (**d**). Results of the quantum chemical calculations with amplitudes drawn at 0.033 a.u. (**e**). Parts of the figure were reproduced with permission from Wiley-VCH. Please click here to view a larger version of this figure.

By means of the same synthesis protocol as applied for K$_4$[PbSe$_4$]·2en·NH$_3$, yet using a different elemental combination and stoichiometry, further metalate materials can be obtained. For example, K$_2$Hg$_2$Se$_3$[24] is a semi- and photoconductor material with a polyanionic substructure that is based on three-dimensionally connected selenidomercurate tubes. The compound can be obtained on large scales and in high yield. It is a promising archetype for thermoelectric applications, even though the very elemental combination exhibits a too-large band gap, as demonstrated by means of DFT calculations with periodic boundary conditions and by ultra-violet (UV)-visible spectroscopy. This causes a rather low electronic conductivity, as rationalized experimentally. However, the band gap can be decreased by synthesizing the heavier homolog, K$_2$Hg$_2$Te$_3$ (**Figure 2**), which indeed gives rise to an increase in the photoconductivity by several orders of magnitude.
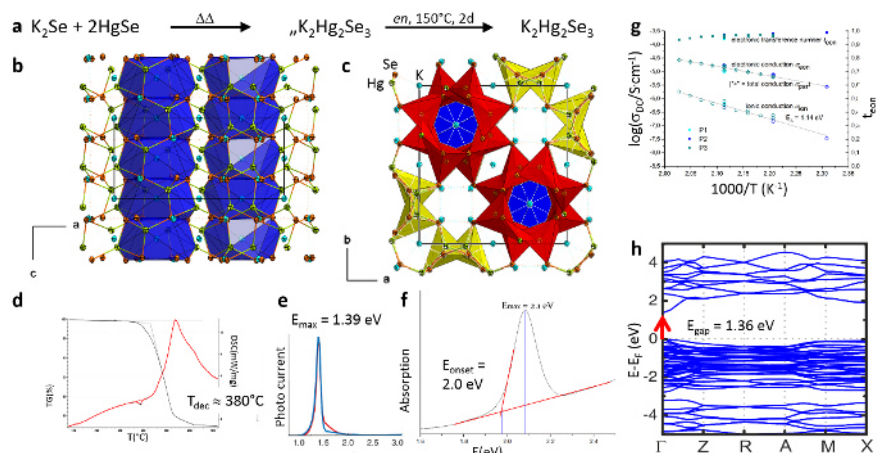
Figure 2: K$_2$Hg$_2$Se$_3$. Reaction pathway for the synthesis of K$_2$Hg$_2$Se$_3$ (**a**). Representation of the structures with channels along *c* (**b**, **c**) according to single-crystal X-ray diffraction, thermal (**d**), and optoelectronic analysis (**e**, **f**). Impedance spectroscopy results (**g**) and calculated band structure (**h**). Parts of the figure were reproduced with permission from the American Chemical Society. Please click here to view a larger version of this figure.

High yield and purity solutions of metalate anions do not only facilitate their isolation and full characterization[25], but they can also be utilized for further reactivity studies, yielding, for example, molecular Chevrel-type compounds, such as [(RhPPh$_3$)$_6$(μ-Ch)$_8$] (Ch = Se, Te) or anionic [Pd$_6$(μ-Te)$_8$]$^{4-}$ (**Figure 3**)[26,27]. Interestingly, the phosphine-saturated (thus, overall neutral) species include mixed valence Rh^{2+}/Rh^{3+} ions, as rationalized by means of quantum chemical calculations. As the charge is highly delocalized over the cluster core, the structure determined by single crystal diffraction does not allow for an assignment of the different formal oxidation states. The anionic telluridopalladate cluster, in contrast, is electron-precise. Pd(II) ions adopt a distorted square-planar coordination environment and are thus interesting for further reactions towards Lewis-basic compounds, like in catalytic processes.
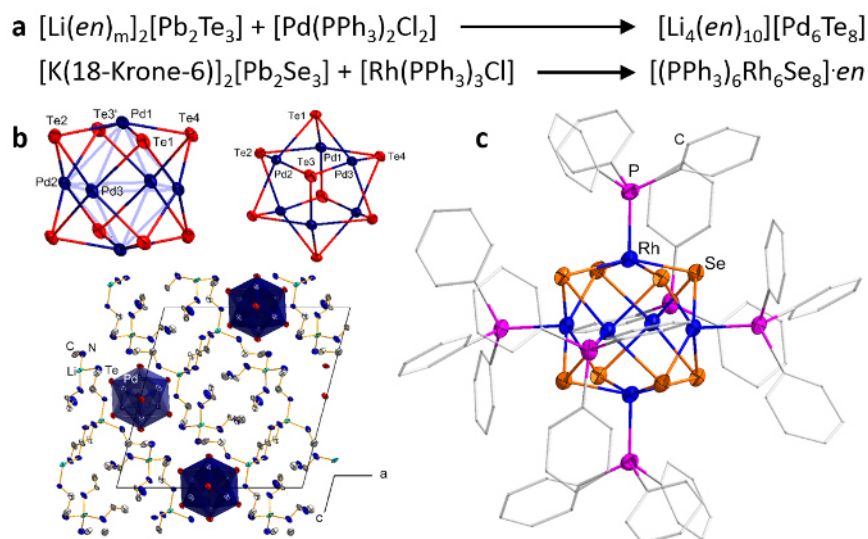
Figure 3: Molecular CHEVREL-type compounds. Reaction pathway for the synthesis of $[Li_4(en)_{10}][Pd_4Te_8]$ and $[(PPh_3)_6Rh_6Se_8]\cdot en$ (**a**). Structural representation as determined by means of single-crystal X-ray diffraction (**b**, **c**). Parts of the figure were reproduced with permission from the American Chemical Society. Please click here to view a larger version of this figure.

Very similar reaction conditions, but a different work-up procedure, afford compounds with $[Rh_3Se_2]$ units, adopting a trigonal bipyramidal shape, with Se at the apical positions and Rh in the basal plane[28]. These units represent the core of different anionic cluster complexes that can be isolated selectively by the addition of a certain counter-ion sequestering agent (**Figure 4**). $[Rh_3(PPh_3)_6(\mu_3\text{-}Se)_2]^-$, with two PPh_3 ligands coordinating each of the Rh(I) atoms, is crystallized as its salt upon the addition of [2.2.2]crypt. The use of 18-crown-6 instead yields a salt of the $[Rh_3(CN)_2(PPh_3)_4(\mu_3\text{-}Se)_2(\mu\text{-}PbSe)]^{3-}$ anion, in which only one of the Rh(I) atoms bears two phosphine ligands, whereas the two others are coordinated by one CN^- ligand each. Additionally, and most remarkably, a μ-PbSe ligand bridges between the latter two metal atoms. The PbSe fragment is the second-heaviest carbon monoxide homolog and the heaviest one observed to date. Quantum chemical calculations helped to show that a corresponding complex with CO instead of PbSe in the bridging position would be disfavored, as the size and bonding properties of PbSe better match the requirements of the cluster core. In line with this, experiments in a CO atmosphere failed to yield a corresponding μ-CO-bridged species.
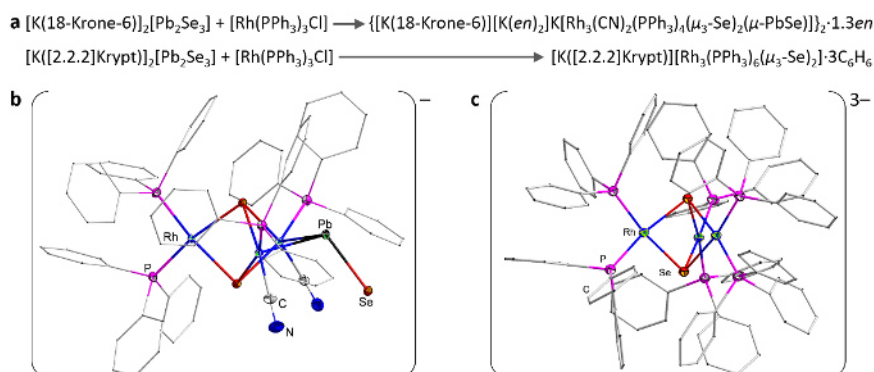
Figure 4: μ-PbSe: a very heavy CO analog. Reaction pathways (**a**) and structural representations, as determined by single-crystal X-ray diffraction for the $[Rh_3(CN)_2(PPh_3)_4(\mu_3\text{-}Se)_2(\mu\text{-}PbSe)]^{3-}$ (**b**) and $[Rh_3(PPh_3)_6(\mu_3\text{-}Se)_2]^-$ (**c**) anions. Parts of the figure were reproduced with permission from Wiley-VCH. Please click here to view a larger version of this figure.

Discussion

The combination of classical high-temperature, solid-state reactions with solution-based methods allows for the generation and isolation of novel compounds that cannot be synthesized by only one of these pathways. Even though, in most cases, a clear identification and full characterization of the intermediate species is difficult or essentially impossible, the general idea is straightforward and can be applied to a variety of elemental combinations. Furthermore, the actual synthetic conditions for the generation of one specific compound are rather flexible, and the presence of further ionic species and/or differing relative proportions of the involved elements affect the yield, but not the formation itself. The synthesis of $K_4[PbSe_4]\cdot 2en\cdot NH_3$,[23] for instance, has to be performed by starting out from a phase of the nominal composition "K_2PbSe_2" for achievement of highest yields, while the same compound is obtained in lower yields upon the use of other phases, like "KPbSe," "K_4PbSe_4," or "K_2PbSe_4." Furthermore, the utilization of technical Pb, which contains up to 30% of Sb, affords the same product, to our surprise, in even better yields than with the phases mentioned before. This suggests a reaction mechanism involving a Sb^{3+}/Sb^{5+} redox step — present, for example, in a phase with the nominal composition "$K_4Pb_xSb_{1-x}Se_4$" — as a sacrificial oxidant for the generation of "Pb^{4+}." The

same applies for the generation of mercurates, thallates, and bismuthates: the solvothermal reaction of "K_2PbSe_2" with $HgSO_4$ yields $K_2Hg_2Se_3$, as does a solvothermal extraction of "$K_xHg_ySe_z$" (where $x \geq y$ and $z \leq 2y$; $K_2Hg_2Se_3$ is the primary reaction product). Again, in most cases of such solvothermal "extractions," $K_2Hg_2Se_3$ can be obtained with elemental proportions not too far off the nominal product of the solid-state fusion reaction. Depending on the respective amounts, $K_2Hg_3Se_4$, K_2Se_x ($x = 1.3$), HgSe, and elemental Hg are obtained as side-products in corresponding yields.

Apparently, it is necessary to provide preformed multinary phases, as can be deduced from the generation of $K_4[HgSe_3] \cdot H_2O$[29], which was synthesized from K_2Se and $HgSO_4 \cdot nH_2O$. Attempts to synthesize this compound from a phase of the nominal composition "K_4HgSe_3," with varying percentages of water within the solvent, failed. Only the abovementioned mercurates, $K_2Hg_2Se_3$ and $K_2Hg_3Se_4$, were obtained instead. Vice versa, $K_2Hg_2Se_3$ could so far not be obtained from solvothermal reactions starting out from K_2Se and $HgSO_4$ or HgSe.

In contrast to the aforementioned flexibility of the synthesis concerning elemental ratios, the change of solvent or the addition of trace amounts of different solvents had a large impact on the reaction product. Whereas N,N-dimethylformamide slowly decomposes into CO and $HNMe_2$, to slowly increase the basicity of the mixture, or forms formate anions, which help with crystallization, primary amines either tend to form ammonia *in situ* or coordinate the metal ions in various ways, such as in $[Ba(trien)_2]^{2+}$ (trien = 2,2'-diaminodiethylamine) or $[(pren)_3Eu(Te_3)_2Eu(pren)_3]$ (pren = 1,3-diaminopropane)[30]. Traces of water may act as a crystal solvent, affect the acidity and basicity of the solution, and/or act as templates by H-bonding.

A different approach towards these metalates is the pathway of *in situ* reduction. Formally chalcogen-rich chalcogenides or elemental chalcogens in the presence of metal chalcogenides are treated with elemental alkali metals in amines. As known for solutions of alkali metals in liquid ammonia, amine solutions of alkali metals possess a high reduction potential. Thus, the chalcogen is reduced, forming soluble chalcogenides that can further react with metal chalcogenides to yield chalcogenidometalates. However, the formal oxidation state of the metal within the metal chalcogenide is usually not affected. Thus, a large variety of metalate species can be obtained via this synthetic approach[25]. Additionally, the application of primary amines, such as 1,2-diaminoethane, yields stable alkali metal solutions that can be stored at RT (with the exception of cesium and, to a lesser extent, rubidium, which cause the instantaneous reduction of the amine). Furthermore, unlike reactions in liquid ammonia, the reactions in amines do not have to be performed at low temperatures. As would be expected, the reduction of tellurium usually proceeds much faster than that of selenium. Additionally, the solubility of telluride species in amines is generally enhanced by an order of magnitude. However, the resulting telluridometalate compounds are usually extremely sensitive to air, moisture, and — depending on the central metal ion — also to light.
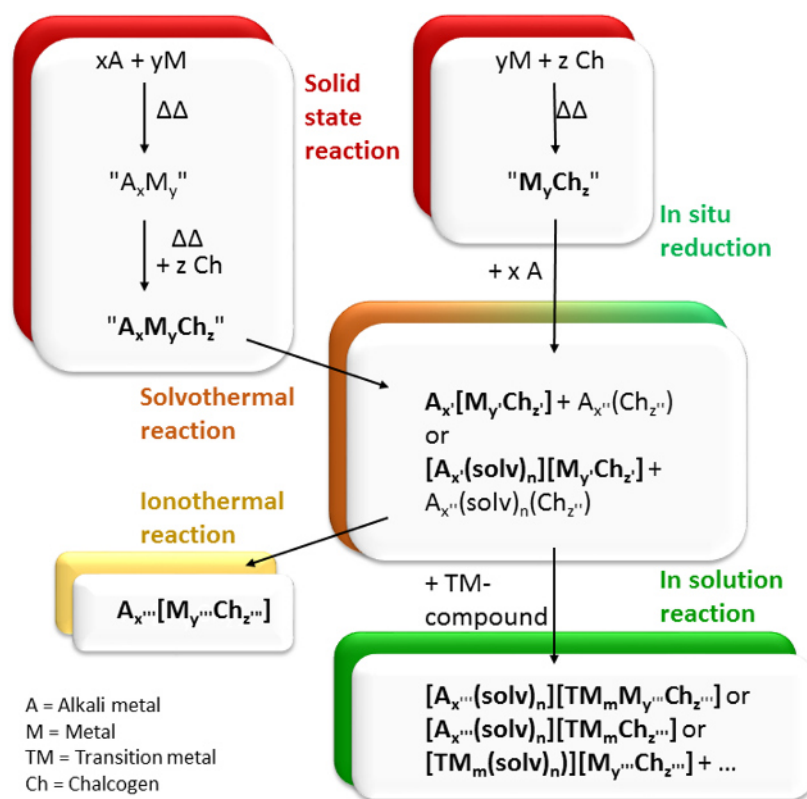
Figure 5: Summary of synthetic approaches. Reaction pathways starting out from the solid-state reactions to generate metalate species by solvothermal reactions or *in situ* reduction and the subsequent derivatization of the metalate species by means of ionothermal reactions or solution-based techniques. Please click here to view a larger version of this figure.

Each of the individual reaction approaches depicted in **Figure 5** has intrinsic limitations. Solid-state reactions usually yield thermodynamic products, and since hardly any phase diagrams for the ternary compounds were investigated, the stoichiometries have to be investigated via an educated trial-and-error approach. The *in situ* reactions do not allow for unusual high oxidation states of the central metal (such as Pb^{+IV}), and the solvent is restricted to primary amines. Transformation reactions in ionic liquids need to start from pure educts, and the exact nature of the

reaction product cannot yet be predicted. This also applies to the reported reactions in solution, which additionally suffer from low yields, thus making subsequent reaction studies and physical investigations cumbersome.

However, apart from all metalate compounds that could be identified and isolated so far (see the summary of synthetic approaches in **Figure 5**), a vast variety of polychalcogenides have been detected and isolated[31,32]. These investigations have been neglected so far, even though they possess intriguing properties and can also be synthesized by a direct approach via the *in situ* method in high yields and purities. In contrast, for the solvothermal reaction pathway, no general pattern is observed for the resulting type of metalate. Neither have the exact influences of solvent and temperature been elucidated thus far. A predictive model, however, seems to be the ultimate goal for the synthesis of this versatile class of materials.

Disclosures

The authors have nothing to disclose.

Acknowledgements

References

1. Zhao, L.-D., *et al.* Ultralow thermal conductivity and high thermoelectric figure of merit in SnSe crystals. *Nature.*, **508** (7496), 373 - 377 (2014).
2. Chung, I., Kanatzidis, M. G. Metal Chalcogenides: A Rich Source of Nonlinear Optical Materials. *Chem. Mater.*, **26** (1), 849 - 869 (2014).
3. Lhuillier, E., *et al.* Two-Dimensional Colloidal Metal Chalcogenides Semiconductors: Synthesis, Spectroscopy, and Applications. *Acc. Chem. Res.*, **48** (1), 22 - 30 (2015).
4. Heine, T., Transition metal chalcogenides: ultrathin inorganic materials with tunable electronic properties. *Acc. Chem. Res.*, **48** (1), 65 - 72 (2015).
5. Gao, M.-R., Xu, Y.-F., Jiang, J., Yu, S.-H., Nanostructured metal chalcogenides: synthesis, modification, and applications in energy conversion and storage devices. *Chem. Soc. Rev.*, **42**, 2986 - 3017 (2013).
6. Jackson, C., *et al.* Multiexciton Solar Cells of CuInSe$_2$ Nanocrystals. *J. Phys. Chem. Lett.* **5** (2), 304 - 309 (2014).
7. Androulakis, J., *et al.* Dimensional Reduction: A Design Tool for New Radiation Detection Materials. *Adv. Mater.* **23** (36), 4163 - 4167 (2011).
8. Sheldrick, W. S., Polychalcogenide Anions: Structural Diversity and Ligand Versatility. *Z. Anorg. Allg. Chem.* **638** (15), 2401 - 2424 (2012).
9. Dehnen, S., Melullis, M., A coordination chemistry approach towards ternary M/14/16 anions. *Coord. Chem. Rev.* **251** (9-10), 1259 - 1280 (2007).
10. Santner, S., Heine, J., Dehnen, S., Synthesis of Crystalline Chalcogenides in Ionic Liquids. *Angew. Chem. Int. Ed.* **55** (3), 876 - 893 (2015).
11. Heine, J., Dehnen, S., From Simple Chalcogenidotetrelate Precursors to Complex Structures and Functional Compounds. *Z. Anorg. Allg. Chem.* **638** (15), 2425 - 2440 (2012).
12. Ruzin, E., Zent, E., Matern, E., Massa, W., Dehnen, S., Syntheses, Structures, and Comprehensive NMR Spectroscopic Investigations of Hetero-Chalcogenidometalates: The Right Mix toward Multinary Complexes. *Chem. Eur. J.* **15** (21), 5230 - 5244 (2009).
13. Leusmann, E., Geringer, E., Weinert, B., Dehnen, S. {[Ir$_3$(cod)$_3$(µ$_3$-S)$_2$](µ$_3$-S)SnCl} $_2$ – a Ternary Ir-Sn-S cluster with the Iridium Atoms in Three Different Chemical Environments. *Dalton Trans.* **45**, 15298–15302 (2016).
14. Pyykkö, P., Relativistic Effects in Chemistry: More Common Than You Thought. *Ann. Rev. Phys. Chem.* **63**, 45 - 64 (2012).
15. Brazel, B., Hoppe, R. Zur Kenntnis von K$_4$PbO$_4$ und Rb$_4$PbO$_4$. *Z. Anorg. Allg. Chem.* **505** (10), 99 - 104 (1983).
16. Jones, C. D. W., DiSalvo, F. J., Haushalter, R. C., Synthesis and X-ray Crystal Structure of K$_4$PbTe$_3$·2(en). *Inorg. Chem.* **37** (4), 821 - 823 (1998).
17. Björgvinsson, M., Sawyer, J. F., Schrobilgen, G. J., Dilead(II) Chalcogenide anions Pb$_2$Ch$_3$$^{2-}$ (Ch = Se, Te): A ^{207}Pb, ^{125}Te, and ^{77}Se Solution NMR Study. X-ray crystal structure of (2,2,2-crypt-K$^+$)$_2$Pb$_2$Se$_3$$^{2-}$. *Inorg. Chem.* **26** (5), 741 - 749 (1987).
18. Scharfe, S., Kraus, F., Stegmaier, S., Schier, A., Fässler, T. F., Zintl Ions, Cage Compounds, and Intermetalloid Clusters of Group 14 and Group 15 Elements. *Angew. Chem. Int. Ed.* **50** (16), 3630 - 3670 (2011).
19. Joannis, C. R., Action du sodammonium et du potassamonium sur quelques métaux. *C. R. Hebd. Seances Acad. Sci.* **113**, 795 - 798, (1891).
20. Joannis, C. R., Sur quelques alliages bien dèfinis de sodium. *C. R. Hebd. Seances Acad. Sci.* **114**, 585 - 587, (1892).
21. Diehl, L., Khodadeh, K., Kummer, D., Strähle, J., Anorganische Polyederverbindungen, III. Zintl's „Polyanionige Salze": Darstellung und Eigenschaften der kristallinen Verbindungen [Na$_4$·7 en]Sn$_9$, [Na$_4$·5 en]Ge$_9$ und [Na$_3$·4 en]Sb$_7$ und ihrer Lösungen. Die Kristallstruktur von [Na$_4$·7 en]Sn$_9$. *Chem. Ber.* **109** (10), 3404 - 3418 (1976).
22. Demazeau, G., Solvothermal Processes: Definition, Key Factors Governing the Involved Chemical Reactions and New Trends. *Z. Naturforsch.* **65b**, 999 - 1006 (2010).
23. Thiele, G., Krüger, T., Dehnen, S. K$_4$[PbSe$_4$]#en#NH$_3$: A Non-Oxide, Non-Halide Inorganic Lead(IV) Compound. *Angew. Chem. Int. Ed.* **53** (18), 4699 - 4703 (2014).
24. Thiele, G., *et al.* K$_2$Hg$_2$Se$_3$: Large-Scale Synthesis of a Photoconductor Material Prototype with a Columnar Polyanionic Substructure. *Chem. Mater.* **27** (11), 4114 - 4118 (2015).
25. Thiele, G., Vondung, L., Dehnen, S. About the Syntheses of Chalcogenidometalates by in-situ Reduction with Elemental Alkali Metals. *Z. Anorg. Allg. Chem.* **641** (2), 247 - 252 (2015).
26. Thiele, G., You, Z., Dehnen, S. Molecular CHEVREL-like Clusters [(RhPPh$_3$)$_6$(µ$_3$-Se)$_8$] and [Pd$_6$(µ$_3$-Te)$_8$]$^{4-}$. *Inorg. Chem.* **54** (6), 2491 - 2493 (2015).
27. Thiele, G., Balmer, M., Dehnen, S. Synthesis, Structure and Electronic Situation of [Rh$_6$Te$_8$(PPh$_3$)$_6$]·4C$_6$H$_6$. *Zeitschrift für Naturforschung B.* **71** (5), 391–394 (2016).

28. Thiele, G., Franzke, Y., Weigend, F., Dehnen, S. {μ-PbSe}: A Heavy CO Homologue as an Unexpected Ligand. *Angew. Chem. Int. Ed.* **54** (38), 11283 - 11288 (2015).

29. Thiele, G., *et al.* Smallest molecular chalcogenidometalate anions of the heaviest metals: syntheses, structures, and their interconversion. *Dalton Trans.* (2016).

30. Thiele, G., *et al.* Solvothermal and ionothermal synthses and structures of amine- and/or (poly-)chalcogenide coordinated metal complexes. *Z. Kristallogr.* **229** (7), 489 - 495 (2014).

31. Thiele, G., Vondung, L., Donsbach, C., Pulz, S., Dehnen, S. Organic Cation and Complex Cation-Stabilized (Poly-)Selenides, [Cation]$_x$(Se$_y$)$_z$: Diversity in Structures and Properties. *Z. Anorg. Allg. Chem.* **640** (14), 2684 - 2700 (2014).

32. Thiele, G., Lichtenberger, N., Tonner, R., Dehnen, S. Syntheses, Structures and Electronic Properties of a New Series of Tellurides of the Type [Sequestrated Cation]$_2$[Te$_x$] (x = 1-4). *Z. Anorg. Allg. Chem.* **639** (15), 2809 - 2815 (2013).

3.3 Formation of Crystalline Telluridomercurates from Ionic Liquids Near Room Temperature

C. Donsbach, S. Dehnen, *Z. Anorg. Allg. Chem.* **2017**, *643*, 14–19.

Abstract: The ternary telluridomercurate $Na_2[HgTe_2]$ (**1**) was formed by fusion of Na_2Te and HgTe at 600 °C and further treated in the ionic liquid $(C_4C_1Im)[BF_4]$ (C_4C_1Im = 1-butyl-3-methylimidazolium) at moderately elevated temperatures (60 °C), leading to replacement of the Na^+ cations with $(C_4C_1Im)^+$ and re-arrangement of the inorganic substructure. As a result, we obtained the telluridomercurate $(C_4C_1Im)_2[HgTe_2]$ (**2**) and the tellurido/ditelluridomercurate $(C_4C_1Im)_2[Hg_2Te_4]$ (**3**) besides polytellurides and HgTe as by-products. The heavy atom compositions of the compounds were confirmed by micro X-ray fluorescence spectroscopy (μ-XFS), and their structures were determined by single-crystal diffraction. The cation-exchanged salts were further investigated by UV/Vis spectroscopy, indicating narrow band-gap optical transitions at 2.80 eV (**2**) and 1.63 eV (**3**), in agreement with their visible yellow or reddish-black color, respectively.

Inhalt: Die Kristallstrukturen dreier Telluridomerkurat-Salze, $Na_2[HgTe_2]$ (**1**), $(C_4C_1Im)_2[HgTe_2]$ (**2**) und $(C_4C_1Im)[Hg_2(Te_2)Te_2]$ (**3**) (C_4C_1Im = 1-Butyl-3-Methylimidazolium), sowie deren Synthese in einer Hochtemperatur-Festkörperreaktion (**1**) und unter ionothermalen Bedingungen (**2**,**3**) wird vorgestellt. Alle drei Verbindungen wurden mittels Einkristall-Röntgenstrukturanalyse charakterisiert. Die anionischen Substrukturen aller drei Verbindungen sind bereits bekannt, im Fall der Verbindungen **1** und **2** allerdings nur deren Analoga mit leichteren Chalkogenidhomologen. Darüber hinaus wurde das relative Verhältnis der Schwerelemente durch micro-Röntgenfluoreszenz-Spektroskopie (μ-XFS) ermittelt. Die optischen Bandlücken der Verbindungen **2** und **3** wurden mittels UV-Vis-Spektroskopie bestimmt.

Verbindung **1** wurde durch Schmelzen einer Mischung äquimolarer Mengen Na_2Te und HgTe unter Schutzgasatmosphäre erhalten und anschließend in evakuierten und abgeschmolzenen Glasampullen in der ionischen Flüssigkeit $C_4C_1Im[BF_4]$ für einen Tag auf 60 °C erhitzt. Nach dem Abkühlen auf Raumtemperatur wurden die Verbindungen **2** und **3** nebeneinander kristallin erhalten. Bemerkenswert sind die relativ milden ionothermalen Synthesebedingungen, unter denen hier bereits eine strukturelle Umwandlung der Chalkogenidometallat-Anionen stattfindet. Das Auftreten von Ditellurid-Fragmenten in Verbindung **3** durch partielle *in-situ*-Oxidation lässt sich auf die extreme

Oxidationsempfindlichkeit von Tellurid-Verbindungen und die zwar seltene, aber bereits beobachtete Oxidation unter ionothermalen Bedingungen zurückführen.

Eigener Anteil: Die Synthese der Verbindungen **1 – 3** wurde von mir geplant und unter meiner Anleitung von Matthäus Drabek durchgeführt. Die Analyse der Verbindungen mittels Einkristall-Strukturanalyse und spektroskopischer Methoden (µ-XFS und UV-Vis-Spektroskopie) inklusive Auswertung erfolgte durch mich. Das Manuskript wurde von mir in Zusammenarbeit mit Stefanie Dehnen verfasst.

SHORT COMMUNICATION

Formation of Crystalline Telluridomercurates from Ionic Liquids near Room Temperature

Carsten Donsbach[a] and Stefanie Dehnen*[a]

Abstract. The ternary telluridomercurate $Na_2[HgTe_2]$ (**1**) was formed by fusion of Na_2Te and $HgTe$ at 600 °C and further treated in the ionic liquid $(C_4C_1Im)[BF_4]$ (C_4C_1Im = 1-butyl-3-methylimidazolium) at moderately elevated temperatures (60 °C), leading to replacement of the Na^+ cations with $(C_4C_1Im)^+$ and re-arrangement of the inorganic substructure. As a result, we obtained the telluridomercurate $(C_4C_1Im)_2[HgTe_2]$ (**2**) and the tellurido/ditelluridomercurate $(C_4C_1Im)_2[Hg_2Te_4]$ (**3**) besides polytellurides and HgTe as by-prod-

ucts. The heavy atom compositions of the compounds were confirmed by micro X-ray fluorescence spectroscopy (μ-XFS), and their structures were determined by single-crystal diffraction. The cation-exchanged salts were further investigated by UV/Vis spectroscopy, indicating narrow band-gap optical transitions at 2.80 eV (**2**) and 1.63 eV (**3**), in agreement with their visible yellow or reddish-black color, respectively.

Introduction

The crystallization of non-oxidic chalcogen compounds from ionic liquids is a relatively young field of research. It is inspired by the constant search for new approaches to novel chalcogenides, which belong to the most promising and the most diverse class of inorganic materials for a variety of different purposes and applications.[1–5]

A particular focus in the search for novel chalcogen compounds is put on heavy metal chalcogenides and related chalcogenidometalates,[6–10] as they exhibit specific opto-electronic and thermoelectric properties, which can be adjusted and fine-tuned by corresponding choice of the elements and the structure motifs within the compounds.[11–14]

Whereas a large variety of sulfide and selenide compounds of heavy metals have been isolated from ionic liquids, to the best of our knowledge, no tellurides were reported to form under analogous reaction conditions.

We have recently reported on formation of several selenidogermanate, selenidostannate, and sulfido- or selenidomercurate salts in ionic liquids, either starting out from molecular precursors or from extended networks of the general composition $[T_xE_y]^{q-}$ (T = Ge and/or Sn; E = S and/or Se] to extend the knowledge on reaction pathways and equilibria in the still young area of low temperature materials synthesis.[15] All of these investigations were done under ionothermal conditions.[16] Aiming at a transfer of these results to tellurides, we are currently investigating telluridomercurate phases with regard to their behavior in ionic liquids and herein we present the first compounds that were obtained this way.

* Prof. Dr. S. Dehnen
E-Mail: dehnen@chemie.uni-marburg.de
[a] Fachbereich Chemie und Wissenschaftliches Zentrum für Materialwissenschaften
Philipps-Universität Marburg
Hans-Meerwein-Straße 4
35043 Marburg, Germany

Results and Discussion

By fusion of Na_2Te and $HgTe$ in a 1:1 ratio at 600 °C, the ternary phase $Na_2[HgTe_2]$ (**1**) was obtained in approximately quantitative yield (Scheme 1). Compound **1** comprises a rare chalcogenidomercurate substructure: co-planar, edge-sharing $[HgTe_3]$ triangles form a 1D strand, with a zigzag chain of alternating Hg and Te atoms as backbone [Hg–(μ-Te) 2.7757(24) Å; (μ-Te)–Hg–(μ-Te) 107.97(13)°]. All of the non-bridging telluride ligands point towards the same side of the chain [Hg–Te 2.7083(41) Å; (μ-Te)–Hg–Te 125.45(7)°]. The Na^+ cations are situated between the strands that are extending parallel to the crystallographic b axis with alternating orientations of $[Hg–Te–]_n$ backbone and terminal telluride ligands, respectively, with regard to neighboring strands. Figure 1 depicts fragments of the crystal structure of **1**. The anionic structural motif is already known as its sulfidomercurate analog from $Ba[HgS_2]$.[17a] Here, the same linear and coplanar arrangement of edge-sharing trigonal $[HgS_3]$ subunits is found as in **1**, yet co-crystallizing with molecular, linear $[HgS_2]^{2-}$ anions. A related one-dimensional selenidomercurate anion was recently found in $K_2[HgSe_2] \cdot H_2O$; in this case, however, the edge sharing trigonal planar $[HgSe_3]$ units are inclined against each other at an angle of 77.6(1)°.[17b] The only other ternary alkali telluridomercurates known so far are the

$$Na_2Te + HgTe \xrightarrow[\substack{\text{2. washing with} \\ \text{pyridine}}]{\substack{\text{1. 600 °C (15 min)} \\ \rightarrow \text{r. t. (1 h)}}} Na_2HgTe_2 \text{ (1; > 90\%)}$$

$$\downarrow \substack{(C_4C_1Im)[BF_4] \\ 60 °C, 1 d}$$

$$(C_4C_1Im)_2[HgTe_2] \text{ (2; 80\%)} + (C_4C_1Im)_2[Hg_2Te_4] \text{ (3; 5\%)}$$
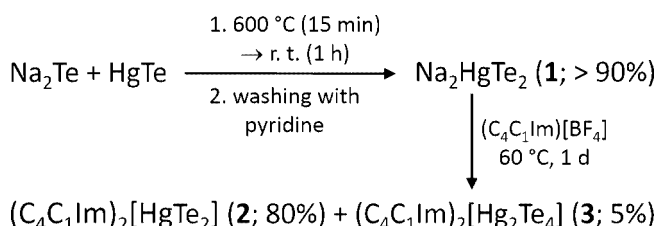
Scheme 1. Overview of the synthetic access of compounds **1**–**3**. Polytellurides that remain dissolved in the mother liquor upon crystallization of **2** and **3**, and an HgTe precipitate explain the non-quantitative product formation.

$K_4[HgTe_3] \cdot H_2O$ with molecular trigonal planar $[HgTe_3]^{4-}$ anions,[17b] $Rb_2[Hg_3Te_4]$ with 1D-$[Hg_3Te_4]^{2-}$ chains,[18] and the partially polytelluride-containing $Rb_4[Hg_5Te_{13}]$ with 1D-$[Hg_5(Te)_3(Te_2)_2(Te_3)_2]^{4-}$ chains.[19]
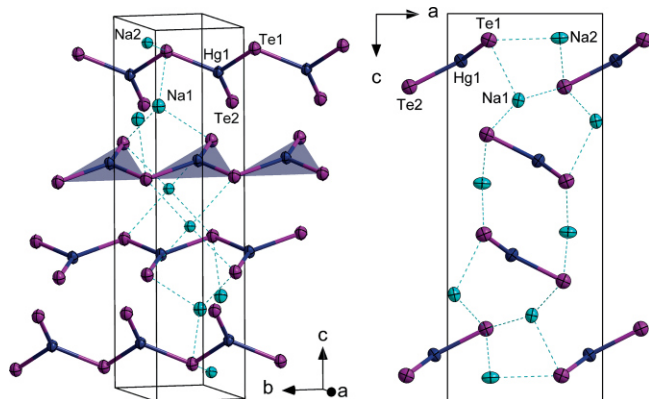
Figure 1. Fragments of the crystal structure of compound **1**, viewed approximately along [100], left, and along [0$\bar{1}$0], right. Hg, Te, and Na atoms are drawn with thermal ellipsoids at the 50 % probability level.

As further indicated in Scheme 1, the treatment of **1** in the ionic liquid $(C_4C_1Im)[BF_4]$, in which the precursor compound **1** dissolved under the given reaction conditions, afforded two new mercurates, $(C_4C_1Im)_2[HgTe_2]$ (**2**) and $(C_4C_1Im)_2[Hg_2Te_4]$ (**3**), under cation exchange and fragmentation (**2**) or re-arrangement of the anionic substructure (**3**), respectively. As a by-product, polytellurides that remain dissolved, and traces of a HgTe precipitate is observed as the thermodynamic sink within this system. The reactions were carried out at remarkably low temperatures of only 60 °C, which is much lower than reported for (trans)formation of related sulfido- or selenidometalates. Figure 2 and Figure 3 show the fractions of the crystal structures of compounds **2** and **3**, respectively.
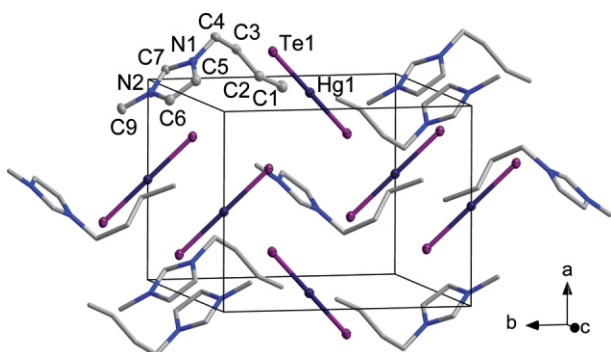
Figure 2. Fragment of the crystal structure of compound **2**. Hg and Te atoms and all C and N atoms of the asymmetric unit are drawn with thermal ellipsoids at the 50 % probability level; further C and N atoms are given as wires for clarity.
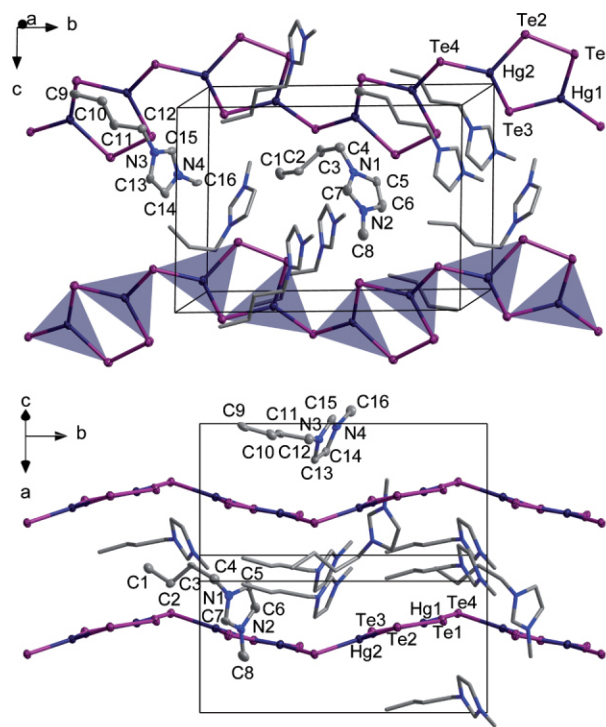
Figure 3. Fragment of the crystal structure of compound **3**, viewed approximately along [100], top, and approximately along [101], bottom. Hydrogen atoms are omitted for clarity. Hg and Te atoms and all C and N atoms of the asymmetric unit are drawn with thermal ellipsoids at the 50 % probability level; further C and N atoms are given as wires for clarity.

At the formation of **2**, the strands were cut into the formally underlying $[HgTe_2]^{2-}$ units, indicating both the relatively low bond energy, and the bond-activating effect of ionic liquids, which is most probably realized by hydrogen H···Te bonds. The $[HgTe_2]^{2-}$ is known as its $[K(crypt-222)]^+$ salt (crypt-222 = 4,7,13,16,21,24-hexaoxa-1,10-diazabicyclo[8.8.8]-hexacosane),[20] and as central building unit in $[Te\{Cr(CO)_5\}_n]$ complexes ($n = 2,3$) of Hg^{II}.[21] In **2**, the Hg atoms are situated on 0,½,½ and ½,0,0, with linear Te–Hg–Te units oriented in one of two nearly perpendicular directions, aligned almost parallel to the *ab* plane [angle between both orientations: 85.6(1)°]. The $(C_4C_1Im)^+$ cations are situated in between the anions, with the imidazolium groups positioned close to 0,0,¼, 0,0,¾, ½,½,¼, ½,½,¾. The Hg–Te bond length [2.5964(2) Å] in **1** is in accordance with that in the known $[K(crypt-222)]^+$ analog [2.5890(25) Å].[20] Both anions are perfectly linear.

In the structure of **3**, another significant re-arrangement of the strands in **1** is observed. This includes an oxidative coupling of the terminal telluride ligands to form ditelluride bridges, which is in agreement with previous reports on partial oxidations in ionic liquids (most probably due to impurities or residual oxygen therein),[15c,22] and a variation of the strand conformation to feature the ditelluride bridges on ever alternating sides of the $[Hg–Te–]_n$ backbone. The achievement of an AABBAA orientation of the terminal telluride ligands (prior to or after their coupling) from the AAAA pattern observed in **1** requires a rotation about the Hg–Te bonds of the backbone.

We assume that this is possible in the molten ionic liquid at 60 °C, but have no proof for it so far. Thus, although this idea of how the substructure of **3** formed from the strand in **1** is the most plausible one from a structural point of view, we cannot exclude, however, that it occurred via complete deconstruction of the telluridomercurate substructure. An analogous construction of a chalcogenidomercurate substructure as found in **3** was reported for the related compounds {[Mn(en)$_3$]$_2$Cl$_2$}[Hg$_2$Te$_4$] (en = 1,2-diaminoethane),[23] and (N(C$_2$H$_5$)$_4$)$_2$[Hg$_2$Te$_4$],[24] which were obtained by solvothermal reaction of alkaline polychalcogenides with Hg$_2$Cl$_2$ and MnCl$_2$ in en or reaction of tetraethylammonium iodide with an en-extracted solution of a ternary phase of the nominal composition K$_2$Hg$_2$Te$_3$, respectively.

The Hg atoms in **3** are positioned near $^3/_8,^7/_8,0$, $^3/_8,0,^7/_8$, $^5/_8,^1/_4,0$, $^5/_8,^1/_2,^1/_8$, and are all coordinated by two μ-bridging Te and one μ^2,η^1:η^1-bridging ditelluride unit. Thereby, a strand of μ–Te linked five-membered [Hg$_2$Te$_3$] rings is formed that extends parallel to the crystallographic b axis. The [Hg$_2$Te$_3$] rings are aligned almost planar, parallel to the (10$\bar{1}$) plane, and form a zigzag chain with two neighboring rings that face each other at an angle of approximately 154°. The imidazolium cations, which are located close to $^1/_4,0,^1/_4$, $^3/_4,^1/_2,^3/_4$, $^1/_8,^5/_8,^1/_2$, $^7/_8,^1/_8,^1/_2$, separate the anionic strands. The Hg–Te distances between Hg and μ-Te units are in the range of 2.6694(14)–2.7263(12) Å, whereas the Hg–Te distances between Hg and μ-Te$_2$ units are slightly longer, 2.7504(14)–2.7715(13) Å. The Te–Te distance in the Te$_2$ fragment is as expected, 2.7361(15) Å. All bond lengths are in good agreement to those of related compounds, in which Hg–(μ-Te) are found in the range 2.654(2)–2.729(5) Å, Hg–(μ^2,η^1:η^1-Te$_2$) are in the range 2.758(2)–2.807(2) Å, and Te–Te bond lengths are 2.751(2)–2.766(7) Å.[23,24]

The Hg atoms in **3** possess a trigonal planar coordination by three Te atoms. The Te–Hg–Te bond angles along the alternating Hg–Te backbone are 121.85(4)–132.80(4)°, whereas they are slightly more acute towards the Te$_2$ unit [110.00(4)–119.93(4)°]. Again, this is in accordance with the values found in the analog compounds [(μ-Te)–Hg–(μ-Te) 124.51(18)–137.12(6)°; (μ-Te)–Hg–(μ^2,η^1:η^1-Te$_2$) 105.45(6)–120.56(6)°].[23,24] However, the relative orientation of the [Hg$_2$Te$_3$] rings against each other differs between the three related compounds. The rings are arranged in a zigzag chain in **3** as well as in (N(C$_2$H$_5$)$_4$)$_2$[Hg$_2$Te$_4$], with dihedral angles between mean planes of 20.14(2)° and 34.98(59)°,[24] respectively. In {[Mn(en)$_3$]$_2$Cl$_2$}[Hg$_2$Te$_4$], however, they are nearly coplanar with all rings pointing towards the same direction [dihedral angle between mean planes: 7.09(3)°].[23] This phenomenon is probably induced by the different cations, and in case of {[Mn(en)$_3$]$_2$Cl$_2$}[Hg$_2$Te$_4$] also because of the presence of further chloride anions in the crystal structure that help stabilizing channels in the cationic substructure.

Besides the anionic substructures that are observed in **1–3** and related compounds, some other inorganic (poly)telluridomercurates have been reported, the structural motifs of which are summarized in Scheme 2. Most of the anions are found along with weakly interacting cations, such as sequestered potassium, transition metal, tetraalkylammonium or tetraphenylphosphonium cations.[18–21,23–29] The entire spectrum of telluridomercurate units comprises molecular anions with linear [HgTe$_2$]$^{2-}$ or trigonal-planar 0D-[HgTe$_3$]$^{4-}$ structure,[20,21,24] whereas no discrete *ortho*-[HgTe$_4$]$^{6-}$ anion has been known to date although tetrahedral subunits are well-known as part of many extended telluridomercurates.[18,19,24,26,28,29] Furthermore, several further mononuclear and polynuclear, molecular anions with bridging or chelating polytelluride ligands have been reported,[23,25–29] as well as several 1D chain anions, most of which include [Hg$_2$Te$_3$] rings as building blocks.[23,24,28]
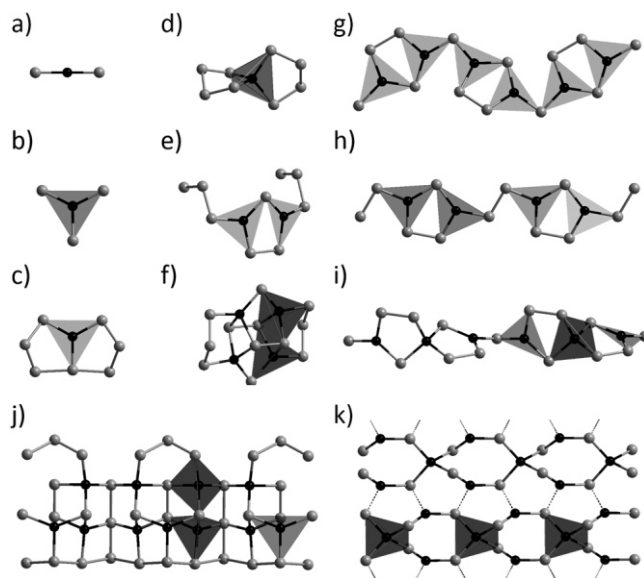
Scheme 2. Overview of all anionic substructures known so far in the system Hg/Te (black/grey): (a) [HgTe$_2$]$^{2-}$,[20,21] (b) [HgTe$_3$]$^{4-}$,[17b,24] (c) [Hg(Te$_7$)]$^{2-}$,[25] (d) [Hg(Te$_4$)$_2$]$^{2-}$,[26] (e) [Hg$_2$(Te)(Te$_2$)(Te$_3$)$_2$]$^{4-}$,[23,27] (f) [Hg$_4$(Te)$_2$(Te$_2$)$_2$(Te$_3$)$_2$]$^{4-}$,[28,29] (g) 1D-[Hg$_2$(Te)$_2$(Te$_2$)]$^{2-}$,[23,24] (h) 1D-[Hg$_2$(Te)(Te$_2$)$_2$]$^{2-}$,[28] (i) 1D-[Hg$_3$(Te)$_3$(Te$_2$)$_2$]$^{5-}$,[24] j) 1D-[Hg$_5$(Te)$_3$(Te$_2$)$_2$(Te$_3$)$_2$]$^{4-}$,[19] (k) 1D-[Hg$_3$Te$_4$]$^{2-}$.[18] Hg atoms are represented as black balls and Te atoms as grey ones. Dotted lines in (k) indicate additional Hg···Te contacts [2.905(1) Å] between the shown 1D strands.

Extending the view from telluridomercurates to chalcogenidomercurates in general, the structural variety is even larger, of course. Sulfido- and selenidomercurates are known as mononuclear complexes with linear, trigonal planar, or tetrahedral coordination around the Hg atoms (e.g. A_2[HgS$_2$], A = Na, K; K$_4$[HgE_3]·H$_2$O, E = Se, Te; A_6[HgCh_4], A/Ch = K/S, K/Se, Rb/S, Rb/Se; Ba[HgS$_2$]),[6c,17,30,31] and they were also observed as 1D chain structures (e.g. K$_2$[HgSe$_2$]·H$_2$O; Ba[HgS$_2$]; Ba$_2$[HgS$_3$]; A_2[Hg$_3E_4$], A/E = K/S,Se, Cs/S,Se),[17,32,33] 2D networks (e.g. Na$_2$[Hg$_3E_4$], E = S, Se),[15f,34] and 3D frameworks (e.g. K$_2$[Hg$_2$Se$_3$], A_2[Hg$_6E_7$], A/E = K/S, K/Se, Rb/S, Rb/Se, Cs/S, Cs/Se),[10b,15f,32,33a,34,35] all of which are based on either linear, trigonal-planar, or tetrahedral [HgE_n] (n = 2–4) building units.

The cation-exchanged salts, **2** and **3**, were further investigated by means of UV/Vis spectroscopy to get an insight in their optical absorption behavior (Figure 4). The spectra reflect well the different extension of the anionic substructures in the two compounds, with the onset of absorption detected at 2.80 eV for **2** and at 1.63 eV for **3**. Both values are in agreement with the visible colors of the two compounds, and they can be understood in terms of the presence of (bonded) polytelluride in **3**, as well as the extend nature of the telluridomercurate anion in it. Extreme air sensitivity of **2** led to decomposition of the sample during preparation, which caused the emergence of a second, red-shifted optical absorption edge generated by the resulting polytelluride decomposition products. This is also in accordance with the observation of darkening of the sample during the measurement.
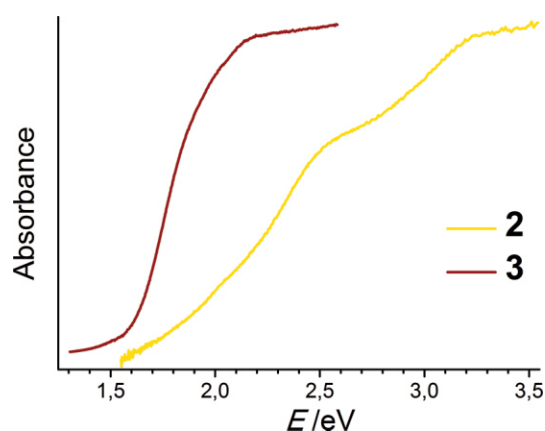
Figure 4. UV/Vis spectra of compound **2** and **3**.

Conclusions

We presented the first telluridometalate salts that were crystallized from ionic liquids. The novel ternary telluridometalate $Na_2[HgTe_2]$, comprising a rare type of a 1D-polymeric $\{[HgTe_2]^{2-}\}_n$ substructure, was used as parent compound to be moderately heated in $(C_4C_1Im)[BF_4]$. From the treatment at 60 °C, two novel salts were obtained upon cation exchange and rearrangement of the anionic substructure, $(C_4C_1Im)_2[HgTe_2]$ (**2**) and $(C_4C_1Im)_2[Hg_2Te_4]$ (**3**). Whereas the $\{[HgTe_2]^{2-}\}_n$ strands were cut into the underlying $[HgTe_2]^{2-}$ monomers at the formation of **2**, the terminal telluride ligands of the parent chains underwent an oxidative coupling into ditelluride bridges at the formation of **3**. Optical absorption spectra of **2** and **3** reflect the different polytelluride content and the dimensionalities of the telluridomercurate anions.[33a] The studies are currently extended towards further telluridometalates of heavy metals.

Experimental Section

General: All manipulations were performed under strict exclusion of air, moisture and light using standard Schlenk and glovebox techniques. Pyridine was dried over CaH_2 and freshly distilled. $(C_4C_1Im)[BF_4]$ was purchased from Sigma-Aldrich and degassed at 1×10^{-3} mbar and 80 °C for 12 h before usage.

Synthesis of 1: Na_2Te and $HgTe$ were fused in a 1:1 ratio in a silica ampoule under ambient pressure with an oxygen/methane burner at 600 °C for 15 min. After cooling to room temperature, the resulting solid was pestled and washed with pyridine to remove polytelluride byproducts until no further colored components were visible in the washing liquid. To obtain single crystals of **1**, 1 g of the raw product

Table 1. Crystallographic data of **1–3**.

	1	**2**	**3**
Empirical formula	$Hg_1Na_2Te_2$	$C_{16}H_{30}Hg_1N_4Te_2$	$C_{16}H_{30}Hg_2N_4Te_4$
Formula weight /g·mol^{-1}	501.77	734.23	1190.02
Crystal color and shape	black metallic block	yellow block	black block
Crystal size /mm^3	$0.03 \times 0.04 \times 0.05$	$0.11 \times 0.13 \times 0.16$	$0.02 \times 0.04 \times 0.06$
Crystal system	orthorhombic	monoclinic	monoclinic
Space group	$Pnma$	$P2_1/n$	$P2_1$
a /Å	7.2708(14)	8.3622(5)	8.9695(18)
b /Å	4.4902(9)	10.6448(5)	14.572(3)
c /Å	18.216(4)	12.7226(8)	10.373(2)
β /°	–	90.321(5)	103.09(3)
V /Å^3	594.7(2)	1132.47(11)	1320.5(5)
Z	4	2	2
ρ_{calc} /g·cm^{-3}	5.60	2.15	2.99
μ(Mo-K_α) /mm^{-1}	35.5	9.3	16.0
Min/max transmission	0.0962/0.3520	0.3033/0.4417	0.1682/0.4654
θ range /°	2.236–26.248	2.495–33.435	2.331–26.360
No. measured refl.	674	18592	7967
No. independent refl.	674	4409	5172
R(int)	0.1068	0.0705	0.0422
No. indep. refl. [$I > 2\sigma(I)$]	359	3823	4866
No. of parameters	31	108	240
R$_1$ [$I>2\theta(I)$]	0.0669	0.0247	0.0297
wR_2 (all data)	0.1701	0.0474	0.0839
S (all data)	0.850	1.046	1.040
Flack parameter	–	–	0.037(8)
$\Delta\rho$max, $\Delta\rho$min /e·Å^{-3}	2.08 / –4.15	1.54 / –1.89	1.25 / –2.60

and 2 mL of pyridine were filled in a glass vial, which was placed in a PTFE-lined steel autoclave with an inner volume of 15 mL and heated in an oven to 150 °C for 4 d before allowing the vessel to slowly cool down to room temperature during 1 d. **1** crystallized as small black blocks with metallic glance.

Synthesis of 2 and 3: Compound **1** (100 mg) and $(C_4C_1Im)[BF_4]$ (0.5 mL) were placed in a pyrex tube. The latter was sealed under vacuum, then sonicated for 1 h at 60 °C, and heated to 60 °C for another 12 h in an oven. After slow cooling to room temperature, **2** crystallized as yellow blocks in approximately 80 % yield alongside with small amounts of dark red blocks of **3** (approximately 5 %) as well as traces of HgTe. The dark color of the solution even after crystallization of **2** and **3** indicated polytelluride by-products to be present.

Single-crystal X-ray Diffraction Studies, Data Collection and Crystallographic Details: Crystals suitable for X-ray diffraction analyses were investigated with a STOE IPDS-II (**1**) or IPDS-2T (**2** and **3**) diffractometer at 100 K using Mo-K_α radiation and a graphite monochromator (λ = 0.71073 Å). Upon numerical absorption correction (STOE X-AREA), the structure solution was performed by direct methods, followed by full-matrix-least-squares refinement against F^2, using SHELXT15, SHELXL15, and OLEX2 software.[36] Table 1 summarizes the crystallographic data for **1**, **2**, and **3**.

Crystallographic data (excluding structure factors) for the structures in this paper have been deposited with the Cambridge Crystallographic Data Centre, CCDC, 12 Union Road, Cambridge CB21EZ, UK. Copies of the data can be obtained free of charge on quoting the depository numbers CCDC-1504527 (**1**), CCDC-1504529 (**2**), and CCDC-1504528 (**3**) (Fax: +44-1223-336-033; E-Mail: deposit@ccdc.cam.ac.uk, http://www.ccdc.cam.ac.uk).

UV/Vis Spectroscopy: UV/Vis spectra were measured with a Varian Cary 5000 dual-beam spectrometer equipped with a Praying Mantis sample holder from Harrik. The diffuse reflection of powdered samples was analyzed.

Micro X-ray Fluorescence Spectroscopy (μ-XFS): Elemental analysis was performed by μ-XFS with a Bruker M4 Tornado, equipped with an Rh-target X-ray tube and a Si drift detector. The emitted fluorescence photons were detected with an acquisition time of 100 s. Upon deconvolution of the spectra, quantification of the elements was achieved based on the Na-K, Te-K and Hg-L radiation. Table 2 summarizes the results.

Table 2. Results of the μ-XSF analyses of compounds **1–3**.

Element	Atom-% measured [calcd.] in **1**	Atom-% measured [calcd.] in **2**	Atom-% measured [calcd.] in **3**
Na	39.0(6) [40.0]	–	–
Te	40.0(5) [40.0]	65.1(8) [66.7]	66.2(8) [66.7]
Hg	21.0(2) [20.0]	34.9(2) [33.3]	33.8(2) [33.3]

Acknowledgements

References

[1] a) M. F. Groh, A. Wolff, M. A. Grasser, M. Ruck, *Int. J. Mol. Sci.* **2016**, *17*, 1452; b) S. Santner, J. Heine, S. Dehnen, *Angew. Chem. Int. Ed.* **2016**, *55*, 886–904.

[2] a) Q. Zhang, I. Chung, J. I. Jang, J. B. Ketterson, M. G. Kanatzidis, *J. Am. Chem. Soc.* **2009**, *131*, 9896–9897; b) K. Biswas, Q. Zhang, I. Chung, J.-H. Song, J. Androulakis, A. J. Freeman, M. G. Kanatzidis, *J. Am. Chem. Soc.* **2010**, *132*, 14760–14762.

[3] a) K.-O. Feldmann, J. Breternitz, M. F. Groh, U. Müller, M. Ruck, T. Wiegand, J. Ren, H. Eckert, O. Schön, K. Karaghiosoff, B. Maryasin, C. Ochsenfeld, J. J. Weigand, *Chem. Eur. J.* **2015**, *21*, 9697–9712; b) M. F. Groh, J. Breternitz, E. Ahmed, A. Isaeva, A. Efimova, P. Schmidt, M. Ruck, *Z. Anorg. Allg. Chem.* **2015**, *641*, 388–393; M. F. Groh, M. Knies, A. Isaeva, M. Ruck, *Z. Anorg. Allg. Chem.* **2015**, *641*, 279–284; c) E. Ahmed, J. Breternitz, M. F. Groh, A. Isaeva, M. Ruck, *Eur. J. Inorg. Chem.* **2014**, 3037–3042.

[4] a) J. R. Li, Z.-L. Xie, X.-W. He, L.-H. Li, X.-Y. Huang, *Angew. Chem. Int. Ed.* **2011**, *50*, 11395–11399; b) W.-W. Xiong, J.-R. Li, B. Hu, B. Tan, R.-F. Li, X.-Y. Huang, *Chem. Sci.* **2012**, *3*, 1200–1204; c) J.-R. Li, W.-W. Xiong, Z.-L. Xie, C.-F. Du, G.-D. Zou, X.-Y. Huang, *Chem. Commun.* **2013**, *49*, 181–183; d) C.-F. Du, J.-R. Li, M.-L. Feng, G.-D. Zou, N.-N. Shen, X.-Y. Huang, *Dalton Trans.* **2015**, *44*, 7364–7372.

[5] J. A. Cody, K. B. Finch, G. J. ReyndersIII, G. C. B. Alexander, H. G. Lim, C. Näther, W. Bensch, *Inorg. Chem.* **2012**, *51*, 13357–13362.

[6] a) A. Banerjee, B. D. Yuhas, E. A. Margulies, Y. Zhang, Y. Shim, M. Wasielewski, M. G. Kanatzidis, *J. Am. Chem. Soc.* **2015**, *137*, 2030–2034; b) I. Chung, M. G. Kanatzidis, *Chem. Mater.* **2014**, *26*, 849–869; c) S. M. Isla, S. Vanishri, H. Li, C. C. Stoumpos, J. A. Peters, M. Sebastian, Z. Liu, S. Wang, A. S. Haynes, J. Im, A. J. Freeman, B. Wessels, M. G. Kanatzidis, *Chem. Mater.* **2015**, *27*, 370–378.

[7] S. V. Kershaw, A. S. Susha, A. L. Rogach, *Chem. Soc. Rev.* **2013**, *42*, 3033–3087.

[8] T. Wu, Q. Zhang, Y. Hou, L. Wang, C. Mao, S.-T. Zheng, X. Bu, P. Feng, *J. Am. Chem. Soc.* **2013**, *135*, 10250–10253.

[9] M. Ruck, F. Locherer, *Coord. Chem. Rev.* **2014**, *285*, 1–10.

[10] a) G. Thiele, T. Krüger, S. Dehnen, *Angew. Chem. Int. Ed.* **2014**, *53*, 4699–4703; b) G. Thiele, S. Lippert, F. Fahrnbauer, P. Bron, O. Oeckler, A. Rahimi-Iman, M. Koch, B. Roling, S. Dehnen, *Chem. Mater.* **2015**, *27*, 4114–4118.

[11] a) L. Fang, J. Im, C. C. Stoumpos, F. Shi, V. David, M. Leroux, A. J. Freeman, W.-K. Kwok, D. Y. Chung, M. G. Kanatzidis, *J. Am. Chem. Soc.* **2015**, *137*, 2311–2317; b) C. D. Morris, H. Li, H. Jin, C. D. Malliakas, J. A. Peters, P. N. Trikalitis, A. J. Freeman, B. W. Wessels, M. G. Kanatzidis, *Chem. Mater.* **2013**, *25*, 3344–3356.

[12] M. A. McGuire, T. J. Scheidemantel, J. V. Badding, F. J. DiSalvo, *Chem. Mater.* **2005**, *17*, 6186–6191.

[13] a) S. Wagner, J. L. Shay, P. Migliorato, H. M. Kasper, *Appl. Phys. Lett.* **1974**, *25*, 434; b) M. G. Panthani, V. Akhavan, B. Goodfellow, J. P. Schmidtke, L. Dunn, A. Dobabalapur, P. F. Barbara, B. A. Korgel, *J. Am. Chem. Soc.* **1998**, *120*, 16770–16777.

[14] P. Bron, S. Johansson, K. Zink, J. Schmedt auf der Günne, S. Dehnen, B. Roling, *J. Am. Chem. Soc.* **2013**, *135*, 15694–15697.

[15] a) Y. Lin, S. Dehnen, *Inorg. Chem.* **2011**, *50*, 7913–7915; b) Y. Lin, W. Massa, S. Dehnen, *J. Am. Chem. Soc.* **2012**, *134*, 4497–4500; c) Y. Lin, W. Massa, S. Dehnen, *Chem. Eur. J.* **2012**, *18*, 13427–13434; d) Y. Lin, D. Xie, W. Massa, L. Mayrhofer, S. Lippert, B. Evers, A. Chernikov, M. Koch, S. Dehnen, *Chem. Eur. J.* **2013**, *19*, 8806–8813; e) S. Santner, S. Dehnen, *Inorg. Chem.*

2015, *54*, 1188–1190; f) C. Donsbach, G. Thiele, L. H. Finger, J. Sundermeyer, S. Dehnen, *Inorg. Chem.* **2016**, *55*, 6725–6730.

[16] a) E. R. Cooper, C. D. Andrews, P. S. Wheatley, P. B. Webb, P. Wormald, R. E. Morris, *Nature* **2004**, *430*, 1012–1016; b) R. E. Morris, *Chem. Commun.* **2009**, 2990–2998; c) R. E. Morris, *Dalton Trans.* **2012**, *41*, 3867–3868.

[17] a) H. D. Rad, R. Hoppe, *Z. Anorg. Allg. Chem.* **1981**, *483*, 18–25; b) G. Thiele, C. Donsbach, R. Riedel, M. Marsch, K. Harms, S. Dehnen, *Dalton Trans.* **2016**, *45*, 5958–5967.

[18] J. Li, Z. Chen, K. C. Lam, S. Mulley, D. M. Proserpio, *Inorg. Chem.* **1997**, *36*, 684–687.

[19] X. Chen, X. Huang, J. Li, *Inorg. Chem.* **2001**, *40*, 1341–1346.

[20] R. C. Burns, J. D. Corbett, *Inorg. Chem.* **1981**, *20*, 4433–4434.

[21] M. Shieh, L.-F. Ho, P.-C. Chen, M.-H. Hsu, H.-L. Chen, Y.-W. Guo, Y.-W. Pan, Y.-C. Lin, *Organometallics* **2007**, *26*, 6184–6196.

[22] a) A. M. Guloy, Z. Tang, R. Ramlau, B. Böhme, M. Baitinger, Y. Grin, *Eur. J. Inorg. Chem.* **2009**, *17*, 2455–2458; b) A. M. Guloy, R. Ramlau, Z. Tang, W. Schnelle, M. Baitlinger, Y. Grin, *Nature* **2006**, *443*, 320–323; c) B. Böhme, S. Hoffmann, M. Baitinger, Y. Grin, *Z. Naturforsch.* **2011**, *66b*, 230–238.

[23] J. Li, Z. Chen, J. L. Kelley, D. M. Proserpio, *Mater. Res. Soc. Symp. Proc.* **1997**, *453*, 29–34.

[24] S. S. Dhingra, C. J. Warren, R. C. Haushalter, A. B. Bocarsly, *Chem. Mater.* **1994**, *6*, 2382–2385.

[25] a) U. Müller, C. Grebe, B. Neumüller, B. Schreiner, K. Dehnicke, *Z. Anorg. Allg. Chem.* **1993**, *619*, 500–506; b) J. M. McConna-chie, M. A. Ansari, J. C. Bollinger, R. J. Salm, J. A. Ibers, *Inorg. Chem.* **1993**, *32*, 3201–3202; c) D. M. Smith, L. C. Roof, M. A. Ansari, J. M. McConnachie, J. C. Bollinger, M. A. Pell, R. J. Salm, J. A. Ibers, *Inorg. Chem.* **1996**, *35*, 4999–5006.

[26] J. C. Bollinger, L. C. Roof, D. M. Smith, J. M. McConnachie, J. A. Ibers, *Inorg. Chem.* **1995**, *34*, 1430–1434.

[27] J. Li, B. G. Rafferty, S. Mulley, D. M. Proserpio, *Inorg. Chem.* **1995**, *34*, 6417–6418.

[28] R. C. Haushalter, *Angew. Chem. Int. Ed. Engl.* **1985**, *24*, 433–435.

[29] K.-W. Kim, M. G. Kanatzidis, *Inorg. Chim. Acta* **1994**, *224*, 163–169.

[30] K. O. Klepp, K. Prager, *Z. Naturforsch.* **1992**, *47b*, 491–496.

[31] H. Sommer, R. Hoppe, *Z. Anorg. Allg. Chem.* **1978**, *443*, 201–211.

[32] M. G. Kanatzidis, Y. Park, *Chem. Mater.* **1990**, *2*, 99–101.

[33] a) E. A. Axtell III, Y. Park, K. Chondroudis, M. G. Kanatzidis, *J. Am. Chem. Soc.* **1998**, *120*, 124–136, b) R. Stromsky, L. W. Zimmermann, I. Hartenbach, Th. Schleid, *Z. Krist.* **2015**, *S35*, 92.

[34] K. O. Klepp, *J. Alloys Compd.* **1992**, *182*, 281–288.

[35] D. E. Bugaris, J. A. Ibers, *Acta Crystallogr., Sect. E* **2008**, *64*, i55-i56.

[36] a) G. M. Sheldrick, *Acta Crystallogr., Sect. A* **2015**, *71*, 3–8; b) G. M. Sheldrick, *Acta Crystallogr., Sect. C* **2015**, *71*, 3–8; c) O. V. Dolomanov, L. J. Bourhis, R. J. Gildea, J. A. K. Howard, H. Puschmann, *J. Appl. Crystallogr.* **2009**, *42*, 339–341.

3.4 Syntheses and properties of selenido mercurates with [HgSe$_2$]$^{2-}$ anions in diverse chemical environments

C. Donsbach, S. Dehnen, *Inorg. Chem. Front.* **2017**, *4*, 336–342.

Abstract: By aminothermal treatment of ternary Cs$_x$Hg$_y$Se$_z$ phases, or of Cs$_2$Se with HgSO$_4$, respectively, in 1,2-diaminoethane (en) and en/water mixtures at 150 °C, four new cesium selenido mercurate compounds Cs$_2$[HgSe$_2$] (**1**), [Cs$_2$(H$_2$O)$_2$][HgSe$_2$] (**2**), Cs[Cs$_3$(H$_2$O)$_{0.5}$][HgSe$_2$](Se$_2$) (**3**) and Cs$_{19}$(Hen)(H$_2$en)(Se$_2$)[HgSe$_2$]$_2$[HgSe$_3$][Hg$_2$Se$_5$]$_2$ (**4**) were synthesized. The precursor phases were prepared by fusion of Cs$_2$Se and HgSe at 600 °C. **2** comprises an unprecedented 1D anionic selenido mercurate substructure. **3** and **4** are rare examples of mercurate compounds with different anions, one of which comprises a new type of a dinuclear chalcogenido mercurate anion. The structures of all four compounds were identified by single crystal X-ray diffraction. Micro X-ray fluorescence spectroscopy (µ-XFS) was used to confirm the heavy atom compositions, and optical absorption measurements were performed to determine the optical band gaps.

Inhalt: Die Kristallstrukturen und aminothermalen Synthese von vier neuen Cäsiumselenidomerkurat-Verbindungen, Cs$_2$[HgSe$_2$] (**1**), [Cs$_2$(H$_2$O)$_2$][HgSe$_2$] (**2**), Cs[Cs$_3$(H$_2$O)$_{0.5}$][HgSe$_2$](Se$_2$) (**3**) und Cs$_{19}$(Hen)(H$_2$en)(Se$_2$)[HgSe$_2$]$_2$[HgSe$_3$][Hg$_2$Se$_5$]$_2$ (**4**), wird präsentiert. Alle Verbindungen wurden mittels Einkristall-Röntgenstrukturanalyse charakterisiert. Außerdem wurden die relativen Verhältnisse der Schwerelemente durch micro-Röntgenfluoreszenz-Spektroskopie (µ-XFS) bestimmt und die optischen Bandlücken mittels UV-Vis-Spektroskopie ermittelt. Die Verbindungen **1** – **3** wurden ausgehend von ternären Mischungen der nominellen Zusammensetzung Cs$_2$Hg$_2$Se$_3$ und Cs$_2$HgSe$_2$, die zuvor in einer Hochtemperatur-Festkörperreaktion aus Cs$_2$Se und HgSe hergestellt wurden, durch solvothermale Reaktion in 1,2-Diaminoethan (en) mit bzw. ohne Zusatz geringer Mengen Wasser bei 150 °C über 3–4 Tage kristallisiert, wobei die Verbindungen **2** und **3** nebeneinander entstehen. Bei der Synthese von Verbindung **4** wurden statt einer ternären Eduktmischung Cs$_2$Se und HgSO$_4$ eingesetzt. Bei Verbindung **2** und **3** handelt es sich um Hydrate. In Verbindung **4** treten neben den Cs$^+$-Kationen auch teilweise protonierte en-Moleküle auf.

Die so erhaltenen Verbindungen weisen eine Reihe unterschiedlicher Anionenstrukturen auf. Besonders bemerkenswert ist das Auftreten zweier Anionenstrukturen der nominellen Zusammensetzung [HgSe$_2$]$^{2-}$ mit unterschiedlichen Topologien, als lineares Molekülanion in Verbindung **1**, **3** und **4** sowie als Strang,

bestehend aus kantenverknüpften [HgSe$_4$]-Bausteinen in **2**, jeweils stabilisiert in unterschiedlichen Umgebungen. Bei Verbindung **3** handelt es sich um ein Doppelsalz der Anionen [HgSe$_2$]$^{2-}$ und (Se$_2$)$^{2-}$, während in Verbindung **4** zusätzlich trigonal-planare [HgSe$_3$]$^{4-}$-Anionen sowie neuartige zweikernige [Hg$_2$Se$_5$]$^{6-}$-Anionen enthalten sind.

Eigener Anteil: Die Synthese der Verbindungen **1 – 4** wurde von mir geplant und unter meiner Anleitung von Matthäus Drabek durchgeführt. Die Analyse der Verbindungen mittels Einkristall-Strukturanalyse und spektroskopischer Methoden (µ-XFS und UV-Vis-Spektroskopie) inklusive Auswertung erfolgte durch mich. Das Manuskript wurde von mir in Zusammenarbeit mit Stefanie Dehnen verfasst.

RESEARCH ARTICLE

Syntheses and properties of selenido mercurates with [HgSe₂]²⁻ anions in diverse chemical environments†

C. Donsbach and S. Dehnen*

By aminothermal treatment of ternary $Cs_xHg_ySe_z$ phases, or of Cs_2Se with $HgSO_4$, respectively, in 1,2-diamino-ethane (*en*) and *en*/water mixtures at 150 °C, four new cesium selenido mercurate compounds $Cs_2[HgSe_2]$ (**1**), $[Cs_2(H_2O)_2][HgSe_2]$ (**2**), $Cs[Cs_3(H_2O)_{0.5}][HgSe_2](Se_2)$ (**3**) and $Cs_{19}(Hen)(H_2en)(Se_2)[HgSe_2]_2[HgSe_3][Hg_2Se_5]_2$ (**4**) were synthesized. The precursor phases were prepared by fusion of Cs_2Se and $HgSe$ at 600 °C. **2** comprises an unprecedented 1D anionic selenido mercurate substructure. **3** and **4** are rare examples of mercurate compounds with different anions, one of which comprises a new type of a dinuclear chalcogenido mercurate anion. The structures of all four compounds were identified by single crystal X-ray diffraction. Micro X-ray fluorescence spectroscopy (μ-XFS) was used to confirm the heavy atom compositions, and optical absorption measurements were performed to determine the optical band gaps.

Introduction

Ternary chalcogenido mercurate phases have been discussed in the recent past as being interesting materials for sensing and in diagnostic applications of hard radiation detection and diagnostics, as these applications require a specific combination of properties.[1] For example, for an efficient interaction with radiation, high atomic numbers are crucial. Furthermore, dark current and electronic noise are only suppressed if the band gap is not too small (≥1.6 eV), and the crystals should exhibit large enough size and hardness. All of these preconditions seem to be achievable in A/Hg/E phases (with A being an alkali(ne earth) metal and E being a chalcogenide), while many other materials have drawbacks at one or the other point.[2]

Due to these intriguing properties, numerous A/Hg/E compounds have been generated in the past two decades, most of them by the Kanatzidis group, who have enormously developed the field of heavy metal–chalcogen compounds in general by applying high-temperature and flux-syntheses. We have recently shown that chalcogenido metalates can be accessed at much lower temperatures under solvothermal or ionothermal reaction conditions.[3] This way, both solvates and solvent-free phases have been observed.[4,5]

Philipps-Universität Marburg, Fachbereich Chemie und Wissenschaftliches Zentrum für Materialwissenschaften, Hans-Meerwein-Straße 4, D-35043 Marburg, Germany.
E-mail: dehnen@chemie.uni-marburg.de
†CCDC 1514745–1514748. For crystallographic data in CIF or other electronic format see DOI: 10.1039/c6qi00481d

In the course of our most recent investigations, we have obtained a series of cesium selenido mercurates by aminothermal extraction of the corresponding parent phases, $Cs_xHg_ySe_z$, with 1,2-diaminoethane (*en*). All of them comprise [HgSe₂]²⁻ units, but their integration in the crystal structure is different for all cases. In this report, we describe and discuss the syntheses, the structural variety and the optical absorption properties, thereby complementing the existing series of Cs/Hg/Se phases.[6–8]

Discussion

Syntheses

General reaction scheme. Compounds **1–3** are accessible *via* aminothermal reactions of ternary $Cs_xHg_ySe_z$ phases in *en* (**1**; *x/y/z* = 2/2/3) or in an *en*/water mixture (40 : 1) (**2**, **3**; *x/y/z* = 2/1/2), maintained at 150 °C for 4 days. The ternary precursor phases are prepared by fusion of Cs_2Se and $HgSe$ at 600 °C in the respective stoichiometric ratio. This way, **1–3** were obtained in 30–50% crystalline yield. The aminothermal reaction of Cs_2Se and $HgSO_4$ in a 2 : 1 ratio in dry *en* yielded **4** in very good yield (approximately 80%), yet along with Cs_2SO_4 as a side product. The formation of further byproducts HgSe and $Cs_2Hg_3Se_4$ is observed in different amounts in each of these reactions. The overall synthetic route is illustrated in Scheme 1. Further details are given in the Experimental section.

Crystal structure description

Crystal structure of $Cs_2[HgSe_2]$ (1). **1** crystallizes in the orthorhombic space group *Pbam* with two formula units per unit

336 | *Inorg. Chem. Front.*, 2017, **4**, 336–342

This journal is © the Partner Organisations 2017
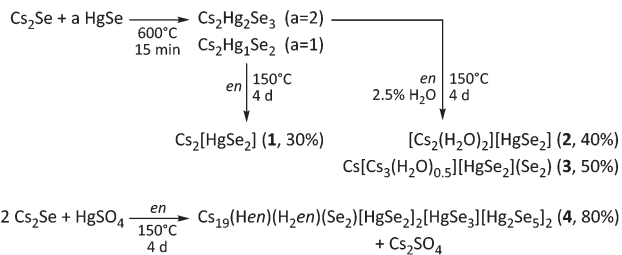
Scheme 1 Overview of the reaction paths in the synthesis of compounds **1–4**.
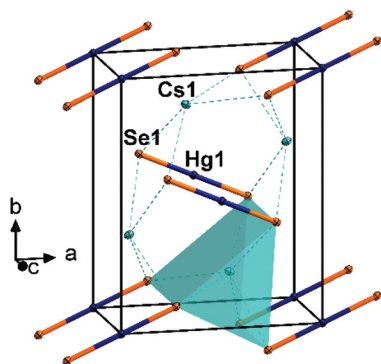
Fig. 1 Fragment of the crystal structure of **1**, viewed approximately along ⟨00$\bar{1}$⟩. The coordination polyhedron of one Cs atom is shown. All atoms are drawn with displacement ellipsoids at the 50% probability level.

Fig. 2 Fragments of the crystal structure of **2**, viewed along ⟨001⟩ (top) and ⟨100⟩ (bottom). The coordination polyhedra around the Hg atoms of the central strand and around one Cs atom are shown. All atoms are drawn with displacement ellipsoids at the 50% probability level.

cell (Fig. 1). It comprises perfectly linear, molecular $[HgSe_2]^{2-}$ anions, whose central Hg atoms are located at the cell corners and in the center of the *ab* plane. The anions are all positioned in the *ab* plane, and they are coplanar but rotated about the *a* axis by 23.8°. The anions appear in two different orientations, which are rotated against each other by 42.3°. The Cs$^+$ cations are located in between the layers of anions. The Hg–Se bond length (2.414(1) Å) is very similar to that found in the analogous $[K(crypt-222)]^+$ salt‡ (2.389(3) Å).[9] Cs atoms are coordinated by six Se atoms in a trigonal prismatic manner (Cs⋯Se 3.6585(7)–3.7205(7) Å), as typical for Cs⋯Se distances (3.489–3.921 Å).[10]

Furthermore, alkali metal chalcogenido mercurates with discrete $[HgE_2]^{2-}$ anions have only been reported as their non-isostructural sulfur analogs, $Na_2[HgS_2]$ and $K_2[HgS_2]$.[11]

Crystal structure of $[Cs_2(H_2O)_2][HgSe_2]$ (2). 2 crystallizes in the orthorhombic space group *Cccm* with four formula units per unit cell (Fig. 2). It exhibits an unprecedented substructure of the chalcogenido mercurate anion, as the $^1_\infty\{[HgSe_2]^{2-}\}$ anions form linear 1D-strands by edge-sharing of $[HgSe_4]$ tetrahedra as the formal subunits. This is significantly different from the molecular $[HgSe_2]^{2-}$ anions found in **1** and in the majority of all compounds with $[HgE_2]^{2-}$ units. Only two

further $^1_\infty\{[HgSe_2]^{2-}\}$ anions, yet with other constitutions, were recently reported for $[K_2(H_2O)][HgSe_2]$ and $Na_2[HgTe_2]$.[4a,12] They consist of chains of corner-sharing, distortedly trigonal planar $[HgE_3]$ subunits that are markedly inclined against each other ($[K_2(H_2O)][HgSe_2]$) or arranged coplanarly ($Na_2[HgTe_2]$), respectively. In **2**, the Hg atoms are coordinated tetrahedrally by four μ-bridging Se atoms, with an Hg–Se bond length of 2.6854(12) Å. This is very close to the value found in $K_2Hg_3Se_4$, which comprises the only comparable situation with μ-bridging Se ligands at a tetrahedral $[HgSe_4]$ unit within a ternary A/Hg/E compound, 2.657(6) Å.[13] In addition, yet ternary anionic substructures $[HgSnSe_4]^{2-}$ that also comprise edge-sharing $[HgSe_4]$ subunits have been reported as their K$^+$ and (DBNH)$^+$ salts.[5,14] § The Hg–Se bond length of 2.687(4) Å found in $K_2[HgSnSe_4]$ is in perfect agreement with the observed bonding situation in **2**.

In the crystal structure of **2**, the collinear anionic strands extend along ⟨001⟩, four along the unit cell edges, and one passing through $\frac{1}{2},\frac{1}{2},0$. This way, non-interacting layers of

‡ crypt-222 = 4,7,13,16,21,24-hexaoxa-1,10-diazabicyclo[8.8.8]hexacosane.

§ DBN = 1,5-diazabicyclo[4.3.0]non-5-ene.

anionic strands are formed in the ac plane (smallest Se···Se distance 5.476(2) Å), separated by the Cs^+ cations, which are located slightly above and below the layers. The Cs^+-shielded layers are further separated in the c direction by crystal water molecules. This results in a coordination of the Cs^+ cations by four water molecules (Cs···O 3.132(11)–3.562(8) Å) and five selenide ligands (Cs···Se 3.656(2)–3.761(1)), and a total coordination number for Cs^+ is nine. The Cs···Se distances are in the typical range (3.489–3.921 Å).[10]

A closer look at the structures of **2** and $[K_2(H_2O)][HgSe_2]$ reveals a notable structure directing effect of crystal water on the structure of alkali metal chalcogenido mercurates of the nominal composition "A_2HgE_2".[12] As crystal water is present in both cases, the aggregation of $[HgSe_2]^{2-}$ to 1D strands seems to be favored in this environment – in contrast to the situation in **1**. In **2**, each of the μ_2-bridging Se^{2-} ligands show coordinative interaction with four Cs^+ cations whereas each of the terminal Se ligands in **1** coordinate to six Cs^+ cations. A similar situation is observed in $[K_2(H_2O)][HgSe_2]$, with each of the μ_2-bridging Se^{2-} ligands coordinating to four K^+ cations, and each of the terminal Se^{2-} ligands coordinating to five K^+ cations. Their coordination spheres are saturated by additional interaction with water molecules. In summary, the cationic framework forms channels that stabilize the 1D anions within.

Crystal structure of $Cs[Cs_3(H_2O)_{0.5}][HgSe_2](Se_2)$ (3). **3** comprises a molecular $[HgSe_2]^{2-}$ unit and a diselenide anion, thus forming a double salt hydrate of $Cs_2[HgSe_2]$ and $Cs_2(Se_2)$. Double salts of this type are quite rare as the only other literature known example of an alkali/alkaline earth metal double salt combining both molecular chalcogenido mercurate and polychalcogenide anions was reported only recently.[15] In $Ba_2[HgS_2](S_3)$, molecular $[HgS_2]^{2-}$ units crystallize along with $(S_3)^{2-}$ anions. Unlike **3**, this compound was obtained from a polysulfide flux reaction, and thus contains no crystal water. The existence of such rare double salts of chalcogenido mercurates co-crystallizing with polychalcogenides has to be considered in the context of a variety of polychalcogenido mercurates that have been reported, such as different salts of $[Hg(E_4)_2]^{2-}$, for example.[16–18] In these compounds, the polychalcogenide anions act as bidentate ligands, coordinating the Hg(II) cations rather than forming discrete anions. It is not clear, however, why the markedly different charge density of Cs^+ versus Ba^{2+} cations does not cause the formation of different structures here.

3 crystallizes in the monoclinic space group $P2_1/n$ with four formula units per unit cell (Fig. 3). The Hg atoms are coordinated by two Se atoms almost linearly (177.31(2)°). A slight deviation from linearity is unusual, since attractive interaction with any neighboring Se atom seems to be absent (nearest Se···Hg distances are above 4.0 Å). However, the nearest Cs···Hg distance is 3.803(1) Å and might therefore induce weak repulsive interactions. The Hg–Se distance of 2.417(1) is in good agreement with the distances in **1** and [K(crypt-222)]$_2$[HgSe$_2$] (see above). The $[HgSe_2]^{2-}$ anions are arranged in two sets of different orientations, approximately along $\langle 111 \rangle$ and $\langle 1\bar{1}1 \rangle$, respectively. The diselenide anions are oriented
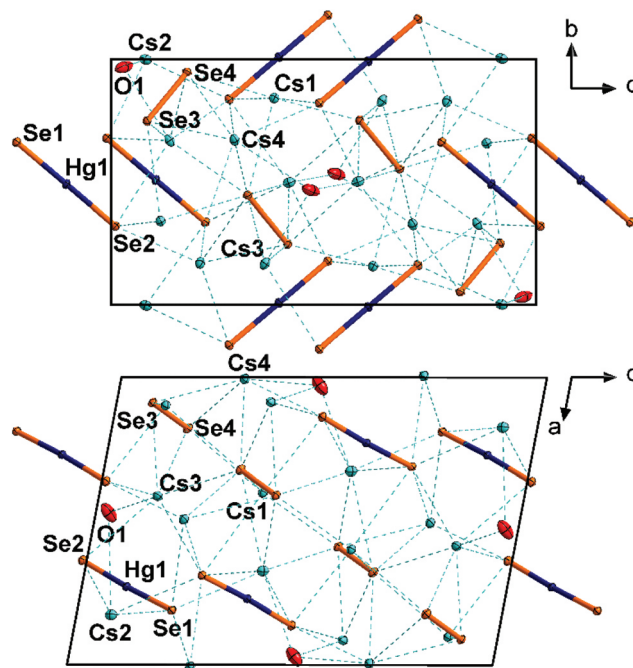
Fig. 3 Fragment of the crystal structure of **3**, viewed along $\langle 100 \rangle$ (top) and $\langle 010 \rangle$ (bottom). All atoms are drawn with displacement ellipsoids at the 50% probability level.

almost collinearly with regard to the mercurate anions. The diselenide Se–Se bond length of 2.387(1) Å is in good agreement with that in known cesium polyselenides such as $Cs_4(Se_2)(Se_3)\cdot en$ (2.394(3)–2.404(3) Å).[19] All cations are separated by Cs^+ cations, which in turn are coordinated by six Se atoms (Cs1, octahedral coordination), seven Se atoms and one additional water molecule (Cs2, irregular coordination), or six Se atoms and 0.5 water molecules (Cs3, Cs4, irregular coordination). The Cs···Se distances (3.443(1)–3.912(1) Å) are as expected.

Crystal structure of $Cs_{19}(Hen)(H_2en)(Se_2)[HgSe_2]_2[HgSe_3][Hg_2Se_5]_2$ (4). **4** crystallizes in the orthorhombic space group $Cmcm$ with four formula units per unit cell (Fig. 4). It comprises four different molecular anions, i.e., three different selenido mercurate anions and one diselenide anion. Besides **3** and $Ba_2[HgS_2](S_3)$,[15] this is another rare example of a salt containing both molecular chalcogenido mercurate and polychalcogenide anions.

The unit cell of **4** contains eight linear $[HgSe_2]^{2-}$ anions with typical structural parameters (Hg–Se 2.419(2)–2.420(2) Å; Se–Hg–Se 179.89(7)°). Furthermore, four slightly distorted, trigonal planar $[HgSe_3]^{4-}$ anions are present in the unit cell (Hg–Se 2.559(2)–2.589(3) Å; Se–Hg–Se 118.32(4)–123.37(7)°). Although the Se–Hg–Se angles vary slightly, these anions are absolutely planar (sum of angles 360.0°). This molecular selenido mercurate anion was recently reported as its potassium salt monohydrate, with similar bond lengths (2.552(2)–2.610(2) Å) but with more notable distortion (Se–Hg–Se 115.03(6)–125.87(6)°, sum of angles 359.97°).[12]

338 | Inorg. Chem. Front., 2017, **4**, 336–342

This journal is © the Partner Organisations 2017

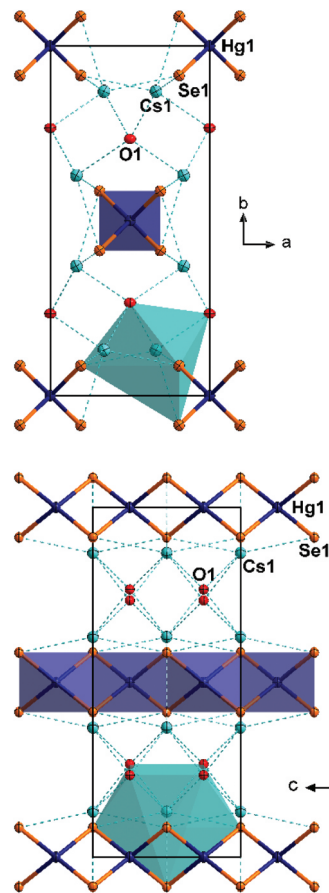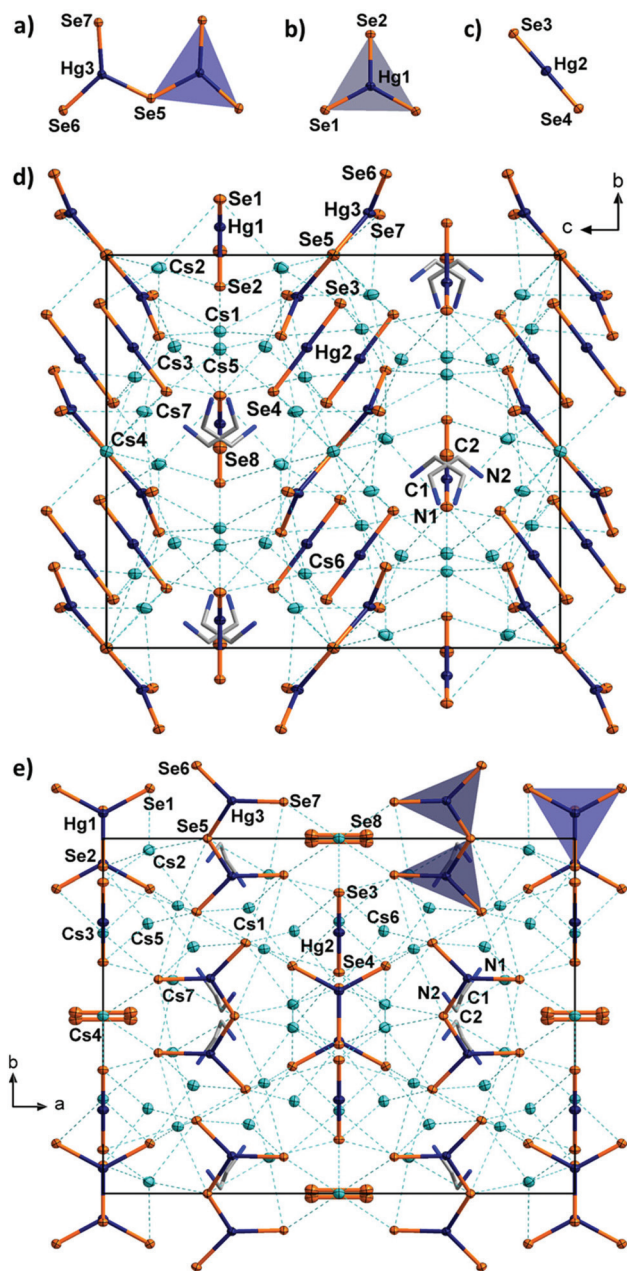**Fig. 4** Molecular selenido mercurate anions in **4**, $[Hg_2Se_5]^{6-}$ (a), $[HgSe_3]^{4-}$ (b), $[HgSe_2]^{2-}$ (c), and fragments of the crystal structure of **4**, viewed along $\langle 100 \rangle$ (d), and $\langle 001 \rangle$ (e), respectively. The coordination environments of one $[HgSe_3]^{4-}$ anion and one $[Hg_2Se_5]^{6-}$ anion are shown as grey and blue triangles, respectively. The Cs, Hg and Se atoms are drawn with displacement ellipsoids at the 50% probability level. Hydrogen atoms are omitted for clarity.

Furthermore, eight symmetry equivalents of an unprecedented third anionic selenido mercurate species, $[Hg_2Se_5]^{6-}$, are observed in the unit cell of **4**. To the best of our knowledge, this dinuclear molecular anion is the first discrete multinuclear chalcogenido mercurate anion without polychalcogenide ligands.[17d,20] The $[Hg_2Se_5]^{6-}$ anion is formed by two trigonal planar $[HgSe_3]$ fragments that are linked *via* a μ_2-bridging Se atom. Hence, it can be formally regarded as being composed

of one of the two other molecular anions, $[HgSe_2]^{2-}$ and $[HgSe_3]^{4-}$, each, which may be the reason for this uncommon co-existence. It can be furthermore considered as a fragment of the anionic 1D-chains that were recently found in $[K_2(H_2O)][HgSe_2]$[12] (but different from the chains observed in **2**). The two $[HgSe_3]$ subunits do not face each other, but are arranged in an almost coplanar manner (dihedral angle 20.04(4)°), which is different from the heavily inclined arrangement in $[K_2(H_2O)][HgSe_2]$ (dihedral angle 77.65(2)°). The Hg–Se distances (2.524(2)–2.542(2) Å for terminal Se ligands, 2.665(1) Å for the μ-bridge) are only slightly longer than those found in $[K_2(H_2O)][HgSe_2]$ (2.510(1) Å for terminal Se ligands, 2.609(1) Å for the μ-bridge). The Se–Hg–Se angles (109.82(4)–129.13(5)°) deviate significantly from ideally 120° (*cf.*, the $[HgSe_3]^{4-}$ anions in **4** and $K_2[K_2(H_2O)][HgSe_3]$) due to the unsymmetrical structure of the $[Hg_2Se_5]^{6-}$ anion.[12] Yet, the $[HgSe_3]$ subunits are still nearly planar (sum of angles around Hg is 359.8°). Besides the three selenido mercurate anions, the complicated crystal structure of **4** further comprises four equivalent diselenide anions per unit cell.

The almost planar $[Hg_2Se_5]^{6-}$ anions and the linear $[HgSe_2]^{2-}$ anions form two sets of non-bonded layers parallel to the *ab* plane (Fig. 4). The anions within each of the sets are oriented approximately parallel to (012) and (01$\bar{2}$), respectively. These layers are intercalated with another set of layers, formed by the planar $[HgSe_3]^{4-}$ anions and the diselenide anions both of which are arranged coplanarly and parallel to (001). All of the diselenide anions are further oriented along $\langle 100 \rangle$. The anions are separated by Cs^+ cations and *en* molecules. The latter are disordered over two positions, which inhibited the localization of protons on the difference fourier map. We assume that three quarters of the amine groups are protonated for charge balance, as further Cs atoms were not observed. Proton transfer and even more complex degradation of *en* are not untypical for reactions involving chalcogenidometalates in *en*. For this, it is most likely that the protons originate from the solvent itself.[21] The Cs^+ cations are situated in different coordination polyhedra, with Cs···Se distances of 3.481(2)–4.030(1) Å, and with coordination numbers five (Cs1, Cs3, Cs5, Cs7) in distorted square pyramids or six (Cs2, Cs4, Cs6) in octahedral coordination, respectively.

Optical absorption properties. UV-visible absorption measurements were performed on single-crystalline samples of compounds **1**–**4** to determine their optical bandgaps. The results (Fig. 5) are in good agreement with the visible color of the compounds, and reflect well the dimensionality of their respective anionic substructure and polyselenide content. **1**, which contains exclusively molecular ("0D") $[HgSe_2]^{2-}$ anions, exhibits the largest bandgap of the four compounds (3.0 eV). Upon increasing the dimensionality of the anionic substructure to 1D, the bandgap decreases slightly to 2.4 eV in **2**, in spite of the presence of one equivalent of crystal water. As reported by the Kanatzidis group, the bandgap is further reduced in the Cs/Hg/Se series upon further increase in dimensionality (2D-$Cs_2[Hg_3Se_4]$: 2.1 eV; 3D-$Cs_2[Hg_6Se_7]$: 1.17 eV),[1,7] continuously approximating the (negative) value for

This journal is © the Partner Organisations 2017

Inorg. Chem. Front., 2017, **4**, 336–342 | **339**
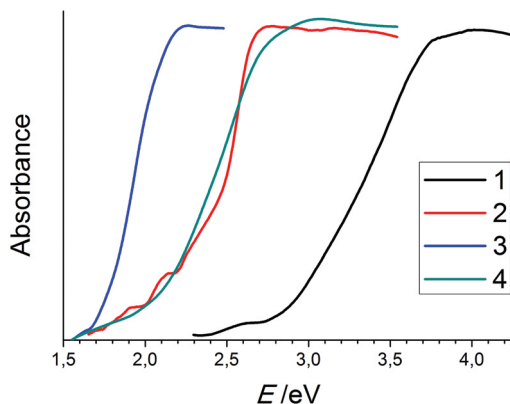
Fig. 5 UV-Visible spectra of compounds **1–4**. The following E_{onset} values were determined by means of the tangent method: 2.9 eV (**1**); 2.4 eV (**2**); 1.7 eV (**3**); 2.1 eV (**4**). Note that the onset of absorption for compound **2** is intrinsically red-shifted due to the beginning of decomposition of the very sensitive compound during sample preparation; for this, only the sharply ascending part of the curve was used to determine the optical gap.

binary HgSe (-0.15 eV).[22] Notably, the bandgap determined for **1** with a molecular $Cs_2[HgSe_2]$ structure is notably smaller than that predicted for a selenido mercurate $Cs_2[HgSe_2]$ with a 1D anionic substructure.[1] Additionally, we also found a significantly smaller bandgap for the 1D analog **2**, although its structure is "diluted" by crystal water.

Considering the incorporation of diselenide anions into a selenido mercurate structure, we observed bandgap narrowing with the increasing diselenide ratio. The bandgap of 2.1 eV in **4** is smaller than that in **1** and even **2**, though it only comprises selenido mercurate anions of the lowest dimensionality. Yet, the incorporation of a diselenide anion results in a significantly lower bandgap. This effect is even more distinct in the case of **3** (1.7 eV), where one 0D mercurate ion is combined with one diselenide ion.

Experimental

General

All manipulations were performed under strict exclusion of air and moisture (unless stated otherwise) using standard Schlenk and glovebox techniques. *En* was dried over CaH_2 and distilled prior to use. Water was degassed three times at 1×10^{-3} mbar, and subsequently saturated with Ar. Cs_2Se was synthesized from the elements in liquid ammonia and HgSe by fusion of the elements in a silica glass ampoule using an oxygen–methane torch. Pure samples of **1–4** suitable for different analyses were prepared by manual selection of the crystals from the raw products due to the presence of side-products. This is not uncommon for solvothermal methods, which represent a certain limitation and drawback of the solvothermal approach.

Synthesis of $Cs_2[HgSe_2]$ (1)

A solid phase with the nominal composition "$Cs_2Hg_2Se_3$" was prepared by fusion of Cs_2Se and HgSe in a 1 : 2 ratio in a silica

glass ampoule with an oxygen–methane torch at about 600 °C, and the resulting solid was pestled after cooling to room temperature. 0.7 g of the raw phase and 2 mL of *en* were placed in a glass vial inside the PTFE inlay (inner volume 15 mL) of a steel autoclave. The autoclave was closed tightly and heated to 150 °C for 4 days before slowly cooling to room temperature over 1 day. **1** crystallizes as light yellow crystals in approximately 30% yield besides small amounts of microcrystalline $Cs_2[Hg_3Se_4]$, HgSe and unidentified amorphous by-products.

Synthesis of $[Cs_2(H_2O)_2][HgSe_2]$ (2) and $Cs[Cs_3(H_2O)_{0.5}][HgSe_2](Se_2)$ (3)

Compounds **2** and **3** were obtained during the same reaction. The synthetic procedure is similar to that applied for the synthesis of **1**. A precursor phase of the nominal composition "$Cs_2Hg_1Se_2$" was prepared from Cs_2Se and HgSe in a 1 : 1 ratio *via* fusion. 0.7 g of the raw phase and 2 mL of *en*, containing 2.5 vol% of water (0.05 mL), were used in the solvothermal reaction. **2** crystallizes as light yellow sticks alongside dark red blocks of **3** in crystalline yields of approximately 40% and 50%, respectively. Small amounts of amorphous by-products are observed.

Synthesis of $Cs_{19}(Hen)(H_2en)(Se_2)[HgSe_2]_2[HgSe_3][Hg_2Se_5]_2$ (4)

For the synthesis of **4**, 400 mg of Cs_2Se (1.16 mmol, 2 eq.), 172 mg of $HgSO_4$ (0.58 mmol, 1 eq.), and 2 mL of *en* were placed in an autoclave and heated to 150 °C for 3 days before cooling to room temperature over 1 day. **4** crystallizes as yellow blocks in approximately 80% yield alongside Cs_2SO_4 and small amounts of microcrystalline $Cs_2[Hg_3Se_4]$, HgSe and unidentified amorphous by-products.

Elemental analyses

The heavy atom composition of compounds **1–4** was determined by means of micro X-ray fluorescence spectroscopy (μ-XFS), using a Bruker M4 Tornado with a Rh target X-ray tube and a Si drift detector. Fluorescence photons emitted by the sample were detected during an acquisition time of 120 s, followed by deconvolution of the spectra. The elements were then quantified based on the Se–K, Cs–L and Hg–L radiation. The results are shown in Table 1.

Single crystal X-ray diffraction studies

Single crystals for X-ray diffraction analyses were selected under paratone oil using a standard light microscope. Suitable crystals were analyzed on a STOE IPDS-2T (**1–3**) or IPDS-II (**4**) diffractometer, respectively, at 100 K using Mo-Kα radiation

Table 1 Results of the μ-XFS analyses of compounds **1–4**

Element	Atom% [calc.] in **1**	Atom% [calc.] in **2**	Atom% [calc.] in **3**	Atom% [calc.] in **4**
Cs	40.4(2) [40.0]	39.4(3) [40.0]	43.7(3) [44.4]	43.0(3) [42.2]
Hg	19.1(1) [20.0]	20.5(1) [20.0]	10.9(1) [11.1]	14.9(1) [15.6]
Se	40.5(1) [40.0]	40.2(3) [40.0]	45.4(2) [44.4]	42.2(2) [42.2]

340 | *Inorg. Chem. Front.*, 2017, **4**, 336–342

This journal is © the Partner Organisations 2017

Table 2 Crystallographic data of **1–4**

Compound	1	2	3	4
CCDC	1514747	1514745	1514746	1514748
Empirical formula	$Cs_2Hg_1Se_2$	$Cs_2H_4Hg_1O_2Se_2$	$Cs_4H_1Hg_1O_{0.5}Se_4$	$C_4H_{19}Cs_{19}Hg_7N_4Se_{19}$
Formula weight/g mol^{-1}	624.33	660.36	1057.08	5552.89
Crystal color and shape	Yellow needle	Yellow needle	Dark red block	Yellow block
Crystal size/mm^3	$0.02 \times 0.03 \times 0.30$	$0.02 \times 0.03 \times 0.28$	$0.04 \times 0.04 \times 0.05$	$0.08 \times 0.09 \times 0.10$
Crystal system	Orthorhombic	Orthorhombic	Monoclinic	Orthorhombic
Space group	*Pbam*	*Cccm*	*P2$_1$/n*	*Cmcm*
a/Å	8.1848(7)	7.5853(8)	10.7624(5)	22.7375(9)
b/Å	10.3302(6)	16.7226(14)	8.8940(3)	17.1603(6)
c/Å	4.7112(3)	7.0333(6)	15.6140(7)	19.7854(5)
β/°	—	—	100.637(3)	—
V/Å^3	398.34(5)	892.15(4)	1468.90(11)	7719.9(5)
Z	2	4	4	4
$\rho_{calc.}$/g cm^{-3}	5.21	4.89	4.78	4.78
$\mu(Mo_{K\alpha})$/mm^{-1}	37.3	33.4	30.1	31.7
Min/max transmission	0.0210/0.5636	0.0304/0.5927	0.3291/0.4951	0.0929/0.1449
θ range/°	3.175–31.771	2.436–26.986	2.127–29.075	1.487–27.144
No. measured refl.	3653	1661	15 391	14 727
No. independent refl.	743	532	3917	4504
R(int)	0.0521	0.1042	0.0440	0.0562
No. indep. refl. ($I > 2\sigma(I)$)	685	479	3018	3129
No. of parameters	17	22	92	158
R_1 ($I > 2\sigma(I)$)	0.0334	0.0564	0.0195	0.0418
wR_2 (all data)	0.0800	0.1448	0.0255	0.1023
S (all data)	1.122	1.076	0.848	0.901
$\Delta\rho_{max}$, $\Delta\rho_{min}$/e Å^{-3}	2.313/−3.267	3.057/−4.479	0.894/−0.861	3.485/−3.293

and a graphite monochromator (λ = 0.71073 Å). Numerical absorption corrections were applied (STOE X-AREA) and the structures were solved *via* direct methods, followed by full-matrix-least-squares refinement against F^2, using SHELXT15, SHELXL15 and the OLEX2 software platform.[23] The crystallographic data of **1–4** are summarized in Table 2.

Optical absorption spectroscopy

UV-visible absorption spectroscopy was performed by analyses of the diffuse reflection of powdered samples. The measurements were carried out using a Varian Cary 5000 dual-beam spectrometer with a Praying Mantis sample holder from Harrick.

Conclusions

In summary, we presented four new cesium selenido mercurate compounds synthesized *via* aminothermal syntheses in 1,2-diaminoethane (*en*). These comprise unprecedented selenido mercurate anionic substructures (**2**, **4**) and the molecular $[HgSe_2]^{2-}$ anion (**1**), which have not been reported in the solid phase without sequestering agents so far. The bandgaps determined for these low-dimensional cesium selenido mercurates match the theory of the influence of dimensionality reduction, thus complementing and supporting the observations made for another set of chalcogenido mercurates of larger dimensionality. Besides, the influence of water on the ability of cesium cations to stabilize anionic substructures of different dimensionalities was investigated. Owing to their good crystal quality, the compounds may be interesting regarding their potential use in sensing or detection of hard radiation.

Notes and references

1 J. Androulakis, S. C. Peter, H. Li, C. D. Malliakas, J. A. Peters, Z. Liu, B. W. Wessels, J.-H. Song, H. Jin, A. J. Freeman and M. G. Kanatzidis, *Adv. Mater.*, 2011, **23**, 4163.

2 (*a*) B. D. Milbrath, A. J. Peurrung, M. Bliss and W. J. Weber, *J. Mater. Res.*, 2008, **23**, 2561; (*b*) D. S. McGregor and H. Hermon, *Nucl. Instrum. Methods Phys. Res., Sect. A*, 1997, **395**, 101; (*c*) A. Owens, *J. Synchrotron Radiat.*, 2006, **13**, 143; (*d*) T. E. Schlesinger, J. E. Toney, H. Yoon, E. Y. Lee, B. A. Brunett, L. Franks and R. B. James, *Mater. Sci. Eng.*, 2001, **32**, 103.

3 (*a*) S. Santner, J. Heine and S. Dehnen, *Angew. Chem., Int. Ed.*, 2016, **54**, 876; (*b*) J. Heine and S. Dehnen, *Z. Anorg. Allg. Chem.*, 2012, **638**, 2425; (*c*) S. Dehnen and M. Mellulis, *Coord. Chem. Rev.*, 2007, **251**, 1259.

4 (*a*) C. Donsbach and S. Dehnen, *Z. Anorg. Allg. Chem.*, 2016, DOI: 10.1002/zaac.201600338; (*b*) C. Donsbach, G. Thiele,

L. H. Finger, J. Sundermeyer and S. Dehnen, *Inorg. Chem.*, 2016, **55**, 6725; (*c*) G. Thiele, S. Lippert, F. Fahrnbauer, P. Bron, O. Oeckler, A. Rahimi-Imam, M. Koch, B. Roling and S. Dehnen, *Chem. Mater.*, 2015, **27**, 4114; (*d*) E. Ruzin, A. Fuchs and S. Dehnen, *Chem. Commun.*, 2006, 4796; (*e*) C. Zimmermann and S. Dehnen, *Z. Anorg. Allg. Chem.*, 2003, **125**, 6618.

5 M. K. Brandmayer, R. Clérac, F. Weigend and S. Dehnen, *Chem. – Eur. J.*, 2004, **10**, 5147.

6 M. G. Kanatzidis, *Chem. Mater.*, 1990, **2**, 353.

7 E. A. Axtell III, Y. Park, K. Chondroudis and M. G. Kanatzidis, *J. Am. Chem. Soc.*, 1998, **120**, 124.

8 R. Stromsky, L. W. Zimmermann, I. Hartenbach and T. Schleid, *Z. Kristallogr.*, 2015, **35**, 92.

9 C.-W. Park, D. M. Smith, M. A. Pell and J. A. Ibers, *Inorg. Chem.*, 1997, **36**, 942.

10 (*a*) H. Sommer and R. Hoppe, *Z. Anorg. Allg. Chem.*, 1977, **429**, 118; (*b*) P. Böttcher, *J. Less-Common Met.*, 1980, **76**, 271.

11 K. O. Klepp and K. Prager, *Z. Naturforsch., B: Chem. Sci.*, 1992, **47**, 491.

12 G. Thiele, C. Donsbach, R. Riedel, M. Marsch, K. Harms and S. Dehnen, *Dalton Trans.*, 2016, **45**, 5958.

13 M. G. Kanatzidis and Y. Park, *Chem. Mater.*, 1990, **2**, 99.

14 W.-W. Xiong, P.-T. Li, T.-H. Zhou, Y. Zhao, R. Xu and Q. Zhang, *J. Solid State Chem.*, 2013, **204**, 86.

15 S. M. Islam, J. Im, A. J. Freeman and M. G. Kanatzidis, *Inorg. Chem.*, 2014, **53**, 4698.

16 (*a*) A. Müller, J. Schimanski, U. Schimanski and H. Bogge, *Z. Naturforsch., B: Anorg. Chem. Org. Chem.*, 1985, **40**, 1277; (*b*) T. D. Bailey, R. M. H. Banda, D. C. Craig, I. G. Dance, I. N. L. Ma and M. L. Scudder, *Inorg. Chem.*, 1991, **30**, 187.

17 (*a*) J. Adel, F. Weller and K. Dehnicke, *Z. Naturforsch., B: Chem. Sci.*, 1988, **43**, 1094; (*b*) G. Krauter, F. Weller and K. Dehnicke, *Z. Naturforsch., B: Chem. Sci.*, 1989, **44**, 444; (*c*) R. M. H. Banda, J. Cusick, M. L. Scudder, D. C. Craig and I. G. Dance, *Polyhedron*, 1989, **8**, 1995; (*d*) S. Magull, B. Neumüller and K. Dehnicke, *Z. Naturforsch., B: Chem. Sci.*, 1991, **46**, 985; (*e*) B. Neumüller, M.-L. Ha-Eierdanz, U. Müller, S. Magull, G. Krauter and K. Dehnicke, *Z. Anorg. Allg. Chem.*, 1992, **609**, 12; (*f*) A. Ahle, K. Dehnicke, K. Maczek and D. Fenske, *Z. Anorg. Allg. Chem.*, 1993, **619**, 1699; (*g*) P. J. Barrie, R. J. H. Clark, R. Withnall, D.-Y. Chung, K.-W. Kim and M. G. Kanatzidis, *Inorg. Chem.*, 1994, **33**, 1212; (*h*) J. C. Bollinger and J. A. Ibers, *Inorg. Chem.*, 1995, **34**, 1859; (*i*) C.-W. Park, D. M. Smith, M. A. Pell and J. A. Ibers, *Inorg. Chem.*, 1997, **36**, 942.

18 J. C. Bollinger, L. C. Roof, D. M. Smith, J. M. McConnachie and J. A. Ibers, *Inorg. Chem.*, 1995, **34**, 1430.

19 G. Thiele, L. Vondung, C. Donsbach, S. Pulz and S. Dehnen, *Z. Kristallogr.*, 2014, **640**, 2684.

20 (*a*) J. Li, B. G. Rafferty, S. Mulley and D. M. Proserpio, *Inorg. Chem.*, 1995, **34**, 6417; (*b*) R. C. Haushalter, *Angew. Chem., Int. Ed. Engl.*, 1985, **24**, 433.

21 (*a*) G. Thiele, T. Krüger and S. Dehnen, *Angew. Chem., Int. Ed.*, 2014, **53**, 4699–4703; (*b*) G. Thiele, Y. Franzke, F. Weigend and S. Dehnen, *Angew. Chem., Int. Ed.*, 2015, **54**, 11283–11288; (*c*) G. Thiele, L. Vondung and S. Dehnen, *Z. Anorg. Allg. Chem.*, 2015, **641**, 247.

22 J. I. Pankove, in *Optical Processes in Semiconductors*, Dover Publication, New York, 1975.

23 (*a*) G. M. Sheldrick, *Acta Crystallogr., Sect. A: Fundam. Crystallogr.*, 2015, **71**, 3; (*b*) G. M. Sheldrick, *Acta Crystallogr., Sect. C: Cryst. Struct. Commun.*, 2015, **71**, 3; (*c*) O. V. Dolomanov, L. J. Bourhis, R. J. Gildea, J. A. K. Howard and H. Puschmann, *J. Appl. Crystallogr.*, 2009, **42**, 339.
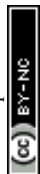
342 | *Inorg. Chem. Front.*, 2017, **4**, 336–342

This journal is © the Partner Organisations 2017

3.5 $[Hg_4Te_8(Te_2)_4]^{8-}$: A Heavy Metal Porphyrinoid Embedded in a Lamellar Structure

C. Donsbach, K. Reiter, D. Sundholm, F. Weigend, S. Dehnen, *Angew. Chem. Int. Ed.* **2018**, *57*, DOI: 10.1002/anie.201803233, *im Druck.*

$[Hg_4Te_8(Te_2)_4]^{8-}$: ein Schwermetall-Porphyrinoid in einer lamellaren Struktur

C. Donsbach, K. Reiter, D. Sundholm, F. Weigend, S. Dehnen, *Angew. Chem.* **2018**, *129*, DOI: 10.1002/ange.201803233, *im Druck.*

Abstract: The use of ionic liquids $(C_nC_1Im)[BF_4]$ with long alkyl chains (n=10, 12) in the ionothermal treatment of $Na_2[HgTe_2]$ led to lamellar crystal structures with molecular Makrocyclic anions $[Hg_8Te_{16}]^{8-}$ (**1**), the heaviest known topological relative of porphyrin. $[Hg_8Te_{16}]^{8-}$ differs from porphyrin by the absence of an electronic π-system, which prevents a "global" aromaticity. Quantum chemical studies reveal instead small ring currents in the pyrrole-type five-membered rings that indicate weak local (σ) aromaticity. As a result of their lamellar nature, the compounds are promising candidates for the formation of sheets containing chalcogenidometalate anions.

Inhalt: Die Kristallstruktur und ionothermale Synthese eines Telluridomerkurat-Salzes mit einer Porphyrin-artigen Anionenstruktur $[Hg_4Te_8(Te_2)_4]^{8-}$ (**1**) wird vorgestellt. Die Verbindung wurde mittels Einkristall-Röntgenstrukturanalyse charakterisiert und das relative Verhältnis der Schwerelemente sowie die optische Bandlücke durch micro-Röntgenfluoreszenz-Spektroskopie (μ-XFS) bzw. UV-Vis-Spektroskopie bestimmt. Außerdem wurden quantenchemische Methoden angewendet, um die optische Bandlücke zu verifizieren, Ringströme im cyclischen Anion zu ermitteln und die Struktur möglicher Übergangsmetallkomplexe mit Anion **1** als Ligand vorherzusagen. Das Anion **1** wurde als $(C_{10}C_1Im)^+$-Salz ($C_{10}C_1Im$ = 1-Decyl-3-Methylimidazolium) durch ionothermale Umsetzung des ternären Telluridomerkurats $Na_2[HgTe_2]$ in einer evakuierten und abgeschmolzenen Glasampulle in der ionischen Flüssigkeit $C_{10}C_1Im[BF_4]$ bei 80 °C über 12 Stunden erhalten. Das analoge $(C_{12}C_1Im)^+$-Salz ($C_{12}C_1Im$ = 1-Dodecyl-3-Methylimidazolium) konnte auf die gleiche Weise erhalten werden. Allerdings waren die Kristalle von $(C_{12}C_1Im)_8[Hg_4Te_8(Te_2)_4]$ von derart unzureichender Qualität, dass nur ein Strukturmodell entwickelt werden konnte, welches jedoch die Zusammensetzung des Salzes bestätigt.

Das Grundgerüst des Anions **1** weist durch die makrocyclische Anordnung von vier μ-Te-verbrückten [Hg(Te$_2$)Te$_2$]-Fünfringen ein zum organischen Porphyrin-Molekül sowie zu den zu **1** valenzisoelektronischen Bordichalkogeniden BS$_2$ und BSe$_2$ analoges Grundgerüst auf. Im Kristall wird die hohe Ladung des Anions durch langkettige Alkylimidazolium-Kationen kompensiert, deren Anordnung um **1** eine Separation von polaren, ionischen Bereichen und unpolaren Bereichen mit einer regelmäßigen, untereinander verzahnten Anordnung der Alkylketten bewirkt. Auf diese Weise entsteht eine lamellare Struktur.

Quantenchemische Rechnungen zeigen vernachlässigbare Ringströme innerhalb des Makrocyclus, aber dennoch signifikante lokale Ringströme innerhalb der [Hg(Te)$_2$Te$_2$]-Fünfringe. Die mit quantenchemischen Methoden bestimmten Strukturen hypothetischer Übergangmetallkomplexe zeigen eine hohe Flexibilität des Anions **1** als Ligand, die zu starken Verformungen und partieller Umordnung von Atomen innerhalb des Makrocyclus führen (siehe Appendix).

Eigener Anteil: Die Synthese der beschriebenen Salze des Anions **1** wurde von mir geplant und durchgeführt. Die Analyse der Verbindungen mittels Einkristall-Strukturanalyse und micro-Röntgenfluoreszenz-Spektroskopie (μ-XFS) inklusive Auswertung erfolgte ebenfals durch mich. Das optische Absorptionsspektrum wurde von Niklas Rinn, André Rinn und Jurek Lange gemessen. Alle quantenchemischen Rechnungen wurden von Kevin Reiter, Florian Weigend und Dage Sundholm durchgeführt und von diesen in Zusammenarbeit mit Stefanie Dehnen ausgewertet. Das Manuskript wurde von mir in Kooperation mit Stefanie Dehnen verfasst und von den weiteren Co-Autoren um kurze Abschnitte zu ihren Beiträgen ergänzt und überarbeitet.

Im Folgenden wird die englischsprachige Version der Publikation gezeigt (C. Donsbach, K. Reiter, D. Sundholm, F. Weigend, S. Dehnen, *Angew. Chem. Int. Ed.* **2018**, *57,* DOI: 10.1002/anie.201803233).

Die deutschsprachige Version (C. Donsbach, K. Reiter, D. Sundholm, F. Weigend, S. Dehnen, *Angew. Chem.* **2018**, *129*, DOI: 10.1002/ange.201803233*)* ist im Appendix (6.2) zu finden.

Inorganic Macrocycles

$[Hg_4Te_8(Te_2)_4]^{8-}$: A Heavy Metal Porphyrinoid Embedded in a Lamellar Structure

Carsten Donsbach, Kevin Reiter, Dage Sundholm, Florian Weigend, and Stefanie Dehnen*

Dedicated to Professor Bernt Krebs on the occasion of his 80th birthday

Abstract: *The use of ionic liquids $(C_nC_1Im)[BF_4]$ with long alkyl chains $(n = 10, 12)$ in the ionothermal treatment of $Na_2[HgTe_2]$ led to lamellar crystal structures with molecular macrocyclic anions $[Hg_8Te_{16}]^{8-}$ (**1**), the heaviest known topological relative of porphyrin. $[Hg_8Te_{16}]^{8-}$ differs from porphyrin by the absence of an electronic π-system, which prevents a "global" aromaticity. Quantum chemical studies reveal instead small ring currents in the pyrrole-type five-membered rings that indicate weak local (σ) aromaticity. As a result of their lamellar nature, the compounds are promising candidates for the formation of sheets containing chalcogenidometalate anions.*

Dimensional reduction of semiconductor materials is currently being actively pursued to control and tune their electronic properties.[1] In this context, post-synthetic methods beyond the formation of nanoparticles, such as stamping or exfoliation techniques, have picked up pace.[2] Preconditions for such methods are twofold: a) the presence of suitable semiconductor substructures and b) relatively weak interactions within these substructures in the parent compound. Both are fulfilled in layered elements such as graphite and phosphorous,[3,4] some binary chalcogenides,[5] and various inorganic-organic hybrid salts.[6]

Semiconductor nanostructures are also found in heavy-metal chalcogenidometalates, which exhibit a large variety of elemental combinations and architectures. High-temperature reactions usually lead to compact structures, whereas solution-based routes afford more-open frameworks with solvated or organic cations. The anionic substructures may comprise lower dimensionalities, down to molecular chalcogenidometalate units.[7]

An elegant way to transform semiconductor-based solids into hybrid compounds with weakly interacting organic cations is achieved by the ionothermal treatment of inorganic chalcogenidometalate salts.[8] The resulting substructures can be as unusual as the $[Cu_5Ga_{30}S_{52}(SH)_2(C_4C_1im)_2]^{11-}$ cluster $(C_4C_1im = 1\text{-butyl-3-methylimidazolyl})$[9] or the 0D-$[Ge_{24}Sn_{32}Se_{132}]^{24-}$ supersphere,[10] the formation of which largely depends on the chosen temperatures, the use of further auxiliaries, and the nature of the ionic liquid.[11]

One variable parameter is the chain lengths of the alkyl substituents on the $(C_nC_1Im)^+$ cations in imidazolium-based ionic liquids. For $n = 1–4$, the cations behave similarly to spherical ones, hence their structure-directing effect does not generally differ from the variation of the ionic radii of the atomic cations. By contrast, longer alkyl chains cause the ionic liquid cations to assemble, for example, into herring-bone or lamellar structures.[12]

In the course of our studies on dimensional reduction of heavy-metal chalcogenidometalates, we are currently focusing on substructures formally derived from the II-VI semiconductor material HgTe.[13] Ionothermal treatment of $Na_2[HgTe_2]$, which is based on one-dimensional $[\text{-Hg(Te)-Te-}]_n$ chains,[14] in the short-chain ionic liquid $(C_4C_1Im)[BF_4]$ $(C_4C_1Im = 1\text{-butyl-3-methylimidazolium})$ at 60°C yielded a salt of another one-dimensional substructure, $[\text{-Hg(}\mu\text{-Te)-}(\mu\text{-Te}_2)Hg\text{-Te-}]_n$. Here, $[Hg_2Te(Te_2)]$ five-membered rings with Te^{2-} and $(Te_2)^{2-}$ ligands (upon partial oxidation of Te^{2-}) are linked through further $\mu\text{-Te}^{2-}$ bridges (Scheme 1, left). However, the use of 1-(do)decyl-3-methylimidazolium ionic liquids $(C_nC_1Im)[BF_4]$ $(n = 10, 12)$ affords salts of the unprecedented molecular anion $[Hg_8Te_{16}]^{8-}$ (**1**; Scheme 1, right) within a lamellar structure.

[*] C. Donsbach, Prof. Dr. S. Dehnen
Fachbereich Chemie and Wissenschaftliches Zentrum für Materialwissenschaften (WZMW), Philipps-Universität Marburg
Hans-Meerwein-Strasse 4, 35043 Marburg (Germany)
E-mail: dehnen@chemie.uni-marburg.de

K. Reiter, Priv.-Doz. Dr. F. Weigend
Institute of Nanotechnology
Karlsruhe Institute of Technology (KIT)
Hermann-von-Helmholtz-Platz 1
76344 Eggenstein-Leopoldshafen (Germany)

Prof. Dr. D. Sundholm
Department of Chemistry, University of Helsinki
P. O. Box 55 (A.I. Virtanens plats 1), 00014 Helsinki (Finland)

Supporting information (syntheses, single-crystal X-ray diffraction including CIF, spectroscopy, and quantum chemical studies) and the ORCID identification number for some of the authors of this article can be found under: https://doi.org/10.1002/anie.201803233.
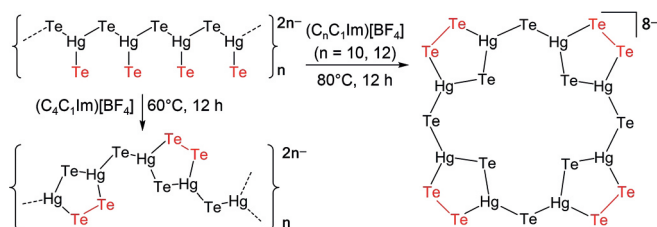
Scheme 1. Diagram of the strand-like anion in $Na_2[HgTe_2]$ (top left)[14] and its treatment in ionic liquids $(C_nC_1Im)[BF_4]$, which yields another strand-like anion in the presence of short-chain alkyl imidazolium cations $(n = 4$, bottom left),[14] or the molecular anion $[Hg_8Te_{16}]^{8-}$ (**1**) in ionic liquids with long-chain alkyl imidazolium cations $(n = 10, 12;$ this work).

These are not the final page numbers! ↗↗

$(C_{10}C_1Im)_8\mathbf{1}$ crystallizes as thin, dark-red plates in the monoclinic space group $P2_1/c$, with four formula units per unit cell. The heavy-element composition of the single-crystalline compound was confirmed by means of micro-X-ray fluorescence spectroscopy (μ-XFS; see Table S11 and Figure S5 in the Supporting Information). Bulk analyses were inhibited by the fine dispersion of the small crystals in the highly viscose ionic liquid, which complicates their isolation. As a consequence of the high anionic charge, the compound is not soluble in common solvents, thus preventing analytical data from being obtained in solution.

The inorganic macrocycle in **1** is built from four of the above-described $[Hg_2Te(Te_2)]$ five-membered rings, which are bridged by four Te^{2-} ligands to form a cyclic tetramer. Hence, the anion **1** is structurally related to organic porphyrins composed of four methylene-bridged pyrrole rings, although the total valence-electron count differs (120 in **1** versus 114 in porphyrin). **1** is thus isoelectronic to the $[B_8E_{16}]$ structures of BE_2 (E = S, Se),[15] but with the difference of being charged and deviating notably from planarity. Figure 1 illustrates the crystal structure of $(C_{10}C_1Im)_8\mathbf{1}$.

Te-bridged $[Hg_2Te(Te_2)]$ motifs have been aligned in one-dimensional chains, as found in the above-mentioned $(C_4C_1Im)^+$ salt,[14] and with $[N(C_2H_5)_4]^+$, $\{[Mn(en)_3]_2Cl_2\}^{2+}$, or $[M(trien)(N_2H_4)]^{2+}$ (M = Mn, Zn; trien = triethylenetetr-

amine) counterions[16a–c] as well as with bridging Te_2^{2-} ligands.[16d] They have also been observed in molecular clusters: in $[Hg_4Te_{12}]^{4-}$,[16c,d] two (folded) $[Hg_2Te(Te_2)]$ rings and two additional $(Te_3)^{2-}$ ligands are linked, and a similar motif is found in the chain-like arrangement of $\{[Hg_5Te_{12}]^{2-}\}_n$, in which the clusters comprising two (folded) $[Hg_2Te(Te_2)]$ rings are bridged by $[HgTe_2(Te_3)]$ units.[16d] However, a cyclic oligomer as found in **1** has not previously been reported. We ascribe the preference of $[Hg_8Te_{16}]^{8-}$ macrocycles over chain-like 1D-$\{[Hg_2Te_4]^{2-}\}$ anions to the perfect fit of the molecular anions within the cationic template. Suggestions for possible anion-formation pathways are given in Scheme S1.

The bond lengths in **1** [Hg-(μ-Te) 2.692(2)–2.710(1), Hg-(μ:η^1:η^1-Te$_2$) 2.762(1)–2.803(1), Te-Te 2.728(2)–2.750(1)] are in good agreement with those of the related 1D-$\{[Hg_2Te_4]^{2-}\}$ anions [Hg-(μ-Te) 2.654(2)–2.729(5) Å; Hg-(μ:η^1:η^1-Te$_2$) 2.750(2)–2.807(2) Å; Te-Te 2.736(2)–2.788(3) Å]. All the metal atoms possess a roughly trigonal planar coordination with three Te atoms (angle sums of $\geq 359.35(2)°$), but the individual Te-Hg-Te angles cover a wide range (102.73(4)–142.39(5)°), with somewhat more obtuse (μ-Te)-Hg-(μ-Te) angles [116.84(7)–137.12(6)° in the 1D strand] and slightly more acute (μ-Te)-Hg-(μ:η^1:η^1-Te$_2$) angles [105.45(6)–127.73(7)° in the 1D strand]. This indicates a significant coordinative flexibility around the Hg atoms that reacts to the respective arrangement of the counterions that vary in size, structure, charge, polarizability, and hydrogen-bonding properties.

As a consequence of the coordinative flexibility of the Hg atoms, the macrocyclic anion **1** as a whole is not planar (Figure 1, bottom right). To optimize the interaction and structural match with the imidazolium cations, opposite pairs of $[Hg_2Te(Te_2)]$ rings are each inclined by about 24.8(1)°. In this way, the endocyclic Te atoms are relatively far apart from each other (Te···Te 7.0808(7)–7.4130(6) Å across the center of **1**).

A closer look at the crystal structure of $(C_{10}C_1Im)_8\mathbf{1}$ reveals segregation into ionic and nonpolar parts. The latter result from van der Waals interactions between the decyl chains that form a membrane-like interlocked double-layer with a width of 17.7 Å (Figure 1, top). The positively charged imidazolium rings of the cations perfectly accommodate the anions as follows: two imidazolium rings are each located in proximity to one of the $[Hg_2Te(Te_2)]$ rings, in total four from the cation layer above and four from the cation layer below the anion, and thus compensate for the relatively high charge of the anions. In this arrangement, the imidazolium rings are arranged orthogonal to the $[Hg_2Te(Te_2)]$ units, thereby maximizing the anion···anion distance. The second compound obtained with longer alkyl chains, $(C_{12}C_1Im)_8\mathbf{1}$, is isostructural to $(C_{10}C_1Im)_8\mathbf{1}$. As a consequence of even thicker nonpolar layers (20.2 Å, Figure S4), the crystals are very fragile and exhibit relatively poor crystallographic quality (see the Supporting Information).

Besides the segregation of such cations into polar/non-polar sections in the solid state,[17] similar effects of nanoscale segregation into microphases of homogeneous polarity were also observed in the liquid state of ionic liquids and confirmed by means of molecular dynamic simulations.[18,19]
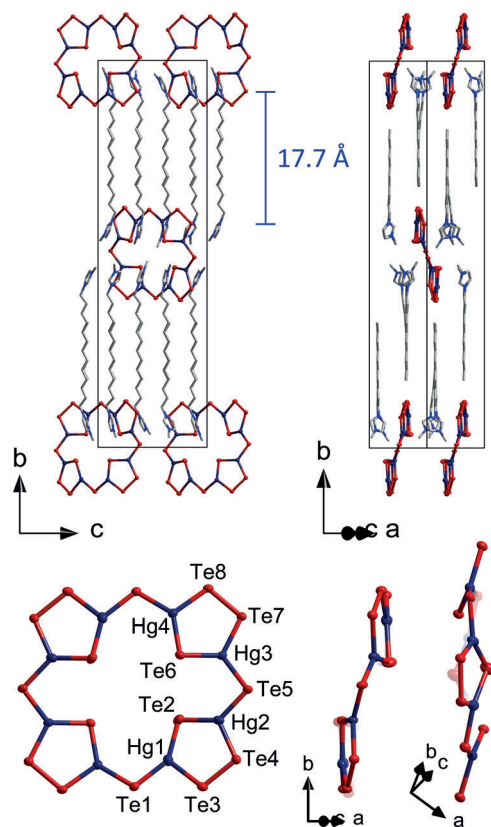
Figure 1. Top: Section of the crystal structure of $(C_{10}C_1Im)_8\mathbf{1}$ in different orientations. Bottom: different views of the molecular structure of the anion $[Hg_8Te_{16}]^{8-}$ (**1**; Hg, Te: thermal ellipsoids at the 50% probability level. C, N: wireframes. H atoms omitted for clarity). External diameters of the anion range from 12.3 Å (Te1···Te1′) to 16.2 Å (Te7···Te7′).[36]

The formation of heavy homologues of well-known molecules is a fascinating area of chemical research, which gives information about the correlation between intrinsic atomic properties and the structural, chemical, and physical properties of molecules. Prominent examples are heavy ethene and ethyne homologues, with their typical impact on their molecular structures.[20] Another recent example is PbSe as a CO-like bridging ligand in $\{[(Ph_3P)_2Rh][(Ph_3P)-(CN)Rh]_2Se_2(\mu\text{-}PbSe)\}^{3-}$.[21] Particularly worth noting are topological mimics of organic compounds by purely inorganic analogues—both with isoelectronic situations as well as with other electron counts. Many simple molecules, such as the benzene analogue borazine, $B_3N_3H_6$,[22] or the P_5^- equivalent of cyclopentadienide, Cp^-,[23] have been well-known for decades, while more complex structures have remained rare. Besides the above-mentioned porphyrin-like structures of BE_2 (E = S, Se), an inorganic double-helix mimicking DNA-like features was recently reported with the ternary, semiconducting phase SnIP.[24]

Quantum chemical studies were applied to compare the electronic similarities and dissimilarities of this porphyrin-related molecule to porphyrin itself (TURBOMOLE,[25] TPSSh functional,[26] def2-TZVP bases,[27] charge compensation with COSMO[28] by employing default parameters). Ring currents were obtained from GIMIC,[29] based on the magnetic response calculated with a local version[30,31] of TURBOMOLE. The ring currents for the two systems are shown in Figure 2.
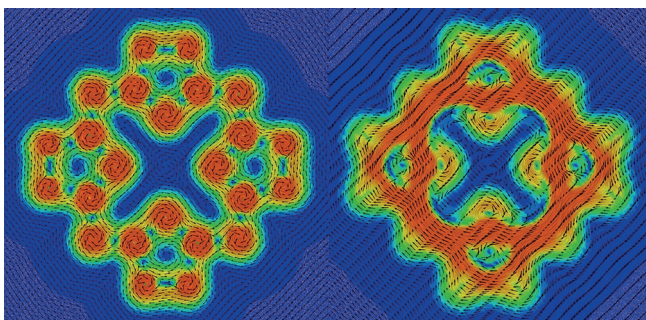
Figure 2. Ring currents, 1 bohr above the molecular plane of the inorganic anion **1** (left) and of the organic porphyrin (right), drawn between 0 a.u. (blue) and 0.07 a.u. (red).

1 exhibits (weak) ring currents in the pyrrole-type five-membered rings. These currents consist of diatropic (clockwise, outside the ring) and paratropic (counterclockwise, inside) contributions of similar size, but with a small surplus of the former leading to net currents of +5.8 nA/T. This is about half as much as for benzene,[32] but—in contrast to the latter—they arise from sigma contributions only. The global net ring current (also consisting of diatropic and paratropic contributions) is essentially zero (0.24 nA/T). The related $[B_8E_{16}]$ cycles (E = S, Se) behave similarly, but with somewhat weaker local currents in the five-membered rings (for details see Figure S9 in the Supporting Information). Organic porphyrins, in contrast, exhibit a global ring current of about 27 nA/T, which in the five rings is split into two subcurrents, each amounting to about 13 nA/T.[32]

These differences correspond to very different electronic structures for the two systems (despite identical topology). The aromaticity and the according currents in porphyrin is based on the delocalized π-electrons. In **1**, there are also delocalized canonical molecular orbitals (MOs), simply for symmetry reasons. The corresponding cluster orbitals (s-, p-, d-, f-, g-type) are the highest-energy MOs representing σ-bonding (Figure S7). However, in contrast to porphyrin, these MOs can be combined into two-center-two-electron bonds and lone pairs of electrons by application of a localization procedure.[33] This yields two lone pairs of electrons per Te atom, and single σ-type bonds between each pair of neighboring atoms (in total, 32 lone pairs of electrons and 28 bonds).

Optical absorption spectra were recorded on a single crystal of $(C_{10}C_1Im)_8\mathbf{1}$ (Figure 3). The onset of absorption is found at 2.2–2.8 eV, with a small shoulder of lower intensity at
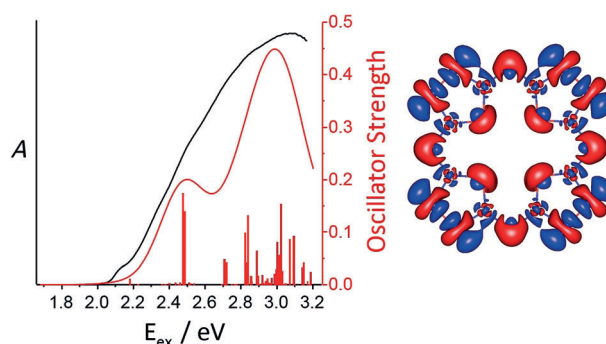
Figure 3. Comparison of the optical absorption spectrum measured on single crystals of $(C_{10}C_1Im)_8\mathbf{1}$ (black line) with calculated singlet excitation energies and oscillator strengths (lowest 250 excitations), plotted as vertical red lines with superimposed Gaussians of fwhm = 0.3 eV (red curve) to simulate the spectrum. The character of the entire band (up to 3.0 eV) is visualized using the nonrelaxed difference densities as described previously.[34] The contributions of the occupied orbitals are plotted in red, those of the unoccupied orbitals in blue.

2.1 eV. This is in excellent agreement with molecular TD-DFT calculations, with the lowest energy electronic transitions at 2.18 eV (HOMO to LUMO), followed by two more-intense transitions at 2.48 eV (HOMO−4 to LUMO+3 and LUMO+4). Excitation results in the electron density essentially being shifted from the μ-Te lone pairs of electrons to antibonding Te–Te MOs. As a consequence of the dimensional reduction, the optical gap is naturally blue-shifted from solid HgTe (−0.3 eV)[35] and 1D-$[Hg_2Te_4]^{2-}$ (1.63 eV)[14] to 0D-$[Hg_8Te_{16}]^{8-}$ (2.16 eV). This shift is still relatively narrow in view of the molecular size (24 atoms), as a consequence of the mixed-valence $Te^{2-}/(Te_2)^{2-}$ situation.

As the absorption energy is likely to change upon complexation of transition-metal atoms, we analyzed the possibility of using **1** as a ligand. The lack of π-electrons in $[Hg_8Te_{16}]^{8-}$ comes along with a high structural flexibility (see above). Quantum chemical calculations show that the macrocycle may accommodate metal ions of different sizes and coordination demands (e.g. Ti^{4+}, Cu^+, Ce^{4+}) by the ring adopting other shapes. Such changes will indeed lead to

These are not the final page numbers! ↗↗

a different absorption behavior (Figure S8). In this way it may be possible to form ternary complexes and clusters with tunable optical gaps within lamellar arrangements. However, as the bonding energies are naturally lower than for the corresponding porphyrin complexes, the experimental isolation of the according complexes remains a challenge.

In summary, we pursued a new approach for dimensional reduction of Hg/Te motifs by ionothermal treatment of $Na_2[HgTe_2]$ in long-chain alkyl imidazolium based ionic liquids. The obtained substructure represents purely inorganic macrocycles, $[Hg_8Te_{16}]^{8-}$, with a porphyrin-related topology that assemble in lamellar crystal structures. The anion notably deviates from planarity to optimize its situation in between the imidazolium units of the lamellar counterion structure. As confirmed by quantum chemical studies, the lack of π-electrons prevents significant aromaticity but leads to high structural flexibility, which may allow the coordination of metal cations, despite the macrocycle's size, by adopting its structure to the requirement of the embedded cation. In this way, lamellar arrangements of all-heavy-element complexes with tunable electronic properties may be accessible.

Conflict of interest

The authors declare no conflict of interest.

Keywords: chalcogenidometalates · dimensional reduction · inorganic macrocylces · ionothermal synthesis · ring currents

[1] a) Y. Pei, C. Chang, Z. Whang, M. Yin, M. Wu, G. Tan, H. Wu, Y. Chen, L. Zhang, S. Ghong, T. Zhu, X. Zhao, L. Huang, J. He, M. G. Kanatzidis, L.-D. Zhao, *J. Am. Chem. Soc.* **2016**, *138*, 16364 – 16371; b) X. Chen, X. Bu, Q. Lin, C. Mao, Y.-G. Zhai, Y. Wang, P. Feng, *Chem. Eur. J.* **2017**, *23*, 11913 – 11919; c) K. Zhao, C. Zhu, P. Qiu, A. B. Blichfeld, E. Eikeland, D. Ren, B. B. Iversen, F. Xu, X. Shi, L. Chen, *Nano Energy* **2017**, *42*, 43 – 50.

[2] a) L. Dou, A. B. Wong, Y. Yu, M. Lai, N. Kornienko, S. W. Eaton, A. Fu, C. G. Bischak, J. Ma, T. Ding, N. S. Ginsberg, L.-W. Wang, A. P. Alivisatos, P. Yang, *Science* **2015**, *349*, 1518 – 1521; b) A. Castellanos-Gomez, M. Buscema, R. Molenaar, V. Singh, L. Janssen, H. S. J. van der Zant, G. A. Steele, *2D Mater.* **2014**, *1*, 011002; c) C. Tan, X. Cao, X.-J. Wu, Q. He, J. Yang, X. Zhang, J. Chen, W. Zhao, S. Han, G.-H. Nam, M. Sindoro, H. Zhang, *Chem. Rev.* **2017**, *117*, 6225 – 6331.

[3] K. S. Novoselov, A. K. Geim, S. V. Morozov, D. Jiang, Y. Zhang, S. V. Dobonos, I. V. Grigorieva, A. A. Firsov, *Science* **2004**, *306*, 666 – 669.

[4] R. Gusmão, Z. Sofer, M. Pumera, *Angew. Chem. Int. Ed.* **2017**, *56*, 8052 – 8072; *Angew. Chem.* **2017**, *129*, 8164 – 8185.

[5] a) G. Zhang, H. Liu, J. Qu, J. Li, *Energy Environ. Sci.* **2016**, *9*, 1190 – 1209; b) L. Li, Z. Chen, Y. Hu, X. Wang, T. Zhang, W. Chen, Q. Wang, *J. Am. Chem. Soc.* **2013**, *135*, 1213 – 1216; c) Y. Sun, H. Cheng, S. Gao, Q. Liu, Z. Sun, C. Xiao, C. Wu, S. Wei, Y. Yie, *J. Am. Chem. Soc.* **2012**, *134*, 20294 – 20297.

[6] a) C. Zhou, H. Lin, Y. Tian, Z. Yuan, R. Clark, B. Chen, L. J. van de Burgt, J. C. Wang, Y. Zhou, K. Hanson, Q. J. Meisner, J. Neu, T. Besara, T. Siegrist, E. Lambers, P. Djurovich, B. Ma, *Chem. Sci.* **2018**, *9*, 586 – 593; b) A. Bayaguud, K. Chen, Y. Wei, *Nano Res.* **2016**, *9*, 3858 – 3867.

[7] a) M. G. Kanatzidis, *Inorg. Chem.* **2017**, *56*, 3158 – 3173; b) M. J. Manosa, M. G. Kanatzidis, *Chem. Sci.* **2016**, *7*, 4804 – 4824; c) G. Thiele, T. Krüger, S. Dehnen, *Angew. Chem. Int. Ed.* **2014**, *53*, 4699 – 4703; *Angew. Chem.* **2014**, *126*, 4787 – 4791; d) S. Dehnen, M. Melullis, *Coord. Chem. Rev.* **2007**, *251*, 1259 – 1280; e) P. Feng, X. Bu, N. Zheng, *Acc. Chem. Res.* **2005**, *38*, 293 – 303.

[8] S. Santner, J. Heine, S. Dehnen, *Angew. Chem. Int. Ed.* **2016**, *55*, 876 – 893; *Angew. Chem.* **2016**, *128*, 886 – 904.

[9] W.-W. Xiong, J.-R. Li, B. Hu, B. Tan, R.-F. Li, X.-Y. Huang, *Chem. Sci.* **2012**, *3*, 1200 – 1204.

[10] Y. Lin, W. Massa, S. Dehnen, *J. Am. Chem. Soc.* **2012**, *134*, 4497 – 4500.

[11] a) R. E. Morris, *Chem. Commun.* **2009**, 2990 – 2998; b) S. Santner, J. Sprenger, M. Finze, S. Dehnen, *Chem. Eur. J.* **2018**, *24*, 1032 – 1035; c) S. Santner, S. Yogendra, J. J. Weigand, S. Dehnen, *Chem. Eur. J.* **2017**, *23*, 1999 – 2004.

[12] a) F. Neve, O. Francescangeli, A. Crispini, J. Charmant, *Chem. Mater.* **2001**, *13*, 2032 – 2041; b) A. Downard, M. J. Earle, C. Hardacre, S. E. J. McMath, M. Nieuwenhuyzen, S. Teat, *Chem. Mater.* **2001**, *13*, 2032 – 2041; c) A. Getsis, B. Balke, C. Felser, A.-V. Mudring, *Cryst. Growth Des.* **2009**, *9*, 4429 – 4437; d) M. Stricker, T. Linder, B. Oelckers, J. Sundermeyer, *Green Chem.* **2010**, *12*, 1589 – 1598.

[13] a) M. Cardona, R. Kremer, R. Lauck, G. Siegle, A. Muñoz, A. H. Romero, *Phys. Rev. B* **2009**, *80*, 195204; b) A. Delin, T. Klüner, *Phys. Rev. B* **2002**, *66*, 035117; c) B. A. Bernevig, T. L. Hughes, S.-C. Zhang, *Science* **2006**, *314*, 1757 – 1761; d) M. König, S. Wiedmann, C. Brüne, A. Roth, H. Buhmann, L. W. Molenkamp, X.-L. Qi, S.-C. Zhang, *Science* **2007**, *318*, 766 – 770; e) A. Roth, C. Brüne, H. Buhmann, L. W. Molenkamp, J. Maciejko, X.-L. Qi, S.-C. Zhang, *Science* **2009**, *325*, 294 – 297.

[14] C. Donsbach, S. Dehnen, *Z. Anorg. Allg. Chem.* **2017**, *643*, 14 – 19.

[15] a) B. Krebs, H.-U. Hürter, *Angew. Chem. Int. Ed. Engl.* **1980**, *19*, 481 – 482; *Angew. Chem.* **1980**, *92*, 479 – 480; b) B. Krebs, H.-U. Hürter, *Acta Crystallogr. Sect. A* **1981**, *37*, C163b.

[16] a) S. S. Dhingra, C. J. Warren, R. C. Haushalter, A. B. Bocarsly, *Chem. Mater.* **1994**, *6*, 2382 – 2385; b) J. Li, Z. Chen, J. L. Kelly, D. M. Proserpio, *Mater. Res. Soc. Symp. Proc.* **1997**, *453*, 29 – 34; c) P. Sun, S. Liu, S. Li, L. Zhang, H. Sun, D. Jia, *Inorg. Chem.* **2017**, *56*, 6152 – 6162; d) R. C. Haushalter, *Angew. Chem. Int. Ed. Engl.* **1985**, *24*, 432 – 433; *Angew. Chem.* **1985**, *97*, 414 – 415.

[17] T. Ito, *Crystals* **2016**, *6*, 24.

[18] A. Triolo, O. Russina, H.-J. Bleif, E. Di Cola, *Phys. Chem. B* **2007**, *111*, 4641 – 4644.

[19] R. Elfgen, O. Hollóczki, B. Kirchner, *Acc. Chem. Res.* **2017**, *50*, 2949 – 2957.

[20] R. C. Fischer, P. P. Power, *Chem. Rev.* **2010**, *110*, 3877 – 3923.

[21] G. Thiele, Y. Franzke, F. Weigend, S. Dehnen, *Angew. Chem. Int. Ed.* **2015**, *54*, 11283 – 11288; *Angew. Chem.* **2015**, *127*, 11437 – 11442.

[22] a) A. Stock, E. Pohland, *Chem. Ber.* **1926**, *59*, 2215 – 2223; b) R. Boese, A. H. Maulitz, P. Stellberg, *Chem. Ber.* **1994**, 127, 1887 – 1889.

[23] O. J. Scherer, J. Schwalb, G. Wolmershäuser, W. Kaim, R. Gross, *Angew. Chem. Int. Ed. Engl.* **1986**, *25*, 363 – 364; *Angew. Chem.* **1986**, *98*, 349 – 350.

[24] D. Pfister, K. Schäfer, C. Ott, B. Gercke, R. Pöttgen, O. Janka, M. Baumgartner, A. Efimova, A. Hohmann, P. Schmidt, S. Venkatachalam, L. van Wüllen, U. Schürmann, L. Kienle, V. Duppel, E. Parzinger, B. Miller, J. Becker, A. Holleitner, R. Weihrich, T. Nilges, *Adv. Mater.* **2016**, *28*, 9783 – 9791.

[25] TURBOMOLE Version 7.2, TURBOMOLE GmbH **2017**. TURBOMOLE is a development of the University of Karlsruhe and the Forschungszentrum Karlsruhe 1989 – 2007, TURBOMOLE GmbH since 2007.

[26] V. Staroverov, G. Scuseria, J. Tao, J. Perdew, *J. Chem. Phys.* **2003**, *119*, 12129.

[27] a) F. Weigend, R. Ahlrichs, *Phys. Chem. Chem. Phys.* **2005**, *7*, 3297 – 3305; b) F. Weigend, *Phys. Chem. Chem. Phys.* **2006**, *8*, 1057 – 1065; c) K. A. Peterson, D. Figgen, E. Goll, H. Stoll, M. Dolg, *J. Chem. Phys.* **2003**, *119*, 11113; d) D. Andrae, U. Häussermann, M. Dolg, H. Stoll, H. Preuß, *Theor. Chim. Acta* **1990**, *77*, 123 – 141.

[28] A. Klamt, G. Schüürmann, *J. Chem. Soc. Perkin Trans. 2* **1993**, 799 – 805.

[29] J. Jusélius, D. Sundholm, J. Gauss, *J. Chem. Phys.* **2004**, *121*, 3952 – 3963.

[30] K. Reiter, M. Kühn, F. Weigend, *J. Chem. Phys.* **2017**, *146*, 054102.

[31] K. Reiter, F. Mack, F. Weigend, *J. Chem. Theory Comput.* **2018**, *14*, 191 – 197.

[32] H. Fliegl, D. Sundholm, *J. Org. Chem.* **2012**, *77*, 3408 – 3414.

[33] S. F. Boys, *Rev. Mod. Phys.* **1960**, *32*, 296 – 299.

[34] X.-X. Yang, I. Isaac, S. Lebedkin, M. Kühn, F. Weigend, D. Fenske, O. Fuhr, A. Eichhöfer, *Chem. Commun.* **2014**, *50*, 11043 – 11045.

[35] *Landolt-Börnstein Tables*, *New Series Vol. III/22a* (Ed.: O. Madelung), Springer, New York, **1986**, pp. 95 – 95.

[36] CCDC 1825252 contain the supplementary crystallographic data for this paper. These data can be obtained free of charge from The Cambridge Crystallographic Data Centre.

Communications

Inorganic Macrocycles

C. Donsbach, K. Reiter, D. Sundholm,
F. Weigend, S. Dehnen* —— ▮▮▮▮–▮▮▮▮

$[Hg_4Te_8(Te_2)_4]^{8-}$: A Heavy Metal
Porphyrinoid Embedded in a Lamellar
Structure
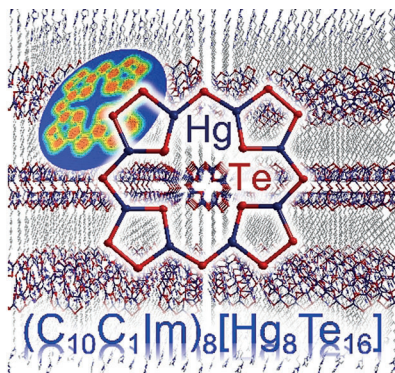
Getting heavy: Ionothermal treatment of $Na_2[HgTe_2]$ with $(C_nC_1Im)[BF_4]$ ($n = 10$, 12) affords salts with lamellar crystal structures of the macrocyclic anion $[Hg_8Te_{16}]^{8-}$ (**1**), the heaviest known topological relative of porphyrin. In accordance with its high structural flexibility, **1** does not exhibit a π-electron system, but possesses small ring currents in the pyrrole-type five-membered rings, which indicates weak local (σ) aromaticity.

↖↖ These are not the final page numbers!

3.6 Formation of [(C$_n$C$_1$imTe)$_4$Hg]$^{2+}$ (n = 6, 8) upon In-Situ Generation of Dialkylimidazole-2-Tellurones in Ionic Liquids at Room Temperature

C. Donsbach, S. Dehnen, **2018**, *Manuskript eingereicht.*

Abstract: The synthesis of a homoleptic Hg(II) complex with *in situ*-formed N-heterocyclic carbene telluride ligands is reported. Tetrakis(1-hexyl-3-methylimidazole-2-tellurone) mercury(II), [(C$_6$C$_1$imTe)$_4$Hg]$^{2+}$ (**1**), and tetrakis(1-octyl-3-methylimidazole-2-tellurone) mercury (II), [(C$_8$C$_1$imTe)$_4$Hg]$^{2+}$ (**2**), emerge from reaction mixtures containing telluridomercurate anions and potassium cations in ionic liquids (C$_n$C$_1$Im)[BF$_4$] (n = 6, 8), if these are exposed to ambient conditions, that is, air, moisture and room temperature. The compounds crystallize with two of the ionic liquid cations each, and form van der Waals dimers via Te···Te interactions in the crystal. Although being coordinated in a homoleptic manner, the orientation of the imidazolium ligands is such that two of them undergo π-stacking interactions, while the others interact with neighboring units via their alkyl chains.

Inhalt: Die Kristallstruktur sowie die Synthese der Tetrafluoroborat-Salze zweier Dialkylimidazol-2-Telluron-Komplexe von Hg(II)-Kationen, [(C$_6$C$_1$imTe)$_4$Hg]$^{2+}$ (**1**) und [(C$_8$C$_1$imTe)$_4$Hg]$^{2+}$ (**2**) (C$_6$C$_1$im = 1-Hexyl-3-Methylimidazol, C$_8$C$_1$im = 1-Methyl-3-Octylimidazol), wird präsentiert. Beide Salze wurden mittels Einkristall-Röntgenstrukturanalyse und Raman-Spektroskopie charakterisiert. Darüber hinaus wurde das relative Verhältnis der Schwerelemente durch micro-Röntgenfluoreszenz-Spektroskopie (μ-XFS) bestimmt und die optische Bandlücke der Verbindungen mittels UV-Vis-Spektroskopie ermittelt. Beide Verbindungen weisen je zwei nahezu tetraedrisch von den entsprechenden Telluron-Liganden koordinierte Hg(II)-Kationen auf, die ein durch dispersive Wechselwirkungen schwach assoziiertes Dimer bilden, das nach außen von den langen Alkylketten der Liganden umgeben ist. Zwischen je zwei Imidazol-Ringen eines Komplexes ist zudem eine schwache π-π-Wechselwirkung zu beobachten.

Die Salze wurden aus der Reaktionsmischung der ionothermalen Reaktion des ternären Telluridomerkurats Na$_2$[HgTe$_2$] in den entsprechenden ionischen Flüssigkeiten C$_n$C$_1$Im[BF$_4$] (n = 6,8; C$_6$C$_1$Im = 1-Hexyl-3-Methylimidazolium, C$_8$C$_1$Im = 1-Methyl-3-Octylimidazolium) erhalten. Die Eduktphase wurde dabei in einer unter Vakuum abgeschmolzenen Glasampulle in der ionischen Flüssigkeit für 12 h auf 60 °C erhitzt. Beim Öffnen der wieder abgekühlten Ampulle kam die Reaktionsmischung methodenbedingt kurzzeitig in Kontakt mit Luftsauerstoff kam. Die Komplexsalze **1**[BF$_4$]$_2$ und **2**[BF$_4$]$_2$

kristallisierten binnen vier Wochen in der geöffneten, aber unter Schutzgasatmosphäre bei Raumtemperatur gelagerten Ampulle. Zur Erklärung der Telluron-Bildung wird die in der Literatur bereits mehrfach beschriebene Deprotonierung von Imidazolium-Kationen zu *N*-heterocyclischen Carbenen unter ionothermalen Bedingungen herangezogen. Ein solches Carben ist in der Lage, zu Te(0) oxidierte Tellurid-Spezies *in-situ* unter Ausbildung eines Tellurons abzufangen, bevor elementares Tellur aus der Lösung abgeschieden wird.

Eigener Anteil: Die Verbindungen **1** und **2** wurden von mir synthetisiert und mittels Einkristall-Strukturanalyse und spektroskopischer Methoden (µ-XFS und UV-Vis-Spektroskopie) charakterisiert. Diese Analysen sowie deren Auswertung erfolgten durch mich. Die schwingungsspektroskopischen Messungen wurden von Bertram Peters und Kristin Kirchberg durchgeführt. Das Manuskript wurde von mir in Zusammenarbeit mit Stefanie Dehnen verfasst.

COMMUNICATION

Formation of [(C$_n$C$_1$imTe)$_4$Hg]$^{2+}$ (n = 6, 8) upon In-Situ Generation of Dialkylimidazole-2-Tellurones in Ionic Liquids at Room Temperature

Carsten Donsbach,[a] and Stefanie Dehnen*[a]

Abstract: The synthesis of a homoleptic Hg(II) complex with *in situ*-formed N-heterocyclic carbene telluride ligands is reported. Tetrakis(1-hexyl-3-methylimidazole-2-tellurone) mercury(II), [(C$_6$C$_1$imTe)$_4$Hg]$^{2+}$ (**1**), and tetrakis(1-octyl-3-methylimidazole-2-tellurone) mercury (II), [(C$_8$C$_1$imTe)$_4$Hg]$^{2+}$ (**2**), emerge from reaction mixtures containing telluridomercurate anions and potassium cations in ionic liquids (C$_n$C$_1$Im)[BF$_4$] (n = 6, 8), if these are exposed to ambient conditions, that is, air, moisture and room temperature. The compounds crystallize with two of the ionic liquid cations each, and form van der Waals dimers via Te···Te interactions in the crystal. Although being coordinated in a homoleptic manner, the orientation of the imidazolium ligands is such that two of them undergo π-stacking interactions, while the others interact with neighboring units via their alkyl chains.

Ionic liquids have evolved very powerful reaction media for the synthesis of a diversity of multinary crystalline chalcogenides with molecular or extended anionic or cationic substructures.[1] In many of the products of these syntheses, the ionic liquid cations, in rare cases also the anions,[2] are embedded, indicating the twofold role of the ionic liquid: as reaction medium and as structure-directing template. However, this still rendered the ionic liquids stable solvent-like environments for the syntheses – comparable with the incorporation of (unreactive) crystal solvent.

In contrast, some studies have emerged in the recent past that report on reactions not only *in* the ionic liquid, but also *with* the cations and/or anions of the reaction medium. This usually took place if temperature has been applied. This apparent "non-innocence" of the ionic liquids was observed at the synthesis of (C$_4$C$_1$C$_1$im)$_8$[NH$_4$]$_3$[Cu$_5$Ga$_{30}$S$_{52}$(SH)$_2$(C$_4$im)$_2$],[3] for instance, in which 1-butyl-2,3-dimethylimidazolium cations of the used ionic liquid, (C$_4$C$_1$C$_1$im)$^+$, acted as ligands at some of the metal atoms upon release of the methyl group in 2-position at temperatures above 160°C. In some cases, the respective methyl group was transferred instead, such as observed in [Co(en)$_{2.5}$(en-Me)$_{0.5}$]$_2$[Sn$_3$Se$_7$],[4] or more recently at the synthesis of methylated chalcogenidometalate clusters and (C$_n$C$_1$Im)$_6$[Hg$_6$Te$_{10}$(TeCH$_3$)$_2$] (n = 6, 8).[5]

The latter example resulted from our current study of the ionothermal treatment of tellurido mercurates, which we pursue with the aim to access compounds with new [Hg$_x$Te$_y$]$^{q-}$ substructures motives, and corresponding fine-tuning of opto-electronic properties.[6] The observed reactivity of the ionic liquid prompted us to continue this study also towards the stability/reactivity of such reaction mixtures against ambient

conditions, that is, against air and moisture at room temperature, which is usually excluded.

Under inert conditions, alkali metal salts of tellurido mercurates exhibit good solubility in imidazolium-based ionic liquids at room temperature, and undergo the following types of reactions at slightly elevated temperatures: (a) rearrangement reactions, leading to tellurido mercurate substructures of different dimensionalities within the resulting imidazolium salts; the dimensionality can be controlled by variation of the alkyl chain lengths of the ionic liquid cation.[7,8] (b) partial oxidation of some of the telluride ligands under formation of ditelluride units. The ionothermal treatment with (C$_n$C$_1$Im)[BF$_4$] (n = 6, 8) further indicated that imidazolium cations can act as a methylation reagent,[5] while the residual de-methylated imidazole units can serve as metal-coordinating ligands.[3]

In our current work, we encountered another possible side-reaction involving the imidazolium cations, that is, their deprotonation towards carbenes, as a feasible way of how to modify the Hg/Te substructures. So far, the formation of carbene species from ionic liquids such as carbene adducts of metal complexes, CO$_2$ as well as chalcogenes has occurred either under basic conditions, or in the presence of open-shell transition metal complexes.[9-13] The underlying formation mechanisms and their effect in carbene-catalyzed reactions or on the solution processes in ionic liquids were investigated by means of quantum chemistry.[14]

Herein, we present the formation and crystal structures of [BF$_4$]$^-$ salts of two unprecedented complexes, tetrakis(1-hexyl-3-methylimidazole-2-tellurone) mercury(II), [(C$_6$C$_1$imTe)$_4$Hg]$^{2+}$ (**1**), and tetrakis(1-octyl-3-methylimidazole-2-tellurone) mercury (II), [(C$_8$C$_1$imTe)$_4$Hg]$^{2+}$ (**2**). Both compounds were obtained in two-steps. First, Na$_2$[HgTe$_2$] was treated ionothermally in the respective (C$_n$C$_1$Im)[BF$_4$] ionic liquid (n = 6, 8), yielding the imidazolium salts of the methylated tellurido mercurate anion, (C$_n$C$_1$Im)$_6$[Hg$_6$Te$_{10}$(TeCH$_3$)$_2$].[5] Upon storage under ambient conditions, the latter are slowly oxidized to afford **1**[BF$_4$]$_2$ and **2**[BF$_4$]$_2$ as single crystals in the course of one month.

In general, both the reaction mixtures of tellurido mercurates in ionic liquids before the ionothermal treatment and the mother liquor afterwards are highly air-sensitive.Exposure to air usually results in slow but inevitable decomposition into the binary solids (HgTe, Na$_2$Te$_x$), accompanied by precipitation of elemental tellurium. Notably, the formation of analog tetrakis(1-alkyl-3-methylimidazole-2-tellurone) mercury(II) complex salts with alkyl chains other than hexyl and octyl could not be observed yet. This can most likely be ascribed to lower concentration of the tellurido mercurate species in the respective ionic liquids. As shown in Scheme 1, we anticipate that the oxidation of Te^{2-} anions (from the tellurium mercurate) by O$_2$ (from air), and the concomitant formation of OH$^-$ anions under deprotonation of the imidazolium cation to afford an N-heterocyclic carbene, represent the first step in the formation cascade. Subsequently, the two intermediate

[a] C. Donsbach, Prof. Dr. S. Dehnen
Fachbereich Chemie and Wissenschaftliches Zentrum für Material-wissenschaften (WZMW), Philipps-Universität Marburg
Hans-Meerwein-Straße 4, 35043 Marburg (Germany)
E-mail: dehnen@chemie.uni-marburg.de

products form imidazole-2-tellurone molecules in this case, which readily coordinate the Hg^{2+} cations to form complexes **1** and **2**. This may explain, why tellurium does not precipitate in this case.
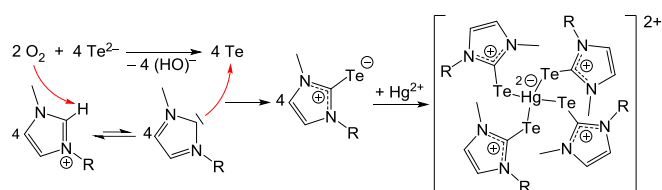
Scheme 1. Proposed reaction scheme for the formation of **1** (R = $-C_6H_{13}$) and **2** (R = $-C_8H_{17}$).

1 crystallizes as its tetrafluoroborate salt in the triclinic space group $P\bar{1}$ with four formula units per unit cell and two formula units per asymmetric unit, respectively (Figure 1). The cation **1** comprises a central Hg atom, which is coordinated in a distortedly tetrahedral manner by four 1-hexyl-3-methylimidazole-2-tellurone ligands. Some of the alkyl chains of the imidazole groups are (partially) disordered. Two of the four alkyl chains are pointing away from the metal center. Hence they do not wrap and shield the cation but rather interlock with alkyl chains of neighboring cations. Thereby, a lose cationic framework is formed, whose voids are occupied by the $[BF_4]^-$ anions for charge compensation. On the other hand, the incomplete shielding of the Hg^{2+} ions by the alkyl chains allows each two of the complexes to closely approach, with one Te_3 face of the central $[HgTe_4]$ tetrahedron facing another Te_3 face of the adjacent tetrahedron. The respective faces are nearly coplanar (angle between two Te_3 mean planes: 1.71(8)°), and the Te_3 faces arrange in a staggered formation. The Hg···Hg distance is 4.976(9) Å and the Te···Te distances range from 3.665(6)–4.055(7) Å. This dimeric entity shows nearly inversion symmetry, which is mainly disturbed by the exact conformation of the alkyl chains. The center of the dimers are located close to ½,¾,¼ and ½,¼,¾. The Hg–Te bond lengths are in the range of 2.769(5)–2.880(4) Å, hence they are slightly longer than those in tetrahedral Hg(II) complexes with organo-Te ligands (2.759(1)–2.795(1) Å).[15] The Te–Hg–Te angles range between 98.80(13) and 122.88(14)° which deviates significantly from the ideal tetrahedral angle of 109.5°. This heavy distortion is most likely caused by π-π interactions between the imidazole rings of those tellurone ligands that enclose the most obtuse Te–Hg–Te angles (shortest C...C contacts: 3.231(18)–3.334(17) Å). This is additionally reflected in an almost coplanar orientation of these rings (angle between the mean planes: 16.72(42)°–17.19(38)°). Opening of the respective Te–Hg–Te angle is the direct consequence of the relatively rigid, planar geometry around the imidazole carbene C atom beside the relatively flexible Te–Hg–Te coordination. None of the other tellurone ligands show intramolecular interactions, but are involved in the aforementioned intermolecular van-der-Waals network. The Te–C bond lengths are 2.061(11)–2.135(14) Å. As expected, they are longer than in non-coordinating imidazole-tellurones (2.050(3)–2.087(10) Å),[16] but slightly shorter on average than reported for the 1,3-diethyl-4,5-dihydro-imidazole-2-tellurone pentacarbonylchromium complex $[(C_2C_2imTe)Cr(CO)_5]$ (2.122(2) Å)[17] owing to the absence of trans-CO ligands. The

Hg–Te–C angles in **1** cover a range of 92.51(29)–102.02(30)°, in good agreement with the respective angle in $(C_2C_2HimTeCr(CO)_5)$ (96.14(1)°).[17]
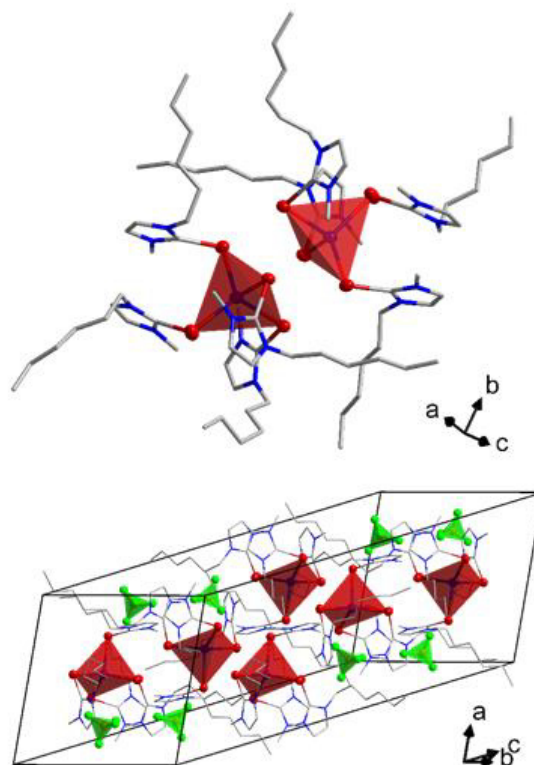
Figure 1. Molecular structure of the dimeric arrangement in **1** (top) and section of the crystal structure of **1**$[BF_4]_2$ (bottom). Hg (dark blue) and Te atoms (red) are represented as thermal ellipsoids at the 50% probability level. B (ocher) and F atoms (green) are shown as balls and sticks. C (grey) and N atoms (blue) are drawn as wireframes. Coordination polyhedra of Hg (red) and B (green) are shown. H atoms and disordered parts with minor occupancy are omitted for clarity.

The tetrafluoroborate salt of **2** crystallizes in the monoclinic space group $P2_1/n$ with four formula units per unit cell. Although it is not isostructural to **1**$[BF_4]_2$, the structure of the cationic complex is analog. **2** comprises higher symmetry than **1**, with the centrosymmetric cation dimers located around 0,0,0 and ½,½,½. (Figure 2). The Hg···Hg distance within this dimer, 4.785(1) Å, is slightly smaller than the corresponding distance in **1,** while the Te···Te distances (3.786(1)–3.931(1) Å) are within the range found in **1**. Significant disorder of the alkyl chains in **2** allows for a higher crystal symmetry. In addition to the general disorder of the alkyl chains, one of the four tellurone ligand is entirely disordered. The $[BF_4]^-$ anions located in the voids of the cationic framework are disordered as well. Hg–Te bond lengths (2.782(1)–2.859(1) Å) and Te–Hg–Te angles (99.70(2)–120.74(2)°) range within the respective values of **1**. Again, two of the four imidazole rings are notably approached (shortest C...C contact: 3.536(7) Å; dihedral angle: 11.99(15)°), indicating significant π-π interactions. Hg–Te–C angles range from 91.98(8)–101.36(11)°, with Te–C bond lengths of 2.073(4)–2.129(3) Å, in accordance with the respective values observed in **1**.

close similarity to **1** and **2**, π-π interactions between imidazole rings have not been observed in the quoted complexes. This can most likely be ascribed to both the absence of long and flexible alkyl substituents and the shorter and more rigid bonding characteristics of the lighter chalcogenone homologs. The respective salts of the literature-known complexes also comprise relatively weakly coordinating anions such as triflate, $[PF_6]^-$, $[BF_4]^-$, $[ClO_4]^-$, and NO_3^-. However, none of these compounds were synthesized in an ionic liquid, but from the respective metal salts and chalcogenones in conventional solvents instead.

The optical band gaps of **1**$[BF_4]_2$ (approximately 2.50 eV) and **2**$[BF_4]_2$ (approximately 2.45 eV) were determined *via* UV-visible spectroscopy, in good agreement with the visible color of both compounds (bright yellow crystals). The corresponding absorption spectra are shown in Figure 3. The band gap is notably red-shifted in comparison to the molecular mononuclear tellurido mercurate $(C_4C_1Im)_2[HgTe_2]$ (2.80 eV), which can be explained by a larger molecular unit as chromophore, namely the tetrahedral $[HgTe_4]$ unit, as compared to the linear $[HgTe_2]$ molecule. The slight difference in the band gap values of the two title compounds corresponds with a closer approach of the molecular units in the crystal: in **2**$[BF_4]_2$, the Hg⋯Hg distance is by 0.19 Å (4%) smaller than in **1**$[BF_4]_2$, and the Te⋯Te distances vary in a more narrow range (see above).

Figure 2. Molecular structure of the dimeric arrangement in **2** (top) and section of the crystal structure of **2**$[BF_4]_2$ (bottom). Hg (dark blue) and Te atoms (red) are represented as thermal ellipsoids at the 50% probability level. B (ocher) and F atoms (green) are shown as balls and sticks. C (grey) and N atoms (blue) are drawn as wireframes. Coordination polyhedral of Hg (red) and B (green) are shown. H atoms and disordered parts with minor occupancy are omitted for clarity.

1 and **2** represent the first examples of metal complexes comprising only tellurone ligands. This is not surprising as tellurones and their complexes are known for their air- and light-sensitivity, which complicated their access and use.[16,17] In this case however, the crystals of **1**$[BF_4]_2$ and **2**$[BF_4]_2$ were found to be relatively stable compared to tellurido mercurates, and only decomposed after several days in paratone oil under ambient conditions. To the best of our knowledge, $[(C_2C_2imTe)Cr(CO)_5]$ is the only metal complex featuring a tellurone ligand so far.[17] Similar complexes of transition metal cations coordinated tetrahedrally by four monodentate chalcogenone ligands have so far only been reported for the lighter homologs S and Se.[18, 19] The imidazole rings of these ligands are functionalized in positions 1 and 3 by alkyl, aryl or ester groups, respectively. Despite their

Figure 3. Optical absorption spectra of pulverized single crystals of **1**$[BF_4]_2$ and **2**$[BF_4]_2$.

In conclusion, we observed the formation of two chalcogenone species as product of a new type of side reaction previously unknown in ionothermal chalcogenido metalate syntheses. The two imidazole tellurone mercury(II) complexes point to an in-situ formation of carbenes from imidazolium based ionic liquids, which has been reported to occur under different conditions before. Thereby, the oxidation products of highly sensitive telluride species could be intercepted. These findings contribute to a more detailed understanding of the reaction processes occurring in ionic liquids in general, and the reactivity of the ionic liquid components in particular.

COMMUNICATION

Experimental Section

General: All manipulations were carried out under inert gas atmosphere (Ar) using Schlenk and glovebox techniques, unless stated otherwise. Pyridine was dried over CaH_2 and distilled prior to use. $(C_6C_1Im)[BF_4]$ and $(C_8C_1Im)[BF_4]$ were purchased from Sigma-Aldrich and degassed by dynamic evaporation ($1 \cdot 10^{-3}$ mbar) for 12 h before use. $Na_2[HgTe_2]$ was synthesized by fusion of stoichiometric amounts of Na_2Te and $HgTe$ in a silica ampoule with an oxygen/methane torch, such as reported previously.[7] The pulverized raw product was washed with pyridine.

Synthesis of 1[BF$_4$]$_2$: 50 mg of $Na_2[HgTe_2]$ and 200 µL of $(C_6C_1Im)[BF_4]$ were placed in a borosilicate glass ampoule with an inner diameter of 7 mm. The ampoule was sealed under vacuum and then placed in an oven where it was heated to 60°C for 12 h. After cooling to room temperature, crystals of $(C_6C_1Im)_6[Hg_6Te_{10}(TeCH_3)_2]$ were observed.[5] The ampoule was opened in air and rapidly mounted in a GL18 threaded joint adapter with a silicone rubber seal. Thereby, the ampoule was purged with inert gas, which still did not exclude the introduction of some oxygen gas. Roughly half of the crystalline product (including some of the mother liquor) was removed. The remaining crystals and the majority of the mother liquor were left under Ar in the closed adapter. Upon storage over four weeks, **1**[BF$_4$]$_2$ crystallizes as yellow blocks among black amorphous side-products like Te and HgTe. Raman shift (signal strength) [cm^{-1}]: 107 (vs), 220 (w), 359 (w), 640 (w), 670 (w), 1017 (vw), 1088 (vw), 1140 (m), 1184 (vw), 1353 (s), 1394 (vs), 1438 (w), 2856-2933 (m), 3166 (vw).

Synthesis of 2[BF$_4$]$_2$: **2**[BF$_4$]$_2$ was synthesized similar to **1**[BF$_4$]$_2$, using $(C_8C_1Im)[BF_4]$ instead of $(C_6C_1Im)[BF_4]$. Similar to the observation made at the synthesis of **1**[BF$_4$]$_2$, crystalline $(C_8C_1Im)_6[Hg_6Te_{10}(TeCH_3)_2]$ was obtained subsequent to the ionothermal reaction.[5] Upon opening, the ampoule was treated the same way as for **1**[BF$_4$]$_2$. **2**[BF$_4$]$_2$ crystallizes as yellow blocks in the course of approximately one month beside the described side-products. Raman shift [cm^{-1}]: 106 (vs), 223 (w), 345 (w), 642 (m), 671 (vw), 1017 (vw), 1086 (w), 1140 (m), 1172 (vw), 1353 (s), 1393 (vs), 1437 (w), 2849-2950 (m), 3166 (w).

Single-crystal X-ray Diffraction Studies, Data Collection and Crystallographic Details: Single crystal X-ray diffraction studies of **1**[BF$_4$]$_2$ were carried out on a STOE StadiVari diffractometer using Cu Kα radiation ($\lambda = 1.54186$) from an X-ray micro source with X-ray optics and a Pilatus 300K Si hybrid pixel array detector. The data was processed by scaling including spherical absorption correction, using STOE X-Area LANA software. X-ray diffraction data of **2**[BF$_4$]$_2$ were collected on a Bruker D8 Quest diffractometer using Mo-Kα radiation from an X-ray micro source tube with X-ray optics and a Photon 100 charge-integrating pixel array detector. The crystal was only cooled to 210 K during the measurement due to extensive splintering and twinning of the crystals occurring below 200°K. The data was scaled applying multiscan absorption correction, using Bruker SADABS software.[20] Structure solution was performed with direct methods, followed by full-matrix-least-squares refinement against F^2, using SHELXT15, SHELXL15 and Olex2 software.[21] The disorder models for the disordered parts of the alkyl chains and for the tetrafluoroborate anions in **2**[BF$_4$]$_2$ were refined with free variables using SADI, SIMU and RIGU restraints. For **2**[BF$_4$]$_2$, stable refinement of one disordered tellurone ligand required application of SAME, FLAT and SIMU restraints as well as some EADP constraints to the respective atoms C, N and Te atoms. Details on the crystallographic data are summarized in Table 1.

Elemental analyses: The heavy element composition of **1**[BF$_4$]$_2$ and **2**[BF$_4$]$_2$ was analyzed by micro X-ray fluorescence spectroscopy (µ-XFS). The measurements were performed using a Bruker M4 Tornado spectrometer equipped with a Rh target X-ray tube with poly capillary optics and a Si drift detector. The fluorescence photons emitted by the sample were detected and the data was processed *via* elemental

parameter methods. The quantitative results, which are shown in Table 2, are based on the Hg-L and Te-L radiation.

Table 1. Crystallographic data of **1**[BF$_4$]$_2$ and **2**[BF$_4$]$_2$.

Compound (CCDC number)	**1**[BF$_4$]$_2$ (1850135)	**2**[BF$_4$]$_2$ (1850136)
Empirical formula	$C_{40} H_{72} B_2 F_8 Hg_1 N_8 Te_4$	$C_{48} H_{88} B_2 F_8 Hg_1 N_8 Te_4$
Formula weight /g·mol^{-1}	1549.64	1661.87
Crystal color and shape	yellow block	yellow block
Crystal size /mm³	0.07×0.06×0.06	0.37×0.12×0.08
Crystal system	Triclinic	monoclinic
Space group	$P\bar{1}$	$P2_1/n$
a /Å	13.1867(2)	20.2531(17)
b /Å	16.4626(4)	13.0239(12)
c /Å	28.0776(6)	24.908(2)
α /°	75.427(2)	90
β /°	79.143(2)	93.135(7)
γ /°	67.643(2)	90
V /Å³	5426.5(2)	6560.2(10)
Z	4	4
ρ_{calc} /g·cm^{-3}	1.897	1.683
Radiation	Cu$_{Kα}$ (λ = 1.54186 Å)	Mo$_{Kα}$ (λ = 0.71073 Å)
Temperature	100 K	210 K
μ /mm^{-1}	22.253 (Cu$_{Kα}$)	4.148 (Mo$_{Kα}$)
Min/max transmission	0.0221/0.1725	0.5843/0.7459
$F(000)$	2952	3208
θ range /°	2.961-67.686	2.264-26.000
No. measured refl.	142357	198714
No. independent refl.	19662	17436
R(int)	0.1170	0.0391
No. indep. refl. ($I > 2\sigma(I)$)	10939	13742
No. of parameters	1257	986
No. of restraints	653	1940
R$_1$ ($I > 2\theta(I)$)	0.0453	0.0292
wR$_2$ (all data)	0.1130	0.0698
S (all data)	0.844	1.086
$\Delta\rho max$, $\Delta\rho min$ /e·Å^{-3}	2.064 / -1.254	1.708 / −1.434

UV-visible spectra: Optical absorption properties of **1**[BF$_4$]$_2$ and **2**[BF$_4$]$_2$ were analyzed by diffuse reflection of pulverized crystalline samples. The measurements were performed with a Varian Cary 5000 dual-beam spectrometer and a Praying Mantis sample holder from Harrick.

Table 2. Results of the μ-XFS analyses of compounds **1**[BF$_4$]$_2$ and **1**[BF$_4$]$_2$.

Element	atom% measured [calc.] in **1**[BF$_4$]$_2$	atom% measured [calc.] in **2**[BF$_4$]$_2$
Te	74.4(24) [75.0]	76.3(42) [75.0]
Hg	25.6(24) [25.0]	23.7(42) [25.0]

Raman spectroscopy: A commercially available Renishaw inVia Raman microscope was used for the Raman measurements of all the samples. The spectra were taken using a 532 nm laser (10 mW) as excitation source and were recorded in a backscattering geometry at room temperature. The excitation laser was focused with a 50 × objective onto the sample surface. The same objective was used to collect the scattered light, which was then dispersed by a spectrometer with a focal length of 250 mm and was finally detected by a charge-coupled device (CCD) camera with a spectral resolution of about 1 cm^{-1}.

Acknowledgements

[1] a) W.-W. Xiong, G. Zhang, Q. Zhang, *Inorg. Chem. Front.* **2014**, *1*, 292-301. b) *S.* Santner, J. Heine, S. Dehnen, *Angew. Chem.* **2016**, *128*, 886–904; *Angew. Chem. Int. Ed.* **2016**, *54*, 876–893.

[2] S. Santner, A. Wolff, M. Ruck, S. Dehnen, *Chem. Eur. J.* **2018**, *24*, https://doi.org/10.1002/chem.201802199.

[3] W.-W. Xiong, J.-R. Li, B. Hu, B. Tan, R.-F. Li, X.-Y. Huang, *Chem. Sci.* **2012**, *3*, 1200–1204.

[4] S. Santner, S. Dehnen, *Inorg. Chem.* **2015**, *54*, 1188–1190.

[5] B. G. H. Peters, S. Santner, C. Donsbach, P. Voelpel, B. Smarsly, S. Dehnen, unpublished results.

[6] Landolt-Börnstein Tables, edited by O. Madelung, New Series Vol. III/22a, Springer, New York, 1986, pp. 95-95.

[7] C. Donsbach, S. Dehnen, *Z. Anorg. Allg. Chem.* **2017**, *643*, 14–19.

[8] C. Donsbach, K. Reiter, D. Sundholm, F. Weigend, S. Dehnen, *Angew. Chem.* **2018**, *130*, https://doi.org/10.1002/ange.201803233; *Angew. Chem. Int. Ed.* **2018**, *57*, http://dx.doi.org/10.1002/anie.201803233.

[9] J. Dupont, J. Spencer, *Angew. Chem.* **2004**, *116*, 5408–5409; *Angew. Chem. Int. Ed.* **2004**, *43*, 5296-5297.

[10] a) L. Xu, W. Chen, J. Xiao, *Organometallics* **2000**, *19*, 1123-1127. b) M. Hasan, I. V. Kozhevnikov, M. R. H. Siddiqui, C. Femoni, A. Steiner, N. Winterton, *Inorg. Chem.* **2011**, *40*, 795-800. c) V. K. Aggarwal, I. Emme, A. Mereu, *Chem. Comm.* **2002**, 1612-1613. d) H. Lebel, M. K. Janes, A. B. Charette, S. P. Nolan, *J. Am. Chem. Soc.* **2004**, *126*, 5046-5047.

[11] N. D. Clement, K. J. Cavell, C. Jones, C. J. Elsevier, *Angew. Chem.* **2004**, *116*, 1297–1297; *Angew. Chem. Int. Ed.* **2004**, *43*, 1277-1277.

[12] G. Gurau, H. Rodríguez, S. O. Kelley, P. Jaiczek, R. S. Kalb, R. D. Rogers, *Angew. Chem.* **2011**, *123*, 12230–12232; *Angew. Chem. Int. Ed.* **2011**, *50*, 12024-12026.

[13] H. Rodríguez, G. Gurau, J. D. Holbrey and R. D. Rogers, *Chem. Commun.* **2011**, *47*, 3222–3224.

[14] a) O. Hollóczki, D. Gerhard, K. Massone, L. Szarvas, B. Németh, T. Veszprémi, L. Nyulászi, *New J. Chem.* **2010**, *34*, 3004-3009. b) O. Hollóczki, L. Nyulászi, *Org. Biomol. Chem.* **2011**, *9*, 2634-2640. c) M. Thomas, M. Brehm, O. Hollóczki, B. Kirchner, *Chem. Eur. J.* **2014**, *20*, 1622-1629. d) Z. Kelemen, B. Péter-Szabó, E. Székely, O. Hollóczki, D. S. Firaha, B. Kirchner, J. Nagy, L. Nyulászi, *Chem. Eur. J.* **2014**, *20*, 13002-13008. S. Gehrke, K. Schmitz, O. Hollóczki, *J. Phys. Chem. B* **2017**, *121*, 4521-4529.

[15] D. M. Smith, L. C. Roof, M. A. Ansari, J. M. McConnachie, J. C. Bollinger, M. A. Pell, R. J. Salm, J. A. Ibers, *Inorg. Chem.* **1996**, *35*, 4999-5006.

[16] a) N. Kuhn, G. Henkel, T. Kratz, *Chem. Ber.* **1993**, *126*, 2047-2049. b) A. J. Arduengo, F. Davidson, H. V. R. Dias, J. R. Goerlich, D. Khasnis, W. J. Marshall, T. K. Prakasha, *J. Am. Chem. Soc.* **1997**, *119*, 12742-12749. c) Ş. P. Yalçın, M. Akkurt, Ü. Yılmaz, H. Küçükbay, O. Büyükgüngör, *Acta Cryst. Sect. E* **2008**, *E64*, o621-o622. d) S. T. Manjare, S. Sharma, H. B. Singh, R. J. Butcher, *J. Organomet. Chem.* **2012**, *717*, 61-74. e) S. T. Manjare, S. Yadav, H. B. Singh, R. J. Butcher, *Eur. J. Inorg. Chem.* **2013**, 5344-5357. f) A. Huffer, B. Jeffery, B. J. Waller, A. A. Danopoulos, *C. R. Chimie* **2013**, *16*, 557-565. g) N. Ghavale, S. T. Manjare, H. B. Singh, R. J. Butcher, *Dalton Trans.* **2015**, *44*, 11893-11900. h) K. Srinivas, P. Suresh, C. N. Babu, A. Sathyanarayana, G. Prabusankar, *RSC Advances* **2015**, *5*, 15579-15590.

[17] M. F. Lappert, T. R. Martin, *Chem. Comm.* **1980**, 635-637.

[18] a) D. J. Williams, J. J. Concepcion, M. C. Koether, K. A. Arrowood, A. L. Carmack, T. G. Hamilton, S. M. Luck, M. Ndomo, C. R. Teel, D. VanDerveer, *J. Chem. Cryst.* **2006**, *36*, 453-457. b) D. J. Williams, D. Gulla, K. A. Arrowood, L. M. Bloodworth, A. L. Carmack, T. J. Evers, M. S. Wilson, J. J. Conception, C. A. S. Brevett, B. E. Huck, D. VanDerveer, *J. Chem. Cryst.* **2009**, *39*, 581-584. c) D. J. Williams, K. A. Arrowood, L. M. Bloodworth, A. L. Carmack, D. Gulla, M. W. Gray, I. M. Maasen, F. Rizvi, S. L. Rosenbaum, K. P. Gwaltney, D. VanDerveer, *J. Chem. Cryst.* **2010**, *40*, 1074-1077. d) B. S. Stadelman, M. M. Kimani, C. A. Bayse, C. D. McMillen, J. L. Brumaghim, *Dalton Trans.* **2016**, *45*, 4697-4711.

[19] a) D. J. Williams, B. J. McKinney, B. Baker, K. P. Gwaltney, D. VanDerveer, *J. Chem. Crystallogr.* **2007**, *37*, 691-694. b) M. M. Kimani, H. C. Wang, J. L. Brumaghim, *Dalton Trans.* **2012**, *41*, 5248-5259. c) C. N. Babu, K. Srivinas, G. Prabusankar, *Dalton Trans.* **2016**, *45*, 6456-6465.

[20] L. Krause, R. Herbst-Irmer, G. M. Sheldrick, D- Stahlke, *J. Appl. Cryst.* **2015**, 48, 3-10.

[21] a) G. M. Sheldrick, *Acta Crystallogr., Sect. A* **2015**, *71*, 3–8. b) G. M. Sheldrick, *Acta Crystallogr., Sect. C* **2015**, *71*, 3–8. c) O. V. Dolomanov, L. J. Bourhis, R. J. Gildea, J. A. K. Howard, H. Puschmann, *J. Appl. Crystallogr.* **2009**, *42*, 339–341.

Entry for the Table of Contents

COMMUNICATION

The $[BF_4]^-$ salts of the very unusual complex cations tetrakis(1-alkyl-3-methylimidazole-2-tellurone) mercury(II), $[(C_nC_1imTe)_4Hg]^{2+}$ (**1**, n = 6 and **2**, n = 8), were observed upon *in situ* formation of the corresponding tellurones in a side reaction of ionothermal chalcogenido metalate syntheses. These reactions point towards carbene formation from imidazolium based ionic liquids. The cations form dimers that undergo Te⋯Te and π-stacking interactions.
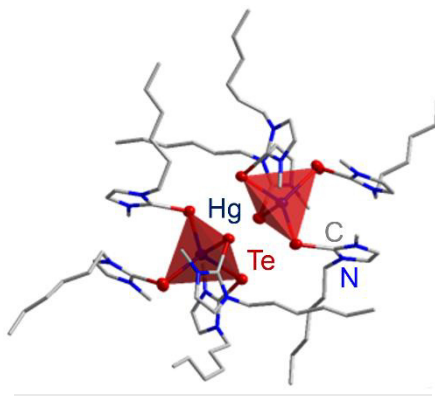
C. Donsbach, S. Dehnen*

Page No. – Page No.

Formation of $[(C_nC_1imTe)_4Hg]^{2+}$ (n = 6, 8) upon In-Situ Generation of Dialkylimidazole-2-Tellurones in Ionic Liquids at Room Temperature

3.7 (C$_4$C$_1$Im)$_6$[Hg$_7$Se$_{10}$]: The Salt of a Molecular Selenido Mercurate Anion Obtained from Ionic Liquids

C. Donsbach, S. Dehnen, **2018**, *Manuskript eingereicht.*

Abstract: A binary selenido mercurate anion exhibiting a novel metalate topology was obtained as its salt (C$_4$C$_1$Im)$_6$[Hg$_7$Se$_{10}$] (**1**)from the treatment of the ternary selenido mercurate K$_2$[Hg$_2$Se$_3$] in the ionic liquid (C$_4$C$_1$Im)[BF$_4$] (C$_4$C$_1$Im = 1-butyl-3-methylimidazolium) in the presence of small amounts of 1,2-diaminoethane (en) at slightly elevated temperatures (80°C). The three-dimensionally extended anionic substructure was disassembled this way, under formation of the unprecedented heptanuclear anion [Hg$_7$Se$_{10}$]$^{6-}$. The light yellow crystals of **1** are extremely sensitive to air and moisture. The structure of **1** was determined by single crystal X-ray diffraction, and its heavy element composition was analyzed and confirmed by micro X-ray fluorescence spectroscopy (µ-XFS).

Inhalt: Die Kristallstruktur und Synthese des (C$_4$C$_1$Im)$^+$-Salzes ((C$_4$C$_1$Im) = 1-Butyl-3-Methyl-Imidazolium), eines neuartigen heptanuklearen Selenidomerkurat-Anions, (C$_4$C$_1$Im)$_6$[Hg$_7$Se$_{10}$] (**1**), werden präsentiert. Die Verbindung wurde mittels Einkristall-Röntgenstrukturanalyse charakterisiert und das relative Verhältnis ihrer Schweratome durch micro-Röntgenfluoreszenz-Strukturanalyse (µ-XFS) bestimmt. Verbindung **1** wird nach ionothermaler Reaktion des ternären Selenidomerkurats K$_2$[Hg$_2$Se$_3$] unter Zusatz geringer Mengen von 1,2-Diaminoethan erhalten. Die dreidimensional ausgedehnte anionische Netzwerkstruktur des Edukts wird hierbei unter Neubildung einer Anionenstruktur geringerer Ausdehnung abgebaut. Derartige strukturdirigierende Effekte durch den Zusatz von Aminen sind bereits aus der ionothermalen Synthese von Selenidostannaten bekannt und konnten nun zum ersten Mal erfolgreich auf Chalkogenidomerkurate angewendet werden.

Eigener Anteil: Die Synthese von Verbindung **1** wurde von mir geplant und unter meiner Anleitung von Matthäus Drabek durchgeführt. Die Analyse der Verbindung mittels Einkristall-Strukturanalyse und micro-Röntgenfluoreszenz-Spektroskopie (*µ*-XFS) inklusive Auswertung erfolgte durch mich. Das Manuskript wurde von mir in Zusammenarbeit mit Stefanie Dehnen verfasst.

SHORT COMMUNICATION

(C4C1Im)6[Hg7Se10]: The Salt of a Molecular Selenido Mercurate Anion Obtained from Ionic Liquids

Carsten Donsbach,[a] and Stefanie Dehnen*[a]

Dedicated to Professor Bernt Krebs on the occasion of his 80th birthday.

Abstract: A binary selenido mercurate anion exhibiting a novel metalate topology was obtained as its salt $(C_4C_1Im)_6[Hg_7Se_{10}]$ (**1**) from the treatment of the ternary selenido mercurate $K_2[Hg_2Se_3]$ in the ionic liquid $(C_4C_1Im)[BF_4]$ (C_4C_1Im = 1-butyl-3-methylimidazolium) in the presence of small amounts of 1,2-diaminoethane (en) at slightly elevated temperatures (80°C). The three-dimensionally extended anionic substructure was disassembled this way, under formation of the unprecedented heptanuclear anion $[Hg_7Se_{10}]^{6-}$. The light yellow crystals of **1** are extremely sensitive to air and moisture. The structure of **1** was determined by single crystal X-ray diffraction, and its heavy element composition was analyzed and confirmed by micro X-ray fluorescence spectroscopy (μ-XFS).

Introduction

Metal-chalcogen compounds represent a broad range of diverse inorganic compounds and materials with different promising properties, in particular with focus on opto-electronic and thermoelectric applications.[1] Ideally, these properties can be fine-tuned by the respective combination of elements and the dimensionality of the structural motifs involved.[2]

In search for systematic approaches of inorganic materials syntheses, different solid state or solution-based techniques are constantly developed.[3] Here, ionic liquids have lately evolved as an interesting reaction medium due to their unique physical and chemical properties, such as low vapor pressure, thermal and chemical stability, as well as their capability to dissolve and stabilize highly charged ionic compounds.[4]

We have recently investigated the formation of various selenido germanate and stannate as well as chalcogenido mercurate salts in ionic liquids at slightly elevated temperatures in order to gain a deeper understanding of the reaction pathways involved in such ionothermal syntheses.[5-7] Both molecular anionic precursor units and extended networks with the general composition $[M_xE_y]^{q-}$ (M = Ge/Sn/Hg, E = S/Se/Te) were used. As shown in the studies involving M = Ge or Sn, the addition of small amounts of amines as ancillary reagents to the reaction mixtures affords a rearrangement of the anionic germanates and stannates substructures, involving increase or reduction of dimensionality.[8] Currently, we are aiming at a transfer of these synthetic strategies to the respective mercurates, the first results of which are presented herein.

Results and discussion

Ionothermal treatment of the ternary selenido mercurate $K_2[Hg_2Se_3]$, which bears a three-dimensional anionic substructure,[9] in $(C_4C_1Im)[BF_4]$ (C_4C_1Im = 1-butyl-3-methylimidazolium) in the presence of en (1%) at 80°C for 4 days

yields the compound $(C_4C_1Im)_6[Hg_7Se_{10}]$ (**1**, Scheme 1). Crystals of the salt are obtained in approximately 10% yield besides unreacted starting material over the course of several months at room temperature.

$$K_2[Hg_2Se_3] \xrightarrow[\text{80 °C, 4 d}]{\substack{(C_4C_1Im)[BF_4] \\ 1\% \text{ en}}} (C_4C_1Im)_6[Hg_7Se_{10}] \quad (1)$$
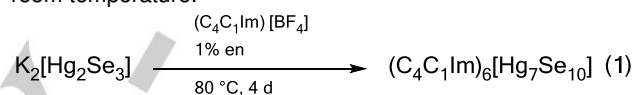
Scheme 1. Reaction scheme for the synthesis of **1**.

Compound **1** crystallizes in the triclinic space group $P\bar{1}$ with two formula units per unit cell (Figure 1). It comprises a unique molecular selenido mercurate anion built from six Hg atoms that show nearly linear or tetrahedral coordination by a total of ten Se atoms.
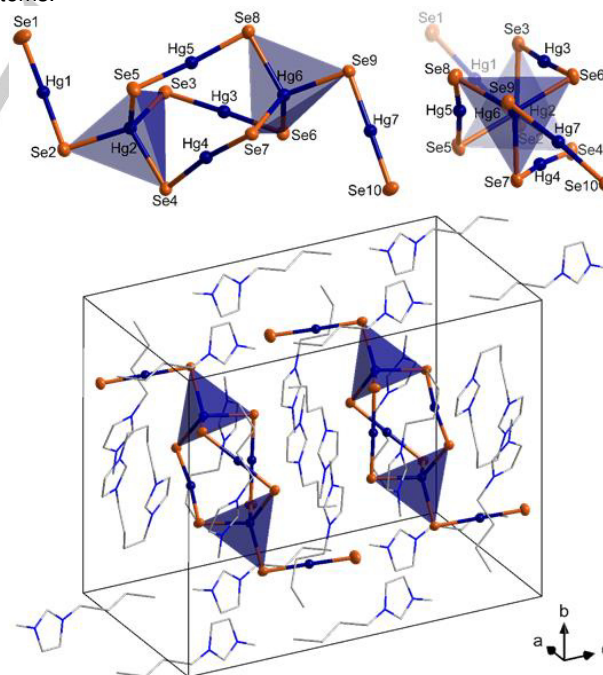
Figure 1. Molecular structure of the anion of **1** shown side-on (top left) and along the Hg2···Hg6 axis (top right) as well as a cut-out of the crystal structure of **1** (bottom). Hg (dark blue) and Se (orange) atoms are shown as thermal ellipsoids on the 50% probability level with coordination polyhedra of the four-coordinate Hg atoms. C (grey) and N (blue) atoms are represented as wireframes. H atoms are omitted for clarity.

[a]   Prof. Dr. S. Dehnen
       E-Mail: dehnen@chemie.uni-marburg.de
[a]   Fachbereich Chemie und Wissenschaftliches Zentrum für Material-
       wissenschaften (WZMW)
       Philipps-Universität Marburg

Within the anion, two [HgSe$_4$] units are linked by three Hg atoms, and linked to a terminal [HgSe] fragment at their forth Se atom. The tetrahedral coordination environment around Hg2 and Hg6 is slightly distorted (Se–Hg–Se 101.31(3)–117.92(3)°) due to the asymmetric 3:1 connection to next Hg atoms, which causes the three Se…Se edges of the [HgSe$_4$] tetrahedra next to the terminal Hg–Se to elongate. The two [HgSe$_4$] units face each other with nearly parallel faces (mean angle between planes: 0.57(2)°). However, the threefold linkage of the [HgSe$_4$] units by further Hg atoms comes along with a twist of the [HgSe$_4$] units against each other around the central Hg2···Hg6 axis by approximately 57°, resulting in a staggered orientation of the coplanar Se$_3$ faces. The terminal [Se–Hg–Se] moieties are also almost linear (Se–Hg–Se 176.62(3)–177.38(4)°). The three linking [Se–Hg–Se] units exhibit slightly more acute angles (Se–Hg–Se 171.62(4)–176.03(3)°). Such deviation from linear coordination geometry is uncommon. The closest secondary Hg···Se contact of the central Hg atoms is found at a distance of 3.67 Å (Hg4···Se5), thus providing only weak electrostatic interaction that would not explain the observed distortion. The three Hg atoms are all pointing inwards, thus closing the void in between, which may be due to weak attractive interactions between them. Weak repulsive interaction between the Hg atoms and the imidazolium rings of adjacent cations (closest Hg…C$_{Im}$ distance: 3.61 Å) may be considered as well.

The Hg–(μ-Se) bond lengths in the [HgSe$_4$] units vary in the range of 2.612(1)–2.714(1) Å. This is typical for Hg atoms in a tetrahedral coordination sphere, see A$_2$[Hg$_3$Se$_4$] (A = K, Rb, Cs, Tl) and Cs$_2$[HgSe$_2$]•H$_2$O (2.671(6)–2.685(2) Å).[10,11] The Hg–(μ–Se) distances in the [Se–Hg–Se] units (2.415(1)–2.438(1) Å) are similar to those found in [(C$_2$H$_5$)$_4$N]$_4$[Hg$_7$Se$_9$] (2.421(8)–2.457(8)).[12] As expected, the Hg–Se bonds towards the terminal selenide ligands are notably shorter (2.385(1)–2.401(1) Å), which again corresponds with the distances reported for compounds containing isolated [HgSe$_2$]$^{2-}$ anions (2.389(3)–2.420(2) Å).[13,13]

In the unit cell, the centers of the [Hg$_7$Se$_{10}$]$^{6-}$ anions are located close to ½,½,¼ and ½,½,¾, with its longest axis (through the terminal Se atoms) oriented approximately along {111}. The relatively high negative charge of the [Hg$_7$Se$_{10}$]$^{6-}$ anion is compensated by six (C$_4$C$_1$Im)$^+$ cations that are evenly arranged between the anions, thereby separating them from one another. The positively charged imidazolium rings of the cations are located close to the anions; their butyl chains both control and fill the voids in between. Different from the observation made with a molecular Hg/Te anion,[6] a separation into ionic and non-polar parts does not occur due to the relatively short alkyl chains of the cation.

Besides the molecular anion in **1**, which comprises an unprecedented topology, several other anionic substructures of (poly)selenido mercurates have been reported in literature (Figure 2). The typical linear, trigonal planar and tetrahedral coordination motifs are found in isolated anions, but also – in some cases heavily distorted – as building units of more complex, extended anionic structures. Most of the mercurates crystallize as salts of rather weakly-interacting cations, such as tetraalkylammonium, tetraphenylphosphonium, cesium or sequestrated alkali cations.[11-12] Aside from known complexes with polyselenide ligands, [Hg(Se$_4$)$_2$]$^{2-}$, [Hg$_2$(Se$_4$)$_3$]$^{4-}$ and [Hg$_7$Se$_8$(Se$_2$)]$^{4-}$,[12,13,14] the

mercurates with unsaturated coordination spheres tend to form polymers in order to increase their coordination number, which seems to be supported by crystallization with weakly-interacting cations. The phenomenon can be observed on the example of three different structures of [HgSe$_2$]$^{2-}$ (see Figure 2: structures a, h and i).[11,15] Hence in the case of **1**, very weakly interacting ionic liquid cations are used to stabilize the [Hg$_7$Se$_{10}$]$^{6-}$ anion with its high charge and a total of five coordinatively unsaturated Hg atoms, preventing possible aggregation.
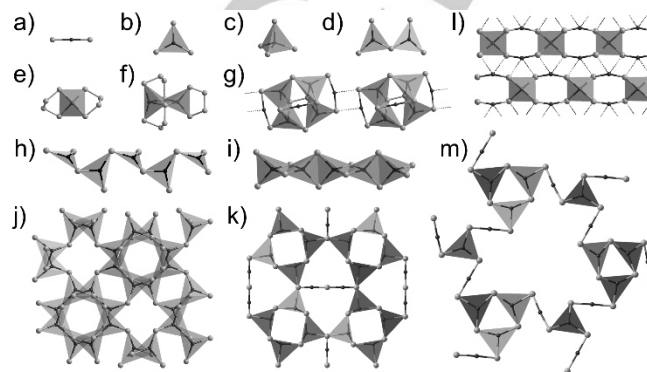
Figure 2. Overview of all anionic substructures known so far in the system Hg/Se (black/grey): a) [HgSe$_2$]$^{2-}$;[11,13] b) [HgSe$_3$]$^{4-}$;[11,15] c) [HgSe$_4$]$^{6-}$;[16] d) [Hg$_2$Se$_5$]$^{6-}$;[11] e) [Hg(Se$_4$)$_2$]$^{2-}$;[13,14] f) [Hg$_2$(Se$_4$)$_3$]$^{4-}$;[14d] g) (1D-)[Hg$_7$Se$_8$(Se$_2$)]$^{4-}$;[12] h) 1D-[HgSe$_2$]$^{2-}$;[15] i) 1D-[HgSe$_2$]$^{2-}$;[11] j) 3D-[Hg$_2$Se$_3$]$^{2-}$;[9] k) 3D-[Hg$_6$Se$_7$]$^{2-}$;[5a] l) 1D/2D-[Hg$_3$Se$_4$]$^{2-}$;[10] m) 2D-[Hg$_7$Se$_9$]$^{4-}$;[12] Coordination polyeders and polyhedra are shown for Hg. Dotted lines indicate additional Hg…Se contacts >3.2 Å.

Conclusions

In conclusion, we presented the imidazolium salt of the heptanuclear molecular selenido mercurate anion [Hg$_7$Se$_{10}$]$^{6-}$, comprising an unprecedented topology. The compound was obtained from the ionic liquid (C$_4$C$_1$Im)[BF$_4$] at moderately elevated reaction temperatures of only 80°C upon addition of small amounts of amine. Under these conditions, the anionic network of K$_2$[Hg$_2$Se$_3$] is fragmented and rearranged to form the molecular units. The synthetic route of amine-assisted dimensional reduction of chalcogenido metalates in ionic liquids has hereby been successfully transferred from tin chemistry to the respective mercurates for the first time. Further studies will focus on synthetic strategies to control the dimensionality of the anionic substructures of chalcogenido mercurates as well as their transformation.

Experimental Section

General: All manipulations were carried out under strict exclusion of air, moisture and light using standard Schlenk and glovebox techniques. K$_2$[Hg$_2$Se$_3$] was synthesized as described in the literature.[9] (C$_4$C$_1$im)[BF$_4$] was purchased from Sigma-Aldrich and degassed at 1×10^{-3} mbar and 80 °C for 12 h before usage. 1,2-diaminoethane was dried over CaH$_2$ and freshly distilled.

Synthesis of 1: 100 mg of K$_2$[Hg$_2$Se$_3$], 0.5 mL of (C$_4$C$_1$Im)[BF$_4$] and 0.05 mL of 1,2-diaminoethane were placed in a borosilicate glass ampoule

with an inner diameter of 7 mm. The vessel was sealed under vacuum to form an ampoule with an inner volume of approximately 5 mL, placed in an oven and heated to 80°C for 4 days. Subsequently, the ampoule was allowed to cool to room temperature. After several months, **1** was obtained as light yellow blocks in approximately 10% yield alongside black crystals of unreacted starting material.

Single-crystal X-ray Diffraction Studies, Data Collection and Crystallographic Details: Single crystals of **1** suitable for X-ray diffraction analysis were investigated on a STOE IPDS-II diffractometer at 100 K using Mo-Kα radiation and a graphite monochromator (λ = 0.71073 Å). Upon numerical absorption correction (STOE X-AREA), the structure was solved by direct methods, followed by full-matrix-least-squares refinement against F^2, using SHELXT15, SHELXL15, and OLEX2 software.[17]

Crystal data of 1: $C_{48}H_{88}Hg_7N_{12}Se_{10}$, 3027.3 g/mol, triclinic, $P\bar{1}$, $Z = 2$, light yellow block (0.13x0.06x0.05 mm³), $a = 11.8929(4)$ Å, $b = 15.3620(5)$ Å, 22.7483(7) Å, $c = 22.7483(7)$ Å, α = 78.607(3)°, β = 81.226(3)°, γ = 67.338(3)°, $V = 3746.0(2)$ Å³, $T = 100$ K, $\rho_{calc} = 2.684$ g/cm³, μ = 19.186 mm^{-1} (Mo$_{Kα}$, λ = 0.71073 Å), $T_{min}/T_{max} = 0.1080/0.4216$, $F(000) = 2720$, θ range: 1.596–29.518°, 69265 reflections measured, 20766 independent reflections ($I>2\sigma(I)$: 11973), 706 parameters, $R_1(I>2\theta(I)) = 0.0356$, wR_2(all data) = 0.690, S(all data) = 0.808, $\Delta\rho_{max}/\Delta\rho_{min} = 2.927/-2.115$. CCDC 1851299 contains the supplementary crystallographic data of the compound in this paper. The data can be obtained free of charge via www.ccdc.cam.ac.uk/data_request/cif.

Micro X-ray Fluorescence Spectroscopy (μ-XFS): The heavy element composition of **1** was analyzed by μ-XFS using a Bruker M4 Tornado, equipped with an Rh-target X-ray tube and a Si drift detector. The emitted fluorescence photons were detected. Upon background correction and deconvolution of the spectra, the data was analyzed based on the Hg-L and Se-K radiation. Figure 3 summarizes the results.

Element	Hg	Se
atom% measured	41.9(13)	58.1(13)
atom% calculated	41.2	58.8
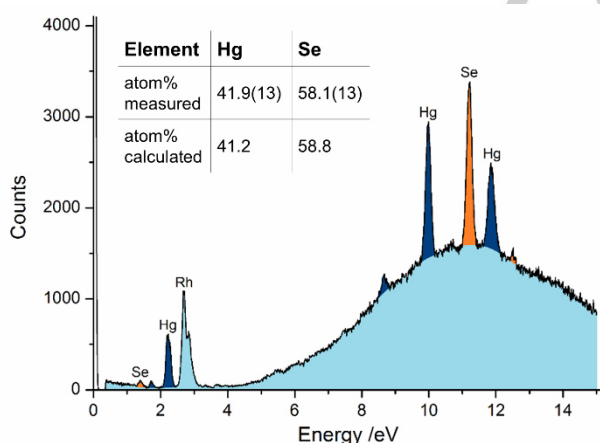
Figure 3. μ-XFS spectrum of a single-crystal of **1** with quantitative results. The intense background signal, including the Rh-L line, is caused by amorphous scattering of the primary beam on the mineral oil the crystal was covered in to prevent oxidation.

Acknowledgements

[1] a) K. Biswas, Q. Zhang, I. Chung, J.-H. Song, J. Androulakis, A. J. Freeman, M. G. Kanatzidis, *J. Am. Chem. Soc.* **2010**, *132*, 14760–14762; b) M. K. Jana, K. Biswas, C. N. R. Rao, Chem. Eur. J. **2013**, 19, 9110–9113; c) I. Chung, M. G. Kanatzidis, *Chem. Mater.* **2014**, *26*, 849–869.

[2] a) J. Androulakis, S. C. Peter, H. Li, C. D. Malliakas, J. A. Peters, Z. Liu, B. W. Wessels, J.-H. Song, H. Jin, A. J. Freeman, M. G. Kanatzidis, *Adv. Mater.* **2011**, *23*, 4163. b) D.-D. Yang, W. Li, W.-W. Xiong, J.-R. Li, X.-Y. Huang, *Dalton Trans.* **2018**, *47*, 5977–5984. c) N.-N. Shen, B. Hu, C.-C. Cheng, G.-D. Zou, Q.-Q. Hu, C.-F. Du, J.-R. Li, X.-Y. Huang., *Cryst. Growth Des.* **2018**, *18*, 962–968.

[3] a) T. Wu, Q. Zhang, Y. Hou, L. Wang, C. Mao, S.-T. Zheng, X. Bu, P. Feng, *J. Am. Chem. Soc.* **2013**, *135*, 10250–10253; b) S. V. Kershaw, A. S. Susha, A. I. Rogach, *Chem. Soc. Rev.* **2013**, *7*, 3033–3087. c) W.-W. Xiong, G. Zhang, Q. Zhang, *Inorg. Chem. Front.* **2014**, *1*, 292–301; d) L. Nie, Y. Zhang, W.-W. Xiong, T.-T. Lim, R. Xu, Q. Yan, Q. Zhang, *Inorg. Chem. Front.* **2016**, *3*, 111–116; e) D.-D. Yang, Y. Song, B. Zhang, N.-N. Shen, G.-L. Xu, W.-W. Xiong, X.-Y. Huang, *Cryst. Growth Des.* **2018**, *18*, 3255–3262.

[4] a) R. E. Morris, *Chem. Comm.* **2009**, 2990–2998; b) W.-W. Xiong, G. Zhang, Q. Zhang, *Inorg. Chem. Front.* **2014**, *1*, 292-301; c) M. F. Groh, A. Wolff, M. A. Grasser, M. Ruck, *Int. J. Mol. Sci.* **2016**, *17*, 1452; d) S. Santner, J. Heine, S. Dehnen, *Angew. Chem. Int. Ed.* **2016**, *55*, 886–904.

[5] a) C. Donsbach, G. Thiele, L. H. Finger, J. Sundermeyer, S. Dehnen, *Inorg. Chem.* **2016**, *55*, 6725–6730; b) S. Santner, S. Yogendra, J. J. Weigand, S. Dehnen, *Chem. Eur. J.* **2017**, *23*, 1999–2004; c) S. Santner, J. Sprenger, M. Finze, S. Dehnen, *Chem. Eur. J.* **2018**, *24*, 3474–3480.

[6] C. Donsbach, K. Reiter, D. Sundholm, F. Weigend, S. Dehnen, *Angew. Chem.* **2018**, *129*, https://doi.org/10.1002/ange.201803233; *Angew. Chem. Int. Ed.* **2018**, *57*, https://doi.org/10.1002/anie.201803233

[7] S. Santner, A. Wolff, M. Ruck, S. Dehnen, *Chem. Eur. J.* **2018**, *24*, https://doi.org/10.1002/chem.201802199.

[8] a) Y. Lin, W. Massa, S. Dehnen, *Chem. Eur. J.* **2012**, *18*, 13427–13434; b) Y. Lin, D. Xie, W. Massa, L. Mayrhofer, S. Lippert, B. Ewers, A. Chernikov, M. Koch, S. Dehnen, *Chem. Eur. J.* **2013**, *19*, 8806–8813.

[9] G. Thiele, S. Lippert, F. Fahrnbauer, P. Bron, O. Oeckler, A. Rahimi-Iman, M. Koch, B. Roling, S. Dehnen, *Chem. Mater.* **2015**, *27*, 4114–4118.

[10] a) M. G. Kanatzidis, Y. Park, Chem. Mater. **1990**, *2*, 99–101; b) E. A. Axtell III, Y. Park, K. Chondroudis, M. G. Kanatzidis, *J. Am. Chem. Soc.* **1998**, *120*, 124–136; c) S. Johnsen, S. C. Peter, S. L. Nguyen, J. H. Song, H. Jin, A. J. Freeman, M. G. Kanatzidis, *Chem. Mater.* **2011**, *23*, 4375–4383. d) K.-W. Kim, *Z. Kristallogr. NCS* **2016**, *231*, 299–300.

[11] C. Donsbach, S. Dehnen, *Inorg. Chem. Front.* **2017**, *4*, 336–342.

[12] K.-W. Kim, M. G. Kanatzidis, *Inorg. Chem.* **1991**, *30*, 1966–1969.

[13] C.-W. Park, D. M. Smith, M. A. Pell, J. A. Ibers, *Inorg. Chem.* **1997**, *36*, 942–943.

[14] a) J. Adel, F. Weller, K. Dehnicke, *Z. Naturforsch. B: Chem. Sci.* **1988**, *43*, 1094–1100; b) G. Krauter, F. Weller, K. Dehnicke, *Z. Naturforsch. B: Chem. Sci.* **1989**, *44*, 444–454; c) R. M. H. Banda, J. Cusick, M. L. Scudder, D. C. Craig, I. G. Dance, *Polyhedron* **1989**, *8*, 1995–1998; d) S. Magull, B. Neumüller, K. Dehnicke, *Z. Naturforsch. B: Chem. Sci.* **1991**, *46*, 985–991; e) B. Neumüller, M.-L. Ha-Eierdanz, U. Müller, S. Magull, G. Krauter, K. Dehnicke, *Z. Anorg. Allg. Chem.* **1992**, *609*, 12–18; f) A. Ahle, K. Dehnicke, K. Maczek, D. Fenske, *Z. Anorg. Allg. Chem.* **1993**, *619*, 1699–1703; g) P. J. Barrie, R. J. H. Clark, R. Withnall, D.-Y. Chung, K.-W. Kim, M. G. Kanatzidis, *Inorg. Chem.* **1994**, *33*, 1212–1216; h) J. C. Bollinger, J. A. Ibers, *Inorg. Chem.* **1995**, *34*, 1859–1867; i) K.-W. Kim, J. Kim, *Z. Kristallogr. NCS* **2014**, *229*, 25–30.

[15] G. Thiele, C. Donsbach, R. Riedel, M. Marsch, K. Harms, S. Dehnen, *Dalton Trans.* **2016**, *45*, 5958–5967.

[16] H. Sommer, R. Hoppe, *Z. Anorg. Allg. Chem.* **1978**, *443*, 201–211.

[17] a) G. M. Sheldrick, *Acta Crystallogr., Sect. A* **2015**, *71*, 3–8; b) G. M. Sheldrick, *Acta Crystallogr., Sect. C* **2015**, *71*, 3–8; c) O. V. Dolomanov, L. J. Bourhis, R. J. Gildea, J. A. K. Howard, H. Puschmann, *J. Appl. Crystallogr.* **2009**, *42*, 339–341.

WILEY-VCH

Entry for the Table of Contents (Please choose one layout)

COMMUNICATION

Ionothermal treatment of the ternary selenidomercurate $K_2[Hg_2Se_3]$ in $C_4C_1im[BF_4]$ affords the salt of an unprecedented selenidomercurate cluster anion (see Figure), which hadds to the large variety of known Hg/Se substructures. Two tetrahedral $[HgSe_4]$ units are facing each other and being linked via three linear Se–Hg–Se moieties. In addition, the fourth selenium ligand at the $[HgSe_4]$ units each binds another Hg–Se fragment, thus forming two further linear Se–Hg–Se units.
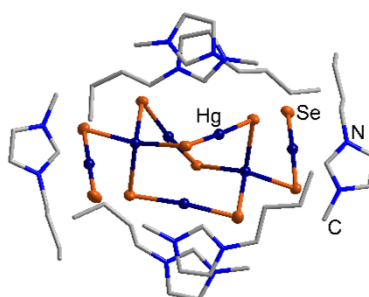
Carsten Donsbach, Stefanie Dehnen*

Page No. – Page No.

$(C_4C_1Im)_6[Hg_7Se_{10}]$: The Salt of a Molecular Selenido Mercurate Anion Obtained from Ionic Liquids

Additional Author information for the electronic version of the article.

Stefanie Dehnen: 0000-0002-1325-9228

3.8   Not so innocent after all? The role of ionic liquid cations as methylation agent

B. Peters, S. Santner, C. Donsbach, S. Dehnen, **2018**, *Manuskript in Vorbereitung*.

Abstract: The uncommon in-situ methylation of molecular chalcogenido metalate anions in ionothermal reactions with alkylimidazolium-based ionic liquids yields a series of organo-functionalized chalcogenido metalate compounds. In particular, we present the syntheses and crystal structures of $(Cat)_x[Sn_{10}S_{16}O_4(S–Me)_4][An]_y$ (**1a–1f**), $(Cat)_6[Mn_4Sn_4Se_{13}(Se–Me)_4]$ (**2**) and $(Cat)_6[Hg_6Te_{10}(Te–Me)_2]$ (**3a, 3b**). Methylation of the S compounds is confirmed by vibrational spectroscopy data and the optical bandgap of the Se compound is determined *via* UV-Vis spectroscopy.

Inhalt: Die *in-situ*-Methylierung molekularer Chalkogenidometallat-Cluster durch 1-Alkyl-(2,)3-(Di-)Methylimidazolium-basierte ionische Flüssigkeiten wird vorgestellt. Hierzu werden Kristallstrukturen und Synthesen der Salze von ingesamt drei unterschiedlichen Anionen präsentiert. Dabei handelt es sich um einen Oxothiostannat-Cluster in $(Cat)_x[Sn_{10}S_{16}O_4(S–Me)_4][BF_4]_y$ (**1a–1f**), einen ternären Selenidometallat-Cluster in $(Cat)_6[Mn_4Sn_4Se_{13}(Se–Me)_4]$ (**2**) und ein neuartiges hexanukleares Telluridomerkurat-Anion in $(Cat)_6[Hg_6Te_{10}(Te–Me)_2]$ (**3a, 3b**). Die Verbindungen wurden mittels Einkristall-Röntgenstrukturanalyse charakterisiert. Die Methylierung der Cluster in **1a** – **1f** wurde durch Raman-spektroskopische Messungen bestätigt. Außerdem wurde die optische Bandlücke von Verbindung **2** mittels UV-Vis-Spektroskopie bestimmt.

Alle neun Verbindungen wurden durch Reaktionen entsprechender Chalkogenidometallate in ionischen Flüssigkeiten mit 1-Alkyl-(2,)3-(Di-)Methyl-imidazolium-Kationen bei 60–180 °C erhalten. Dabei wurden molekulare Anionenstrukturen gebildet, die bis auf die Hg/Te-Spezies bereits in ihrer nicht-methylierten Form bekannt sind. In den vorgestellten Reaktionen wurden jedoch Methylgruppen von Imidazolium-Kationen auf die terminalen Chalkogenatome der Cluster übertragen. Durch die organische Funktionalisierung verlängern sich die terminalen Metall-Chalkogen-Bindungen signifikant, was eine entsprechende Verzerrung der gesamten Clustergeometrie bewirkt.

Eigener Anteil: Die Synthese der Verbindungen **3a** und **3b** wurde von mir geplant und durchgeführt. Die Analyse der Verbindungen mittels Einkristall-Strukturanalyse und micro-Röntgenfluoreszenz-Spektroskopie (µ-XFS) inklusive Auswertung erfolgte durch mich. Die Verbindungen **1a** – **1e** wurden von Bertram Peters synthetisiert und charakterisiert. Die

schwingungsspektroskopischen Messungen wurden von Bertram Peters in Zusammenarbeit mit Pascal Vöpel und Kristin Kirchberg durchgeführt. Verbindung **2** wurde von Silke Santner synthetisiert und charakterisiert. Das optische Absorptionsspektrum von Verbindung **2** wurde von mir in Kooperation mit Silke Santner gemessen. Das Manuskript wurde von mir in Zusammenarbeit mit Bertram Peters, Silke Santner und Stefanie Dehnen verfasst.

COMMUNICATION

Not so innocent after all? The role of ionic liquid cations as methylation agent

B. G. H. Peters,[a] S. Santner,[a] C. Donsbach,[a] and S. Dehnen[a]*

The uncommon in-situ methylation of molecular chalcogenido metalate anions in ionothermal reactions with alkylimidazolium-based ionic liquids yields a series of organo-functionalized chalcogenido metalate compounds. In particular, we present the syntheses and crystal structures of $(Cat)_x[Sn_{10}S_{16}O_4(S–Me)_4][An]_y$ (**1a–1f**), $(Cat)_6[Mn_4Sn_4Se_{13}(Se–Me)_4]$ (**2**) and $(Cat)_6[Hg_6Te_{10}(Te–Me)_2]$ (**3a**, **3b**). Methylation of the S compounds is confirmed by vibrational spectroscopy data and the optical bandgap of the Se compound is determined via UV-Vis spectroscopy.

Introduction

Ionic liquids are regarded as ideal or even "green" solvents, as they usually behave extremely indifferent in many types of reactions. To some extent, this is also valid for reactions under slightly elevated temperature, that is, under ionothermal conditions. However, in recent years, it has become obvious that certain compounds, in particular chalcogenides, do react with the ionic liquids.[1] Besides the well-known incorporation of ionic liquid cations,[2-8] we have also observed the methylation of amines that are added as auxiliary for the control of the basicity of the reaction medium.[9] We have also reported the distinct influence of the ionic liquid anion on the course of the reactions, though the incorporation of the anions in the finally isolated reaction products has remained rare so far.[10,11]

These results prompted us to systematically investigate their chemical behavior and their use as reactive solvents for the formation of organic derivatives of chalcogenido metalate anions, thereby also extending our studies towards the still rare class of corresponding sulfides and tellurides for exploring the effect of different nucleophilicities. Herein we show that ionic liquids can be purposefully used for the formation of methylated sulfido, selenido, and tellurido stannate cluster anions, which has not been possible so far with common methylation reagents.[5,12]

The treatment of different chalcogenido metalate salts, $Na_4[SnS_4]\cdot14H_2O$,[13] $Li_4[SnS_4]\cdot13H_2O$,[14] $K_4[SnSe_4]\cdot4MeOH$,[15] $Na_2[HgTe_2]$,[16] in ionic liquids of the type $(C_m(C_n)C_1Im)X^§$ afforded nine new salts comprising each one of three types of molecular chalcogenido metalate anions, $[Sn_{10}S_{16}O_4(S–Me)_4]^{4-}$ (in **1a–1e**), $[Mn_4Sn_4Se_{13}(Se–Me)_4]^{6-}$ (in **2**), $[Hg_6Te_{10}(Te–Me)_2]^{6-}$ (in **3a** and **3b**). Scheme 1 summarizes the syntheses.
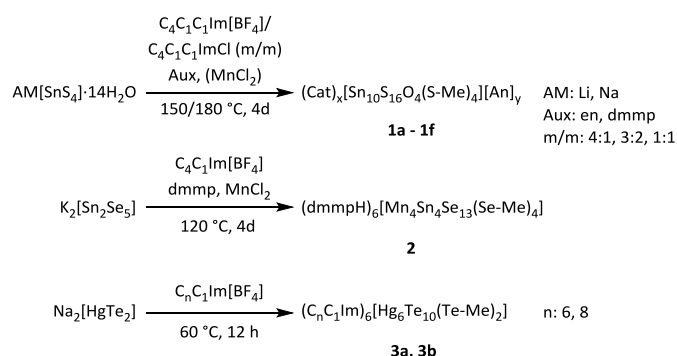
Scheme 1: Overview of the ionothermal synthesis of salts comprising different methylated chalcogenido metalate anions $[M_xTM_yE_z]^{q-}$ in **1 – 3** (M = Sn, E = O,S; M = Sn, TM = Mn, E = Se; M = Hg, E = Te), performed in imidazolium-based ionic liquids with different substitution pattern. The scheme indicates the respective reaction conditions, that is, the presence of auxiliaries (Aux) and/or additives (TMCl₂), temperatures (T), and reaction durations (t).§§

The title compounds are exceptional in several ways. First, they belong to the rare examples of molecular cluster anions obtained from ionic liquids. Second, the anion in **1a – 1f** comprises the first known sulfido stannate anions synthesized by ionothermal treatment, and with this contributes to the still small collection of sulfido metalate anions obtained via this route. Third, the anion in **2** represents the first ternary TM/Sn/E anions that was formed in ionic liquids and not in solution or by flux techniques. Finally, the anion in **3a** and **3b** belongs to the rare family of molecular Hg/Te clusters and adopts a so far unknown composition and architecture. The most important aspect of all of the title compounds, however, is the presence of the terminal methyl groups.

The only reasonable source of the Me groups is the ionic liquid cation. Previously, the transfer of one Me group onto a molecule of 1,2-diaminoethane was reported.[9] In another case, the demethylated fragment of an imidazolium cation was found to coordinate Ga or In atoms in cluster molecules.[17] In our case, the whereabouts of the abstracted methyl group have been re-

[a.] Fachbereich Chemie und Wissenschaftliches Zentrum für Materialwissenschaften (WZMW), Philipps-Universität Marburg, Hans-Meerwein-Straße 4, 35043 Marburg, Germany. E-mail: dehnen@chemie.uni-marburg.de

† Electronic Supplementary Information (ESI) available. See DOI: 10.1039/x0xx00000x

solved. Although in-situ methylation of highly charged chalcogenido metalate anions has not been achieved in ionic liquids nor in conventional solvents before, these findings indicate significant nucleophilicity of the terminal ligands of chalcogenido metalate anions, regardless of the nature of the chalcogen. Below, we describe the structures the new chalcogenido metalate anions along with some further properties of the title compounds.

$(C_4C_1C_1Im)_5[Sn_{10}S_{16}O_4(S-Me)_4][BF_4]$ (compound **1a**) crystallizes in the orthorhombic crystal system (space group *Pbcm*), with $a = 17.727(4)$ Å, $b = 35.611(7)$ Å, $c = 31.733$ Å, $V = 20.032(7) \cdot 10^3$ Å^3. Besides imidazolium cations, the asymmetric unit contains two types of anions: one $[BF_4]^-$ anion (similar to the previously reported $(C_4C_1C_1Im)_5[Sn_9Se_{20}][BF_4]$),[14] and one methylated thiooxostannate anion, $[Sn_{10}S_{16}O_4(S-Me)_4]^{4-}$. The inorganic cluster structure of the latter represents an "oxide-filled" version of a T3-type supertetrahedron, $[Sn_{10}S_{20}O_4]^{8-}$, which has been reported previously with other counterions.[18,19]
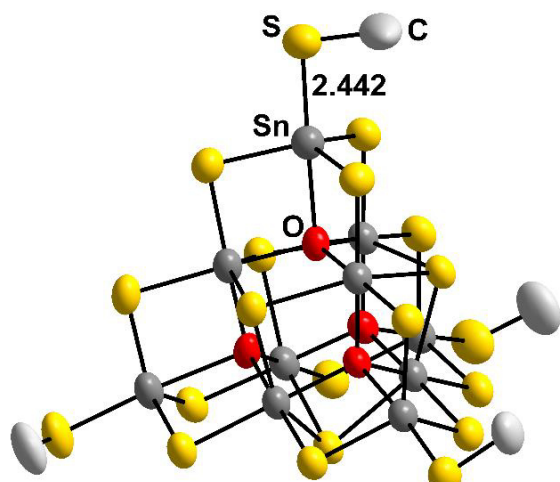
Figure 1. Molecular structure of the cluster anion in **1b**. Thermal ellipsoids are drawn at the 50% probability level; hydrogen atoms are omitted for clarity. Color code: grey - Sn, yellow - S, red - O, white - C.

Similar to **1a**, five further compounds **1b**–**1f** containing the methylated thiooxostannate anion could be obtained. The molecular structure of the cluster anion is shown in Figure 1 using the example of **1b**. The co-crystallizing constituents of the ionic liquid are shown in Figure 2. The cations are located close to the anions with the imidazolium rings oriented parallel to the cluster faces, thereby separating them from each other. The voids are occupied by the $[BF_4]^-$ anions. Not all butyl substituents of the cations in **1b** could be refined due to their heavy positional disorder.

For the same reason, neither the organic cations nor the methyl groups could be refined in **1c** and **1d**. In **1e** and **1f** some of the methyl groups could be identified, but the position of the organic cations could not be refined. However, the unprecedented methylation of the terminal S atoms in **1** has a notable impact on the cluster structure, as it leads to an elongation of the terminal Sn–S bonds (2.402–2.602 Å compared to the purely inorganic analogs (2.355–2.374 Å).[18] In turn, the respective Sn atoms are pushed towards the cluster center, with Sn–O distances between 2.418–2.775 Å, which are smaller than in the purely inorganic structures (2.604–2.713 Å). Consequently, the (μ-S)–Sn–(μ-S) bond angles are relatively more obtuse (114.86(19)–118.55(16)°), while the (μ-S)–Sn–S(Me) angles are relatively more acute. The Sn–S–C angles possess typical values of 98.5(8)–100.5(7)°.

In compound **1c**, 136 cluster anions are located in the unit cell, being arranged in pseudo-tubes along the [101] direction. In contrast, the unit cell of **1d** comprises eight anions only. In these two compounds, the cations could not be detected by single crystal X-ray diffraction due to positional disorder (as often observed for cations in the literature),[20,10]

To confirm the existence of the terminal methyl groups, crystals of **1a**–**1f** were investigated by Raman spectroscopy. The characteristic bands of the lattice vibrations of the oxothiostannate cluster core (most intensive bands at approximately 175, 320-330, and 350 cm^{-1}) show a slight red-shift in comparison to the values reported for the non-methylated cluster (ca. 193, 327, 336, 357 and 385 cm^{-1}).[19]

Table 1   Crystallographic details and relevant bond lengths in the oxothiostannate clusters of compounds **1a** – **1f**.

compound	**1A**	**1B**	**1C**	**1D**	**1E**	**1F**
crystal color & shape	colorless rods	colorless plates	colorless trigonal plates	colorless octahedra	colorless blocks	colorless blocks
space group	*Pbcm*	P$\bar{1}$	Fd$\bar{3}$m	Fd$\bar{3}$m	I$\bar{4}c_2$	P6$_3$/mmc
a,b,c /Å	17.727(4)	13.1046(5)	73.537(3)	27.266(11)	29.1874(4)	18.9987(7)
	35.611(7)	21.8727(10)			29.1874(4)	18.9987(7)
	31.733(6)	27.9377(12)			57.5222(14)	31.8798(11)
α,β,γ /°		79.966(4)				
		79.823(3)				
		84.995(3)				
V /Å^3	20032(7)	7748(1)	397665(49)	20270(25)	49003(2)	9966(1)
Z	8	4	136	8	24	4
Sn–S$_{term.}$ /Å^3	2.435–2.457	2.422–2.470	2.446–2.602	----	2.402–2.463	2.431–2.531
Sn$_{term}$–O /Å^3	2.421–2.536	2.418–2.496	2.502–2.775	-----	2.457–2.509	2.473–2.503

COMMUNICATION
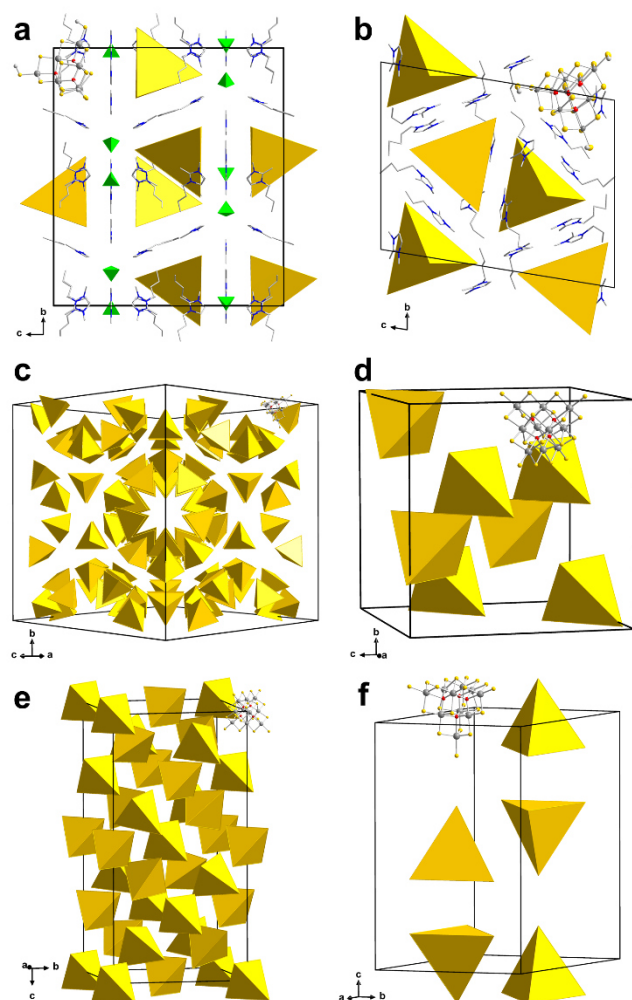
Figure 2. Sections of the crystal strutures of **1a** (a), **1b** (b), **1c** (c), **1d** (d), **1e** (e) and **1f** (f). $[Sn_{10}S_{16}O_4(S–Me)_4]^{4-}$ anions are shown as yellow tetrahedra, green tetrahedra represent $[BF_4]^-$ anions. Counterions are shown as wires. Color code: grey - Sn, yellow - S, red - O, white - C, blue - N.

Figure 3. Raman spectrum of compound **1c**, measured on suspension of single crystals in NVH® oil (the small signals (+) are caused by the oil).

One additional band is observed at 698 cm^{-1}, which is missing in the vibrational spectrum of the purely inorganic cluster anion. This can be assigned to the symmetric valence vibration of the S–C$_{Me}$ bond. This can be assigned to the symmetric valence vibration of the S–C$_{Me}$ bond. Furthermore the signal of the symmetric valence vibration of the C$_{Me}$–H bond can be found at 1515 cm^{-1}. Another signal group, assigned to the imidazolium counter ion, is located between 2850 and 3000 cm^{-1}. A characteristic splitting of this signal is observed in all four spectra, which proves the presence of imidazolium groups as cations in these compounds. Vibrations of the tetrafluoroborate anions (in **1a**) could not be identified. Figure 3 shows the spectrum of compound **1c** as an example; a full set of spectra of **1a** – **1f** is provided in the ESI.‡

Compounds **1a** – **1f** contribute to the rare examples of crystalline sulfides gained from ionic liquids. Further examples are $(C_2C_1Im)_3[Re_3S_4Br_9]Br$,[21] various nickel thiophosphate compounds,[7] and several compounds containing supertetrahedral clusterions like $[Cu_5Tr_{30}S_{52}X_{4-n}(C_4Im)_n]^{(13-n)-}$ (Tr= Ga,In; X= SH/Cl).[22] To explore whether the observed, unprecedented methylation occurrs only due to the presence of more nucleophilic sulfide ligands, or whether it can also occur to other chalcogenidometalates under the given reaction conditions, we investigated syntheses of related selenidometalates and telluridometalates as well.

Compound **2** crystallizes in the trigonal crystal system (space group $R\bar{3}$) with six formula units within the unit cell. **2** contains the molecular anion $[Mn_4Sn_4Se_{13}(Se–Me)_4]^{6-}$, which is the first known methyl derivative of the otherwise well-known $[Mn_4Sn_4Se_{17}]^{10-}$ pentasupertetrahedral P1 cluster anion.[23-25] This type of anion consists of a $[SeMn_4]$ tetrahedral cluster core, where each face of the tetrahedron is capped by a $[SnSe_4]$ tetrahedron. Based on according experiments in solution, it was assumed that such cluster anions are not nucleophilic enough to be alkylated. This seems not to be the case under ionothermal conditions, which allows the methylation of the terminal chalcogen atoms. As discussed for compounds **1a** – **1f**, the methylation affects the bond lengths within the cluster anion: the bond between the Sn atom and the former terminal Se atom is elongated (around 0.05 Å), while unlike **1a** – **1f**, all other bonds are unaffected (Figure 4). For further information on the bond lengths see ESI.‡

Above each edge of the supertetrahedra, one (dmmpH)$^+$ (dmmp = 2,6-dimethylmorpholine) cation is located. The posi-

tions of the H atoms in the crystal structure have been calculated such that opposite μ-Se atoms are connected by N–H···Se hydrogen bonds (2.5574(12)–2.8760(8) Å, Figure 1c). The cluster anions are arranged in {110} in pairs and twisted against each other. Their center of gravity is located at $nb/3$ ($n = 1,2$); two adjacent anion pairs are shifted by $c/3$. The anions possess the same orientation along a and b and are twisted along c, as illustrated in Figure 4 with simplified tetrahedral representation. The cations are located along the tetrahedral faces in between the clusters.

Both, **2** (orange crystals), comprising the inorganic-organic hybrid P1 cluster anion, and $[Cs_{10}(H_2O)_{15.5}][Mn_4Sn_4Se_{17}]$ (red crystals), comprising the purely inorganic *P*1 cluster anion, were investigated by UV-Vis spectroscopy (Figure S6). The band gaps E_g of these two compounds, and their comparison with the value reported for the related Na^+ salt $[Na_{10}(H_2O)_{34}][Mn_4Sn_4Se_{17}]$ (yellow to orange crystals)[23] and K^+ salt $[K_{10}(H_2O)_{16}(MeOH)_{0,5}][Mn_4Sn_4Se_{17}]$ (orange to red crystals),[24] shows that the E_g value of **2** (2.18 eV) is positioned between the one for the Cs^+ salt (1.92 eV) and those ones for the Na^+ (2.3 eV) and K^+ salts (2.27 eV). This correlates with the crystal colors.
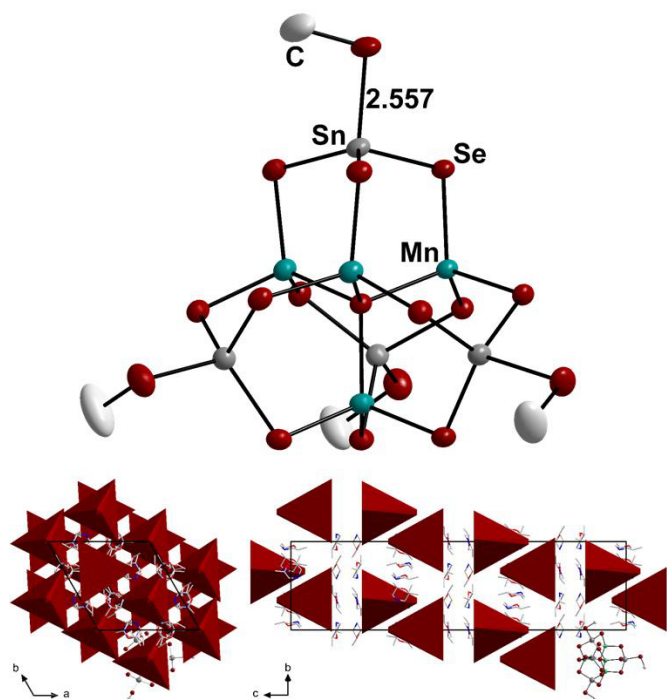
Figure 4. Molecular structure of the anion in **2**, with specification of the bond lengths (top). N–H···Se bridges (dark red) between the protons of the (dmmpH)+ cations and the cluster anion in **2** (top right). H atoms bonded to a C atom are omitted for clarity. Arrangement of the cluster anions (in polyhedral representation) in the unit cell of **2** (bottom), viewed along the crystallographic *a* and *c* axes (left and right, respectively). Color code: grey – Sn, dark red – Se, teal – Mn, red – O, blue – N, white – C.

Several reasons can be used for justification of the E_g values. The compounds differ in their counter ions. For the mentioned hydrate salts a blue shift from the Cs^+ salt to the Na^+ salt in literature is observed, due to the increasing amount of crystal water with increasing charge density of the cation. This causes an expansion of the crystal structure. The same effect might be caused by the presence of a protonated amine as counter ion

which might be a reason for the blue shift. Which has to be considered as well are the different charges in the methylated (–6) and the inorganic (–10) cluster anions. This results in a blue shift as mentioned in literature for $[Cu_5Ga_{30}S_{52}X]^{n-}$ for different kinds of cluster corners (E_g = 3.08 eV (X = $(SH)_4$, n = –13), 3.62 eV (X = $(SH)_{1,5}Cl(C_4Im)_{1,5}$, $n = –11.5$ (C_4Im = 1-Butyl-2-methylimidazole)) and 3.68 eV (X = $(SH)_2(C_4Im)_2$, $n = –11$)). At last differences in packing density of the crystal structures can cause different excitation energies.[17]

$(C_6C_1Im)_6[Hg_6Te_{10}(Te–Me)_2]$ (**3a**) and $(C_8C_1Im)_6[Hg_6Te_{10}(Te–Me)_2]$ (**3b**) both crystallize in the triclinic crystal system (space group $P\bar{1}$) with one formula unit per unit cell. They are the respective imidazolium salts of the dimethylated molecular anion $[Hg_6Te_{10}(Te–Me)_2]^{6-}$. Methylation of the cluster occurred in-situ during its formation under mild ionothermal conditions. This indicates a significant nucleophilicity of highly charged telluridometalate anions. Additionally, the anion bears two ditelluride ligands. These are formed through partial oxidation of the starting material in-situ by residues of oxygen in the ionic liquid or by the ionic liquid itself, a phenomenon we recently reported on.[16] The unprecedented hexanuclear telluridomercurate anion has C2 symmetry and comprises four tetrahedral [HgTe$_4$] and two trigonal planar [HgTe$_3$] units. As illustrated in Figure 5, each half of the anion is built by two edge-sharing [HgTe$_4$] tetrahedra. These are connected to another Hg atom on the outer side by two μ-bridging Te atoms – one from each [HgTe$_4$] tetrahedron – forming the trigonal planar [HgTe$_3$] fragment which is completed by a terminal methyltelluride ligand. On the inner side both halves of the anion are connected by two μ-bridging Te atoms and two $\mu_4,\eta^2:\eta^2$-bridging ditelluride units. All atoms including the terminal methyl groups are arranged nearly planarly except for the two ditelluride units, which are located above and below the plane formed by the remaining Hg and Te atoms. The central unit of the anion is also found in a tetranuclear telluridomercurate anion $[Hg_4Te_{12}]^{4-}$,$[Hg_4Te_{12}]$ in which a tritelluride ligand is substituted for the terminal [HgTe$_3$] unit. The Hg–Te bond lengths between Hg and μ-bridging Te atoms are in the range of 2.656(6)–2.713(9) Å, while those between Hg atoms and μ-bridging Te$_2$ units are slightly larger with 2.935(1)–2.962(1) Å. These values accord well with those found in $[Hg_4Te_{12}]^{4-}$ anions (Hg– (μ-Te) 2.686(1)–2.717(3) Å; Hg– (μ-Te$_2$) 2.925(4)–3.041(2) Å). The Te–Hg–Te bond angles at the tetrahedrally coordinated Hg atoms of 92.01(2)°–125.53(17)° match those of the $[Hg_4Te_{12}]^{4-}$ anions closely (Te–Hg–Te 90.68(2)°–138.31(3)°). Hence, substitution of the terminal tritelluride for the [HgTe$_3$] fragment does not affect the tetranuclear core. The trigonal planar [HgTe$_3$] unit is distorted with enlarged Te–Hg–Te angles between the μ-Te atoms of 136.16(17)–137.08(3)° to provide a sufficiently wide bite angle in coordination of the inner Hg atoms. Therefore, the Te–Hg–Te bond angles towards the terminal Me–Te group are reduced to 103.83(26)–119.67(13)°. The Hg–Te distances towards the methylated Te atom are in the range of 2.767(7)–2.812(7) Å. Thus, they are marginally larger compared to non-methylated Te atoms in the trigonal planar coordination of Hg atoms like in $K_4[HgTe_3]\cdot H_2O$ and $Na_2[HgTe_2]$ (2.745(1)–2.778(1) Å).[16,26] The Te–C bond

length of 2.174(34)–2.187(46) Å is fairly typcial (2.184(5)–2.194(4) Å).[27]

The position of the anion in the unit cell is body-centered with its mean plane tilted near ($\frac{3}{2}$11) and (211), respectively. In 5, two Te atoms of the trigonal planar [HgTe3] unit as well as the methyl group are slightly disordered. The imidazolium rings of the cations bearing their positive charge are located in the vicinity of the anions compensating their charge and separating the anions. The respective hexyl and octyl chains are heavily disordered in both **3a** and **3b**. Still, a heterogeneous arrangement of the alkyl chains between the anions can be noticed as they are located mostly above and below the anions in direction of the crystallographic *c* axis. Hence, ironic layers of tilted anions and imidazolium cations are formed in the *ab* plane, which are shielded by alkyl chains in direction of the *c* axis as shown in Figure 5 (bottom). Due to their shorter chain length, a distinct lamellar structure as found in the mercurate $(C_{10}C_1Im)[Hg_8Te_{16}]$ obtained from the same precursor, is not formed.[28]
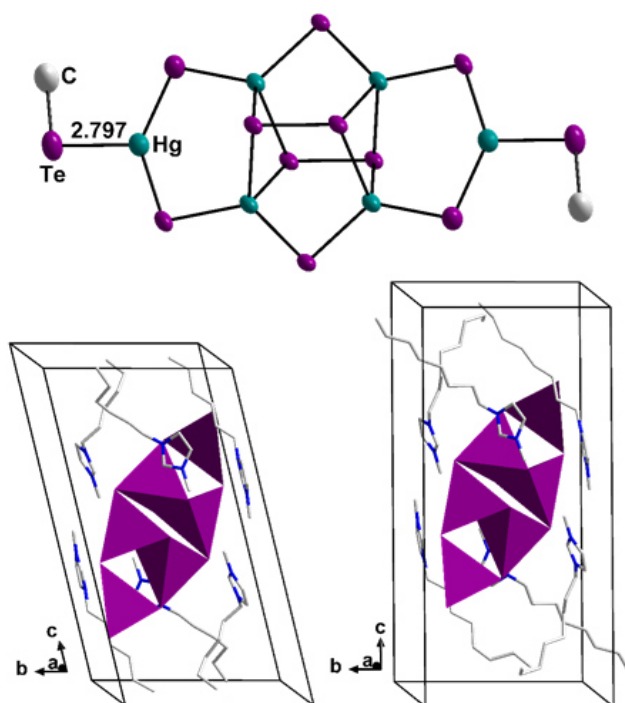
Figure 5. Molecular structure of the $[Hg_6Te_{10}(Te–Me)_2]^{6-}$ anions in **3b** (top). Thermal ellipsoids are drawn at the 50 % probability level. H atoms are omitted for clarity. Sections of the crystal structures of **3a** (bottom left) and **3b** (bottom right). The cations are represented as wires and H atoms are omitted for clarity. The anion is represented only as coordination polyhedra of its Hg atoms. Color code: teal - Hg, violet - Te, white - C, blue - N).

In conclusion, we presented the products of a rather peculiar side-reaction occurring in ionothermal syntheses involving tri(/di)alkylimidazolium based ionic liquids – the demethylation of the imidazolium cation. In a series of different ionothermal reactions of chalcogenido metalate precursors with examples for S, Se and Te, the in-situ formation of methylated metalate anions is achieved. The respective sulfido metalate products are different salts of the oxothiostannate cluster $[Sn_{10}S_{16}O_4(S-Me)_4]^{4-}$ (**1a–1f**). Their methylation has been confirmed by Raman spectroscopy. In **2**, methylation of a ternary *P*1-type selenido metalate cluster ($[Mn_4Sn_4Se_{13}(Se-Me)_4]^{6-}$) is oberved. The

tellurido metalate species **3a** and **3b** are both salts of the same hexanuclear anion $[Hg_6Te_{10}(Te-Me)_2]^{6-}$ which is unique as its non-methylated analog has not been found yet. These results point towards a significant nucleophilicity of chalcogenido metalate clusters which may open access to new strategies in the functionalization of chalcogenido metalates which will be the scope of future investigations.

Conflicts of interest

There are no conflicts to declare.

Notes and references

‡ Electronic Supporting Information (ESI) provide details on syntheses, experimental methods, crystallographic data, Raman spectra of compounds **1a** – **1f** and the UV-Vis spectrum of compound **2**.

§ In the formulae, $(C_m(C_n)C_oIm)^+$ denote tri(/di)-alkylated imidazolium cations, with n, m and o specifying the chain lengths of the alkyl substituents in the respective 1, 2 and 3 positions of the imidazole ring; X = [BF$_4$], Cl.

§§ en = 1,2-diaminoethane, dmmp = 2,6-dimethylmorpholine.

1 S. Santner, J. Heine. S. Dehnen, *Angew. Chem.* **2016**, *128*, 886–904.

2 Z. Wang, C.-F. Du, C.-C. Cheng, N.-N. Shen, J.-R. Li, X.-Y. Huang, *Inorganic Chemistry Communications* **2016**, *74*, 58–61.

3 Y. Lin, S. Dehnen, *Inorg. Chem.* **2011**, *50*, 7913–7915.

4 J.-R. Li, Z.-L. Xie, X.-W. He, L.-H. Li, X.Y. Huang, *Angew. Chem. Int. Ed.* **2011**, *50*, 11395 –11399.

5 Y. Lin, D. Xie, W. Massa, L. Mayrhofer, S. Lippert, B. Ewers, A. Chernikov, M. Koch, S. Dehnen, *Chem. Eur. J.* **2013**, *19*, 8806 –8813

6 H. Sakamoto, Y. Watanabe, T. Saito, *Inorg. Chem.* 2006, 45, 4578–4579.

7 J. A. Cody, K. B. Finch, G. J. Reynders III, G. C. B. Alexander, H. G. Lim, C. Näther, W. Bensch, *Inorg. Chem.* 2012, 51, 13357 – 13362.

8 W.-W. Xiong, J.-R. Li, B. Hu, B. Tan, R.-F. Li, X.-Y. Huang, *Chem. Sci.* **2012**, *3*, 1200–1204.

9 S. Santner, S. Dehnen, *Inorg. Chem.* **2015**, *54*, 1188–1190.

10 S. Santner, S. Yogendra, J. J. Weigand. S. Dehnen, *Chem. Eur. J.* **2017**, *23*, 1999-2004.

11 S. Dehnen, S. Santner, M. Finze, J. Sprenger, Chem. Eur. J. 2018, 24, 3474–3480.

12 Y. Lin, S. Dehnen, Inorg. Chem. 2011, 50, 7913–7915

13 W. Schiwy, S. Pohl, B. Krebs, *Z. Anorg. Allg. Chem.* **1973**, *402*, 77–86.

14 T. Kaib, S. Haddadpour, M. Kapitein, P. Bron, C. Schröder, H. Eckert, B. Roling, S. Dehnen, *Chem. Mater.* **2012**, *24*, 2211–2219.

15 S. Dehnen, M. K. Brandmayer, *J. Am. Chem. Soc.* **2003**, *125*, 6618–6619.

16 C. Donsbach, S. Dehnen, *Z. Anorg. Allg. Chem.* **2017**, *643*, 14-19.

17 W.-W. Xiong, J.-R. Li, B. Hu, B. Tan, R.-F. Li, X.-Y. Huang, *Chem. Sci.* **2012**, *3*, 1200–1204.

18 T. Kaib, M. Kapitein, S. Dehnen, *Z. Anorg. Allg. Chem.* 2011, *637*, 1683-1686.

19 W. Schiwy, B. Krebs, *Angew. Chem.* 1975, *87*, 451-452.

20 a) X. M. Zhang, D. Sarma, Y. Q. Wu, L. Wang, Z. X. Ning, F. Q. Zhang, M. G. Kanatzidis, *J. Am. Chem. Soc.* **2016**, *138*, 5543 –5546; b) Q. Lin, X. Bu, C. Mao, X. Zhao, K. Sasan, P. Feng, *J. Am. Chem. Soc.* **2015**, *137*, 6184 –6187; c) J. Lin, Q. Zhang, L. Wang, X. Liu, W. Yan, T. Wu, X. Bu, P. Feng, *J. Am. Chem. Soc.* **2014**, *136*, 4769 –4779; d) T. Wu, Q. Zhang, Y. Hou, L. Wang, C. Mao, S.-T. Zheng, X. Bu, P. Feng, *J. Am. Chem. Soc.* **2013**, *135*, 10250–10253.

21 H. Sakamoto, Y. Watanabe, T. Saito, *Inorg. Chem.* **2006**, *45*, 4578–4579.

22 W.-W. Xiong, J.-R. Li, B. Hu, B. Tan, R.-F. Li, X.-Y. Huang, *Chem. Sci.* **2012**, *3*, 1200–1204.

23 E. Ruzin, C. Zimmermann, P. Hillebrecht, S. Dehnen, *Z. Anorg. Allg. Chem.* **2007**, *633*, 820–829.

24 M. K. Brandmayer, R. Clerac, F. Weigend, S. Dehnen, *Chem. Eur. J.* **2004**, *10*, 5147–5157.

25 S. Santner, S. Dehnen, *Inorg. Chem.* **2015**, *54*, 1188–1190.

26 G. Thiele, C. Donsbach, R. Riedel, M. Marsch, K. Harms, S. Dehnen, *Dalton Trans.* **2016**, *45*, 5958–5967.

27 J. Ścianowski, A. J. Pacuła, A. Wojtczak, *Tetrahedron: Asymm.* **2015**, *26*, 400–403.

28 C. Donsbach, K. Reiter, D. Sundholm, F. Weigend, S. Dehnen, *Angew. Chem. Int. Ed.* **2018**, *57*, DOI: 10.1002/anie.201803233, *im Druck*; *Angew. Chem.* **2018**, *129*, DOI: 10.1002/ange.201803233, *im Druck*.

4. Zusammenfassung und Ausblick[*]

Im Rahmen dieser Arbeit sollten ionothermale Synthesemethoden aus dem Bereich der Chalkogenidotetrelate auf neue Verbindungen, insbesondere Chalkogenidomerkurate, übertragen und dabei weiterentwickelt werden. Das Ziel war nicht nur die Synthese neuer Materialien, sondern auch die Erweiterung der Kenntnisse über die Reaktivitäten und Abläufe in ionothermalen Reaktionen.

Neben Synthesen in ionischen Flüssigkeiten (ILs) wurden hierbei auch Hochtemperatur-Festkörperreaktionen und solvothermale Reaktionen in Aminen durchgeführt. Dies geschah mit dem Ziel, neue Chalkogenidomerkurate darzustellen um das Spektrum an Ausgangsverbindungen für die ionothermalen Untersucherungen zu erweitern. Außerdem ermöglichte dies einen Vergleich der Reaktivitäten der Verbindungen in konventionellen Lösungsmitteln und ionischen Flüssigkeiten. So lieferten die aminothermalen Untersuchungen neuer Mischungen im ternären System Cs/Hg/Se eine Reihe neuer Cäsiumselenidomerkurat-Verbindungen (**1[3.4]**, **2[3.4]**, **3[3.4]**, **4[3.4]**).

Zwei wichtige Parameter, deren Einfluss auf den Ablauf ionothermaler Reaktionen untersucht wurde, sind die Reaktionstemperatur und die Dauer des Erhitzens. Während die Reaktionen von Selenidotetrelaten in Imidazolium-basierten ILs im Temperaturbereich zwischen 120 und 150 °C bei Heizdauern von 3–4 Tagen gute Ergebnisse liefern, zeigte sich bei Reaktionen des Telluridomerkurats **1[3.3]** über 100 °C eine vermehrte Zersetzung der ternären Präkursoren unter Abscheidung von binärem HgTe. Stattdessen werden hierbei bereits nach 12–24-stündigem Erwärmen auf moderate 60–80 °C kristalline Telluridomerkurat-Salze (**2[3.3]**, **3[3.3]**, $(C_{10}C_1Im)_8$**1[3.5]**, $(C_{12}C_1Im)_8$**1[3.5]**, **3a[3.8]**, **3b[3.8]**) erhalten. Dabei wurde außerdem eine partielle Oxidation der Tellurid-Liganden im Produkt beobachtet, entweder durch Verunreinigungen in der IL oder durch Bestandteile der IL selbst. Dieses Phänomen trat bei allen ionothermalen Reaktionen von Telluridomerkuraten auf. Ein Ziel weiterführender Arbeiten zur ionothermalen Synthese von Telluridomerkuraten sollte die Entwicklung nicht oxidierender Bedingungen sein.

Anhand der Reaktion des Telluridomerkurats **1[3.3]** in 1-Alkyl-3-Methylimidazolium-basierten ionischen Flüssigkeiten mit Kationen unterschiedlicher Kettenlänge konnte unter anderem ein deutlicher Templateffekt der IL-Kationen beobachtet werden. Während in ILs mit Kationen kurzer Kettenlänge (Butyl-Rest) ein einkerniges Anion (**2[3.3]**) oder eines mit einer eindimenisional ausgedehnten Strangstruktur (**3[3.3]**) stabilisiert werden kann, wird

---

[*] In diesem Kapitel werden alle Verbindungen mit der Nummerierung ihrer jeweiligen Originalpublikation referenziert. Um Dopplungen auszuschließen, wird dieser die Nummer des der jeweiligen Publikation zugeordneten Kapitels in eckigen Klammern nachgestellt.

bei IL-Kationen mittlerer Kettenlänge (Hexyl- oder Octy-Rest), ein sechskerniges Telluridomerkurat-Anion gebildet (**3a[3.8]**, **3b[3.8]**). Bei größeren Kettenlängen der IL-Kationen (Decyl- oder Dodecyl-Rest) ist die Bildung eines achtkernigen Anions mit einer außergewöhnlichen Porphyrin-artigen Struktur (**1[3.5]**) zu beobachten, dessen Salz eine lamellare Struktur aufweist. Die Synthese weiterer Chalkogenidometallate mit lamellarer Struktur und deren Exfoliation zur Herstellung neuer 2D-Materialien könnte ein vielversprechendes Ziel künftiger Studien sein.

Diese Untersuchungen offenbarten außerdem zweimal ein ungewöhnliches reaktives Verhalten der Imidazolium-Kationen der ILs. Bei der Reaktion des Telluridomerkurats **1[3.3]** in ILs mit 1-Hexyl-3-Methylimidazolium- und 1-Methyl-3-Octylimidazolium-Kationen wurde eine Methylierung der terminalen Tellurid-Liganden des Produktanions durch die IL-Kationen beobachtet (**3a[3.8]**, **3b[3.8]**). Imidazolium-Kationen können jedoch nicht nur Methylgruppen übertragen, sondern auch leicht unter Bildung eines *N*-heterocyclischen Carbens (NHC) an Position 2 des Imidazoliumrings deprotoniert werden, wie die Entstehung der Telluron-Komplexe **1[3.6]** und **2[3.6]** zeigt. Beide hier beschriebenen Reaktionsmöglichkeiten von Imidazolium-Kationen sind bereits bekannt, allerdings wurde zuvor noch nie die Methylierung eines Chalkogenidometallats oder die *in-situ*-Bildung eines Tellurons in ILs beobachtet. Die im Zuge ihrer Methylierung beobachtete Nukleophilie der Clusteranionen könnte eine Möglichkeit zur organischen Funktionalisierung molekularer Chalkogenidometallate bieten. Die Präsenz von Carbenen in Imidazolium-basierten ILs und ihr potentieller Einfluss in ionothermalen Reaktionen mit Chalkogenidometallaten sollten künftig ebenfalls genauer betrachtet werden. Aufgrund der beobachteten Reaktivität Imidazolium-basierter ILs könnte auch ein genereller Wechsel der verwendenten ILs hin zu solchen mit vermeintlich weniger reaktiven Kationen wie etwa Pyrrolidinium- oder Pyridinium-Kationen in Erwägung gezogen werden, was jedoch die Gefahr stark veränderter Reaktivitäten birgt, die eine Übertragung der bislang in Imidazolium-basierten ILs gewonnenen Erkenntnisse erheblich erschweren könnte.

Neben der Variation der Alkylkette von Imidazolium-Kationen wurden im Zuge dieser Arbeit ILs mit neuartigen Hydrogenchalkogenid-Anionen untersucht. Diese Anionen zeigten interessante Reaktivitäten in ionothermalen Reaktionen mit Selenidomerkuraten. In einer Hydrogensulfid-basierten IL wurde ein temperaturabhängiger Chalkogenaustausch zwischen dem Merkurat und der IL beobachtet (**2[3.1]**, **3[3.1]**, **4[3.1]**), was eine Feinabstimmung der optischen Absorptionseigenschaften der Produkte erlaubt. Außerdem gelang mithilfe dieser IL die Synthese des Merkurats **1[3.1]**, dessen Schwefel-Analogon bislang nur bei deutlich höheren Temperaturen im Polychalcogenid-Flux erhalten werden konnte. Darüber hinaus wurde hierbei bislang kein

Kationenaustausch der Alkalimetall-Kationen der Edukte gegen IL-Kationen beobachtet. Die Möglichkeiten einer Niedertemperatur-Alternative zu Polychalkogenid-*Flux*-Synthesen und einer effizienten Synthesemethode für fein abstimmbare optoelektronische Materialien machen diese ILs zu einem vielversprechenden Reaktionsmedium. Zukünftige Studien auf diesem Gebiet sollten versuchen, die gefundenen Synthesemethoden auf andere Metallate zu übertragen und Strategien zur Rückgewinnung solcher reaktiver ILs nach der Reaktion zu entwickeln.

Durch den ionothermalen Abbau eines Selenidomerkurats mit ausgedehnter Netzwerkstruktur (Top-Down-Ansatz) konnte ein neuartiges molekulares Anion (**1[3.7]**) synthetisiert werden. Durch Kombination molekularer Selenidostannat-Vorläufer sowohl mit molekularen Selenidomerkuraten (Bottom-Up-Ansatz) als auch solchen mit ausgedehnter Netzwerkstruktur (gemischter Top-Down-Bottom-Up-Ansatz) konnten Salze mit komplexen ternären Anionenstrukturen dargestellt werden (siehe Appendix 6.5 Weitere Strukturen). Die vollständige Bestimmung der Kristallstrukturen dieser Verbindungen steht derzeit noch aus. Aufgrund der positiven bisherigen Ergebnisse sollten die Untersuchungen zur Synthese ternärer Strukturen im System Hg/Sn/Se weitergeführt werden.
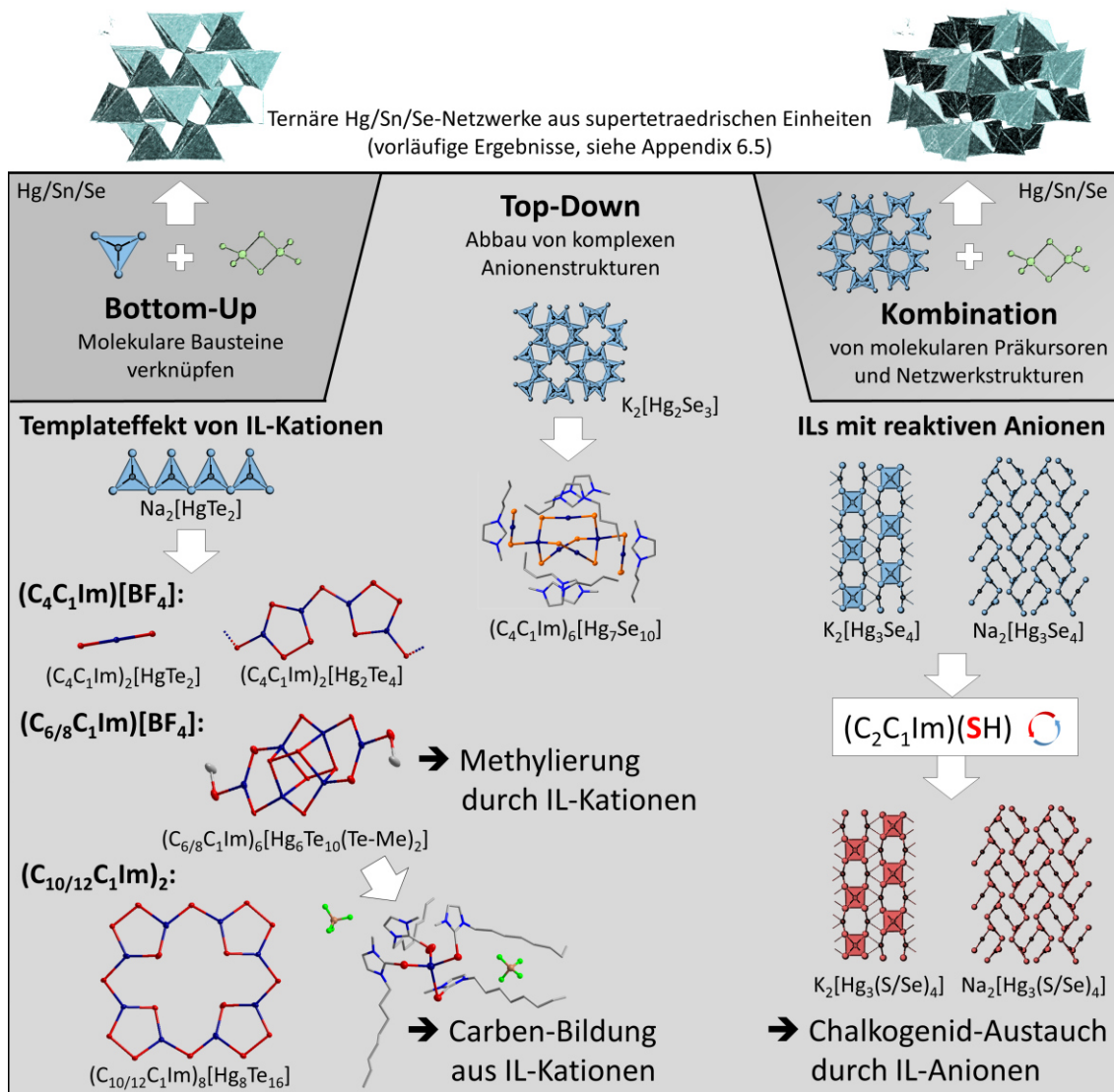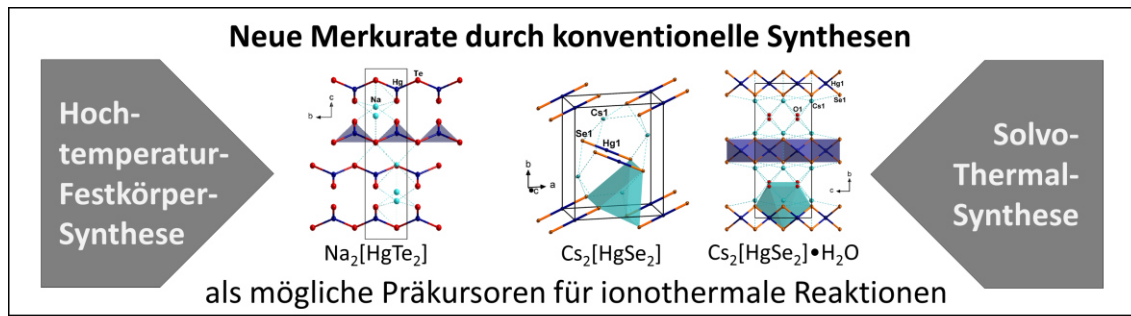
Abbildung 8: Überblick über die in dieser Arbeit präsentierten Reaktionen und Verbindungen. (C_nC_1Im): 1-Alkyl-3-Methylimidazolium, *n* gibt die Anzahl der C-Atome im Alkylrest an.

5. Summary and Outlook[†]

The aim of this work was the transfer of synthetic methods from the ionothermal syntheses of chalcogenido tetrelates to new compounds, especially chalcogenido mercurates, as well as further development of the methods. Beside the synthesis of new materials, the main focus was to gain a deeper understandung of the reactivities and processes involved in ionothermal reactions.

Additionally, high temperature solid-state reactions and aminothermal reactions were performed in order to obtain novel chalcogenido mercurate phases as precursors for ionothermal treatment. Solvothermal reactions in traditional solvents were continued as part of comparative reactivity studies parallel to the ionothermal ones. During the course of these investigations, a series of new cesium selenido mercurate compounds could be characterized (**1[3.4]**, **2[3.4]**, **3[3.4]**, **4[3.4]**).

Reaction temperature and time are two key parameters in ionothermal syntheses. Hence, their effects on the reaction processes were investigated. While reactions of selenido tetrelates in imidazolium based ionic liquids have yielded good results at temperatures of 120–150 °C and with reaction times of 3–4 days, the tellurido mercurate precursor **1[3.3]** starts to decompose under precipitation of binary HgTe under ionothermal conditions above 100 °C. Instead, crystalline tellurido mercurate salts (**2[3.3]**, **3[3.3]**, $(C_{10}C_1Im)_8$**1[3.5]**, $(C_{12}C_1Im)_8$**1[3.5]**, **3a[3.8]**, **3b[3.8]**) are yielded after short ionothermal treatment for 12–24 hours at only 60–80 °C. In all ionothermal reactions with tellurido mercurates, partial oxidation of the telluride ligands was observed. This oxidation may be ascribed to impurities of the IL or to potential oxidative properties of the IL itself. Continued research in ionothermal synthesis of tellurido mercurates should focus on the development of non-oxidizing conditions.

During the course of these investigations, two cases of unexpected reactivity of IL cations could be observed. By ionothermal treatment of the mercurate **1[3.3]** in ionic liquids with 1-hexy-3-methylimidazolium and 1-methyl-3-octylimidazolium cations, methylation of the terminal telluride ligands was observed in the product anion (**3a[3.8]**, **3b[3.8]**). Another possible side reaction of imidazolium cations is the formation of *N*-heterocyclic carbenes (NHC) upon deprotonation of the imidazolium ring at position 2 as found in the formation of the tellurone complexes **1[3.6]** und **2[3.6]**. The nucleophilicity

---

[†] In this chapter, all compounds are referenced by the numbers given in the original publications. To avoid double draws, the number of the chapter the respective publication is discussed in is added in brackets.

of chalcogenido metalate cluster anions observed in the methylation reaction may provide access to new reaction pathways towards organo-functionalized chalcogenido metalate materials. The presence of carbenes in imidazolium based ionic liquids and their potential effects on ionothermal reactions of chalcogenido metalates should be investigated in future studies. Due to the side reactions observed, a transition to other classes of less reactive ionic liquid cations should be taken into consideration. However, this comes at the risk of unpredictable results as current reaction methods are based on the specific reactivities found in imidazolium based ILs.

In this work, reaction studies involving ILs with novel hydrochalcogenide anions were performed as well. Reactions of selenido mercurates in a hydrosulfide IL showed promising results. A temperature dependent exchange of chalcogen atoms between the mercurate and the IL was observed (**2[3.1]**, **3[3.1]**, **4[3.1]**) enabling fine-tuning of optical absorption properties. Furthermore, the mercurate **1[3.1]** was obtained from this ionic liquid. Its isostructural analogs have only been accessible via *flux* syntheses in molten polychalcogenide salts. These are promising results for potential application of hydrochalcogenide ILs as a low-temperature alternative to *flux* syntheses and as a reactive medium for the efficient synthesis of tunable opto-electronic materials. Future studies should focus on the application of this method to other metalates and potential strategies for the recovery of reactive ILs.

In a top-down approach, ionothermal treatment of a selenido mercurate with a three-dimensional anionic substructure yielded the salt of a novel molecular anion (**1[3.7]**). In further reactions, both the bottom-up and a mixed approach were realized by combination of different metalate precursors, yielding salts with complex ternary anion structures featuring supertetrahedral building units (see Appendix 6.5). Due to promising first results, investigations on the syntheses of ternary metalates of the system Hg/Sn/Se should be continued.
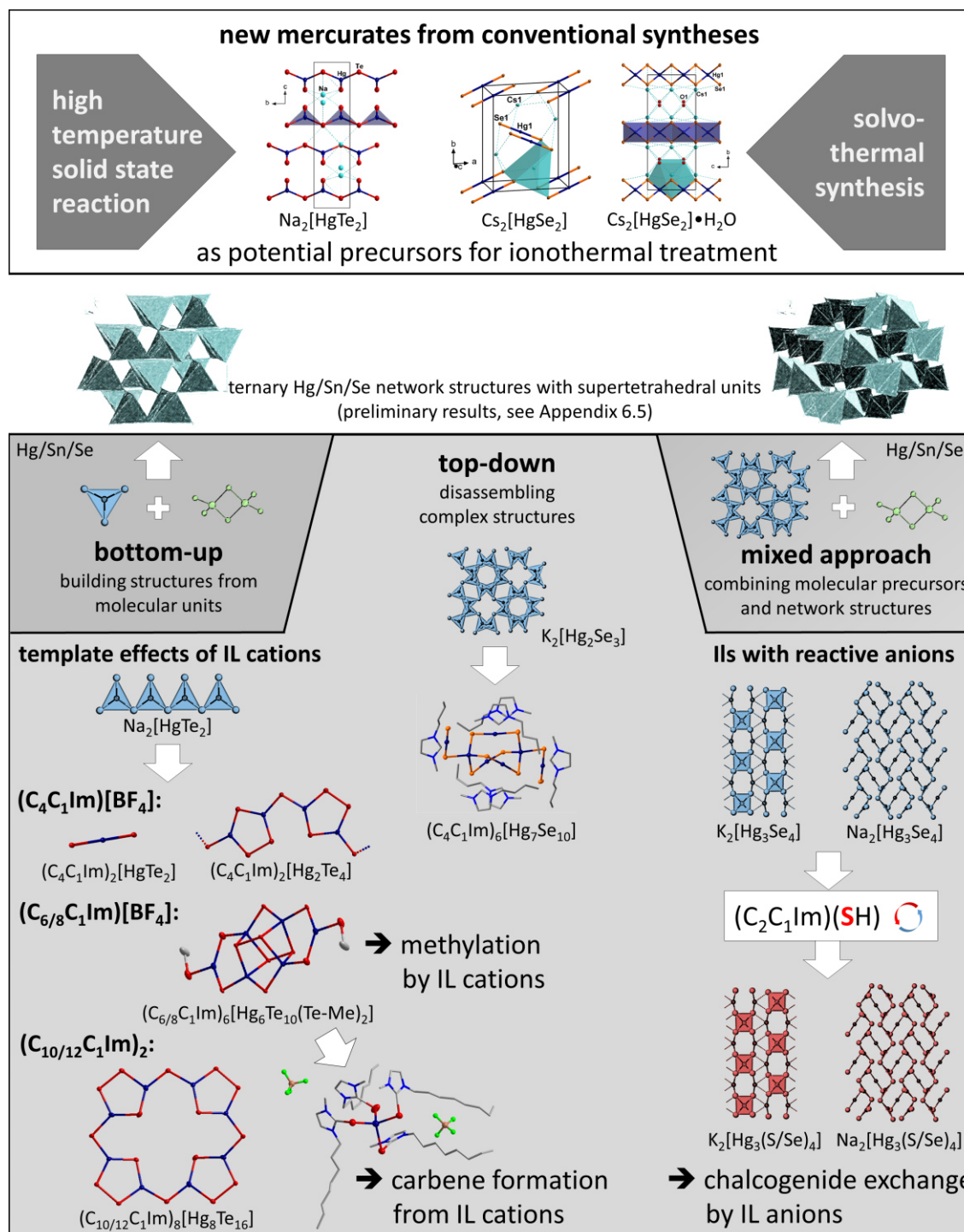
Abbildung 9: Overview of the reactions and structures presented in this work.
(C_nC_1Im): 1-alkyl-3-methylimidazolium, *n* denotes the number of C atoms in the alkyl chain.

6. Appendix

6.1 Abkürzungsverzeichnis

18c6	1,4,7,10,13,16-Hexaoxacyclooctadecan
nD	n-dimenional (n = 0-3)
$(C_k(C_l)C_mIm)X$	IL, bestehend aus einem Imidazolium-Kation und dem Anion X. $C_{k/l/m}$ beschreibt die Alkylsubstitution an den Positionen 1, 2 und 3 des Imidazoliumrings. Die Variablen k, l und m bezeichnen die Anzahl der C-Atome in der jeweiligen Seitenkette.
dmmp	2,6-Dimethylmorpholin
en	1,2-Diaminoethan
IL	ionische Flüssigkeit (engl. ionic liquid), Plural „ILs"
IR	infrarot
Me	Methyl
NMR	Kernspinresonanz (engl. nuclear magnetic resonance)
Pn	pentasupertetraederischer Cluster, n = 1,2,...
Tn	supertetraedrischer Cluster, n = 1,2,...
UV-Vis	optische Strahlung des sichtbaren und ultravioletten Bereichs
µ-XFS	micro-Röntgenfluoreszenz-Spektroskopie

6.2 Manuskript "[Hg$_4$Te$_8$(Te$_2$)$_4$]$^{8-}$: ein Schwermetall-Porphyrinoid in einer lamellaren Struktur" (3.5)

[Hg$_4$Te$_8$(Te$_2$)$_4$]$^{8-}$: ein Schwermetall-Porphyrinoid in einer lamellaren Struktur

$[Hg_4Te_8(Te_2)_4]^{8-}$: ein Schwermetall-Porphyrinoid in einer lamellaren Struktur

Carsten Donsbach, Kevin Reiter, Dage Sundholm, Florian Weigend und Stefanie Dehnen*

Professor Bernt Krebs zum 80. Geburtstag gewidmet

Abstract: *Die Produkte der ionothermalen Behandlung von $Na_2[HgTe_2]$ in ionischen Flüssigkeiten $(C_nC_1Im)[BF_4]$ mit langen Alkylketten (n = 10, 12) weisen lamellare Kristallstrukturen auf, deren molekulare makrocyclische Anionen, $[Hg_8Te_{16}]^{8-}$ (**1**), die schwersten bekannten topologischen Verwandten von Porphyrin darstellen. $[Hg_8Te_{16}]^{8-}$ unterscheidet sich von Porphyrin naturgemäß infolge des fehlenden π-Elektronen-Systems, weshalb auch keine "globale" Aromatizität zu beobachten ist. Quantenchemische Studien belegen jedoch (schwache) Ringströme in den Pyrrol-artigen Fünfringen, was auf das Vorhandensein einer schwachen (σ-)Aromatizität schließen lässt. Aufgrund ihrer lamellaren Natur könnten sich die Verbindungen zur Bildung von Einzelschichten mit solchen Chalkogenidometallat-Anionen eignen.*

Die Dimensionsreduktion von Halbleitermaterialien wird derzeit aktiv betrieben, um deren elektronische Eigenschaften gezielt zu beeinflussen.[1] Zusätzlich zur etablierten Bildung von Nanopartikeln haben inzwischen post-synthetische Methoden wie Stempel- oder Exfolationstechniken an Bedeutung gewonnen.[2] Für die Letztgenannten müssen allerdings zwei Voraussetzungen erfüllt sein: a) das Vorhandensein einer geeigneten Halbleiter-Substruktur und b) relativ schwache Wechselwirkungen zwischen diesen Substrukturen in der Volumenphase. Diese Voraussetzungen sind z. B. bei schichtartigen Elementstrukturen wie im Graphit oder Phosphor erfüllt,[3,4] außerdem in manchen binären Chalkogeniden[5] oder anorganisch-organischen Hybrid-Salzen.[6]

Halbleiter-Nanostrukturen finden sich auch in Chalkogenidometallaten schwerer Metalle, die eine große Vielfalt an Elementzusammensetzungen und Architekturen aufweisen. Hochtemperaturreaktionen führen normalerweise zu dichten Festkörperstrukturen, wogegen Syntheserouten in Lösung die Bildung offenerer Netzwerkstrukturen mit solvatisierten oder organischen Kationen ermöglichen. Die anionischen Substrukturen können hierbei niedrigere Dimensionalitäten aufweisen, bis hinunter zu molekularen Chalkogenidometallat-Einheiten.[7]

Das Überführen Halbleiter-basierter Festkörper in Hybridverbindungen mit schwach wechselwirkenden organischen Kationen gelingt auf elegante Weise durch ionothermale Behandlung anorganischer Chalkogenidometallatsalze.[8] Die dabei entstehenden Substrukturen können sehr ungewöhnlich sein, etwa der Cluster $[Cu_5Ga_{30}S_{52}(SH)_2(C_4C_1Im)_2]^{11-}$ $(C_4C_1Im = 1\text{-Butyl-3-methylimidazolyl})$[9] oder das supersphärische Anion 0D-$[Ge_{24}Sn_{32}Se_{132}]^{24-}$,[10] dessen Bildung stark von der gewählten Temperatur, dem Zusatz von Auxiliaren und der Natur der eingesetzten ionischen Flüssigkeit abhängt.[11]

Ein variabler Parameter ist die Kettenlänge der Alkylsubstituenten am $(C_nC_1Im)^+$-Kation in Imidazolium-basierten ionischen Flüssigkeiten. Für $n = 1$–4 verhalten sich die Kationen weitgehend wie sphärische Kationen, sodass sich ihr strukturdirigierender Einfluss nicht grundlegend von der Variation des Ionenradius atomarer Kationen unterscheidet. Längere Alkylketten hingegen können zur Assemblierung der Kationen führen, wodurch z. B. Fischgrätenanordnungen oder lamellare Strukturen entstehen.[12]

Im Zuge unserer Untersuchungen zur Dimensionsreduktion von Chalkogenidometallaten schwerer Metalle beschäftigen wir uns derzeit mit Substrukturen, die sich formal vom II-VI-Halbleitermaterial HgTe[13] ableiten lassen. Die ionothermale Behandlung von $Na_2[HgTe_2]$ mit eindimensionalen $[\text{-Hg(Te)-Te-}]_n$-Ketten[14] in der kurzkettigen ionischen Flüssigkeit $(C_4C_1Im)[BF_4]$ $(C_4C_1Im = 1\text{-Butyl-3-methylimidazoli-um})$ bei 60 °C führte zur Bildung eines Salzes mit einer anderen eindimensionalen Substruktur, $[\text{-Hg}(\mu\text{-Te})(\mu\text{-Te}_2)\text{-Hg-Te-}]_n$. Darin sind fünfgliedrige Ringe der Zusammensetzung $[Hg_2Te(Te_2)]$ mit Te^{2-}- und $(Te_2)^{2-}$-Liganden (infolge partieller Oxidation von Te^{2-}) enthalten, die über zusätzliche $\mu\text{-Te}^{2-}$-Brücken verknüpft sind (Schema 1, links). Das Salz, das nach dem Einsatz von ionischen Flüssigkeiten mit 1-(Do-)Decyl-3-methylimidazolium-Kationen, $(C_nC_1Im)[BF_4]$ $(n = 10, 12)$ isoliert wird, enthält stattdessen das sehr ungewöhnliche molekulare Anion $[Hg_8Te_{16}]^{8-}$ (**1**; Schema 1, rechts) in einer lamellaren Struktur.

[*] C. Donsbach, Prof. Dr. S. Dehnen
Fachbereich Chemie und Wissenschaftliches Zentrum für Materialwissenschaften (WZMW)
Philipps-Universität Marburg
Hans-Meerwein-Straße 4, 35043 Marburg (Deutschland)
E-Mail: dehnen@chemie.uni-marburg.de

K. Reiter, Priv.-Doz. Dr. F. Weigend
Institut für Nanotechnologie
Karlsruher Institut für Technologie (KIT)
Hermann-von-Helmholtz-Platz 1, 76344 Eggenstein-Leopoldshafen (Deutschland)

Prof. Dr. D. Sundholm
Department of Chemistry, University of Helsinki
P. O. Box 55 (A.I. Virtanens plats 1), 00014 University of Helsinki (Finnland)

Hintergrundinformationen (Synthesen, Einkristall-Strukturuntersuchungen inclusive CIF, Spektroskopie und quantenchemische Studien) und die Identifikationsnummer (ORCID) eines Autors sind unter https://doi.org/10.1002/ange.201803233 zu finden.
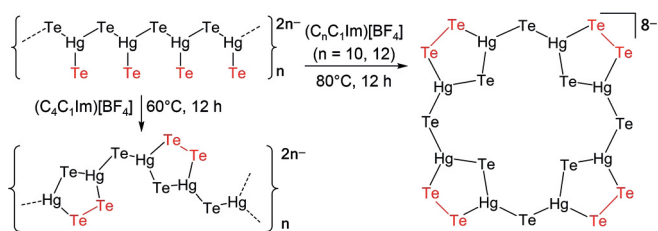
Schema 1. Diagramm des strangartigen Anions in $Na_2[HgTe_2]$ (oben links)[14] und dessen Behandlung in ionischen Flüssigkeiten (C_nC_1Im)-$[BF_4]$, wodurch ein anderer strangartiger Anionentyp in Gegenwart kurzkettiger Alkylimidazolium-Kationen entsteht ($n=4$, unten links),[14] in ionischen Flüssigkeiten mit langkettigen Alkylimidazolium-Kationen ($n=10, 12$; diese Arbeit) hingegen das Anion $[Hg_8Te_{16}]^{8-}$ (**1**).

$(C_{10}C_1Im)_8$**1** kristallisiert in Form dünner, dunkelroter Plättchen mit vier Formeleinheiten pro Elementarzelle in der monoklinen Raumgruppe $P2_1/c$. Die Schweratomzusammensetzung der einkristallinen Verbindung wurde durch mikro-Röntgenfluoreszenzspektroskopie (µ-RFA) bestätigt (Tabelle S11 und Abbildung S5 der Hintergrundinformationen). Volumenanalysen ließen sich wegen der feinen Dispersion der kleinen Kristalle in der hochviskosen ionischen Flüssigkeit nicht durchführen. Aufgrund der hohen Anionenladung ist die Verbindung in gewöhnlichen Lösungsmitteln unlöslich, was jegliche Analytik in Lösung verhindert.

Der anorganische Makrocyclus in **1** wird von vier der oben beschriebenen $[Hg_2Te(Te_2)]$-Fünfringe gebildet, die über vier Te^{2-}-Liganden zu einem cyclischen Tetramer verknüpft werden. Somit ist das Anion **1** strukturell mit organischem Porphyrin verwandt, das vier Methylen-verbrückte Pyrrolringe enthält, wenngleich die Gesamtvalenzelektronenzahlen verschieden sind (120 in **1**, 114 in Porphyrin). **1** ist zudem isoelektronisch zu den $[B_8E_{16}]$-Strukturen von BE_2 ($E=S$, Se),[15] im Unterschied zu diesen jedoch geladen und nicht ganz planar. Abbildung 1 illustriert die Kristallstruktur von $(C_{10}C_1Im)_8$**1**.[36]

Te-verbrückte $[Hg_2Te(Te_2)]$-Motive kennt man aus eindimensionalen Ketten: in den oben erwähnten $(C_4C_1Im)^+$-Salzen,[14] mit den Gegenionen $[N(C_2H_5)_4]^+$, $\{[Mn(en)_3]_2Cl_2\}^{2+}$ oder $[M(trien)(N_2H_4)]^{2+}$ ($M=Mn$, Zn; trien = Triethylentetramin)[16a–c] und mit verknüpfenden Te_2^{2-}-Einheiten.[16d] Sie wurden zudem in molekularen Clustern beobachtet: in $[Hg_4Te_{12}]^{4-}$ sind zwei (gefaltete) $[Hg_2Te(Te_2)]$-Ringe mit zwei $(Te_3)^{2-}$-Liganden verknüpft,[16c,d] und ein ähnliches Motiv findet sich in einer $\{[Hg_5Te_{12}]^{2-}\}_n$-Kette, in der Cluster mit zwei (gefalteten) $[Hg_2Te(Te_2)]$-Ringen über $[HgTe_2(Te_3)]$-Einheiten verknüpft sind.[16d] Ein cyclisches Oligomer wie in **1** war bisher nicht bekannt. Wir führen die gegenüber der Entstehung von 1D-$\{[Hg_2Te_4]^{2-}\}$-Ketten bevorzugte Bildung der $[Hg_8Te_{16}]^{8-}$-Makrocyclen auf die perfekte Einpassung des molekularen Anions in das kationische Templat zurück. Schema S1 zeigt Vorschläge für Bildungsmechanismen.

Die Bindungslängen in **1** [Hg-(μ-Te) 2.692(2)–2.710(1), Hg-(μ:η^1:η^1-Te_2) 2.762(1)–2.803(1), Te-Te 2.728(2)–2.750(1)] stimmen gut mit denen in den 1D-$\{[Hg_2Te_4]^{2-}\}$-Anionen überein [Hg-(μ-Te) 2.654(2)–2.729(5) Å; Hg-(μ:η^1:η^1-Te_2) 2.750(2)–2.807(2) Å; Te-Te 2.736(2)–2.788(3) Å]. Alle Metallatome befinden sich in einer idealisiert trigonal-planaren
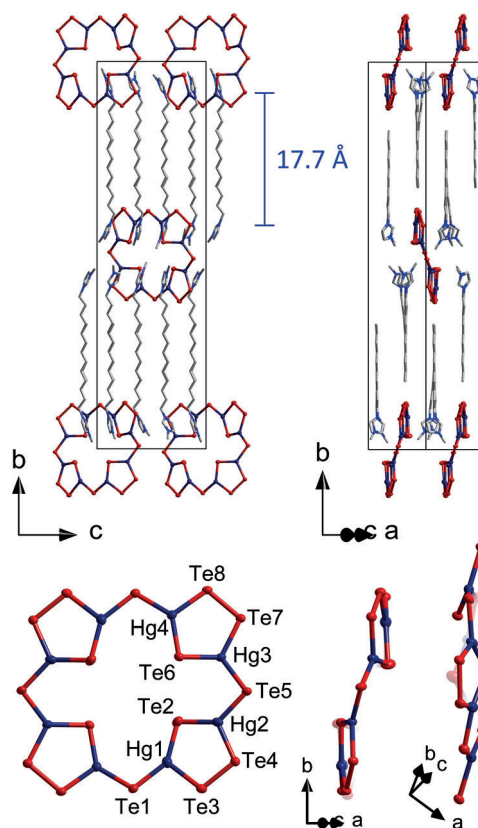
Abbildung 1. Oben: Ausschnitt aus der Kristallstruktur von $(C_{10}C_1Im)_8$**1** in unterschiedlichen Orientierungen. Unten: Molekülstruktur des Anions $[Hg_8Te_{16}]^{8-}$ (**1**) in unterschiedlichen Blickrichtungen (Hg, Te: thermische Auslenkungsparameter mit 50% Wahrscheinlichkeit; C, N: Stab-Darstellung; H-Atome nicht gezeigt). Äußere Durchmesser des Anions: 12.3 Å (Te1⋯Te1′) bis 16.2 Å (Te7⋯Te7′).[36]

Koordinationsumgebung durch drei Te-Atome (Winkelsummen $\geq 359.35(2)°$), aber die individuellen Te-Hg-Te-Winkel überspannen einen weiten Bereich (102.73(4)–142.39(5)°). Die (μ-Te)-Hg-(μ-Te)-Winkel sind hierbei gegenüber denen in den 1D-Strängen etwas stumpfer [116.84(7)–137.12(6)° in den Ketten], die (μ-Te)-Hg-(μ:η^1:η^1-Te_2)-Winkel sind etwas spitzer [105.45(6)–127.73(7)° in den Ketten]. Dies lässt auf eine erhebliche koordinative Flexibilität der Hg-Atome schließen, was eine gute Anpassung an die jeweilige Anordnung der in Größe, Struktur, Polarisierbarkeit und H-Brückenbindungs-Tendenz unterschiedlichen Gegenionen ermöglicht.

Infolge dieser koordinativen Flexibilität der Hg-Atome ist das makrocyclische Anion **1** als Ganzes nicht planar (Abbildung 1, unten rechts). Zur Optimierung der Wechselwirkung mit den Imidazolium-Kationen und der Einpassung in ihre Struktur sind einander gegenüberliegende $[Hg_2Te(Te_2)]$-Ringe um etwa 24.8(1)° aus der mittleren Ebene herausgedreht. Dadurch sind die endocyclischen Te-Atome relativ weit voneinander entfernt (Te⋯Te 7.0808(7)–7.4130(6) Å über das Zentrum von **1** gemessen).

Eine genaue Betrachtung der Kristallstruktur von $(C_{10}C_1Im)_8$**1** zeigt, dass hier eine Segregation in ionische und unpolare Teile vorliegt. Letztere resultieren aus Van-der-Waals-Wechselwirkungen der Decyl-Ketten, die membranar-

↖↖ These are not the final page numbers!

tige, ineinandergeschobene Doppelschichten mit einer Dicke von 17.7 Å bilden (Abbildung 1, oben). Die positiv geladenen Imidazolium-Ringe der Kationen betten die Anionen perfekt ein: Je zwei Imidazolium-Ringe befinden sich in enger Nachbarschaft zu einem der [Hg$_2$Te(Te$_2$)]-Ringe, insgesamt vier aus der Kationen-Schicht oberhalb und vier aus der Kationen-Schicht unterhalb des Anions, wodurch die relativ hohe Anionenladung exakt ausgeglichen wird. Die Imidazolium-Ringe sind hierbei orthogonal zu den [Hg$_2$Te(Te$_2$)]-Einheiten ausgerichtet, was den Anion···Anion-Abstand maximiert. Die zweite Verbindung wurde mit längeren Alkylketten in der ionischen Flüssigkeit erhalten. (C$_{12}$C$_1$Im)$_8$**1** ist isostrukturell zu (C$_{10}$C$_1$Im)$_8$**1**. Wegen nochmals dickerer unpolarer Schichten (20.2 Å; Abbildung S4) sind die Kristalle sehr fragil und von geringer kristallographischer Qualität (siehe Hintergrundinformationen).

Außer der Segregation solcher Kationen in polare/unpolare Bereiche im Festkörper[17] hat man auch in den Flüssigphasen ionischer Flüssigkeiten ähnliche Effekte nanoskaliger Segregationen in Mikrophasen homogener Polarität beobachtet und mittels Moleküldynamik-Simulationen bestätigt.[18,19]

Die Bildung schwerer Homologe gut bekannter Moleküle ist ein faszinierendes Gebiet chemischer Forschung, das Einblicke in den Zusammenhang von intrinsischen Atomeigenschaften und den strukturellen, chemischen und physikalischen Eigenschaften von Molekülen gibt. Zu den prominentesten Beispielen gehören schwere Ethen- und Ethin-Homologe und die zugehörigen, typischen Auswirkungen auf die Molekülstrukturen.[20] Ein anderes, jüngeres Beispiel ist PbSe, das in {[(Ph$_3$P)$_2$Rh][(Ph$_3$P)(CN)Rh]$_2$Se$_2$(μ-PbSe)}$^{3-}$ als CO-artiger Brückenligand auftritt.[21] Besonders hervorzuheben sind rein anorganische topologische Verwandte von organischen Verbindungen – sowohl in isoelektronischer Form als auch unter Toleranz anderer Elektronenzahlen. Viele einfache Moleküle wie das Benzol-analoge Borazin, B$_3$N$_3$H$_6$,[22] oder P$_5^-$ als anorganisches Äquivalent von Cyclopentadienid, Cp$^-$,[23] kennt man seit Jahrzehnten, während komplexere Strukturen viel seltener sind. Abgesehen von den oben erwähnten Porphyrin-artigen Strukturen von BE$_2$ (E = S, Se) wurde kürzlich mit der ternären, halbleitenden Phase SnIP auch eine entfernt an den Bau der DNA erinnernde anorganische Doppelhelix publiziert.[24]

Zur Untersuchung von Gemeinsamkeiten und Unterschieden in der elektronischen Struktur dieses Porphyrinartigen Moleküls zu Porphyrin selbst wurden Methoden der Quantenchemie herangezogen (TURBOMOLE,[25] TPSSh-Funktional,[26] def2-TZVP-Basissätze,[27] Kompensation der negativen Ladung mit COSMO[28] unter Verwendung der Standardwerte). Die Berechnung von Ringströmen erfolgte mit GIMIC[29] auf Grundlage der magnetischen Antwort des Moleküls, die mit einer lokalen Version[30,31] des Programmpakets TURBOMOLE berechnet wurde. Die Ringströme für beide Systeme sind in Abbildung 2 dargestellt.

1 zeigt (schwache) Ringströme in den Pyrrol-artigen Fünfringen. Diese Ströme haben einem diatropen (im Uhrzeigersinn, auf der Außenseite des Rings) und einen paratropen Anteil (gegen den Uhrzeigersinn, auf der Innenseite). Beide Anteile sind von ähnlicher Größe, jedoch mit einem
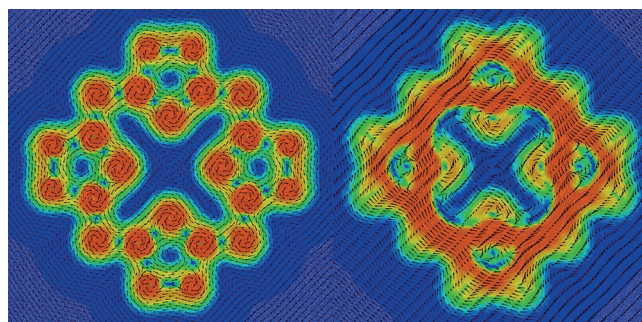
Abbildung 2. Ringströme, 1 bohr oberhalb der Molekülebene des anorganischen **1** (links) und des organischen Porphyrins (rechts), dargestellt zwischen 0 (blau) und 0.07 atomaren Einheiten (rot).

leichten Überhang zugunsten des Erstgenannten, der zu einem Nettostrom von +5.8 nA/T führt. Dies ist dem Betrage nach etwa die Hälfte des Ringstroms im Benzol,[32] aber im Unterschied zum Letztgenannten hat er ausschließlich σ-artige Beiträge. Der Ringstrom durch das Molekül als Ganzes (ebenfalls als Summe dia- und paramagnetischer Beiträge) ist nahe null (0.24 nA/T). Ähnliche Ergebnisse erhält man für die mit **1** verwandten Systeme [B$_8$E$_{16}$] (E = S, Se), allerdings mit noch etwas schwächeren lokalen Strömen (Einzelheiten sind Abbildung S9 zu entnehmen). Im Unterschied hierzu zeigt das organische Porphyrin einen großen globalen Ringstrom von etwa 27 nA/T, der sich in den Fünfringen in zwei Teilströme von jeweils 13 nA/T[32] aufteilt.

Mit diesen Unterschieden in der magnetischen Antwort gehen – bei gleicher Topologie – ebenso deutliche Unterschiede in der elektronischen Struktur einher. Die Aromatizität und die entsprechenden Ringströme des Porphyrins haben ihre Ursache in den delokalisierten π-Elektronen. Auch in **1** findet man delokalisierte Molekülorbitale, allein schon aus Gründen der Symmetrie; die radialsymmetrischen Orbitale (mit s-, p-, d-, f-, g-Charakter) mit der höchsten Energie stellen die σ-Bindungen dar (Abbildung S7). Diese Orbitale können jedoch mithilfe einer Lokalisierungsprozedur ausnahmslos in Zwei-Elektronen-zwei-Zentren-Bindungen und freie Elektronenpaare transformiert werden.[33] Man erhält so zwei freie Elektronenpaare je Te-Atom und jeweils eine σ-artige Einfachbindung zwischen benachbarten Atomen (insgesamt 32 freie Elektronenpaare und 28 Bindungen).

Optische Absorptionsspektren wurden an einem Einkristall von (C$_{10}$C$_1$Im)$_8$**1** aufgenommen (Abbildung 3). Die Absorption setzt demnach bei 2.2–2.8 eV ein, mit einer kleinen Schulter niedriger Intensität bei 2.1 eV. Dies ist in ausgezeichneter Übereinstimmung mit den Ergebnissen zeitabhängiger Dichtefunktionalrechnungen (an **1**), bei denen als niedrigste Anregung der HOMO-LUMO-Übergang bei 2.18 eV gefunden wurde, gefolgt von zwei intensiveren Übergängen bei 2.48 eV (HOMO−4 nach LUMO+3 und LUMO+4). Diese Anregungen sind charakterisierbar als Übergang der Elektronen aus den freien Elektronenpaaren der μ-Te-Atome in die antibindenden Orbitale zwischen benachbarten Te-Atomen. Infolge der Dimensionsreduktion ist die optische Bandlücke naturgemäß von festem HgTe (−0.3 eV)[35] über 1D-[Hg$_2$Te$_4$]$^{2-}$ (1.63 eV)[14] hin zu 0D-

These are not the final page numbers! ↗↗
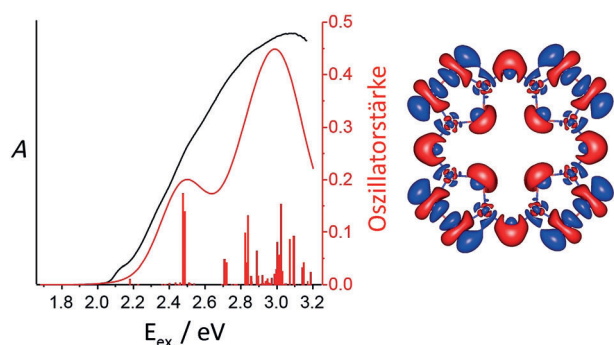
Abbildung 3. Links: Vergleich des an $(C_{10}C_1Im)_8\mathbf{1}$-Einkristallen aufgenommenen optischen Anregungsspektrums (schwarze Linie) mit berechneten Singulett-Anregungsenergien und Oszillatorstärken (niedrigste 250 Anregungen). Diese sind als vertikale Linien dargestellt sowie – zur Simulation des Spektrums – als überlagerte Gaußfunktionen gezeichnet (Halbwertsbreite 0.3 eV; rote Linie). Rechts: räumlicher Charakter der Absorptionsbande in ihrer Gesamtheit (bis 3.0 eV) unter Verwendung nichtrelaxierter Differenzdichten,[34] mit Beiträgen von besetzten Orbitalen in Rot, von unbesetzten in Blau.

$[Hg_8Te_{16}]^{8-}$ (2.16 eV) blauverschoben. Dennoch ist sie relativ schmal, wenn man die Molekülgröße (24 Atome) bedenkt, was man auf die gemischtvalente Ligandensituation $Te^{2-}/(Te_2)^{2-}$ zurückführen kann.

Da sich die Absorptionsenergie durch Komplexierung von Übergangsmetallatomen vermutlich ändern würde, analysierten wir die Möglichkeit, **1** als Ligand zu verwenden. Die Abwesenheit von π-Elektronen in $[Hg_8Te_{16}]^{8-}$ geht einher mit einer großen strukturellen Flexibilität (siehe oben). Quantenchemische Rechnungen ergaben, dass der Makrocyclus Metallionen unterschiedlicher Größe und Bedürfnisse bezüglich der Koordinationsgeometrie komplexieren könnte (z.B. Ti^{4+}, Cu^+, Ce^{4+}), indem sich die Form des Rings geeignet anpasst. Tatsächlich würde dadurch ein anderes Absorptionsverhalten hervorgerufen (Abbildung S8). Auf diesem Weg könnten demnach ternäre Komplexe und Cluster mit fein einstellbaren optischen Lücken innerhalb lamellarer Strukturen zugänglich werden. Da die Bindungsenergien hier jedoch naturgemäß kleiner sind als bei entsprechenden Porphyrinkomplexen, bleibt die experimentelle Isolierung solcher Komplexe eine anspruchsvolle Aufgabe.

Zusammenfassend haben wir über die Ionothermalbehandlung von $Na_2[HgTe_2]$ mit langkettigen, Alkylimidazolium-basierten ionischen Flüssigkeiten einen neuen Zugang zu dimensionsreduzierten Hg/Te-Motiven eröffnet. Als anionische Substruktur wurden rein anorganische $[Hg_8Te_{16}]^{8-}$-Makrocyclen mit Porphyrin-artiger Topologie beobachtet, die in lamellare Kristallstrukturen eingebettet sind. Bemerkenswerterweise weicht das Anion von einer planaren Struktur ab, um die Wechselwirkung mit den Imidazolium-Einheiten der lamellaren Gegenionenstruktur zu optimieren. Quantenchemische Studien ergaben, dass mangels π-Elektronen keine ausgeprägte Aromatizität vorliegt, was jedoch zu einer großen Flexibilität der Struktur führt. Dadurch könnte trotz der Größe des Makrocyclus eine Koordination von Metallkationen möglich sein, da sich der Ring den Erfordernissen des eingeschlossenen Ions anpassen kann. Auf diese Weise könnten lamellare Anordnungen von nur aus schweren

Elementen bestehenden Komplexen mit fein einstellbaren optischen Eigenschaften zugänglich werden.

Interessenkonflikt

Die Autoren erklären, dass keine Interessenkonflikte vorliegen.

[1] a) Y. Pei, C. Chang, Z. Whang, M. Yin, M. Wu, G. Tan, H. Wu, Y. Chen, L. Zhang, S. Ghong, T. Zhu, X. Zhao, L. Huang, J. He, M. G. Kanatzidis, L.-D. Zhao, *J. Am. Chem. Soc.* **2016**, *138*, 16364–16371; b) X. Chen, X. Bu, Q. Lin, C. Mao, Y.-G. Zhai, Y. Wang, P. Feng, *Chem. Eur. J.* **2017**, *23*, 11913–11919; c) K. Zhao, C. Zhu, P. Qiu, A. B. Blichfeld, E. Eikeland, D. Ren, B. B. Iversen, F. Xu, X. Shi, L. Chen, *Nano Energy* **2017**, *42*, 43–50.

[2] a) L. Dou, A. B. Wong, Y. Yu, M. Lai, N. Kornienko, S. W. Eaton, A. Fu, C. G. Bischak, J. Ma, T. Ding, N. S. Ginsberg, L.-W. Wang, A. P. Alivisatos, P. Yang, *Science* **2015**, *349*, 1518–1521; b) A. Castellanos-Gomez, M. Buscema, R. Molenaar, V. Singh, L. Janssen, H. S. J. van der Zant, G. A. Steele, *2D Mater.* **2014**, *1*, 011002; c) C. Tan, X. Cao, X.-J. Wu, Q. He, J. Yang, X. Zhang, J. Chen, W. Zhao, S. Han, G.-H. Nam, M. Sindoro, H. Zhang, *Chem. Rev.* **2017**, *117*, 6225–6331.

[3] K. S. Novoselov, A. K. Geim, S. V. Morozov, D. Jiang, Y. Zhang, S. V. Dobonos, I. V. Grigorieva, A. A. Firsov, *Science* **2004**, *306*, 666–669.

[4] R. Gusmão, Z. Sofer, M. Pumera, *Angew. Chem. Int. Ed.* **2017**, *56*, 8052–8072; *Angew. Chem.* **2017**, *129*, 8164–8185.

[5] a) G. Zhang, H. Liu, J. Qu, J. Li, *Energy Environ. Sci.* **2016**, *9*, 1190–1209; b) L. Li, Z. Chen, Y. Hu, X. Wang, T. Zhang, W. Chen, Q. Wang, *J. Am. Chem. Soc.* **2013**, *135*, 1213–1216; c) Y. Sun, H. Cheng, S. Gao, Q. Liu, Z. Sun, C. Xiao, C. Wu, S. Wei, Y. Yie, *J. Am. Chem. Soc.* **2012**, *134*, 20294–20297.

[6] a) C. Zhou, H. Lin, Y. Tian, Z. Yuan, R. Clark, B. Chen, L. J. van de Burgt, J. C. Wang, Y. Zhou, K. Hanson, Q. J. Meisner, J. Neu, T. Besara, T. Siegrist, E. Lambers, P. Djurovich, B. Ma, *Chem. Sci.* **2018**, *9*, 586–593; b) A. Bayaguud, K. Chen, Y. Wei, *Nano Res.* **2016**, *9*, 3858–3867.

[7] a) M. G. Kanatzidis, *Inorg. Chem.* **2017**, *56*, 3158–3173; b) M. J. Manosa, M. G. Kanatzidis, *Chem. Sci.* **2016**, *7*, 4804–4824; c) G. Thiele, T. Krüger, S. Dehnen, *Angew. Chem. Int. Ed.* **2014**, *53*, 4699–4703; *Angew. Chem.* **2014**, *126*, 4787–4791; d) S. Dehnen, M. Melullis, *Coord. Chem. Rev.* **2007**, *251*, 1259–1280; e) P. Feng, X. Bu, N. Zheng, *Acc. Chem. Res.* **2005**, *38*, 293–303.

[8] S. Santner, J. Heine, S. Dehnen, *Angew. Chem. Int. Ed.* **2016**, *55*, 876–893; *Angew. Chem.* **2016**, *128*, 886–904.

[9] W.-W. Xiong, J.-R. Li, B. Hu, B. Tan, R.-F. Li, X.-Y. Huang, *Chem. Sci.* **2012**, *3*, 1200–1204.

[10] Y. Lin, W. Massa, S. Dehnen, *J. Am. Chem. Soc.* **2012**, *134*, 4497 – 4500.

[11] a) R. E. Morris, *Chem. Commun.* **2009**, 2990 – 2998; b) S. Santner, J. Sprenger, M. Finze, S. Dehnen, *Chem. Eur. J.* **2018**, *24*, 1032 – 1035; c) S. Santner, S. Yogendra, J. J. Weigand, S. Dehnen, *Chem. Eur. J.* **2017**, *23*, 1999 – 2004.

[12] a) F. Neve, O. Francescangeli, A. Crispini, J. Charmant, *Chem. Mater.* **2001**, *13*, 2032 – 2041; b) A. Downard, M. J. Earle, C. Hardacre, S. E. J. McMath, M. Nieuwenhuyzen, S. Teat, *Chem. Mater.* **2001**, *13*, 2032 – 2041; c) A. Getsis, B. Balke, C. Felser, A.-V. Mudring, *Cryst. Growth Des.* **2009**, *9*, 4429 – 4437; d) M. Stricker, T. Linder, B. Oelckers, J. Sundermeyer, *Green Chem.* **2010**, *12*, 1589 – 1598.

[13] a) M. Cardona, R. Kremer, R. Lauck, G. Siegle, A. Muñoz, A. H. Romero, *Phys. Rev. B* **2009**, *80*, 195204; b) A. Delin, T. Klüner, *Phys. Rev. B* **2002**, *66*, 035117; c) B. A. Bernevig, T. L. Hughes, S.-C. Zhang, *Science* **2006**, *314*, 1757 – 1761; d) M. König, S. Wiedmann, C. Brüne, A. Roth, H. Buhmann, L. W. Molenkamp, X.-L. Qi, S.-C. Zhang, *Science* **2007**, *318*, 766 – 770; e) A. Roth, C. Brüne, H. Buhmann, L. W. Molenkamp, J. Maciejko, X.-L. Qi, S.-C. Zhang, *Science* **2009**, *325*, 294 – 297.

[14] C. Donsbach, S. Dehnen, *Z. Anorg. Allg. Chem.* **2017**, *643*, 14 – 19.

[15] a) B. Krebs, H.-U. Hürter, *Angew. Chem. Int. Ed. Engl.* **1980**, *19*, 481 – 482; *Angew. Chem.* **1980**, *92*, 479 – 480; b) B. Krebs, H.-U. Hürter, *Acta Crystallogr. Sect. A* **1981**, *37*, C163b.

[16] a) S. S. Dhingra, C. J. Warren, R. C. Haushalter, A. B. Bocarsly, *Chem. Mater.* **1994**, *6*, 2382 – 2385; b) J. Li, Z. Chen, J. L. Kelly, D. M. Proserpio, *Mater. Res. Soc. Symp. Proc.* **1997**, *453*, 29 – 34; c) P. Sun, S. Liu, S. Li, L. Zhang, H. Sun, D. Jia, *Inorg. Chem.* **2017**, *56*, 6152 – 6162; d) R. C. Haushalter, *Angew. Chem. Int. Ed. Engl.* **1985**, *24*, 432 – 433; *Angew. Chem.* **1985**, *97*, 414 – 415.

[17] T. Ito, *Crystals* **2016**, *6*, 24.

[18] A. Triolo, O. Russina, H.-J. Bleif, E. Di Cola, *Phys. Chem. B* **2007**, *111*, 4641 – 4644.

[19] R. Elfgen, O. Hollóczki, B. Kirchner, *Acc. Chem. Res.* **2017**, *50*, 2949 – 2957.

[20] R. C. Fischer, P. P. Power, *Chem. Rev.* **2010**, *110*, 3877 – 3923.

[21] G. Thiele, Y. Franzke, F. Weigend, S. Dehnen, *Angew. Chem. Int. Ed.* **2015**, *54*, 11283 – 11288; *Angew. Chem.* **2015**, *127*, 11437 – 11442.

[22] a) A. Stock, E. Pohland, *Chem. Ber.* **1926**, *59*, 2215 – 2223; b) R. Boese, A. H. Maulitz, P. Stellberg, *Chem. Ber.* **1994**, *127*, 1887 – 1889.

[23] O. J. Scherer, J. Schwalb, G. Wolmershäuser, W. Kaim, R. Gross, *Angew. Chem. Int. Ed. Engl.* **1986**, *25*, 363 – 364; *Angew. Chem.* **1986**, *98*, 349 – 350.

[24] D. Pfister, K. Schäfer, C. Ott, B. Gercke, R. Pöttgen, O. Janka, M. Baumgartner, A. Efimova, A. Hohmann, P. Schmidt, S. Venkatachalam, L. van Wüllen, U. Schürmann, L. Kienle, V. Duppel, E. Parzinger, B. Miller, J. Becker, A. Holleitner, R. Weihrich, T. Nilges, *Adv. Mater.* **2016**, *28*, 9783 – 9791.

[25] TURBOMOLE Version 7.2, TURBOMOLE GmbH **2017**. TURBOMOLE is a development of the University of Karlsruhe and the Forschungszentrum Karlsruhe 1989 – 2007, TURBO-MOLE GmbH since 2007.

[26] V. Staroverov, G. Scuseria, J. Tao, J. Perdew, *J. Chem. Phys.* **2003**, *119*, 12129.

[27] a) F. Weigend, R. Ahlrichs, *Phys. Chem. Chem. Phys.* **2005**, *7*, 3297 – 3305; b) F. Weigend, *Phys. Chem. Chem. Phys.* **2006**, *8*, 1057 – 1065; c) K. A. Peterson, D. Figgen, E. Goll, H. Stoll, M. Dolg, *J. Chem. Phys.* **2003**, *119*, 11113; d) D. Andrae, U. Häussermann, M. Dolg, H. Stoll, H. Preuß, *Theor. Chim. Acta* **1990**, *77*, 123 – 141.

[28] A. Klamt, G. Schüürmann, *J. Chem. Soc. Perkin Trans. 2* **1993**, 799 – 805.

[29] J. Jusélius, D. Sundholm, J. Gauss, *J. Chem. Phys.* **2004**, *121*, 3952 – 3963.

[30] K. Reiter, M. Kühn, F. Weigend, *J. Chem. Phys.* **2017**, *146*, 054102.

[31] K. Reiter, F. Mack, F. Weigend, *J. Chem. Theory Comput.* **2018**, *14*, 191 – 197.

[32] H. Fliegl, D. Sundholm, *J. Org. Chem.* **2012**, *77*, 3408 – 3414.

[33] S. F. Boys, *Rev. Mod. Phys.* **1960**, *32*, 296 – 299.

[34] X.-X. Yang, I. Isaac, S. Lebedkin, M. Kühn, F. Weigend, D. Fenske, O. Fuhr, A. Eichhöfer, *Chem. Commun.* **2014**, *50*, 11043 – 11045.

[35] *Landolt-Börnstein Tables*, *New Series Vol. III/22a* (Hrsg.: O. Madelung), Springer, New York, **1986**, S. 95 – 95.

[36] CCDC 1825252 enthält die ausführlichen kristallographischen Daten zu dieser Veröffentlichung. Die Daten sind kostenlos beim Cambridge Crystallographic Data Centre erhältlich.

Zuschriften

Anorganische Makrocyclen

C. Donsbach, K. Reiter, D. Sundholm,
F. Weigend, S. Dehnen* —— ▮▮▮▮–▮▮▮▮

$[Hg_4Te_8(Te_2)_4]^{8-}$: ein Schwermetall-
Porphyrinoid in einer lamellaren Struktur

$(C_{10}C_1Im)_8[Hg_8Te_{16}]$
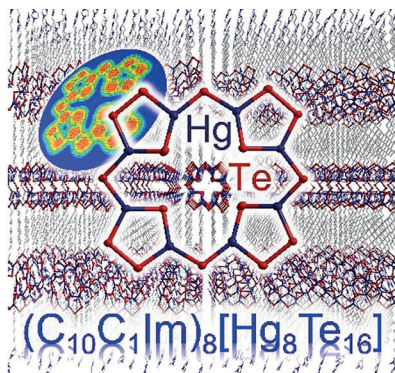
Aus der Ionothermalbehandlung von
$Na_2[HgTe_2]$ in $(C_nC_1Im)[BF_4]$ ($n = 10, 12$)
resultieren lamellar strukturierte Salze
des makrocyclischen Anions $[Hg_8Te_{16}]^{8-}$
(**1**), des schwersten bekannten topologi-
schen Analogons von Porphyrin. Ent-
sprechend seiner großen strukturellen
Flexibilität hat **1** allerdings kein π-Elek-
tronensystem. Kleine Ringströme in den
Pyrrol-artigen Fünfringen lassen auf
schwache lokale (σ-)Aromatizität schlie-
ßen.

6.3 **Supporting Information zum Manuskript "[Hg$_4$Te$_8$(Te$_2$)$_4$]$^{8-}$: A Heavy Metal Porphyrinoid Embedded in a Lamellar Structure" (3.5)**

Supporting Information

[Hg$_4$Te$_8$(Te$_2$)$_4$]$^{8-}$: A Heavy Metal Porphyrinoid Embedded in a Lamellar Structure

Carsten Donsbach, Kevin Reiter, Dage Sundholm, Florian Weigend, and Stefanie Dehnen*

anie_201803233_sm_miscellaneous_information.pdf

Supporting Information

Contents:

1. Synthesis Details

1.1. General

Owing to the starting material's and products' high sensitivity towards air and moisture, all manipulations were performed under Ar atmosphere using standard Schlenk and glovebox techniques. $(C_{10}C_1Im)_8[BF_4]$ and $(C_{12}C_1Im)_8[BF_4]$ were purchased from Iolitec or ABCR, respectively, and degassed at $< 1 \cdot 10^{-3}$ mbar for 12 hours prior to use. Pyridine was dried over CaH_2 and distilled. $Na_2[HgTe_2]$ was prepared according to the literature, by fusion of Na_2Te and $HgTe$ in a 1:1 ratio at 600 °C, followed by washing with pyridine.[S1]

1.2. Synthesis of $(C_{10}C_1Im)_8[Hg_8Te_{16}]$ ($(C_{10}C_1Im)_8\mathbf{1}$)

50 mg of $[Na_2[HgTe_2]$ and 250 mL of $(C_{10}C_1Im)[BF_4]$ were placed in a borosilicate glass ampoule (inner diameter: 7 mm, length: *ca.* 15 cm). The ampoule was sealed under vacuum and placed in an oven at 80 °C for 12 hours. Then, the oven was turned off and the ampoule was allowed to cool to room temperature within 6 hours. $(C_{10}C_1Im)_8[Hg_8Te_{16}]$ = $(C_{10}C_1Im)_8\mathbf{1}$ crystallized as thin light brownish red platelets (Figure S1) in approximately 50% yield.
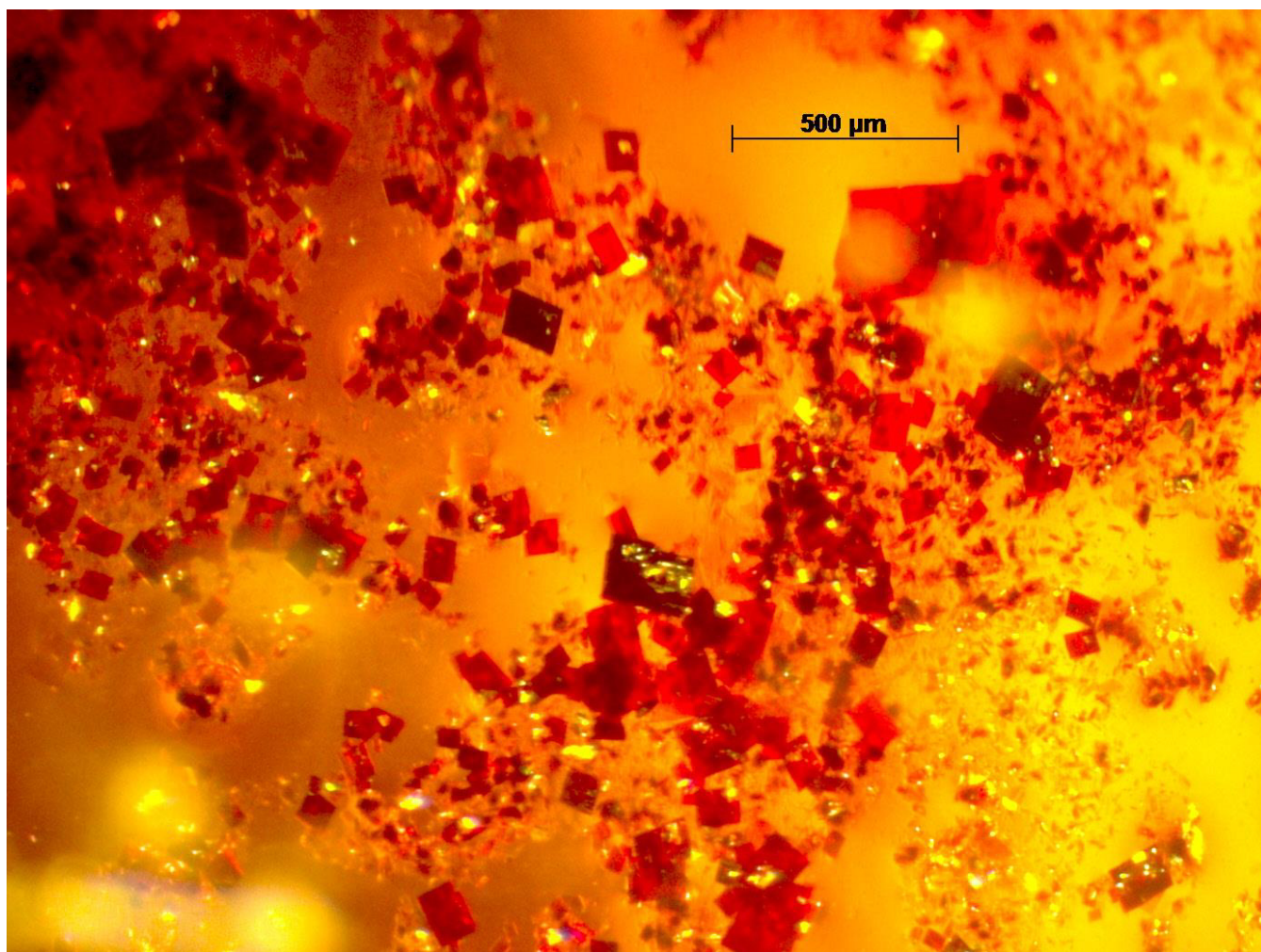
Figure S1. Photograph of the crystals of $(C_{10}C_1Im)_8[Hg_8Te_{16}]$ = $(C_{10}C_1Im)_8\mathbf{1}$.

1.3. Synthesis of $(C_{12}C_1Im)_8[Hg_8Te_{16}]$ $((C_{12}C_1Im)_81)$

$(C_{12}C_1Im)_8$**1** is synthesized in the same way as described for $(C_{12}C_1Im)_8$**1**, yet in the ionic liquid $(C_{12}C_1Im)_8[BF_4]$. However, the crystalline product is hardly isolable from the reaction mixture, as $(C_{12}C_1Im)_8[BF_4]$ is solid at room temperature. Tiny red platelets of $(C_{12}C_1Im)_8$**1** can be spotted temporarily in the melt while the ampoule is cooling down to room temperature (Figure S2). As we have not been able to selectively dissolve the ionic liquid, the product had to be separated mechanically from the solid (and crystalline) reaction medium upon cooling to ambient temperature under a microscope for further investigation. Hence, determination of the yield or any further measurements except for X-ray diffraction analysis have been prohibited. Furthermore, the X-ray data obtained from the product were rather poor (see sections 3.1. and 3.3.).
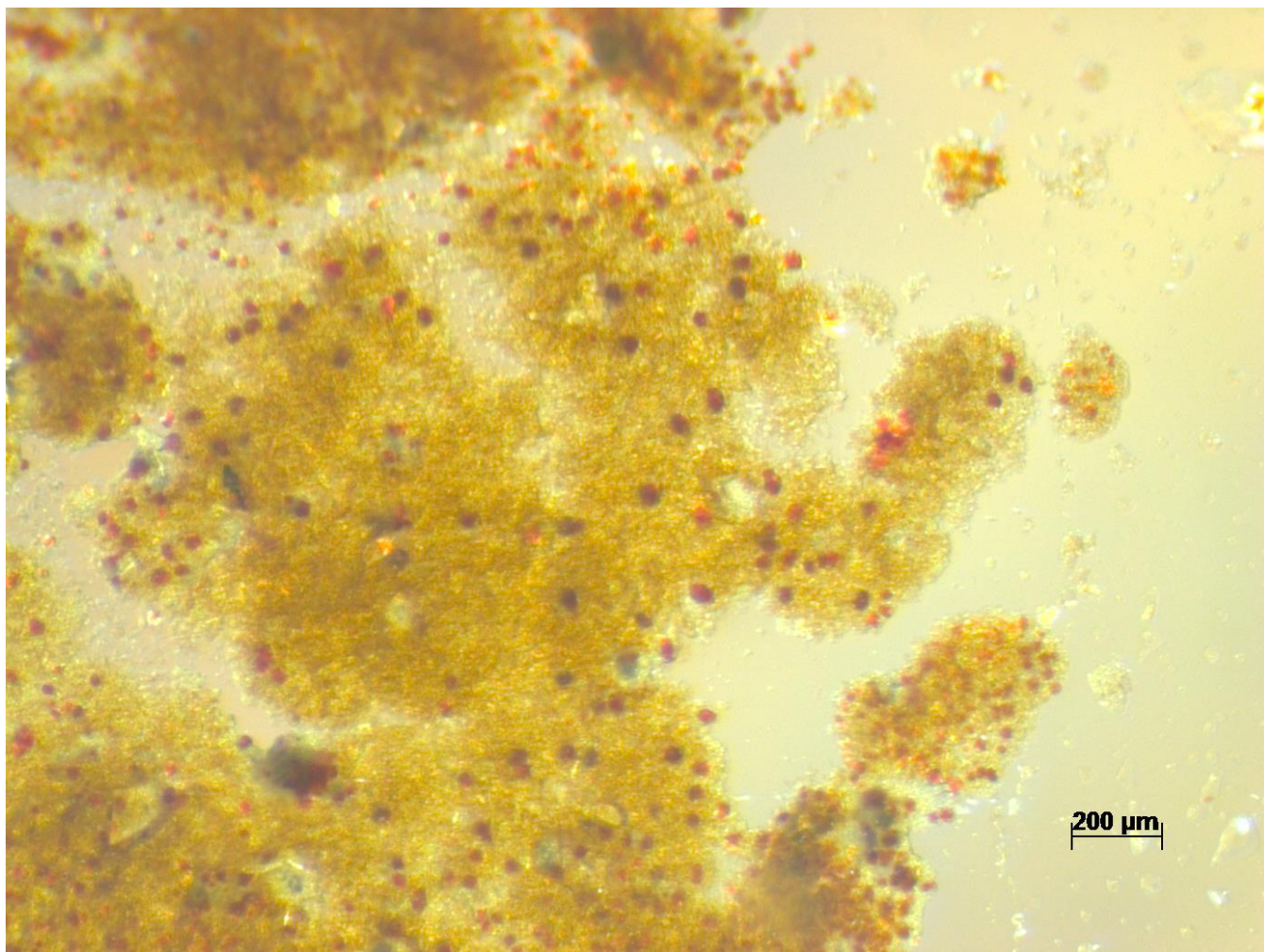
Figure S2. Photograph of the crystals of $(C_{12}C_1Im)_8[Hg_8Te_{16}]$ = $(C_{12}C_1Im)_8$**1** in the already recrystallized mixture after the reaction.

2. Possible Reaction Pathways

The exact formation of the molecular anion **1** is unknown, but fort sure, the anionic substructure of the starting material is re-organized, accompanied by (partial) oxidative coupling of the telluride ligands. Dichalcogenide anions are relatively readily formed in ionic liquids, which are less "innocent" in this regard than originally anticipated.[S1,S2] Either residues of oxygen or constituents of the ionic liquid itself may act as oxidizing agent.

In the telluridomercurate anions of the starting material, $[HgTe_3]$ triangles are linked by edge-sharing into one-dimensional $[-Hg(Te)-Te-]_n$ chains with all of the terminal Te atoms pointing towards the same side of the chain. Thus, generation of Te–Te bonds to form the $[-Hg(\mu-Te)(\mu-Te_2)Hg-Te-]_n$ units may, in theory, occur without deconstruction of the chain. However, for the assembly of the oligomeric structure of **1**, at least every tenth Hg–Te bond needs to be cut, and the five-membered rings need to re-arrange by rotation about Hg–Te bonds.

1 may thus form directly from the 1D-$[HgTe_2]^{2-}$ anions of the staring material, which could be dissolved or suspended in the reaction medium as polymeric or oligomeric fragments. Several steps, including rearrangement of the chain by flipping around Hg–(μ-Te) bonds, oxidative coupling of neighboring terminal Te atoms, and ring closure via nucleophilic substitution, are involved, but their order may vary. Scheme S1 summarizes different possible scenarios.

One way is the preliminary formation of 1D-$[Hg_2Te_4]^{2-}$ anions by rearrangement of the 1D-$[HgTe_2]^{2-}$ chains and oxidative coupling of terminal telluride ligands. These anions consist of five membered $[Hg_2Te_3]$ rings that are linked by μ-bridging Te atoms and have already been found in ionic liquids as their imidazolium salt,[S1] By further rearrangement of the 1D-$[Hg_2Te_4]^{2-}$ chains the, tetrameric porphyrinoid structure of **1** can be pre-formed, followed by ring closure through nucleophilic attack of a μ-bridging telluride ligand on a Hg atom. Within this step, fragments of the 1D-$[Hg_2Te_4]^{2-}$ chains are released from both the attacking side as well as the attacked Hg atoms.

The oxidative coupling does not necessarily have to occur in the beginning, so that the octanuclear tellurido mercurate complex is pre-formed by rearrangement of the 1D-$[HgTe_2]^{2-}$ anions first. Subsequent ring closure and oxidative coupling in each order then yields **1**.

As it is unclear whether the 1D-$[HgTe_2]^{2-}$ anions dissolve or suspend in the reaction medium at all, another tellurido mercurate species might be the actual starting point. By breaking the μ-Te bridges in the 1D-$[HgTe_2]^{2-}$ chains, linear $[HgTe_2]^{2-}$ molecules are formed first. These anions have been observed in ionic liquids as their imidazolium salt as well.[S1] By stepwise oligomerization and subsequent ring closure, the unoxidized form of the cyclic octanuclear tellurido mercurate anion **1** can be obtained. In the final step, the porphyrinoid structure of **1** is realized by oxidative coupling of each two neighboring terminal Te atoms. Naturally, formation of the ditelluride units may occur before during the oligomerization process as well.
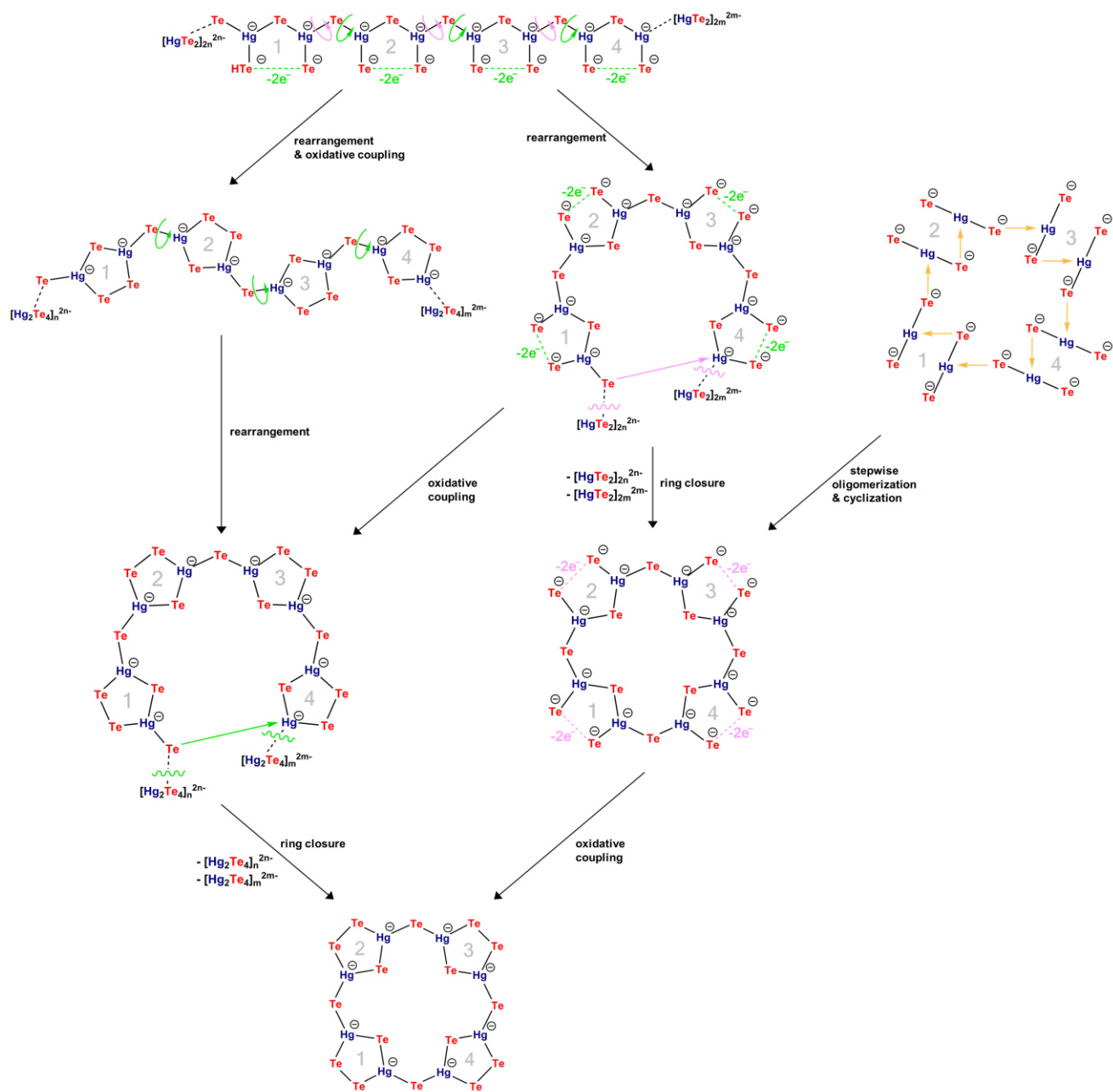
Scheme S1. Schematic illustration of possible reaction pathways at the formation of **1** (for explanations, see the text above).

3. Single Crystal X-Ray Diffraction Analyses

3.1. General

Single crystal X-ray diffraction data were collected on a STOE StadiVari diffractometer using Cu Kα radiation (λ = 1.54186) from an X-ray micro source with X-ray optics and a Pilatus 300K Si hybrid pixel array detector. Data scaling and spherical absorption correction were applied using STOE X-Area LANA software. Structure solution was carried out using direct methods, followed by full-matrix-least-squares refinement against F^2, using SHELXT15, SHELXL15 and Olex2 software.[S3-S5] The 2015 version of SHELXL was used due to compatibility issues of the RESI command in the recent version.

Upon crystal structure refinement of $(C_{10}C_1Im)_8$**1** the anisotropic displacement parameters of the organic cations were treated with SIMU and RIGU restraints on several C and N atoms as well as an EADP constraint on C37 and C38.

The extremely weak diffraction data of $(C_{12}C_1Im)_8$**1** only allowed refinement of a rough structural model. Here, SIMU, RIGU and ISOR commands had to be applied to restrain the anisotropic displacement parameters of the Hg and Te atoms. Hg2/Te5 and Hg4/Te6 were further treated with EADP commands. The positions and equivalent isotropic displacement parameters of the C and N atoms were restraint using the SADI, FLAT and SIMU commands. Besides, the light atoms were refined with isotropic displacement parameters only and the positions of H atoms were not calculated.

Details on the crystallographic data are summarized in Table S1.

Table S1. Crystallographic data of $(C_{10}C_1Im)_8$**1** and preliminary crystal data of $(C_{12}C_1Im)_8$**1.**

Compound	$(C_{10}C_1Im)_8$**1** (CCDC 1825252)	$(C_{12}C_1Im)_8$**1** (not deposited)
Empirical formula	$C_{112} H_{216} Hg_8 N_{16} Te_{16}$	$C_{128} H_{248} Hg_8 N_{16} Te_{16}$
Formula weight /g·mol^{-1}	5433.31	5657.73
Crystal color and shape	brown plate	brown plate
Crystal size /mm^3	0.13×0.03×0.003	0.05×0.015×0.002
Crystal system	monoclinic	monoclinic
Space group	$P2_1/c$	$P2_1/c$
a /Å	9.8573(2)	9.8333(7)
b /Å	52.5806(6)	57.767(11)
c /Å	14.9014(2)	14.9565(5)
β /°	95.8910(10)	95.897(6)
V /Å^3	7682.6(2)	8450.9(11)
Z	2	2
ρ_{calc} /g·cm^{-3}	2.349	2.223
μ(Cu$_{K\alpha}$) /mm^{-1}	37.783	34.383
F(000)	4944.0	5200.0
Min/max transmission	0.0644 / 0.3642	0.0010 / 0.0126
θ range /°	6.196–35.998	6.12–61.846
No. of measured reflections	75374	19517
No. of independent reflections	13820	2611
R(int)	0.0995	0.2399 [a]
No. of indep. reflections ($I>2\sigma(I)$	8380	1331
No. of restraints	123	2081 [a]
No. of parameters	687	349
R_1 ($I>2\theta(I)$)	0.0599	0.1793 [a]
wR_2 (all data)	0.1482	0.4822 [a]
S (all data)	0.909	1.140
$\Delta\rho max$, $\Delta\rho min$ /e·Å^{-3}	4.01 / –1.69	2.22 / –1.59

[a] Please note that the very poor X-ray data obtained from the product do not allow for a satisfying refinement. Thus the data shown here serve as an information about the existence of the compound and its cell metrics; the refinements result only allow for the provision of a structure model.

3.2. Molecular Structure of $(C_{10}C_1Im)_8[Hg_8Te_{16}] = (C_{10}C_1Im)_8\mathbf{1}$

A detailed discussion of the molecular structure of $(C_{10}C_1Im)_8\mathbf{1}$ is given in the main text. Bond lengths and angles of the anion **1** are depicted in Figure S3. Atomic coordinates, equivalent isotropic displacement parameters, anisotropic displacement parameters, bond lengths and bond angles for the molecular structure of $(C_{10}C_1Im)_8\mathbf{1}$ are given in Tables S1–S6.
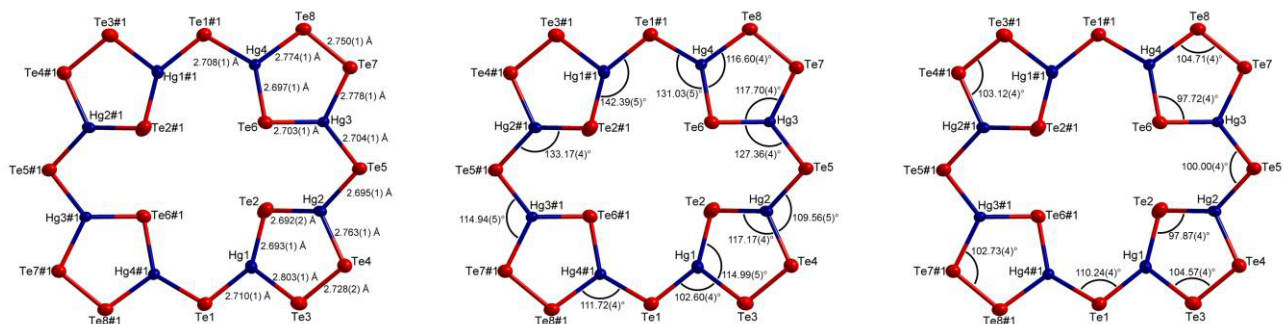
Figure S3. Bond lengths [Å] and angles [°] of **1** (symmetry operations: #1 = 1-X,1-Y,1-Z): Hg–(μ,η^2-Te) 2.692(2)–2.710(1), Hg–($\mu:\eta^1:\eta^1$-Te$_2$) 2.762(1)–2.803(1), Te–Te 2.728(2)–2.750(1); (μ,η^2-Te)–Hg–(μ,η^2-Te) 127.36(4)–142.39(5), (μ,η^2-Te)–Hg–($\mu:\eta^1:\eta^1$-Te$_2$) 102.60(4)–117.70(4), Hg–Te–Te 102.73(4)–104.71(4), Hg–Te–Hg 97.72(4)–110.24(4).

Table S2. Fractional atomic coordinates ($\times 10^4$) and equivalent isotropic displacement parameters ($\mathring{A}^2 \times 10^3$) for $(C_{10}C_1Im)_8$**1**. U_{eq} is defined as 1/3 of the trace of the orthogonalized U_{ij} tensor.

Atom	x	y	z	U(eq)
C1	4923(17)	1793(3)	11550(12)	55(4)
C2	5450(17)	2032(3)	11074(10)	45(4)
C3	4957(17)	2272(3)	11508(10)	45(4)
C4	5406(17)	2517(3)	11082(9)	46(4)
C5	4959(17)	2757(3)	11501(10)	45(4)
C6	5385(17)	3003(3)	11027(10)	43(4)
C7	4833(18)	3245(3)	11452(9)	46(4)
C8	5183(17)	3486(3)	10972(10)	46(4)
C9	4578(15)	3717(3)	11374(9)	37(3)
C10	4875(17)	3958(3)	10864(10)	43(4)
C11	3262(16)	4317(3)	11041(10)	42(4)
C12	4494(14)	4542(3)	12070(9)	35(3)
C13	5217(16)	4332(3)	11898(8)	37(3)
C14	2197(16)	4728(3)	11505(11)	54(4)
C15	7370(20)	1778(3)	9056(11)	64(5)
C16	7850(20)	2012(3)	8658(10)	53(4)
C17	7354(17)	2254(3)	9033(9)	44(4)
C18	7883(15)	2496(2)	8586(9)	39(3)
C19	7409(16)	2740(3)	9011(9)	40(3)
C20	7923(16)	2976(3)	8591(9)	41(4)
C21	7510(16)	3225(3)	8997(9)	41(4)
C22	8011(15)	3463(2)	8516(10)	42(4)
C23	7705(16)	3716(3)	8967(10)	44(4)
C24	8041(15)	3930(3)	8401(10)	45(4)
C25	6628(14)	4261(3)	9066(8)	33(3)
C26	8054(18)	4568(3)	9278(10)	48(4)
C27	8686(15)	4373(3)	8900(9)	37(3)
C28	5735(15)	4645(3)	9782(10)	45(4)
C29	-115(18)	1775(3)	6513(10)	53(4)
C30	376(17)	2013(3)	6105(10)	48(4)
C31	-137(17)	2257(3)	6531(10)	48(4)
C32	389(17)	2496(3)	6103(10)	47(4)
C33	-107(14)	2743(3)	6522(9)	40(3)
C34	401(17)	2980(3)	6076(10)	46(4)
C35	-8(18)	3230(3)	6482(9)	47(4)
C36	472(17)	3463(3)	6013(10)	49(4)
C37	140(20)	3716(4)	6431(14)	79(4)
C38	730(20)	3910(4)	5806(14)	79(4)
C39	-510(20)	4276(4)	6314(11)	67(4)
C40	1010(20)	4576(4)	6230(13)	75(5)
C41	1520(20)	4344(3)	6012(10)	56(4)
C42	-1210(20)	4720(4)	6633(15)	88(6)
C43	2272(18)	1781(3)	4060(11)	56(4)
C44	2844(18)	2015(3)	3593(11)	51(4)
C45	2341(17)	2263(3)	4028(10)	47(4)
C46	2868(16)	2499(3)	3602(9)	41(4)

C47	2420(16)	2748(3)	4022(9)	41(4)
C48	2887(17)	2989(3)	3553(10)	47(4)
C49	2478(16)	3240(3)	3980(10)	46(4)
C50	2959(17)	3461(3)	3510(10)	47(4)
C51	2551(17)	3716(3)	3895(9)	45(4)
C52	3080(20)	3933(3)	3343(11)	61(5)
C53	3704(16)	4353(3)	4036(9)	37(3)
C54	1676(16)	4549(3)	3933(10)	49(4)
C55	1531(16)	4306(3)	3630(9)	39(3)
C56	3753(16)	4804(3)	4536(9)	42(4)
Hg1	5283.4(7)	4161.2(2)	6532.0(4)	49.43(18)
Hg2	2982.9(8)	4588.7(2)	8066.0(4)	49.66(19)
Hg3	1604.6(6)	5330.3(2)	7789.2(4)	38.67(15)
Hg4	2461.2(7)	5848.6(2)	5901.6(4)	40.01(16)
N1	4416(13)	4191(2)	11251(7)	39(3)
N2	3279(12)	4531(2)	11534(7)	34(3)
N3	7789(12)	4180(2)	8774(8)	38(3)
N4	6770(12)	4491(2)	9392(7)	36(3)
N5	2782(13)	4186(2)	3705(8)	40(3)
N6	3087(13)	4568(2)	4198(7)	41(3)
N7	620(18)	4165(3)	6049(9)	63(3)
N8	-313(17)	4526(3)	6394(8)	65(4)
Te1	6350.7(11)	3861.9(2)	5301.4(6)	43.0(2)
Te2	5038.6(15)	4650.2(2)	7027.9(7)	63.4(3)
Te3	3971.2(11)	3808.6(2)	7558.6(7)	45.9(3)
Te4	2401.2(11)	4097.8(2)	8566.6(6)	41.3(2)
Te5	1362.7(11)	4917.6(2)	8843.7(6)	41.8(2)
Te6	2315.1(11)	5339.3(2)	6085.2(6)	41.8(2)
Te7	994.3(11)	5791.0(2)	8566.9(6)	40.2(2)
Te8	1601.4(11)	6139.3(2)	7290.4(6)	40.5(2)

Table S3. Anisotropic displacement parameters ($Å^2 \times 10^3$) for $(C_{10}C_1Im)_8\mathbf{1}$. The anisotropic displacement factor exponent takes the form: $-2\pi^2[h^2a^{*2}U_{11}+2hka^*b^*U_{12}+...]$.

Atom	U_{11}	U_{22}	U_{33}	U_{23}	U_{13}	U_{12}
C1	51(10)	31(9)	80(12)	-11(8)	-5(9)	-6(7)
C2	56(10)	36(9)	42(8)	6(7)	1(8)	-9(7)
C3	54(10)	38(9)	42(8)	-1(7)	1(8)	-2(7)
C4	58(10)	43(9)	36(8)	10(7)	7(8)	-3(8)
C5	60(10)	27(8)	48(9)	-10(6)	10(8)	4(7)
C6	56(10)	30(8)	45(8)	-9(6)	7(8)	4(7)
C7	64(11)	38(9)	33(8)	3(6)	-5(8)	3(8)
C8	53(10)	45(10)	40(8)	3(7)	1(8)	-8(8)
C9	44(9)	29(8)	36(8)	2(6)	5(7)	-4(6)
C10	53(10)	29(8)	46(9)	-7(6)	-3(8)	-1(7)
C11	42(9)	47(10)	40(8)	11(7)	9(8)	-4(7)
C12	38(8)	26(7)	41(8)	8(6)	0(7)	0(6)
C13	53(10)	33(8)	22(7)	0(6)	-4(7)	0(7)
C14	46(10)	61(11)	53(10)	2(8)	-3(8)	33(8)
C15	120(17)	17(8)	60(10)	-7(7)	28(11)	4(9)
C16	81(13)	37(9)	41(9)	-2(7)	7(9)	7(8)
C17	65(11)	30(8)	41(8)	2(6)	14(8)	-3(7)
C18	45(9)	28(8)	42(8)	-3(6)	1(7)	4(6)
C19	47(9)	27(8)	44(8)	-4(6)	-9(8)	3(6)
C20	56(10)	26(8)	41(8)	-2(6)	8(8)	-1(7)
C21	56(10)	30(8)	35(8)	0(6)	0(8)	1(7)
C22	42(9)	24(8)	58(9)	11(7)	3(8)	1(6)
C23	45(9)	35(9)	51(9)	1(7)	-3(8)	10(7)
C24	32(8)	49(10)	51(9)	0(7)	-8(8)	-4(7)
C25	33(8)	33(8)	34(7)	5(6)	4(7)	2(6)
C26	55(10)	41(9)	49(9)	-2(7)	0(9)	2(8)
C27	31(8)	31(8)	48(9)	6(6)	-3(7)	9(6)
C28	35(8)	43(9)	55(9)	1(7)	-4(8)	5(7)
C29	70(12)	44(10)	46(9)	12(7)	5(9)	3(8)
C30	48(10)	54(10)	42(9)	-17(7)	11(8)	-8(8)
C31	48(10)	46(10)	51(9)	-5(7)	4(8)	1(7)
C32	51(10)	45(9)	42(9)	-5(7)	-11(8)	-3(7)
C33	30(8)	57(10)	32(8)	-6(7)	-1(7)	0(7)
C34	54(10)	39(9)	43(9)	1(7)	3(8)	-11(7)
C35	69(11)	40(9)	34(8)	-4(7)	13(8)	-4(8)
C36	51(10)	56(11)	36(8)	2(7)	-9(8)	-6(8)
C37	90(10)	54(6)	90(9)	18(6)	-11(8)	7(6)
C38	90(10)	54(6)	90(9)	18(6)	-11(8)	7(6)
C39	69(9)	86(8)	44(9)	-23(8)	-3(8)	0(7)
C40	90(10)	67(8)	71(11)	3(9)	18(10)	1(7)
C41	70(9)	63(7)	33(8)	4(7)	-4(8)	3(6)
C42	86(13)	78(12)	96(15)	-33(11)	-14(12)	1(10)
C43	68(12)	33(9)	64(11)	-4(8)	-1(10)	-4(8)
C44	58(11)	44(10)	51(9)	0(7)	5(9)	-5(8)
C45	59(11)	32(8)	47(9)	-16(7)	0(8)	-2(7)
C46	50(9)	38(9)	36(8)	-1(6)	5(7)	0(7)

C47	50(9)	29(8)	46(9)	0(6)	8(8)	0(6)
C48	55(10)	40(9)	47(9)	0(7)	8(8)	-2(7)
C49	39(9)	40(9)	55(10)	10(7)	-9(8)	-7(7)
C50	50(10)	51(10)	42(9)	-8(7)	11(8)	-3(8)
C51	58(10)	34(9)	40(8)	0(6)	-1(8)	-5(7)
C52	88(14)	41(8)	54(10)	-9(7)	5(10)	-4(8)
C53	42(7)	41(6)	28(7)	5(5)	0(6)	-4(5)
C54	41(6)	58(10)	51(9)	7(8)	18(7)	-8(6)
C55	39(8)	41(9)	34(8)	1(6)	-17(7)	-14(7)
C56	51(10)	35(8)	40(8)	-2(6)	-1(8)	-8(7)
Hg1	54.0(4)	55.6(4)	38.5(3)	-0.9(3)	4.1(3)	4.9(3)
Hg2	69.5(5)	37.4(4)	41.0(4)	-3.0(3)	0.4(3)	8.1(3)
Hg3	43.7(3)	30.7(3)	41.0(3)	1.8(2)	1.4(3)	-1.3(3)
Hg4	44.9(4)	37.6(3)	37.0(3)	3.9(3)	1.8(3)	0.9(3)
N1	50(8)	36(7)	30(6)	2(5)	4(6)	-13(6)
N2	46(7)	26(6)	32(6)	0(5)	8(6)	8(5)
N3	37(7)	23(6)	49(7)	1(5)	-17(6)	-1(5)
N4	47(7)	24(6)	37(6)	3(5)	11(6)	3(5)
N5	45(7)	30(5)	44(7)	6(5)	3(6)	0(5)
N6	49(6)	39(6)	34(6)	-4(5)	2(6)	-10(5)
N7	81(9)	66(6)	42(7)	-2(6)	-1(7)	-5(6)
N8	72(8)	87(8)	34(7)	-9(7)	4(7)	-5(6)
Te1	53.9(6)	34.0(5)	41.6(5)	3.1(4)	7.0(5)	-1.7(4)
Te2	97.7(10)	45.2(7)	50.0(6)	7.5(5)	19.9(7)	-8.3(6)
Te3	47.1(6)	34.7(5)	56.5(6)	-4.0(4)	7.8(5)	-0.3(4)
Te4	49.6(6)	37.7(5)	36.6(5)	-0.9(4)	4.0(5)	2.8(4)
Te5	58.3(6)	28.5(5)	38.7(5)	-1.4(4)	6.0(5)	-3.6(4)
Te6	50.2(6)	33.6(5)	41.8(5)	-3.6(4)	6.4(5)	3.3(4)
Te7	51.7(6)	32.4(5)	36.4(5)	-1.5(4)	3.2(5)	1.3(4)
Te8	51.4(6)	28.8(5)	40.6(5)	-0.4(4)	1.3(5)	0.1(4)

Table S4. Bond lengths for $(C_{10}C_1Im)_8$**1** (symmetry operation: i = 1–x, 1–y, 1–z).

Atom	Atom	Length/Å	Atom	Atom	Length/Å
C1	C2	1.56(2)	C36	C37	1.52(2)
C2	C3	1.52(2)	C37	C38	1.53(3)
C3	C4	1.52(2)	C38	N7	1.40(2)
C4	C5	1.496(19)	C39	N7	1.35(2)
C5	C6	1.55(2)	C39	N8	1.34(2)
C6	C7	1.546(19)	C40	C41	1.37(2)
C7	C8	1.51(2)	C40	N8	1.37(2)
C8	C9	1.50(2)	C41	N7	1.30(2)
C9	C10	1.522(19)	C42	N8	1.42(2)
C10	N1	1.447(18)	C43	C44	1.55(2)
C11	N1	1.326(19)	C44	C45	1.56(2)
C11	N2	1.344(18)	C45	C46	1.51(2)
C12	C13	1.352(19)	C46	C47	1.536(19)
C12	N2	1.371(18)	C47	C48	1.54(2)
C13	N1	1.397(17)	C48	C49	1.54(2)
C14	N2	1.481(16)	C49	C50	1.46(2)
C15	C16	1.47(2)	C50	C51	1.53(2)
C16	C17	1.50(2)	C51	C52	1.53(2)
C17	C18	1.553(19)	C52	N5	1.477(19)
C18	C19	1.525(18)	C53	N5	1.324(18)
C19	C20	1.501(19)	C53	N6	1.316(18)
C20	C21	1.513(19)	C54	C55	1.36(2)
C21	C22	1.547(18)	C54	N6	1.410(19)
C22	C23	1.538(19)	C55	N5	1.379(18)
C23	C24	1.46(2)	C56	N6	1.468(17)
C24	N3	1.457(18)	Hg1	Te1	2.7095(12)
C25	N3	1.335(17)	Hg1	Te2	2.6932(14)
C25	N4	1.305(17)	Hg1	Te3	2.8029(12)
C26	C27	1.35(2)	Hg2	Te2	2.6920(15)
C26	N4	1.356(19)	Hg2	Te4	2.7635(12)
C27	N3	1.346(17)	Hg2	Te5	2.6953(12)
C28	N4	1.469(17)	Hg3	Te5	2.7040(11)
C29	C30	1.49(2)	Hg3	Te6	2.7028(11)
C30	C31	1.54(2)	Hg3	Te7	2.7780(11)
C31	C32	1.52(2)	Hg4	Te1^i	2.7078(11)
C32	C33	1.55(2)	Hg4	Te6	2.6969(11)
C33	C34	1.52(2)	Hg4	Te8	2.7746(11)
C34	C35	1.52(2)	Te3	Te4	2.7275(14)
C35	C36	1.51(2)	Te7	Te8	2.7501(13)

Table S5. Bond angles for $(C_{10}C_1Im)_8\mathbf{1}$ (symmetry operation: i = 1–x, 1–y, 1–z).

Atom	Atom	Atom	Angle/°	Atom	Atom	Atom	Angle/°
C3	C2	C1	109.8(12)	C55	C54	N6	103.2(14)
C2	C3	C4	113.8(12)	C54	C55	N5	109.8(13)
C5	C4	C3	115.5(12)	Te1	Hg1	Te3	102.61(4)
C4	C5	C6	114.1(12)	Te2	Hg1	Te1	142.39(4)
C7	C6	C5	112.1(12)	Te2	Hg1	Te3	114.98(4)
C8	C7	C6	112.9(13)	Te2	Hg2	Te4	117.17(4)
C9	C8	C7	111.6(12)	Te2	Hg2	Te5	133.17(4)
C8	C9	C10	111.7(12)	Te5	Hg2	Te4	109.56(4)
N1	C10	C9	115.1(12)	Te5	Hg3	Te7	114.94(3)
N1	C11	N2	109.2(14)	Te6	Hg3	Te5	127.36(4)
C13	C12	N2	107.6(13)	Te6	Hg3	Te7	117.69(3)
C12	C13	N1	107.0(14)	Te1[1]	Hg4	Te8	111.72(4)
C15	C16	C17	115.5(14)	Te6	Hg4	Te1i	131.03(4)
C16	C17	C18	113.7(12)	Te6	Hg4	Te8	116.60(3)
C19	C18	C17	112.5(12)	C11	N1	C10	128.8(13)
C20	C19	C18	113.0(12)	C11	N1	C13	107.9(13)
C19	C20	C21	115.5(12)	C13	N1	C10	123.2(13)
C20	C21	C22	113.6(12)	C11	N2	C12	108.3(12)
C23	C22	C21	114.3(12)	C11	N2	C14	126.8(14)
C24	C23	C22	110.3(12)	C12	N2	C14	124.9(12)
N3	C24	C23	114.5(13)	C25	N3	C24	126.7(12)
N4	C25	N3	110.8(13)	C25	N3	C27	106.6(12)
C27	C26	N4	107.5(14)	C27	N3	C24	126.7(13)
N3	C27	C26	107.8(14)	C25	N4	C26	107.3(12)
C29	C30	C31	113.5(13)	C25	N4	C28	127.3(13)
C32	C31	C30	112.0(13)	C26	N4	C28	125.4(12)
C31	C32	C33	112.9(12)	C53	N5	C52	125.5(14)
C34	C33	C32	112.4(12)	C53	N5	C55	107.6(12)
C35	C34	C33	114.9(12)	C55	N5	C52	126.2(14)
C36	C35	C34	114.0(13)	C53	N6	C54	110.4(13)
C35	C36	C37	115.6(14)	C53	N6	C56	126.0(14)
C36	C37	C38	103.0(16)	C54	N6	C56	123.4(13)
N7	C38	C37	115.9(19)	C39	N7	C38	125.2(19)
N8	C39	N7	109.5(19)	C41	N7	C38	127.9(19)
C41	C40	N8	104.8(19)	C41	N7	C39	106.8(18)
N7	C41	C40	111(2)	C39	N8	C40	107.6(18)
C43	C44	C45	109.3(13)	C39	N8	C42	130.0(19)
C46	C45	C44	111.9(12)	C40	N8	C42	122.3(19)
C45	C46	C47	113.9(12)	Hg4[1]	Te1	Hg1	110.24(4)
C46	C47	C48	113.9(12)	Hg2	Te2	Hg1	97.86(4)
C49	C48	C47	114.6(12)	Te4	Te3	Hg1	104.57(4)
C50	C49	C48	111.9(13)	Te3	Te4	Hg2	103.11(4)
C49	C50	C51	114.0(13)	Hg2	Te5	Hg3	99.99(4)
C50	C51	C52	109.5(13)	Hg4	Te6	Hg3	97.73(3)
N5	C52	C51	112.6(13)	Te8	Te7	Hg3	102.73(4)
N6	C53	N5	109.0(14)	Te7	Te8	Hg4	104.71(4)

Table S6. Hydrogen atom coordinates ($Å×10^4$) and isotropic displacement parameters ($Å^2×10^3$) for $(C_{10}C_1Im)_8$**1**.

Atom	x	y	z	U(eq)
H1A	5420.67	1642.48	11377.88	82
H1B	3946.6	1770.7	11366.59	82
H1C	5069.18	1815.82	12205.95	82
H2A	6459.21	2030.86	11125.71	54
H2B	5110.11	2029.66	10425.58	54
H3A	5301.8	2271.66	12156.05	54
H3B	3948.07	2268.42	11466.55	54
H4A	6413.82	2517.07	11112.65	55
H4B	5048.84	2516.59	10436.08	55
H5A	5349.25	2761.95	12139.99	54
H5B	3953.76	2754.95	11491.73	54
H6A	6392.3	3011.73	11067.13	52
H6B	5035.5	2995.62	10380.28	52
H7A	3829.63	3231.47	11438.9	55
H7B	5216.77	3255.51	12091.87	55
H8A	6186.45	3504.34	11010.72	56
H8B	4834.98	3472.75	10325.96	56
H9A	4957.97	3733.88	12012.37	44
H9B	3578.81	3694.44	11360.31	44
H10A	5871.84	3969.64	10834.56	52
H10B	4437.5	3943.08	10238.31	52
H11	2537.85	4264.43	10611.12	51
H12	4776.91	4673.09	12487	42
H13	6103.16	4289.17	12167.31	44
H14A	1385.22	4656.17	11738.57	80
H14B	1965.98	4783.76	10881	80
H14C	2524.89	4873.34	11877.17	80
H15A	7646.3	1630.51	8715.05	96
H15B	6372.25	1782.3	9033.14	96
H15C	7764.44	1764.29	9684.57	96
H16A	7574.24	2008.27	8000.42	63
H16B	8863.47	2012.08	8742.06	63
H17A	7643.45	2259.75	9688.54	53
H17B	6344.77	2254.5	8951.95	53
H18A	8892.3	2493.13	8642.28	46
H18B	7556.28	2495.77	7934.83	46
H19A	6399.99	2743.97	8949.46	48
H19B	7728.23	2739.86	9662.65	48
H20A	7590.27	2976.35	7940.78	49
H20B	8931.55	2968.72	8638.44	49
H21A	7880.7	3229.91	9639.92	49
H21B	6503.05	3230.85	8972.44	49
H22A	9007.98	3448.38	8492.64	50
H22B	7576.38	3464.56	7886.35	50
H23A	6727.08	3723.76	9064.2	53
H23B	8247.22	3728.25	9563.09	53

H24A	9016.94	3918.49	8301.1	54
H24B	7500.88	3914.46	7805.58	54
H25	5810.93	4164.51	9041.23	40
H26	8438.98	4729.85	9434.22	58
H27	9600.08	4372.13	8750.2	45
H28A	4868.9	4551.98	9736.86	67
H28B	5610.86	4805.99	9452.99	67
H28C	6034.07	4679.62	10418.21	67
H29A	236.62	1626.72	6210.62	80
H29B	-1114.61	1771.3	6439.13	80
H29C	209.66	1769.66	7156.76	80
H30A	70.5	2013.07	5451.48	57
H30B	1385.48	2013.12	6175.35	57
H31A	-1146.7	2258.7	6456.56	58
H31B	165.41	2257.83	7184.98	58
H32A	84.02	2494.57	5448.61	56
H32B	1398.91	2492.88	6173.4	56
H33A	-1117.01	2744.88	6462.67	48
H33B	215.37	2746.65	7173.43	48
H34A	1408.52	2973.02	6111.72	55
H34B	49.5	2978.08	5428.86	55
H35A	-1014.95	3235.64	6461.57	56
H35B	367.14	3234.97	7123.99	56
H36A	57.33	3460.72	5378.66	58
H36B	1472.65	3450.67	6002.91	58
H37A	589.89	3731.24	7055.02	95
H37B	-852.19	3738.98	6436.94	95
H38A	1703.26	3869.89	5777.56	95
H38B	257.09	3887.11	5191.96	95
H39	-1320.73	4188.58	6425.31	80
H40	1462.38	4735.03	6260.2	90
H41	2422.3	4318.02	5854.32	67
H42A	-834.15	4799.65	7199.99	132
H42B	-2102.59	4646.3	6708.99	132
H42C	-1309.68	4849.09	6155.27	132
H43A	2532.5	1790.81	4712.2	83
H43B	2647.77	1625.21	3822.15	83
H43C	1275.97	1778.58	3942.86	83
H44A	2528.23	2012.96	2940.11	61
H44B	3853.23	2010.32	3661.83	61
H45A	1331.52	2265.35	3959.06	56
H45B	2651.22	2262.22	4681.19	56
H46A	2545.26	2499.01	2950.6	50
H46B	3877.29	2492.65	3659.05	50
H47A	2789.85	2752.46	4664.94	50
H47B	1412.61	2749.57	3997.63	50
H48A	3892.16	2984.3	3562.83	56
H48B	2497.55	2985.87	2914.01	56
H49A	1472.62	3248.09	3963.54	55
H49B	2864.8	3245.36	4619.31	55

H50A	2590.86	3451.94	2866.74	57
H50B	3965.54	3453.31	3536.47	57
H51A	2939.75	3730.67	4532.71	54
H51B	1545.59	3726.49	3874.93	54
H52A	4079.59	3914.57	3337.17	73
H52B	2658.95	3920.28	2712.65	73
H53	4657.95	4323.57	4139.98	45
H54	992.43	4675.28	3959.49	59
H55	692.23	4229.18	3401.64	47
H56A	3702.51	4930.53	4050.92	64
H56B	4710.57	4769.33	4743.74	64
H56C	3289.72	4869.69	5039.51	64

3.3. Molecular Structure Model of $(C_{12}C_1Im)_8[Hg_8Te_{16}] = (C_{12}C_1Im)_8\mathbf{1}$

The crystals of $(C_{12}C_1Im)_8\mathbf{1}$ are very thin and fragile, but still twinned by layering. In addition to that, they had to be separated from the solid reaction mixture mechanically (see 1.3.) which greatly hindered proper sample preparation. As the crystals furthermore proofed quite sensitive to X-rays, a very weak diffraction dataset could be gained only. Nevertheless, the presence of the anion $\mathbf{1}$ was confirmed by structure solution and refinement. Owing to the weak data, the bond lengths and angles in this structure model are not be discussed here in detail.

$(C_{12}C_1Im)_8\mathbf{1}$ crystallizes isotypically to $(C_{10}C_1Im)_8\mathbf{1}$. The crystallographic b axis is elongated by 5.18 Å, while the other cell constants are nearly identical. This is caused by the longer alkyl chains of the cation, also increasing the width of the double-layer, formed by the interlocked alkyl chains, by roughly 2.5 Å to a total of about 20.2 Å. As shown in Figure S4, the dodecyl chains of the imidazolium cation do not seem interlock as neatly as the decyl chains in $(C_{10}C_1Im)_8\mathbf{1}$. However, this phenomenon can't be considered significant as the poor data set only allows for a C–C bond precision below 0.12 Å.

The atomic coordinates, equivalent isotropic displacement parameters, anisotropic displacement parameters, bond lengths and bond angles for the molecular structure of $(C_{12}C_1Im)_8\mathbf{1}$ are listed in Tables S7–S10.
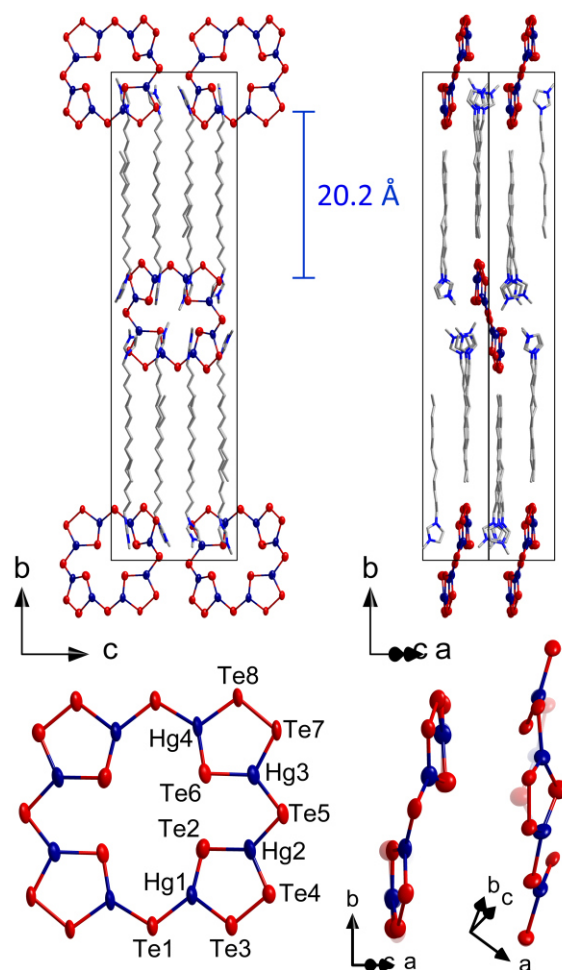
Figure S4. Cut-out of the crystal structure model of $(C_{12}C_1Im)_8\mathbf{1}$. Hg (dark blue) and Te (red) atoms are drawn as thermal ellipsoids on the 40% probability level. C and N are shown as wireframes. The positions of H atoms were not calculated at all.

18

Table S7. Fractional atomic coordinates ($\times 10^4$) and equivalent isotropic displacement parameters ($\text{Å}^2 \times 10^3$) for $(C_{12}C_1Im)_8\mathbf{1}$. U_{eq} is defined as 1/3 of the trace of the orthogonalized U_{ij} tensor.

Atom	x	y	z	U(eq)
Hg1	2987(12)	5375(2)	8073(7)	114(5)
Hg2	5274(11)	5763(2)	6531(7)	114(5)
Hg3	7537(10)	5770(2)	4080(7)	102(5)
Hg4	8372(10)	5301(2)	2205(7)	102(4)
Te1	1341(16)	5071(3)	8820(12)	106(7)
Te2	5060(20)	5318(4)	7001(13)	142(8)
Te3	3999(17)	6083(4)	7577(12)	111(7)
Te4	2482(16)	5814(3)	8564(11)	102(7)
Te5	6360(18)	6043(4)	5289(12)	114(5)
Te6	7647(15)	5318(3)	3913(11)	102(4)
Te7	9020(17)	5720(3)	1425(11)	103(7)
Te8	8399(17)	6041(3)	2712(11)	98(7)
C1_1	-130(130)	8383(12)	6540(100)	20(50)
C2_1	480(120)	8162(12)	6260(90)	30(40)
C3_1	-160(120)	7945(10)	6570(90)	30(40)
C4_1	320(150)	7725(10)	6180(80)	30(40)
C5_1	-90(150)	7508(10)	6610(70)	40(40)
C6_1	240(140)	7289(10)	6150(60)	30(40)
C7_1	-40(130)	7070(9)	6640(80)	30(40)
C8_1	750(80)	6863(10)	6380(100)	50(40)
C9_1	150(120)	6634(10)	6580(90)	40(40)
C10_1	700(160)	6432(11)	6100(70)	50(40)
C11_1	520(180)	6201(12)	6530(90)	80(40)
C12_1	1090(140)	6001(13)	6050(90)	100(40)
N1_1	830(100)	5763(12)	6180(60)	120(40)
C13_1	-470(90)	5660(16)	6220(80)	110(40)
N2_1	-270(110)	5419(15)	6370(60)	110(40)
C14_1	1150(110)	5372(13)	6410(90)	120(50)
C15_1	1830(90)	5585(15)	6300(100)	110(40)
C16_1	-1320(140)	5250(20)	6450(100)	100(70)
C1_2	2460(150)	8368(12)	3950(100)	30(50)
C2_2	3020(130)	8147(12)	3630(90)	30(40)
C3_2	2510(140)	7931(10)	4040(70)	20(40)
C4_2	2750(150)	7712(10)	3540(50)	30(40)
C5_2	2530(150)	7493(9)	4040(70)	30(40)
C6_2	2970(130)	7277(9)	3600(80)	30(40)
C7_2	2480(120)	7056(9)	3960(80)	20(40)
C8_2	3040(120)	6840(9)	3590(70)	10(30)
C9_2	2460(110)	6618(9)	3910(90)	30(40)
C10_2	3150(120)	6403(9)	3630(100)	40(40)
C11_2	2590(130)	6182(10)	3960(90)	40(40)
C12_2	3120(110)	5966(11)	3570(70)	50(40)
N1_2	2760(80)	5734(10)	3750(40)	40(30)
C13_2	3660(70)	5561(11)	4140(60)	30(30)
N2_2	2900(90)	5354(11)	4200(50)	40(30)
C14_2	1530(80)	5399(14)	3850(70)	40(40)

C15_2	1440(70)	5634(15)	3570(70)	30(40)
C16_2	3410(130)	5141(17)	4560(80)	80(60)
C1_3	2480(180)	1635(13)	730(110)	80(60)
C2_3	1990(180)	1848(12)	1170(100)	90(50)
C3_3	2370(170)	2072(11)	760(80)	70(40)
C4_3	1970(160)	2285(11)	1240(90)	70(40)
C5_3	2490(140)	2508(10)	890(90)	50(40)
C6_3	2100(150)	2721(9)	1370(70)	40(40)
C7_3	2430(140)	2945(9)	950(70)	30(40)
C8_3	2110(150)	3157(9)	1450(60)	30(40)
C9_3	2250(150)	3381(10)	970(60)	30(40)
C10_3	2020(150)	3595(10)	1500(50)	20(40)
C11_3	2130(150)	3818(11)	1010(60)	30(40)
C12_3	1960(120)	4032(11)	1550(60)	30(40)
N1_3	2240(80)	4252(10)	1200(40)	50(30)
C13_3	3530(80)	4332(14)	990(60)	80(40)
N2_3	3360(90)	4562(13)	660(50)	80(40)
C14_3	1970(100)	4624(13)	670(80)	90(40)
C15_3	1270(80)	4432(15)	1010(80)	70(40)
C16_3	4410(130)	4700(20)	380(80)	70(60)
C1_4	5130(160)	8376(12)	1660(90)	40(50)
C2_4	5440(130)	8159(11)	1170(70)	0(40)
C3_4	4940(120)	7940(10)	1560(80)	10(40)
C4_4	5400(150)	7722(10)	1140(60)	20(40)
C5_4	5190(150)	7505(9)	1660(60)	40(40)
C6_4	5600(120)	7286(9)	1220(90)	40(40)
C7_4	5040(140)	7069(9)	1590(90)	40(40)
C8_4	5470(130)	6848(10)	1180(90)	50(40)
C9_4	4950(160)	6632(10)	1570(70)	50(40)
C10_4	5100(180)	6416(11)	1050(70)	60(40)
C11_4	4740(180)	6197(12)	1500(70)	60(40)
C12_4	4850(130)	5981(12)	960(80)	80(40)
N1_4	4450(90)	5763(11)	1280(50)	100(40)
C13_4	3160(90)	5654(15)	1050(60)	80(40)
N2_4	3180(100)	5438(14)	1500(60)	100(40)
C14_4	4470(120)	5414(17)	2010(80)	90(40)
C15_4	5250(100)	5614(18)	1870(80)	100(40)
C16_4	2100(140)	5280(20)	1460(100)	140(70)

Table S8. Anisotropic displacement parameters ($\text{Å}^2 \times 10^3$) for $(C_{12}C_1Im)_8\mathbf{1}$. The anisotropic displacement factor exponent takes the form: $-2\pi^2[h^2a^{*2}U_{11}+2hka^*b^*U_{12}+\ldots]$.

Atom	U_{11}	U_{22}	U_{33}	U_{23}	U_{13}	U_{12}
Hg1	99(10)	175(14)	72(9)	21(9)	30(8)	2(10)
Hg2	94(8)	166(11)	90(8)	-8(7)	53(7)	-7(8)
Hg3	65(9)	176(14)	70(9)	7(8)	35(7)	3(8)
Hg4	48(7)	166(11)	97(9)	8(7)	27(6)	0(7)
Te1	51(13)	181(19)	92(15)	14(14)	34(11)	14(13)
Te2	139(18)	168(19)	127(18)	-15(15)	61(14)	17(15)
Te3	72(14)	170(19)	98(15)	10(14)	40(11)	17(13)
Te4	72(14)	150(17)	85(15)	-1(12)	16(11)	-3(12)
Te5	94(8)	166(11)	90(8)	-8(7)	53(7)	-7(8)
Te6	48(7)	166(11)	97(9)	8(7)	27(6)	0(7)
Te7	83(14)	170(20)	68(13)	6(12)	38(11)	12(13)
Te8	92(15)	146(17)	61(13)	7(11)	35(11)	2(13)

Table S9. Bond lengths for $(C_{12}C_1Im)_8\mathbf{1}$ (symmetry operation: i = 1–x, 1–y, 1–z).

Atom	Atom	Length/Å	Atom	Atom	Length/Å
Hg1	Te1	2.70(2)	C12_2	N1_2	1.41(5)
Hg1	Te2	2.74(2)	N1_2	C13_2	1.4200
Hg1	Te4	2.70(2)	N1_2	C15_2	1.4200(11)
Hg2	Te2	2.68(3)	C13_2	N2_2	1.4200
Hg2	Te3	2.80(2)	N2_2	C14_2	1.4200(12)
Hg2	Te5	2.76(2)	N2_2	C16_2	1.41(5)
Hg3	Te5	2.74(2)	C14_2	C15_2	1.4200
Hg3	Te6	2.63(2)	C1_3	C2_3	1.49(3)
Hg3	Te8	2.77(2)	C2_3	C3_3	1.49(3)
Hg4	Te1^i	2.67(2)	C3_3	C4_3	1.50(3)
Hg4	Te6	2.723(19)	C4_3	C5_3	1.50(3)
Hg4	Te7	2.79(2)	C5_3	C6_3	1.49(3)
Te3	Te4	2.70(3)	C6_3	C7_3	1.49(3)
Te7	Te8	2.78(3)	C7_3	C8_3	1.49(3)
C1_1	C2_1	1.49(3)	C8_3	C9_3	1.49(3)
C2_1	C3_1	1.49(3)	C9_3	C10_3	1.49(3)
C3_1	C4_1	1.49(3)	C10_3	C11_3	1.50(3)
C4_1	C5_1	1.49(3)	C11_3	C12_3	1.49(3)
C5_1	C6_1	1.49(3)	C12_3	N1_3	1.41(5)
C6_1	C7_1	1.49(3)	N1_3	C13_3	1.4200
C7_1	C8_1	1.49(3)	N1_3	C15_3	1.4200
C8_1	C9_1	1.49(3)	C13_3	N2_3	1.4200
C9_1	C10_1	1.50(3)	N2_3	C14_3	1.4200
C10_1	C11_1	1.50(3)	N2_3	C16_3	1.42(5)
C11_1	C12_1	1.50(3)	C14_3	C15_3	1.4200
C12_1	N1_1	1.41(5)	C1_4	C2_4	1.50(3)
N1_1	C13_1	1.4200(16)	C2_4	C3_4	1.50(3)
N1_1	C15_1	1.4200(11)	C3_4	C4_4	1.49(3)

C13_1	N2_1	1.4200		C4_4	C5_4	1.49(3)
N2_1	C14_1	1.4200(19)		C5_4	C6_4	1.50(3)
N2_1	C16_1	1.41(5)		C6_4	C7_4	1.49(3)
C14_1	C15_1	1.4200(13)		C7_4	C8_4	1.49(3)
C1_2	C2_2	1.49(3)		C8_4	C9_4	1.49(3)
C2_2	C3_2	1.50(3)		C9_4	C10_4	1.49(3)
C3_2	C4_2	1.50(3)		C10_4	C11_4	1.50(3)
C4_2	C5_2	1.50(3)		C11_4	C12_4	1.49(3)
C5_2	C6_2	1.49(3)		C12_4	N1_4	1.41(5)
C6_2	C7_2	1.49(3)		N1_4	C13_4	1.4200
C7_2	C8_2	1.49(3)		N1_4	C15_4	1.4200
C8_2	C9_2	1.49(3)		C13_4	N2_4	1.4200
C9_2	C10_2	1.49(3)		N2_4	C14_4	1.4200(11)
C10_2	C11_2	1.49(3)		N2_4	C16_4	1.41(5)
C11_2	C12_2	1.49(3)		C14_4	C15_4	1.4200(10)

Table S10. Bond angles for $(C_{12}C_1Im)_8\mathbf{1}$ (symmetry operation: i = 1–x, 1–y, 1–z)

Atom	Atom	Atom	Angle/°		Atom	Atom	Atom	Angle/°
Te1	Hg1	Te2	132.6(8)		N1_2	C12_2	C11_2	128(4)
Te4	Hg1	Te1	111.3(7)		C12_2	N1_2	C13_2	125.9(10)
Te4	Hg1	Te2	116.1(7)		C12_2	N1_2	C15_2	126.1(10)
Te2	Hg2	Te3	115.9(7)		C15_2	N1_2	C13_2	108.0
Te2	Hg2	Te5	141.7(7)		N2_2	C13_2	N1_2	108.00(9)
Te5	Hg2	Te3	102.4(7)		C13_2	N2_2	C14_2	108.0
Te5	Hg3	Te8	110.2(7)		C16_2	N2_2	C13_2	125.9(10)
Te6	Hg3	Te5	131.1(7)		C16_2	N2_2	C14_2	126.1(10)
Te6	Hg3	Te8	118.1(6)		C15_2	C14_2	N2_2	108.00(10)
Te1ⁱ	Hg4	Te6	128.5(8)		C14_2	C15_2	N1_2	108.00(9)
Te1ⁱ	Hg4	Te7	114.6(6)		C1_3	C2_3	C3_3	115(3)
Te6	Hg4	Te7	116.9(7)		C2_3	C3_3	C4_3	115(3)
Hg4ⁱ	Te1	Hg1	100.4(6)		C3_3	C4_3	C5_3	115(3)
Hg2	Te2	Hg1	96.9(7)		C6_3	C5_3	C4_3	115(3)
Te4	Te3	Hg2	103.3(8)		C5_3	C6_3	C7_3	116(3)
Te3	Te4	Hg1	105.4(7)		C8_3	C7_3	C6_3	115(3)
Hg3	Te5	Hg2	109.1(8)		C9_3	C8_3	C7_3	116(3)
Hg3	Te6	Hg4	98.3(7)		C8_3	C9_3	C10_3	116(3)
Te8	Te7	Hg4	102.3(7)		C9_3	C10_3	C11_3	115(3)
Hg3	Te8	Te7	103.9(8)		C12_3	C11_3	C10_3	115(3)
C1_1	C2_1	C3_1	116(3)		N1_3	C12_3	C11_3	120(4)
C2_1	C3_1	C4_1	115(3)		C12_3	N1_3	C13_3	126.1(10)
C5_1	C4_1	C3_1	116(3)		C12_3	N1_3	C15_3	125.9(10)
C6_1	C5_1	C4_1	116(3)		C15_3	N1_3	C13_3	108.0
C5_1	C6_1	C7_1	116(3)		N2_3	C13_3	N1_3	108.00(7)
C6_1	C7_1	C8_1	115(3)		C13_3	N2_3	C14_3	108.00(8)
C9_1	C8_1	C7_1	116(3)		C16_3	N2_3	C13_3	126.0(10)
C8_1	C9_1	C10_1	115(3)		C16_3	N2_3	C14_3	126.0(10)
C9_1	C10_1	C11_1	115(3)		N2_3	C14_3	C15_3	108.0

C10_1	C11_1	C12_1	115(3)		N1_3	C15_3	C14_3	108.00(7)
N1_1	C12_1	C11_1	127(5)		C3_4	C2_4	C1_4	115(3)
C12_1	N1_1	C13_1	126.0(10)		C4_4	C3_4	C2_4	115(3)
C12_1	N1_1	C15_1	126.0(10)		C5_4	C4_4	C3_4	116(3)
C13_1	N1_1	C15_1	108.0		C4_4	C5_4	C6_4	115(3)
N1_1	C13_1	N2_1	108.00(9)		C7_4	C6_4	C5_4	115(3)
C13_1	N2_1	C14_1	108.00(16)		C6_4	C7_4	C8_4	116(3)
C16_1	N2_1	C13_1	126.0(10)		C7_4	C8_4	C9_4	115(3)
C16_1	N2_1	C14_1	126.0(10)		C10_4	C9_4	C8_4	116(3)
C15_1	C14_1	N2_1	108.0		C9_4	C10_4	C11_4	115(3)
C14_1	C15_1	N1_1	108.00(13)		C12_4	C11_4	C10_4	115(3)
C1_2	C2_2	C3_2	116(3)		N1_4	C12_4	C11_4	122(4)
C4_2	C3_2	C2_2	115(3)		C12_4	N1_4	C13_4	126.0(10)
C3_2	C4_2	C5_2	116(3)		C12_4	N1_4	C15_4	126.0(10)
C6_2	C5_2	C4_2	115(3)		C13_4	N1_4	C15_4	108.0
C7_2	C6_2	C5_2	116(3)		N1_4	C13_4	N2_4	108.00(8)
C6_2	C7_2	C8_2	116(3)		C14_4	N2_4	C13_4	108.00(8)
C9_2	C8_2	C7_2	115(3)		C16_4	N2_4	C13_4	126.1(10)
C8_2	C9_2	C10_2	115(3)		C16_4	N2_4	C14_4	125.9(10)
C9_2	C10_2	C11_2	115(3)		C15_4	C14_4	N2_4	108.0
C12_2	C11_2	C10_2	115(3)		N1_4	C15_4	C14_4	108.00(11)

4. Micro X-Ray Fluorescence Spectroscopy (µ-XRF)

Micro X-ray fluorescence spectroscopy (µ-XRF) was used to determine the heavy atom composition of crystalline samples of $(C_{10}C_1Im)_8$**1**. The measurement was carried out using a Bruker M4 Tornado spectrometer with an Rh target X-ray tube, poly-capillary optics and a Si drift detector. The fluorescence photons emitted by the sample were detected, followed by data processing *via* elemental parameter methods. The quantification of the elements is based on the Hg-L and Te-L fluorescent spectral lines. The notable deviation from the calculated values can be explained by the small thickness and light matrix of the sample, causing relative underestimation of higher energy signals. The relative results are summarized in Table S11, the deconvoluted spectrum is shown in Figure S5.

Insufficient size and thickness of the samples of $(C_{12}C_1Im)_8$**1** hampered elemental analysis of the second compound (see section 1.3.).

Table S11. Results of the µ-XRF analysis of $(C_{10}C_1Im)_8$**1.**

Element	Radiation	Atom% calculated	Atom% measured
Hg	L	33.33	31.22(5)
Te	L	66.67	68.78(24)
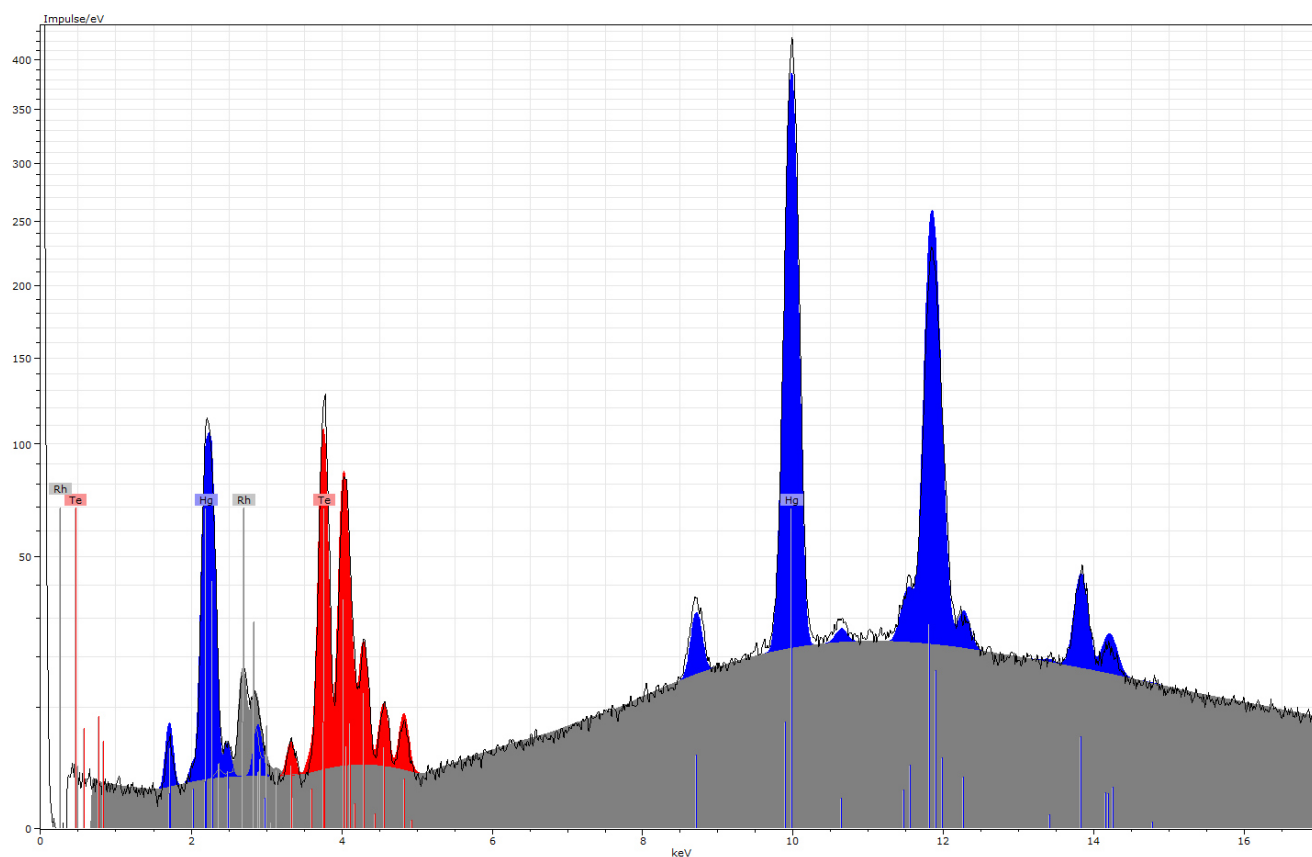
Figure S5. Micro X-ray fluorescence spectrum shown with deconvolution. The Rh signal (dark grey) is generated by diffuse scattering of the primary beam.

5. Optical Absorption Measurements

The optical absorption spectra were measured with the aid of a transmission microscope at ambient conditions and room temperature on a single crystalline sample covered in mineral oil. An objective with a numerical aperture of 0.5 and 32× magnification is used together with a standard tungsten-halogen bulb for illumination. A 50 μm pinhole is positioned in the image plane of the microscope. A beam splitter between the objective and the sample holder is used to keep optical control of the sample alignment. Thereby the real image is displayed on a metal oxide-semiconductor color camera chip (5.632 mm × 4.224 mm; 2560 px × 1920 px). The light transmitted through the sample is analyzed with a Czerny-Turner-spectrometer in combination with a Roper Scientific liquid nitrogen cooled silicon charge-coupled device camera. This setup covers a field of view of 220 μm × 160 μm and a region of interest of less than 2 μm × 2 μm.

6. Quantum Chemical Investigations

6.1. Methods and Accuracy

Quantum chemical studies were done with TURBOMOLE[S6] employing the TPSSh functional[S7] with def2-TZVP bases[S8] and corresponding Coulomb auxiliary bases[S9] as well as effective core potentials.[S10] Charge compensation was realized with COSMO[S11] employing default parameters. The molecular structure of **1** was optimized both in C_i symmetry (according to the experimentally found local symmetry) and without symmetry restrictions (point group C_1), which led to identical results. Despite a flattening of the structure due to the absence of counterions (see Figure S6), the agreement of calculated and experimentally found structural parameters is excellent (see Table S12), with maximum deviations of bond lengths by 0.07 Å. The metal complexes (see section 6.2.) were optimized without symmetry restrictions.

Table S12. Comparison of structural parameters in the calculated anion $[Hg_8Te_{16}]^{8-}$ (**1**) with those found in the crystal structure of $(C_{10}C_1Im)_8$**1.**

Length/Å	DFT	X-Ray
Hg–Te (μ-Te within [Hg₂Te(Te₂)] unit)	2.720 – 2.728	2.692(1) – 2.703(1)
Hg–Te (μ-Te between [Hg₂Te(Te₂)] units)	2.753 – 2.758	2.695(1) – 2.710(1)
Hg–Te (Te₂ unit)	2.835 – 2.858	2.762(1) – 2.803(1)
Te–Te (Te₂ unit)	2.756	2.728(2) – 2.750(1)
Angle/°	DFT	X-Ray
Hg–Te–Hg (μ-Te within [Hg₂Te(Te₂)] unit)	97.299 – 97.428	97.73(3) – 97.86(4)
Hg–Te–Hg (μ-Te between [Hg₂Te(Te₂)] units)	99.112 – 100.058	99.99(4) – 110.24(4)
(μ–Te)–Hg–(Te₂)	106.162 – 109.833	102.61(4) – 117.69(3)
(μ-Te)–Hg–(μ-Te)	132.716 – 136.604	127.36(4) – 142.39(4)
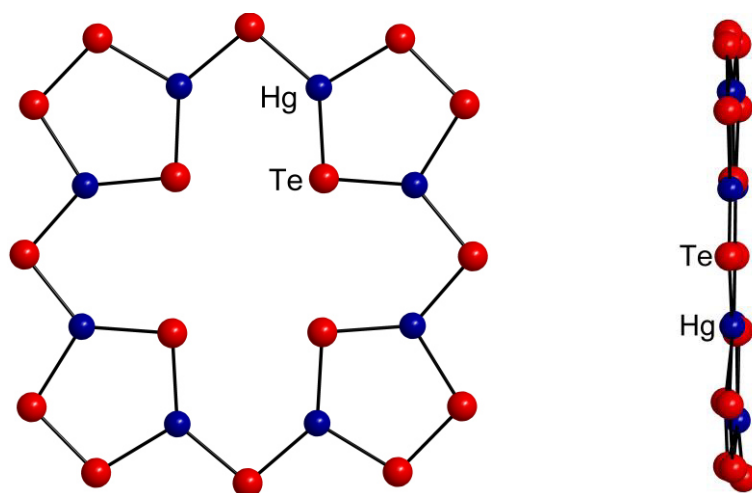
Figure S6. Two views of the calculated molecular structure of the $[Hg_8Te_{16}]^{8-}$ anion (**1**).

6.2. Molecular Orbitals of 1

Figure S7 illustrates the highest-energy MOs representing σ-bonding, representing s-type (119 a_g), p-type (119 a_u), d-type (117 a_g, 120 a_g) or g-type (118a_g) MOs.
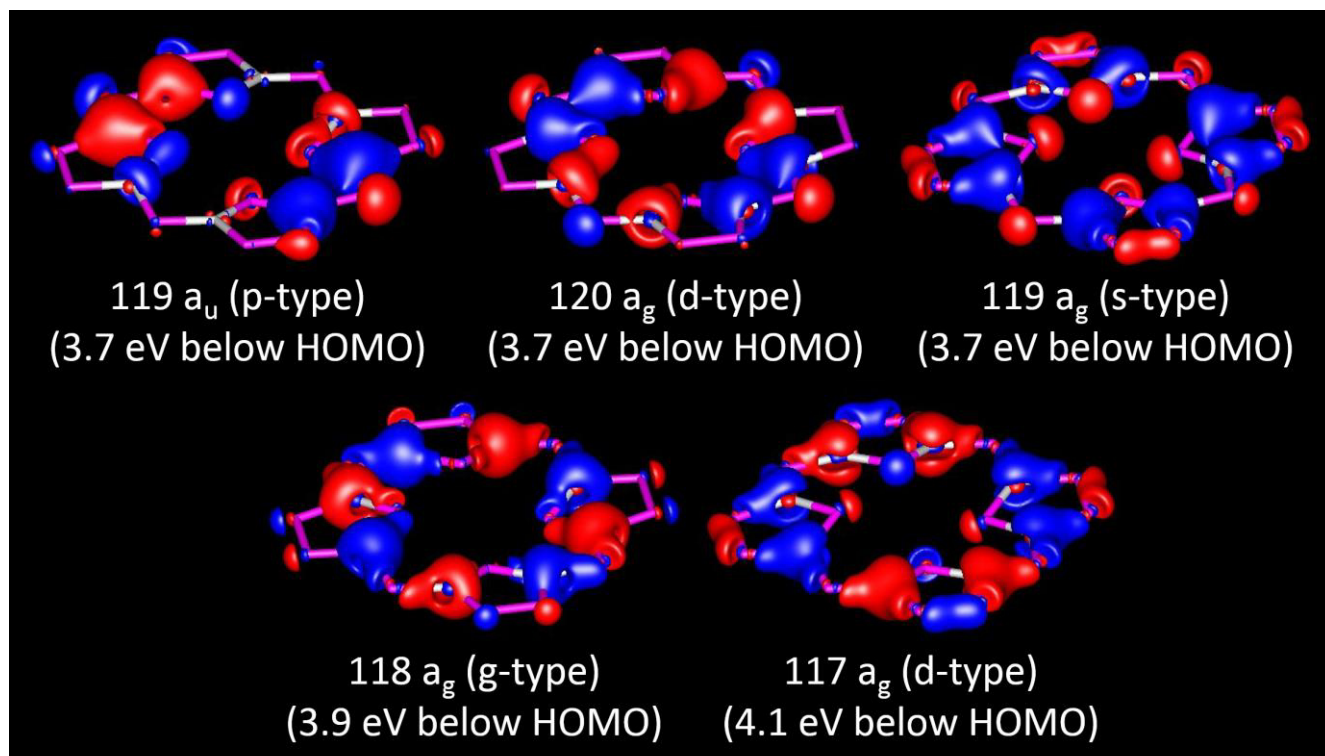
Figure S7. Selected canonical MOs (C_i symmetry) in the calculated $[Hg_8Te_{16}]^{8-}$ anion (**1**), with the shape of cluster s-, p-, d-, or g- orbitals.

6.3. Calculation of Transition Metal Complexes of 1

Optimized structures of some hypothetical metal complexes $[M@1]^{(8-q)-}$ (M^{q+} = Zn^{2+}, Cu^+, Ce^{4+}, or Ti^{4+}) are shown in Figure S8 as examples.
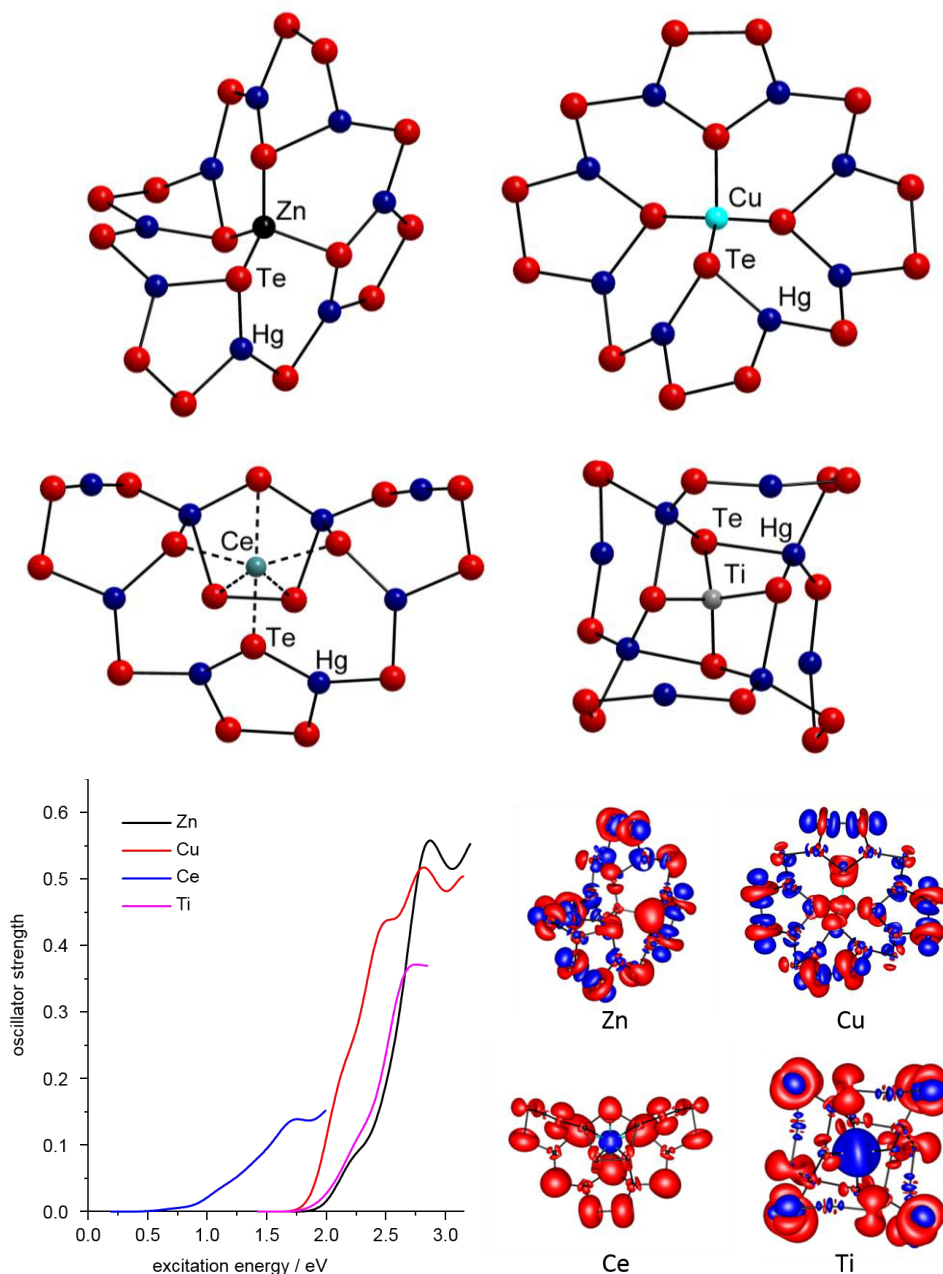
Figure S8. Top: Molecular structures of calculated metal complexes of **1**, indicating the conformational flexibility of the macrocycle. Bottom left: Calculated optical absorption spectra of the respective complex anions (TD-DFT). Calculated singlet excitation energies and oscillator strengths (lowest 150 excitations), plotted as superimposed Gaussians of fwhm = 0.3 eV to simulate the spectra. Bottom right: The characters of the respective bands are visualized using the nonrelaxed difference densities as described previously.[S12] The contributions of the occupied orbitals are plotted in red and those of the unoccupied orbitals in blue.

Insertion of Zn^{2+} or Cu^+ into the $[Te_{16}Hg_8]^{8-}$ framework mainly causes distortion in order to allow for a tetrahedral coordination of the metal ion. For Ce^{4+} and Ti^{4+}, the ring undergoes more significant rearrangements, either to comply with the larger preferred coordination number in the case of Ce^{4+}, or to match the very small ionic radius of Ti^{4+}.

The calculated optical absorption spectra of the complexes indicate the most significant red-shift to occur for the structurally most significantly affected Ce^{4+} complex (onset of absorption at ca. 0.8 eV), followed by the Cu^+ complex with least structural changes (onset of absorption at ca. 1.6 eV). The Ti^{4+} and Zn^{2+} complexes cause an only small red-shift (onset of absorption at ca. 1.9 or 2.0 eV, respectively). Regarding the character of the band, it is very similar to that of the empty macrocycle (see Figure 3 in the main document) for the Cu^+ and Zn^{2+} complexes. In the case of the Ce^{4+} complex, the electron density is shifted towards the Ce(4f) orbitals during the excitation (LUMO···LUMO+6), and for the Ti^{4+} complex, it is shifted towards Te–Te antibonding molecular orbitals and towards Ti(3d) orbitals.

These few examples already clearly illustrate the easy variation of the structures and absorption characteristics of such ternary complexes.

To estimate the experimental availability of such complexes, we investigated bond energies. However, as direct calculation of bond energies for the metal ion complexation is unreliable due to strong solvent effects for the atomic cation in COSMO, we instead calculated the exchange energies for the hypothetical exchange reaction with organic porphyrin, shown in equation (S1):

$$\{M^{q+}@[C_{20}H_{12}N_4]^{2-}\} + [Te_{16}Hg_8]^{8-} \rightarrow [C_{20}H_{12}N_4]^{2-} + \{M^{q+}@[Te_{16}Hg_8]^{8-}\} \quad \text{(S1)}$$
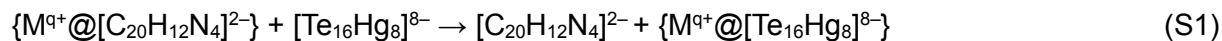
These reactions are endothermic for all tested metal ions, as expected; calculated reaction energies for $M^{q+} = Zn^{2+}$, Cu^+, Ce^{4+}, or Ti^{4+} amount to 279, 232, 27, or 112 kJ/mol, respectively.

6.4. Calculation of Ring Currents in [B₈S₁₆] and [B₈S₁₆]

Quantum chemical studies were also done on the previously known porphyrine-related structures of [B_8S_{16}] and [B_8Se_{16}][S13] for comparison. These were done with the same methods as used for the new molecule, thus representing an update of previous calculations done in the 1980s with Hückel MO calculations.[S14]

Figure S9 illustrates the resulting ring currents. Like for the anion in **1**, it indicates the presence of nearly no global ring current (S: 0.81 nA/T, Se: 0.79 nA/T), and a weak ring current was calculated in the five-membered rings (S: 3.25 nA/T, Se: 3.28 nA/T), which is a bit weaker than that calculated for the anion in **1** (5.8 nA/T). In organic porphyrin, the situation is very different. Here, the global ring current of 27 nA/T splits at the pyrrolic rings into outer and inner pathways of about the same strength, whereas the local ring current in the pyrrolic rings is weaker than 1 nA/T.[S15]
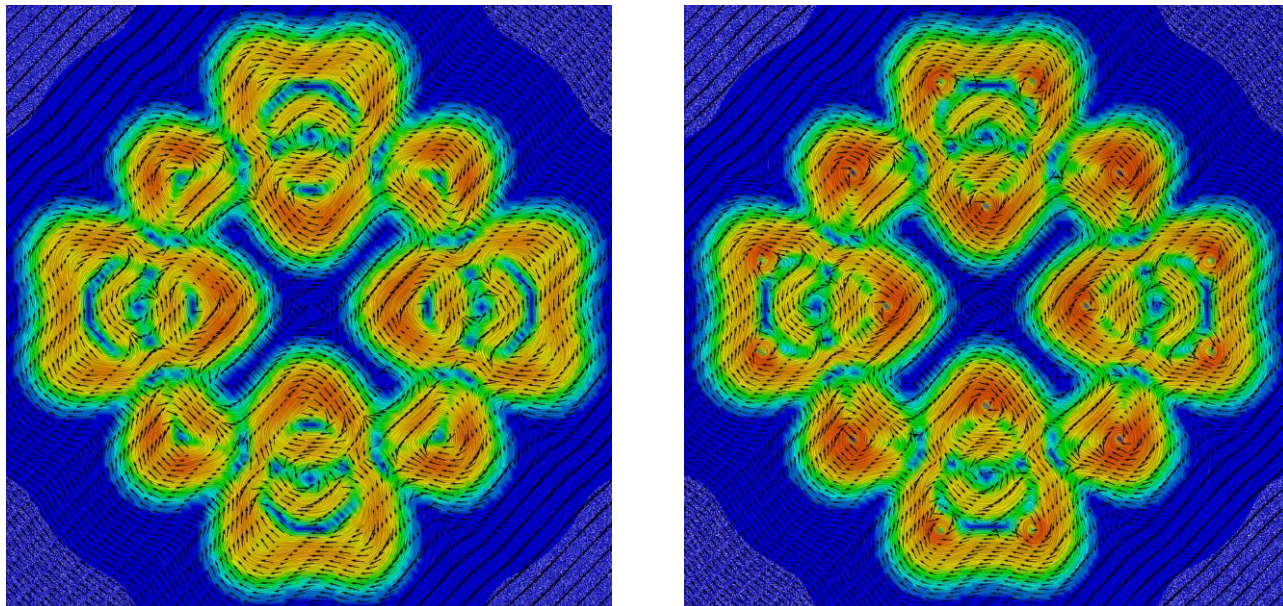

Figure S9. Ring currents, 1 bohr above the molecular plane of [B_8S_{16}] (left) and [B_8Se_{16}] (right), drawn between 0 a.u. (blue) and 0.07 a.u. (red).

7. References for the Supporting Information

[S1]   C. Donsbach, S. Dehnen, *Z. Anorg. Allg. Chem.* **2017**, *643*, 14–19.

[S2]   Y. Lin, W. Massa, S. Dehnen, *Chem. Eur. J*. **2012**, *18*, 13427–13434.

[S3]   G. M. Sheldrick, *Acta Crystallogr., Sect. A* **2015**, *71*, 3–8.

[S4]   G. M. Sheldrick, *Acta Crystallogr., Sect. C* **2015**, *71*, 3–8.

[S5]   O. V. Dolomanov, L. J. Bourhis, R. J. Gildea, J. A. K. Howard, H. Puschmann, *J. Appl. Crystallogr.* **2009**, *42*, 339–341.

[S6]   TURBOMOLE Version 7.2, TURBOMOLE GmbH 2017. TURBOMOLE is a development of the University of Karlsruhe and the Forschungszentrum Karlsruhe 1989-2007, TURBOMOLE GmbH since 2007.

[S7]   V. Staroverov, G. Scuseria, J. Tao, J. Perdew, *J. Chem. Phys.* **2003**, *119*, 12129.

[S8]   a) F. Weigend, R. Ahlrichs, *Phys. Chem. Chem. Phys*., **2005**, *7*, 3297–3305. b) D. Andrae, U. Häussermann, M. Dolg, H. Stoll, H. Preuß, *Theor. Chim. Acta.* **1990**, *77*, 123-141.

[S9]   F. Weigend, *Phys. Chem. Chem. Phys*. **2006**, *8*, 1057–1065.

[S10] K. A. Peterson, D. Figgen, E. Goll, H. Stoll, M. Dolg, *J. Chem. Phys.* **2003**, *119*, 11113.

[S11] A. Klamt, G. Schüürmann, *J. Chem. Soc., Perkin Trans. 2* **1993**, 799.

[S12] X.-X. Yang, I. Issac, S. Lebedkin, M. Kühn, F. Weigend, D. Fenske, O. Fuhr, A. Eichhöfer, *Chem. Commun.* **2014**, *50*, 11043−11045.

[S13] a) B. Krebs, H.-U. Hürter, *Angew. Chem.* **1980**, *92*, 479–480; *Angew. Chem. Int. Ed. Engl.* **1980**, 19, 481–482; b) B. Krebs, H.-U. Hürter, *Acta Crystallogr. A* **1981**, *37*, C163b.

[S14] B. M. Gimarc and N. Trinajstić, *Inorg. Chem.* **1982**, *21*, 21–25.

[S15] H. Fliegl, D. Sundholm, *J. Org. Chem.* **2012**, *77*, 3408–3414.

6.4 Supporting Information zum Manuskript "Not so innocent after all? The role of ionic liquid cations as methylation agent" (3.8)

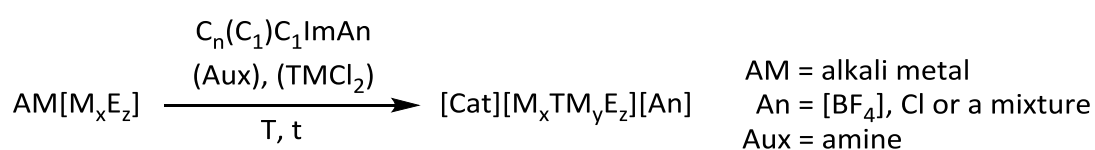# Not so innocent after all? The role of ionic liquid cations as methylation agent

Bertram G. H. Peters,[1] Silke Santner,[1] Carsten Donsbach,[1] and Stefanie Dehnen[1]*

[1] Fachbereich Chemie und Wissenschaftliches Zentrum für Materialwissenschaften (WZMW), Philipps-Universität Marburg, Hans-Meerwein-Straße 4, 35043 Marburg, Germany.

SUPPORTING INFORMATION

Syntheses

General. All reactions were performed in borosilicate glass ampoules. All reactants were treated under argon atmosphere by using standard *Schlenk* technique and gloveboxes. Ionic liquids of the type $(C_m(C_n)C_1Im)[BF_4]$ and $(C_m(C_n)C_1Im)Cl$ were purchased from Sigma Aldrich; in the formulae, $(C_m(C_n)C_oIm)^+$ denote tri(/di)-alkylated imidazolium cations, with *n*, *m* and *o* specifying the chain lengths of the alkyl substituents in the respective 1, 2 and 3 positions of the imidazole ring. Chalcogenidostannate salts were prepared according to the quoted literature procedures. Amines ethane-1,2-diamine (*en*) or 2,6-dimethylmorpholine (DMMP) were dried and freshly distilled prior to use. Products of the ionothermal reactions were analyzed by X-ray powder diffraction, single-crystal X-ray diffraction, micro X-ray fluorescence spectroscopy (μ-XFS), and Raman spectroscopy.

$$AM[M_xE_z] \xrightarrow[\text{T, t}]{\substack{C_n(C_1)C_1ImAn \\ (Aux),\ (TMCl_2)}} [Cat][M_xTM_yE_z][An]$$

AM = alkali metal
An = [BF$_4$], Cl or a mixture
Aux = amine

Scheme S1: . General ionothermal synthesis of chalcogenido metalates with different ionic liquids, auxiliaries (Aux) and transition metal chlorides (TMCl$_2$) as additives at different temperatures (T) with different reaction durations (t).

Synthesis of $(C_4C_1C_1Im)_5[Sn_{10}S_{16}O_4(S–Me)_4][BF_4]$ (1a). Compound **1a** was obtained by the reaction of Li$_4$SnS$_4$·13H$_2$O[S1] in a mixture of $(C_4C_1C_1Im)[BF_4]$ and $(C_4C_1C_1Im)Cl$ in a 3:2 ratio. As an auxiliary, 50 μL of *en* were added. The reaction mixture was heated at 150°C for 4 d. After a few weeks, compound **1a** crystallizes as colorless bars.

Synthesis of $(C_4C_1C_1Im)_4[Sn_{10}S_{16}O_4(S–Me)_4]$ (1b). Compound **1b** was obtained by the reaction of Na$_4$SnS$_4$·14H$_2$O[S2] in a mixture of $(C_4C_1C_1Im)[BF_4]$ and $(C_4C_1C_1Im)Cl$ in a 1:1 ratio. As an auxiliary, 50 μL of *en* were added and as an additive, 11 mg of MnCl$_2$ were added. The reaction mixture was heated at 180°C for 4 d. After a few weeks, compound **1b** crystallizes as colorless bars.

Synthesis of $[Cat]_x[Sn_{10}S_{20}O_4][An]_y$ (1c). Compound **1c** was obtained by the reaction of Na$_4$SnS$_4$·14H$_2$O[S2] in a mixture of $(C_4C_1C_1Im)[BF_4]$ and $(C_4C_1C_1Im)Cl$ in a 3:2 ratio. As an auxiliary, 75 μL of DMMP were added. The reaction mixture was heated at 180°C for 4 d. After a few weeks, compound **1c** crystallizes as colorless trigonal prisms or octahedral blocks.

Synthesis of $[Cat]_x[Sn_{10}S_{20}O_4][An]_y$ (1d). Compound **1d** was obtained by the reaction of Li$_4$SnS$_4$·13H$_2$O[S1] in a mixture of $(C_4C_1C_1Im)[BF_4]$ and $(C_4C_1C_1Im)Cl$ in a 4:1 ratio. As an auxiliary, 100 μL of *en* were added. The reaction mixture was heated at 150°C for 4 d. After a few weeks **1d** crystallizes in colorless octahedral blocks.

Synthesis of $(C_4C_1C_1Im)_4[Sn_{10}S_{16}O_4(S–Me)_4]$ (1e and 1f). Compound **1e** and **1f** were obtained by the reaction of $Na_4SnS_4·14H_2O^{[S2]}$ in a mixture of $(C_4C_1C_1Im)[BF_4]$ and $(C_4C_1C_1Im)Cl$ in a 3:2 ratio. As an additive, 11 mg of $MnCl_2$ were added. The reaction mixture was heated at 150°C for 4 d. After a few days, compounds **1e** and **1f** crystallize as colorless blocks.

Synthesis of $(dmmpH)_6[Mn_4Sn_4Se_{13}(Se–Me)_4]$ (2). Compound **2** was obtained by the reaction of 60 mg of $K_2[Sn_2Se_5]^{[S3]}$ and 20 mg of $MnCl_2$ in the presence of 50 µL of DMMP in 0.5 mL of $(C_4C_1Im)[BF_4]$. Upon heating of the reaction mixture at 120 °C for 96 h, compound **4** crystallized as orange blocks.

Synthesis of $(C_6C_1Im)_6[Hg_6Te_{10}(Te–Me)_2]$ (3a) and $(C_8C_1Im)_6[Hg_6Te_{10}(Te–Me)_2]$ (3b). Compounds **3a** und **3b** were synthesized in the reaction of 50 mg of $Na_2[HgTe_2]^{[S4]}$ in 250 µL of $(C_6C_1Im)[BF_4]$ or $(C_8C_1Im)[BF_4]$, respectively. The mixture was heated at 60 °C overnight. Red plates of **3a** and **3b** were obtained in nearly quantitative crystalline yield upon cooling to room temperature.

Single-crystal X-ray Diffraction Studies, Data Collection, Refinement and Crystallographic Details

Crystals suitable for X-ray diffraction analyses were investigated with a STOE IPDS-II (**1d**), IPDS-2T (**2**), StadiVari (**1b**, **1e**, **1f**) or a Bruker D8 Quest (**1a**, **1c**, **3a**, **3b**) diffractometer at 100 K using. On the STOE IPDS-II and IPDS-2T diffractometers, diffraction experiments were run with Mo-$K\alpha$ radiation and a graphite monochromator (λ = 0.71073 Å). The STOE StadiVari diffractometer used Cu Kα radiation (λ = 1.54186) from an X-ray micro source with X-ray optics and a Pilatus 300K Si hybrid pixel array detector. On the Bruker D8 Quest diffractometer, Mo-Kα radiation from an X-ray micro source tube with X-ray optics and a Photon 100 charge-integrating pixel array detector were used. Upon numerical absorption correction (STOE X-AREA; **1d**, **2**), scaling with spherical absorption correction (STOE X-Area Lana; **1b**, **1e**, **1f**) or scaling with multiscan absorption correction (Bruker SADABS; **1a, 1c, 3a, 3b**),respectively, the structure solution was performed by direct methods, followed by full-matrix-least-squares refinement against $F2$, using SHELXT15, SHELXL15, and OLEX2 software.[S5] Table S1 summarizes the crystallographic data for **1a – 3b**.

Table 1. Crystallographic data of **1a – 3b**.

Compound (CCDC number)	1a	1b	1c	1d	1e	1f	2	3a	3b
Empirical formula	$BC_{39.5}F_4N_9O_4S_{20}Sn_{10}$	$C_{33.5}N_8O_4S_{20}Sn_{10}$	$O_4S_{20}Sn_{10}$	$O_4S_{20}Sn_{10}$	$O_4S_{20}Sn_{10}$	$O_4S_{20}Sn_{10}$	$C_{40}H_{96}Mn_4N_6O_6Se_{17}Sn_4$	$C_{62}H_{120}Hg_6N_{12}Te_{12}$	$C_{74}H_{144}Hg_6N_{12}Te_{12}$
Formula weight /g·mol^{-1}	2561.38	2405.43	49.95	1895.13	2004.19	1892.06	2794.06	3768.43	3936.74
Color & shape	colorless rod	colorless needle	colorless block	colorless block	colorless block	colorless block	orange block	red plate	red plate
Crystal size /mm³	0.06x0.12x0.3	0.06x0.08x0.3	0.1x0.2x0.3				0.15x0.14x0.14	0.11x0.09x0.01	0.27x0.15x0.01
Crystal system & space group	orthorhombic $Pbcm$	triclinic $P\bar{1}$	cubic $Fd\bar{3}m$	cubic $Fd\bar{3}m$	Tetragonal $I\bar{4}c_2$	Hexagonal $P6_3/mmc$	trigonal $R\bar{3}$	triclinic $P\bar{1}$	triclinic $P\bar{1}$
a /Å	17.727(4)	13.1046	73.537(3)	27.266(11)	29.1874(4)	18.9987	16.4857(3)	10.0647(14)	10.0664(8)
b /Å	35.611(7)	21.8727	73.537(3)	27.266(11)	29.1874(4)	18.9987	16.4857(3)	11.591(2)	11.5576(9)
c /Å	31.733(6)	27.9377	73.537(3)	27.266(11)	57.5222(14)	31.8798	54.2335(15)	21.309(3)	24.550(2)
α /°	90	79.966	90	90	90	90	90	78.961(5)	89.172(3)
β /°	90	79.828	90	90	90	90	90	83.155(4)	85.585(3)
γ /°	90	84.995	90	90	90	120	120	83.555(5)	83.936(2)
V /Å³	20032(7)	7748.1(6)	397672(45)	20270(25)	49003.4	9965.4(8)	12764.8(6)	2385.5(7)	2831.7(4)
Z	8	4	136	8	24	4	6	1	1
ρ_{calc} /g·cm^{-3}	1.699	2.062	1.075	1.240	1.630	1.261	2.181	2.623	2.309
Radiation (λ /Å)	Mo$_{K\alpha}$ (0.71073)	Cu$_{K\alpha}$ (1.54186)	Mo$_{K\alpha}$ (0.71073)	Mo$_{K\alpha}$ (0.71073)	Cu$_{K\alpha}$ 1.54186	Cu$_{K\alpha}$ (1.54186)	Mo$_{K\alpha}$ (0.71073)	Mo$_{K\alpha}$ (0.71073)	Mo$_{K\alpha}$ (0.71073)
Temperature	100K	100K	100K	100K	100K	100K	100 K	100 K	100 K
μ /mm^{-1}	2.903	30.511	2.458	2.836	28.771	23.546	9.035	13.253	11.170
Min/max transmission		0.0001/ 0.0233					0.3342/ 0.3997	0.0050/ 0.0249	0.0074/ 0.0277
$F(000)$	9472.0	4434.0	115872.0	6816.0	21792.0	3408.0	7824	1680	1776
θ range /°	2.566–26.853	3.432–68.000	2.216–14.399	2.113–20.051	2.635–81.472	2.686–76.928	2.471–26.853	2.186–27.500	2.261–27.998
No. measured refl.	163419	71389	79634	3835	147460	49585	42399	52343	88604
No. indep. refl. (restr. to $I>2\sigma(I)$)	21715	27594 (20671)	3318	495	25928 (9386)	3860 (1426)	5975 (4125)	10898 (8587)	13672 (9797)
No. of parameters	680	1132	263	22	509	70	249	729	632
No. of restraints	3	1	0	0	0	0	9	1416	2296
R(int)	0.1476	0.0894	0.2785	0.2186	0.2194	0.0853	0.0954	0.0494	0.0602
R_1 ($I>2\theta(I)$)	0.0522	0.1098	0.1529	0.0909	0.1044	0.1379	0.0551	0.0599	0.0499
wR_2 (all data)	0.1619	0.3375	0.4457	0.2744	0.3215	0.4722	0.1578	0.1451	0.1292
S (all data)		1.309			0.855	1.348	1.038	1.110	1.067
Flack parameter					0.07(3)				
$\Delta\rho max$, $\Delta\rho min$ /e·Å^{-3}	1.90/-1.01	2.66/-1.62	1.25/-1.40	1.12/-0.63	1.48/-1.53	1.34/-1.03	3.27/-1.46	4.14/-2.33	2.10/-1.53

Details of the crystals structures

Comparison of the anion in 1b with the purely inorganic cluster [Sn$_{10}$O$_4$S$_{20}$]$^{10-}$.[S6]
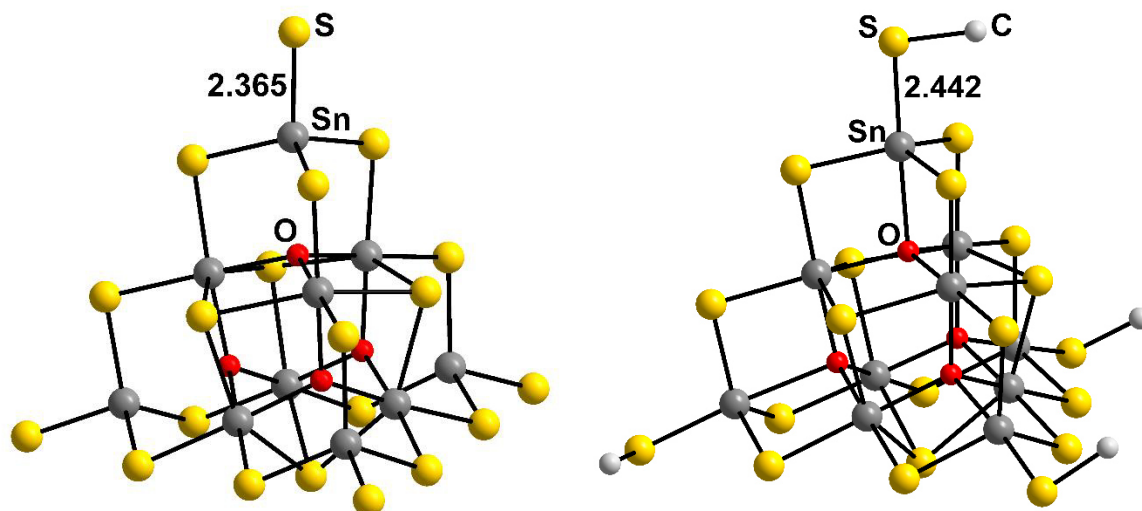
Figure S1: Comparison of the molecular structure of the cluster anions in in [Li$_8$(H$_2$O)$_{29}$][Sn$_{10}$O$_4$S$_{20}$] (left) and **1b** (right) with specification of the bond lengths to the (former) terminal S atoms.[S6] The atoms are drawn as balls and sticks with arbitrary atomic radii, H atoms are omitted. Color code: grey – Sn, yellow – S, red – O, white – C.

Comparison of the anion in 2 with the purely inorganic cluster [Mn$_4$Sn$_4$Se$_{17}$]$^{10-}$.[S7]
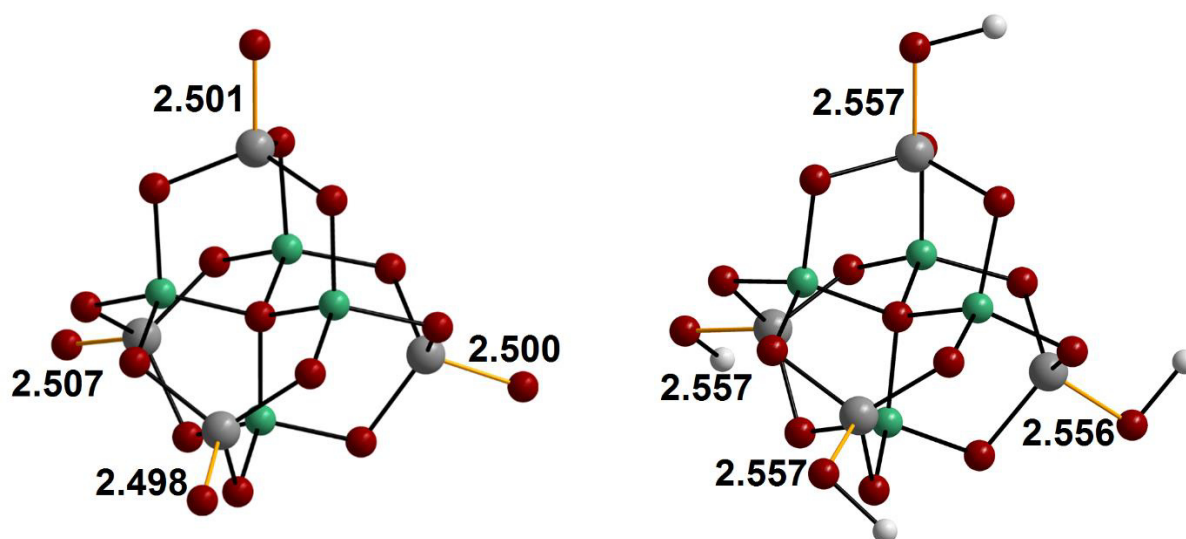
Figure S2: Comparison of the molecular structure of the cluster anions in [Cs$_{10}$(H$_2$O)$_{15.5}$][Mn$_4$Sn$_4$Se$_{17}$] (left) and **2** (right) with specification of the bond lengths to the (former) terminal Se atoms.[S7] The atoms are drawn as balls and sticks with arbitrary atomic radii, H atoms are omitted. Color code: grey – Sn, dark red – Se, teal – Mn, white – C.

Hydrogen bonding situation in the crystal structure of 2.
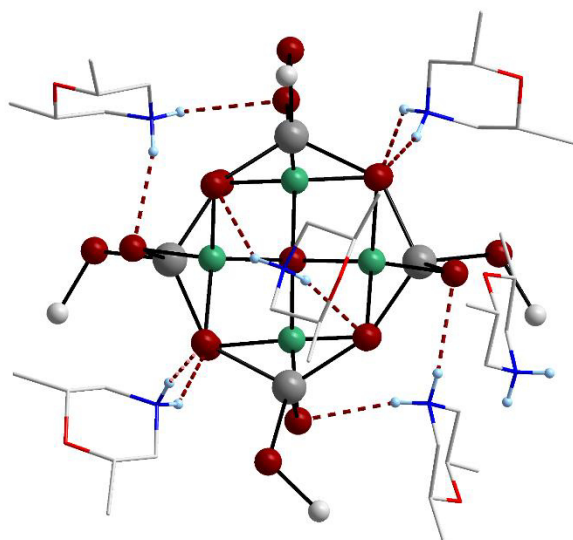
Figure S3: Section of the crystal structure of **2** showing the anion and the six closest (dmmpH)⁺ cations. Hydrogen bonds between the nitrogen bonded H atoms of the cations and Se atoms of the cluster are represented as dashed red lines. The anion is drawn as balls and sticks with arbitrary atomic radii and the cations as wireframes. All H atoms except for the nitrogen bonded ones are omitted. Color code: grey – Sn, dark red – Se, teal – Mn, red – O, blue – N, white – C, light blue – H.

Comparison of the anions in 3a and 3b with related tellurido mercurates.
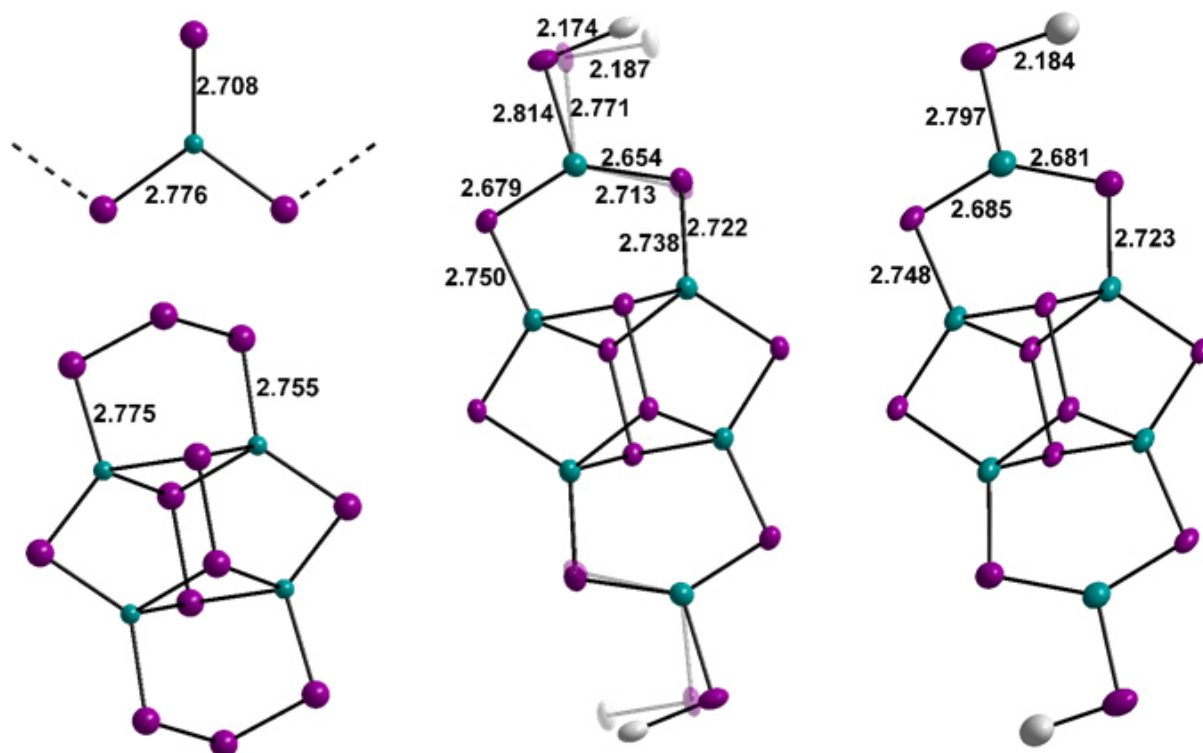
Figure S4: Molecular structure of the $[Hg_6Te_{10}(Te-Me)_2]^{6-}$ anions in **3a** (center) and **3b** (right), compared to the molecular structure of the anions in $Na_2[HgTe_2]$ (top left) and $\{N(C_4H10)_4\}_4[Hg_4Te_{12}]$ (bottom left).[S4,S8] The atoms are shown as balls with arbitrary diameter the literature-known compounds and as thermal ellipsoids at the 50 % probability level for **3a** and **3b**. H atoms are omitted and disordered parts with minor occupancy are represented semi-transparent. Lengths of specific Hg–Te bonds are shown to illustrate the effect of the methylation. Color code: teal – Hg, violet – Te.

Vibrational spectroscopy data of 1a – 1d

Raman spectroscopy: A commercially available Renishaw inVia Raman microscope was used for the Raman measurements of **1a – 1f**. The spectra were measured using a 532 nm laser (10 mW) as excitation source and were recorded in a backscattering geometry at room temperature. The excitation laser was focused with a 50 × objective onto the sample surface. The same objective was used to collect the scattered light, which was then dispersed by a spectrometer with a focal length of 250 mm and finally detected by a charge-coupled device (CCD) camera with a spectral resolution of about 1 cm^{-1}.
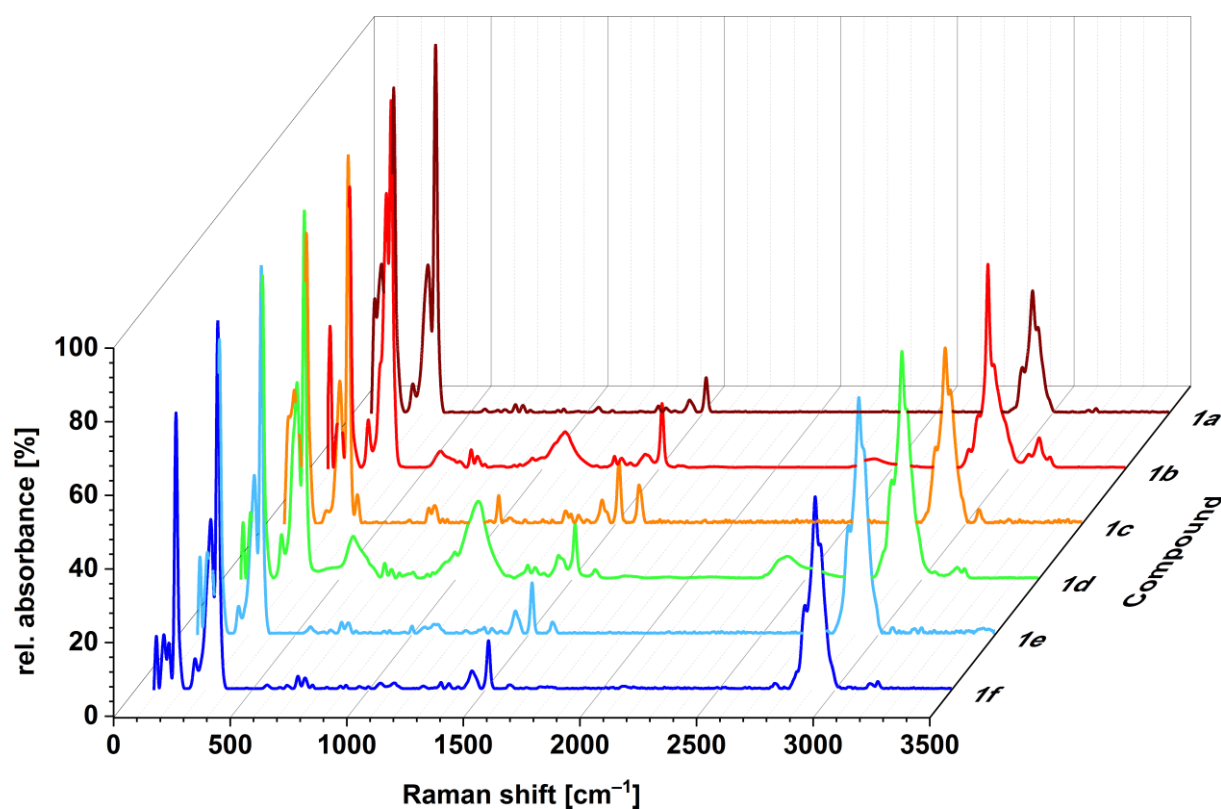
Figure S5: Raman spectra of **1a** (brown)), **1b** (red), **1c** (orange), **1d** (green), **1e** (light blue) and **1f** (blue). The broad signals at approximately 560 cm^{-1}, 1100 cm^{-1} 2350 cm^{-1} were caused by Paratone oil or unidentified decomposition products.

Optical absorption spectroscopy of 2

Optical absorption measurements: The optical absorption properties of **2** were analyzed using diffuse reflection of powdered crystalline samples. The measurements were performed with a Varian Cary 5000 dual-beam spectrometer and a Praying Mantis sample holder from Harrick.
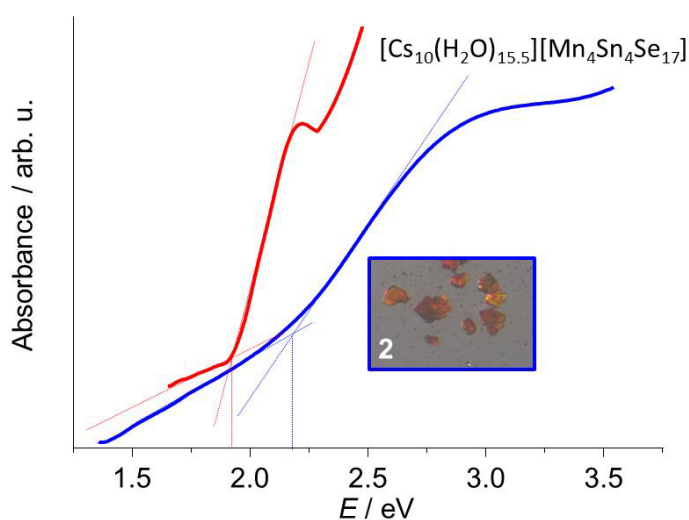
Figure S6: Optical absorption spectra of **2** and $[Cs_{10}(H_2O)_{15.5}][Mn_4Sn_4Se_{17}]$.[S7]

References

[S1] T. Kaib, S. Haddadpour, M. Kapitein, P. Bron, C. Schröder, H. Eckert, B. Roling, S. Dehnen, *Chem. Mater.* **2012**, *24*, 2211–2219.

[S2] W. Schiwy, S. Pohl, B. Krebs, *Z. Anorg. Allg. Chem.* **1973**, *402*, 77–86.

[S3] K. O. Klepp, *Z. Naturforsch. B* **1992**, *47*, 197–200.

[S4] C. Donsbach, S. Dehnen, *Z. Anorg. Allg. Chem.* **2017**, *643*, 14-19.

[S5] a) G. M. Sheldrick, *Acta Crystallogr., Sect. A* **2015**, *71*, 3–8; b) G. M. Sheldrick, *Acta Crystallogr., Sect. C* **2015**, *71*, 3–8; c) O. V. Dolomanov, L. J. Bourhis, R. J. Gildea, J. A. K. Howard, H. Puschmann, *J. Appl. Crystallogr.* **2009**, *42*, 339–341.

[S6] T. Kaib, M. Kapitein, S. Dehnen, *Z. Anorg. Allg. Chem.* 2011, *637*, 1683–1686.

[S7] S. Santner, S. Dehnen, *Inorg. Chem.* **2015**, *54*, 1188–1190.

[S8] R. C. Haushalter, *Angew. Chem. Int. Ed. Engl.* **1985**, *24*, 433–435.

6.5 Weitere Strukturen

Aus ionothermalen Reaktionen von Selenidomerkuraten mit einem Selenidostannat wurden Kristalle zweier neuer Verbindungen mit ternären Metallatstrukturen (**A1** und **A2**) erhalten.

$$K_4[HgSe_3]\cdot H_2O \;+\; Li_4[Sn_2Se_6]\cdot xH_2O \quad \xrightarrow[\;(C_4C_1Im)\,[BF_4]/Cl\;]{120°C,\;3\,d} \quad \{K@[Hg_{4.5}Sn_{11.5}Se_{32}]\}^{8-} \quad (A1)$$

$$K_2[Hg_2Se_3] \;+\; Li_4[Sn_2Se_6]\cdot xH_2O \quad \xrightarrow[\;(C_4C_1Im)\,[BF_4]/Cl\;]{120°C,\;3\,d} \quad [Hg_{10.8}Sn_{15.2}Se_{50}]^{17.6-} \quad (A2)$$
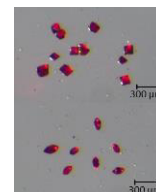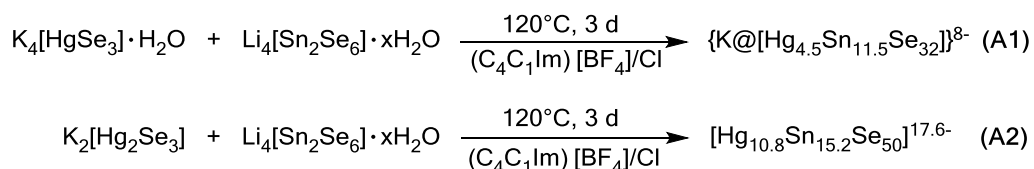
Abbildung 10: Reaktionsschema zur Synthese der Verbindungen **A1** und **A2**.

Die Anionenstruktur von **A1** besteht aus eckenverknüpften T4-supertetraedrischen Baueinheiten, in deren Mitte eine [M$_4$E]-Einheit (M = Sn/Hg, E = Se) fehlt. Wahrscheinlich befindet sich ein Kalium-Kation im Inneren dieses Hohlraums. Eine ähnliche Anordnung wurde erst kürzlich mit Cäsium-Kationen in einem ternären Sn/Ge/Se-Cluster-Anion gefunden.[116]

In der Anionenstruktur von **A2** finden sich neben den T4-supertetraedrischen Baueinheiten, die einen ähnlichen Hohlraum aufweisen wie in **A1**, T3-supertretraedrische Metallat-Cluster. Die Cluster sind auch in **A2** eckenverknüpft zu einer Raumnetzstruktur, wobei T3- und T4-Cluster alternierend angeordnet sind. Der Hohlraum der T4-Einheit in **A2** enthält weniger Elektronendichte in zentraler Position (15.28 e$^-$/Å) als in **A1**, dafür deutlich mehr auf den äußeren vier Positionen (16.25 e$^-$/Å).

Die Röntgenfluoreszenz-Analyse bestätigt die ternäre Zusammensetzung der Verbindungen. Die Sn und Hg Atome können in der Kristallstruktur jedoch auf keiner Metallposition eindeutig zugeordnet werden, so dass von einer Mischbesetzung auf allen Positionen ausgegangen werden muss. Entsprechend wurden die Strukturmodelle unter Verwendung von EXYZ und EADP constraints verfeinert.

Die Kationen können aufgrund der hohen Kristallsymmetrie und ihrer zu erwartenden Fehlordnung nicht lokalisiert werden. Daher wurde der freie Hohlraum der Strukturen mithilfe des SQUEEZE-Algorithmus bestimmt (**A1**: 56,5%, **A2**: 54.6%).[117]
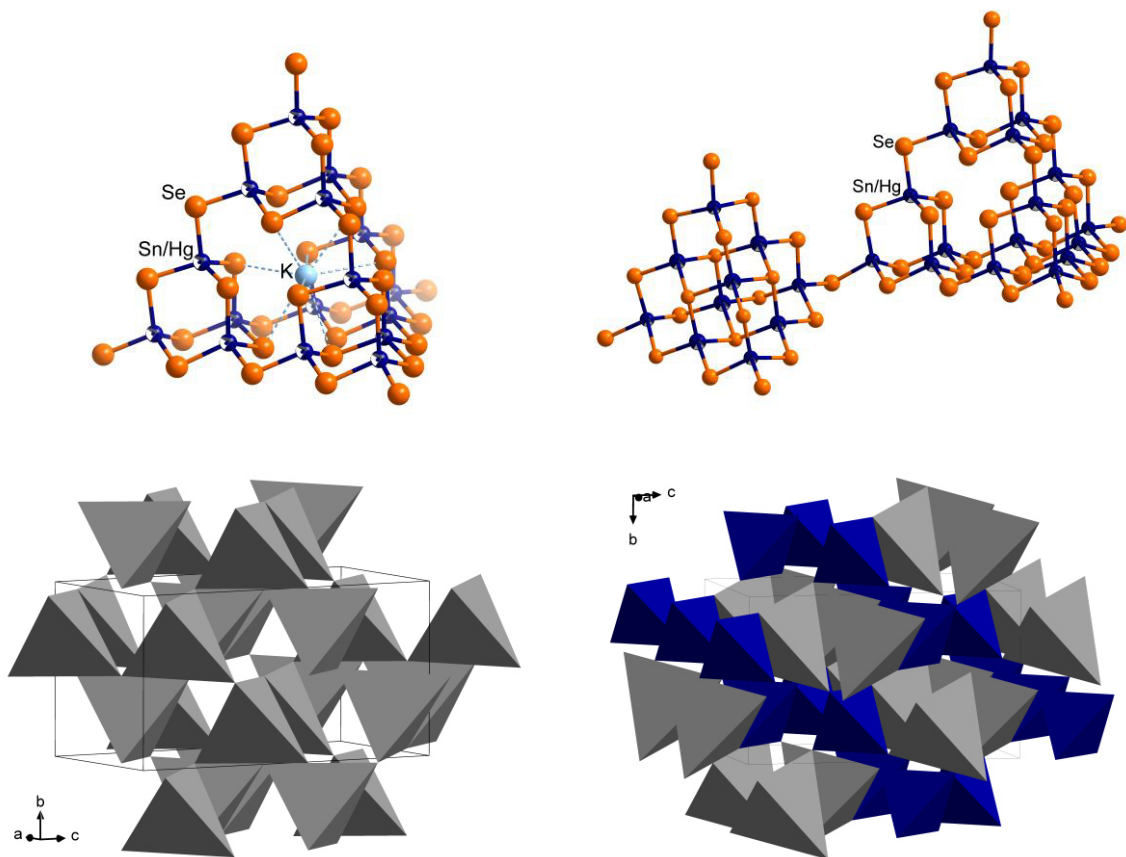
Abbildung 11: Ausschnitte aus den Kristallstrukturmodellen von **A1** (linke Seite) und **A2** (rechte Seite). Oben sind die supertetraedrischen Clusterbausteine gezeigt: *T*4 (hohl, jedoch gefüllt mit K-Kationen) in **A1** sowie *T*3 und *T*4 (derzeit mit unbesetztem Hohlraum verfeinert) in **A2**. Die Atome sind als Kugeln mit beliebigem Radius dargestellt. Unten sind Ausschnitte aus der Kristallstruktur dargestellt um die räumliche Anordnung der eckenverknüpften supertetraedrischen Cluster (vereinfacht als Tetraeder dargestellt: T4 = grau, T3 = blau) zu verdeutlichen.

Details zur micro-Röntgenfluoreszenz-Analyse (µ-XFS)

Das Verhältnis der Schweratome in Kristallen von **A1** und **A2** wurde mittels Röntgenfluoreszenz-Analyse unter Verwendung eines Bruker M4 Tornado Spektrometers bestimmt. Das Gerät ist mit einer Rh-Röntgenröhre samt Polykapillarlinse und einem Si-Drift-Detektor ausgestattet. Die von der Probe emittierte Strahlung wird detektiert und die Daten über die Fundamentalparametermethode ausgewertet.

Tabelle:1: Daten der Elementanalyse der Salze von **A1** und **A2** per µ-XFS

	zur Quantifizierung verwendete Linien	**A1** Atom% gemessen	**A1** Atom% aus der Strukturverfeinerung	**A2** Atom% gemessen	**A2** Atom% aus der Strukturverfeinerung
Hg	Hg-L	7,1(1)	9,2	10,3(4)	14,2
Sn	Sn-L	20,6(13)	23,5	19,4(27)	20,0
Se	Se-K	62,0(2)	65,3	68,1(26)	65,8
K	K-K	7,8(13)	2,0	1,2(3)	0,0
Cl	Cl-K	2,4(1)	0,0	1,0(2)	0,0
Verhältnis Hg:Sn		0,345	0,391	0,530	0,71

Details zur Einkristall-Röntgenstrukturanalyse

Kristalle von **A1** wurden auf einem STOE IPDS-2T Einkristalldiffraktometer mit Mo-Kα-Strahlung und einem Graphit-Monochromator vermessen. Diffraktionsexperimente an Kristallen der Verbindung **A2** wurden an einem Bruker D8 Quest Einkristalldiffraktometer, ausgestattet mit einer Mo-Mikrofokusröhre und Röntgen-Spiegeloptik. Nach numerischer Absorptionskorrektur mit der STOE X-Area Software bzw. nach einer Multiscan-Absorptionskorrektur mit Bruker SADABS wurden die Strukturen auf der Olex2 Software-Plattform mittels direkter Methoden gelöst (Shelxt15) und mit der Methode der kleinsten Quadrate gegen F^2 verfeinert (Shelxl15).[118] Der Platon SQUEEZE Algorithmus wurde verwendet, da die Kationen, welche mehr als die Hälfte des Kristallvolumens einnehmen, nicht verfeinert werden konnten.[117] Die kristallographischen Daten der Verbindungen **A1** und **A2** sind in Tabelle 2 zusammengefasst.

Tabelle 2: Kristallografische Daten zu **A1** und **A2**.

Verbindung	A1	A2
Summenformel	$Hg_{4.5}K_1Se_{32}Sn_{11.5}$	$Hg_{10.8}Se_{50}Sn_{15.2}$
Molare Masse /g·mol^{-1}	4833.31	7916.62
Kristallfarbe und -form	Rotes Oktaeder	Roter Block
Kristallgröße /mm³	0.1×0.1×0.1	0.07×0.05×0.04
Kristallsystem	tetragonal	tetragonal
Raumgruppe	$I4_1/acd$	$I4_1/a$
a /Å	23.802(3)	22.5738(6)
c /Å	44.683(7)	37.8532(13)
V /Å³	25314(8)	19289.1(12)
Z	8	4
ρ_{calc} /g·cm^{-3}	2.536	2.726
$\mu(Mo_{K\alpha})$ /mm^{-1}	16.898	19.912
Min/max Transmission	0.2164/0.3000	0.3750/0.4899
θ-Bereich /°	1.515–19.997	1.669–25.023
Gemessene Reflexe	15272	49725
Unabhängige Reflexe	2961	8523
R(int)	0.1748	0.0926
Unabhängige Reflexe ($I>2\sigma(I)$)	1421	5694
Parameter	116	177
R$_1$ ($I>2\theta(I)$)	0.0664	0.0926
wR$_2$ (all data)	0.1832	0.3123
S (all data)	0.936	1.085
Δρmax, Δρmin /e·Å^{-3}	0.595/-0.766	16.255/-2.872

Tabelle 3: Atomkoordinaten und äquivalente isotrope Auslenkungsparameter U(eq) für Verbindung **A1**.

Atom	x	y	z	U(eq)
Se2	6046.9(14)	6213.1(16)	2445.4(7)	122.2(12)
Se9	7411.5(14)	7301.1(15)	3745.4(6)	123.9(13)
Se4	5000	7500	2453.9(9)	125.3(18)
Se5	4809.3(14)	6329.2(15)	3119.9(6)	120.6(12)
Se8	6032.8(15)	6265.3(16)	3787.7(6)	123.5(12)
Se6	6132.2(14)	7485.1(16)	3131.8(7)	123.5(12)
Se7	7327.2(14)	6154.8(16)	3120.2(7)	129.8(13)
Se3	5975.8(17)	4955.9(16)	3129.8(7)	135.5(14)
Se1	7285.0(18)	5000	2500	143(2)
Hg4	6703.3(8)	6772.8(9)	3431.8(4)	113.2(11)
Sn4	6703.3(8)	6772.8(9)	3431.8(4)	113.2(11)
Hg3	5445.8(8)	5686.0(8)	3428.0(3)	113.2(10)
Sn3	5445.8(8)	5686.0(8)	3428.0(3)	113.2(10)
Hg2	5531.6(8)	6852.3(9)	2805.8(4)	111.8(10)
Sn2	5531.6(8)	6852.3(9)	2805.8(4)	111.8(10)
Hg1	6595.3(7)	5591.1(8)	2805.6(3)	122.3(9)
Sn1	6595.3(7)	5591.1(8)	2805.6(3)	122.3(9)
K1	5000	7500	3750	187(8)

Tabelle 4: Atomkoordinaten und äquivalente isotrope Auslenkungsparameter U(eq) für Verbindung **A2**.

Atom	x	y	z	U(eq)
Se3	8827.7(15)	2766.8(14)	6974.2(9)	92.8(10)
Se7	9186.7(14)	4054.1(16)	6208.0(8)	93.9(10)
Se4	7876.1(12)	4384.6(13)	6989.5(7)	77.2(8)
Se6	10455.3(13)	3674.6(15)	7009.5(9)	91.4(9)
Se2	10000	2500	7787(1)	86.9(12)
Se8	10755.1(14)	4947.1(13)	6269.1(8)	87.1(9)
Se5	9542.7(11)	5332.2(12)	7001.9(7)	72.6(7)
Se1	9164.1(13)	4059.1(13)	7792.7(7)	77.9(8)
Se9	8109.4(10)	5570.4(13)	7664.3(7)	75.7(8)
Se13	9369.0(9)	6820.0(11)	7566.8(6)	61.3(7)
Se11	8063.8(9)	6727.9(10)	8379.0(6)	54.5(6)
Se10	9478.7(10)	5489(1)	8341.5(6)	62.5(6)
Se12	9267.3(8)	8151.6(9)	8338.3(5)	46.5(5)
Hg7	10000	7500	7959.7(7)	58.1(8)
Hg6	8678.4(5)	7438.7(4)	8756.5(2)	60.2(5)
Sn3	8393.0(7)	3616.5(7)	6612.1(4)	70.1(7)
Sn2	9584.3(7)	3280.2(7)	7377.2(4)	75.2(7)
Sn4	9952.3(6)	4479.0(7)	6642.1(4)	64.5(5)
Sn1	8747.3(6)	4799.4(7)	7354.7(4)	73.8(7)
Sn5	8825.0(6)	6197.5(6)	8008.9(4)	64.5(5)
Hg3	8393.0(7)	3616.5(7)	6612.1(4)	70.1(7)
Hg2	9584.3(7)	3280.2(7)	7377.2(4)	75.2(7)
Hg4	9952.3(6)	4479.0(7)	6642.1(4)	64.5(5)
Hg1	8747.3(6)	4799.4(7)	7354.7(4)	73.8(7)
Hg5	8825.0(6)	6197.5(6)	8008.9(4)	64.5(5)
Sn6	8678.4(5)	7438.7(4)	8756.5(2)	60.2(5)
Sn7A	9810(70)	7560(50)	7880(40)	58.1(8)

6.6   Lebenslauf

Name: Carsten Donsbach

Geburtsdatum:

Geburtsort:

Familienstand:

Ausbildung:

6.7　Liste der Publikationen

[16]　Not so innocent after all? The role of ionic liquid cations as methylation agent

B. Peters, S. Santner, C. Donsbach, S. Dehnen, **2018**, *Manuskript in Vorbereitung.*

[15]　 $(C_4C_1Im)_6[Hg_7Se_{10}]$: The Salt of a Molecular Selenido Mercurate Anion Obtained from Ionic Liquids

C. Donsbach, S. Dehnen, **2018**, *Manuskript eingereicht.*

[14]　Formation of $[(C_nC_1imTe)_4Hg]^{2+}$ (n = 6, 8) upon In-Situ Generation of Dialkylimidazole-2-Tellurones in Ionic Liquids at Room Temperature

C. Donsbach, S. Dehnen, **2018**, *Manuskript eingereicht.*

[13]　$[Hg_4Te_8(Te_2)_4]^{8-}$: A Heavy Metal Porphyrinoid Embedded in a Lamellar Structure

C. Donsbach, K. Reiter, D. Sundholm, F. Weigend, S. Dehnen, *Angew. Chem. Int. Ed.* **2018**, *57*, DOI: 10.1002/anie.201803233, *im Druck*; *Angew. Chem.* **2018**, *129*, DOI: 10.1002/ange.201803233, *im Druck.*

[12]　Hybrid Disila-Crown Ethers as Hosts for Ammonium Cations: The O–Si–Si–O Linkage as an Acceptor for Hydrogen Bonding

F. Dankert, K. Reuter, C. Donsbach, C. von Hänisch, *Inorganics* **2018**, *6(1)*, 15.

[11]　Alkali and Alkaline Earth Metal Derivatives of Disila-Bridged Podands: Coordination Chemistry and Structural Diversity

F. Dankert, C. Donsbach, C.-N. Mais, K. Reuter, C. von Hänisch, *Inorg. Chem.* **2018**, *57(1)*, 351-359.

[10]　A Structural Study of Mismatched Disila-Crown Ether Complexes

K. Reuter, F. M. Dankert, C. Donsbach, C. von Hänisch, *Inorganics* **2017**, *5(1)*, 11.

[9]　Syntheses and properties of selenido mercurates with $[HgSe_2]^{2-}$ anions in diverse chemical environments

C. Donsbach, S. Dehnen, *Inorg. Chem. Front.* **2017**, *4*, 336–342.

[8]　A structural study of alkaline earth metal complexes with hybrid disila-crown ethers

F. Dankert, K. Reuter, C. Donsbach, C. von Hänisch, *Dalton Trans.* **2017**, *46*, 8727.

[7]   Formation of Crystalline Telluridomercurates from Ionic Liquids Near Room Temperature
        C. Donsbach, S. Dehnen, *Z. Anorg. Allg. Chem.* **2017**, *643*, 14–19.

[6]   Combining Solid-state and Solution-based Techniques: Synthesis and Reactivity of
        Chalcogenidoplumbates(II or IV)
        G. Thiele, C. Donsbach, I. Nußbruch, S. Dehnen, *J. Vis. Exp.* **2016**, *118*, e54789.

[5]   Mercurates from a Revised Ionothermal Synthesis Route: The Pseudo-Flux Approach
        C. Donsbach, G. Thiele, L.H. Finger, J. Sundermeyer, S. Dehnen, *Inorg. Chem.* **2016**,
        55, 6725–6730.

[4]   Bidentate Lewis Acid Catalyzed Domino Diels-Alder Reaction of Phthalazine for the
        Synthesis of Bridged Oligocyclic Tetrahydronaphthalenes
        L. Schweighauser, I. Bodoky, S. N. Kessler, D. Häussinger, C. Donsbach, H. A. Wegner,
        Org. Lett., **2016**, *18*, 1330–1333.

[3]   Smallest molecular chalcogenidometalate anions of the heaviest metals: syntheses,
        structures, and their interconversion
        G. Thiele, C. Donsbach, R. Riedel, M. Marsch, K. Harms, S. Dehnen, *Dalton Trans.* **2016**,
        45, 5958–5967.

[2]   Organic Cation and Complex Cation-Stabilized (Poly-)Selenides, $[Cation]_x(Se_y)_z$:
        Diversity in Structures and Properties
        G. Thiele, L. Vondung, C. Donsbach, S. Pulz, S. Dehnen, *Z. Anorg. Allg. Chem.* **2014**,
        640, 2684–2700.

[1]   Solvothermal and ionothermal syntheses and structures of amine- and/or
        (poly-)chalcogenide coordinated metal complexes
        G. Thiele, S. Santner, C. Donsbach, M. Assmann, M. Müller, S. Dehnen, *Z. Kristallogr.*
        2014, *229*, 489–495.

7. Literaturverzeichnis

[1]   S.-S. Wang, G.-Y. Yang, *Chemical Reviews* **2015**, *115*, 4893–4962.

[2]   A. Mrotzek, M. G. Kanatzidis, *Acc. Chem. Res.* **2003**, *36*, 111–119.

[3]   N. Zheng, X. Bu, H. Vu, P. Feng, *Angew. Chem.* **2005**, *117*, 5433–5437; *Angew. Chem. Int. Ed.* **2005**, *44*, 5299–5303.

[4]   Z. Zhang, J. Zhang, T. Wu, X. Bu, P. Feng, *J. Am. Chem. Soc.* **2008**, *130*, 15238–15239.

[5]   Y.Liu, P. D. Kanhere, C. L. Wong, Y. Tian, Y. Feng, F. Boey, T. Wu, H. Chen, T. J. White, Z. Chen, Q. Zhang, *J. Solid State Chem.* **2010**, *183*, 2644–2649.

[6]   K.-Y. Wang, M.-L. Feng, D.-N. Kong, S.-J. Liang, L.Wu, X.-Y. Huang, *Cryst. Eng. Comm.* **2012**, *14*, 90–94.

[7]   X. Chen, X. Bu, Q. Lin, C. Mao, Q.-G. Zhai, Y. Wang, P. Feng, *Chem. Eur. J.* **2017**, *23*, 11913–11919.

[8]   N.-N. Shen, B. Hu, C,.C, Cheng, G.-D. Zou, Q.-Q. Hu, C.-F. Du, J.-R. Li, X.-Y. Huang, *Cryst. Growth Des.* **2018**, *18*, 962–968.

[9]   N. Kamaya, K. Homma, Y. Yamakawa, M. Hirayama, R. Kanno, M. Yonemura, T. Kamiyama, Y. Kato, S. Hama, K. Kawamoto, A. Mitsui, *Nat. Mater.* **2011**, *10*, 682–686.

[10]   P.Bron, S. Johansson, K. Zick, J. Schmedt auf der Günne, S. Dehnen, B. Roling, *J. Am. Chem. Soc.* **2013**, *135*, 15694–15697.

[11]   N. Zheng, X. Bu, P. Feng, *Nature* **2003**, *426*, 428–432.

[12]   M.-L. Feng, D.-N. Kong, Z.-L. Xie, X.-Y. Huang, *Angew. Chem.* **2008**, *120*, 8751–8754; *Angew. Chem. Int. Ed.* **2008**, *47*, 8623–8626.

[13]   M. J. Manos, C. D. Malliakas, M. G. Kanatzidis, *Chem. Eur. J.* **2007**, *13*, 51–58.

[14]   M. J. Manos, K. Chrissafis, M. G. Kanatzidis, *J. Am. Chem. Soc.* **2006**, *128*, 8875–8883.

[15]   M. J. Manos, R. G. Iyer, E. Quarez, J. H. Liao, M. G. Kanatzidis, *Angew. Chem.* **2005**, *117*, 3618–3621; *Angew. Chem. Int. Ed.* **2005**, *44*, 3552–3555.

[16]   N. Ding, M. G. Kanatzidis, *Chemistry of Materials* **2007** *19*, 3867–3869.

[17]   a) N. Zheng, X. Bu, B. Wang, P. Feng, *Science* **2002**, *298*, 2366–2369; b) X. Bu, N. Zheng, P. Feng, *Chem. Eur. J.* **2004**, *10*, 3356–3362.

[18]   a) N. Zheng, X. Bu, P. Feng, *J. Am. Chem. Soc.* **2003**, *125*, 1138–1139.

[19]   K. F. Hsu, S. Loo, F. Guo, W. Chen, J. S. Dyck, C. Uher,T. Hogan, E. K. Polychroniadis, M. G. Kanatzidis, *Science* **2004**, *303*, 818 –821.

[20]   S. Johnsen, S. C. Peter, S. L. Nguyen, J.-H. Song, H. Jin, A. J. Freeman, M. G. Kanatzidis, *Chem. Mater.* **2011**, *23*, 4375–4383.

[21]   H. Li, C. D. Malliakas, Z. Liu, J. A. Peters, M. Sebastian, L. Zhao, D. Y. Chung, B. W. Wessels, M. G. Kanatzidis, *Cryst. Growth Des.* **2014**, *14*, 5949–5956.

[22]   H. Chen, Y.-K. Chen, H. Lin, J.-N. Shen, L.-M. Wu, X.-Tao, Wu., *Inorg. Chem.* **2018**, *57*, 916–920.

[23]   K. O. Klepp, K. Prager, *Z. Naturforsch.* **1992**, *47b*, 491–496.

[24]   S. M. Islam, J. Im, A. J. Freeman, Mg. G. Kanatzidis, *Inorg. Chem.* **2014**, *53*, 4698–4704.

[25]   C.-W. Park, D. M. Smith, M. A. Pell, J. A. Ibers, *Inorg. Chem.* **1997**, *36*, 942–943.

[26]   R. C. Burns, J. D. Corbett, *Inorg. Chem.* **1981**, *20*, 4433–4434.

[27]   M. Shieh, L.-F. Ho, P.-C. Chen, M.-H. Hsu, H.-L. Chen, Y.-W. Guo, Y.-W. Pan, Y.-C. Lin, *Organometallics* **2007**, *26*, 6184–6196.

[28]   G. Thiele, C. Donsbach, R. Riedel, M. Marsch, K. Harms, S. Dehnen, *Dalton Trans.* **2016**, *45*, 5958–5967.

[29]   S. S. Dhingra, C. J. Warren, R. C. Haushalter, A. B. Bocarsly, *Chem. Mater.* **1994**, *6*, 2382–2385.

[30]   H. Sommer, R. Hoppe, *Z. Anorg. Allg. Chem.* **1978**, *443*, 201–211.

[31]   H. D. Rad, R. Hoppe, *Z. Anorg. Allg. Chem.* **1981**, *483*, 18–25.

[32]   S. M. Islam, S. Vanishri, H. Li, C. C. Stoumpos, J. A. Peters, M. Sebastian, Z. Liu, S. Wang, A. S. Haynes, J. Im, A. J. Freeman, B. Wessels, M. G. Kanatzidis, *Chem. Mater.* **2015**, *27*, 370–378.

[33]   M. G. Kanatzidis, *Chem. Mater.* **1990**, *2*, 353–363.

[34]   E. A. Axtell III, Y. Park, K. Chondroudis, M. G. Kanatzidis, *J. Am. Chem. Soc.* **1998**, *120*, 124–136,

[35]   K. O. Klepp, *J. Alloys Compd.* **1992**, *182*, 281–288.

[36]   K.-W. Kim, M. G. Kanatzidis, *Inorg. Chem.* **1991**, *30*, 1966–1969.

[37]   G. Thiele, S. Lippert, F. Fahrnbauer, P. Bron, O. Oeckler, A. Rahimi-Iman, M. Koch, B. Roling, S. Dehnen, *Chem. Mater.* **2015**, *27*, 4114–4118.

[38]   A. Müller, J. Schimanski, U. Schimanski, *Angew. Chem.* **1984**, *96*, 158–159; *Angew. Chem. Int. Ed. Engl.* **1984**, *23*, 159–160.

[39]   A. Müller, J. Schimanski, U. Schimanski, *Z. Naturforsch. B: Chem. Sci.* **1985**, *40*, 1277.

[40]   T. D. Bailey, R. M. H. Banda, D. C. Craig, I. G. Dance, I. N. L. Ma, M. L. Scudder, *Inorg. Chem.* **1991**, *30*, 187.

[41]   K.-W. Kim, J. Kim, *Z. Kristallogr. NCS* **2014**, *229*, 25–30.

[42]   J. Adel, F. Weller, K. Dehnicke, *Z. Naturforsch. B: Chem. Sci.* **1988**, *43*, 1094–1100.

[43]   G. Krauter, F. Weller, K. Dehnicke, *Z. Naturforsch. B: Chem. Sci.* **1989**, *44*, 444–454.

[44]   R. M. H. Banda, J. Cusick, M. L. Scudder, D. C. Craig, I. G. Dance, *Polyhedron* **1989**, *8*, 1995–1998.

[45]   S. Magull, B. Neumüller, K. Dehnicke, *Z. Naturforsch. B: Chem. Sci.* **1991**, *46*, 985–991.

[46]   B. Neumüller, M.-L. Ha-Eierdanz, U. Müller, S. Magull, G. Krauter, K. Dehnicke, *Z. Anorg. Allg. Chem.* **1992**, *609*, 12–18.

[47]   A. Ahle, K. Dehnicke, K. Maczek, D. Fenske, *Z. Anorg. Allg. Chem.* **1993**, *619*, 1699–1703.

[48]   P. J. Barrie, R. J. H. Clark, R. Withnall, D.-Y. Chung, K.-W. Kim, M. G. Kanatzidis, *Inorg. Chem.* **1994**, *33*, 1212–1216.

[49]   J. C. Bollinger, J. A. Ibers, *Inorg. Chem.* **1995**, *34*, 1859–1867.

[50]   K.-W. Kim, J. Kim, *Z. Kristallogr. NCS* **2014**, *229*, 25–30.

[51]   J. C. Bollinger, L. C. Roof, D. M. Smith, J. M. McConnachie, J. A. Ibers, *Inorg. Chem.* **1995**, *34*, 1430–1434.

[52]   U. Müller, C. Grebe, B. Neumüller, B. Schreiner, K. Dehnicke, *Z. Anorg. Allg. Chem.* **1993**, *619*, 500–506.

[53]   J. M. McConnachie, M. A. Ansari, J. C. Bollinger, R. J. Salm, J. A. Ibers, *Inorg. Chem.* **1993**, *32*, 3201–3202.

[54]   D. M. Smith, L. C. Roof, M. A. Ansari, J. M. McConnachie, J. C. Bollinger, M. A. Pell, R. J. Salm, J. A. Ibers, *Inorg. Chem.* **1996**, *35*, 4999–5006.

[55]   J. Li, Z. Chen, J. L. Kelley, D. M. Proserpio, *Mater. Res. Soc. Symp. Proc.* **1997**, *453*, 29–34.

[56]   J. Li, B. G. Rafferty, S. Mulley, D. M. Proserpio, *Inorg. Chem.* **1995**, *34*, 6417–6418.

[57]   R. C. Haushalter, *Angew. Chem.* **1985**, *97*, 414–415; *Angew. Chem. Int. Ed. Engl.* **1985**, *24*, 433–435.

[58]   K.-W. Kim, M. G. Kanatzidis, *Inorg. Chim. Acta* **1994**, *224*, 163–169.

[59]   P. Sun, S. Liu, S. Li, L. Zhang, H. Sun, D. Jia, *Inorg. Chem.* **2017**, *56*, 6152.

[60]   S. S. Dhingra, C. J. Warren, R. C. Haushalter, A. B. Bocarsly, *Chem. Mater.* **1994**, *6*, 2382–2385.

[61]   M. K. Brandmayer, R. Clerac, F. Weigend, S. Dehnen, *Chem. Eur. J.* **2004**, *10*, 5147–5157.

[62]   E. Ruzin, A. Fuchs, S. Dehnen, *Chem. Commun.*, **2006**, *0*, 4796–4798.

[63]   S.S. Dhingra, R. C. Haushalter, *Chem. Mater.* **1994**, *6*, 2376–2381.

[64]   Y. Wang, M. Baiyin, S. Ji, X. Liu, Y. An, G. Ning, *Chem. Res. Chin. Univ.* **2006**, *22*, 411.

[65]   J.-H. Chou, M. G. Kanatzidis, *J. Solid State Chem.* **1996**, *123*, 115.

[66]   J.-H. Chou, M. G. Kanatzidis, *Chem. Mater.* **1995**, *7*, 5.

[67]   G. A. Marking, J. A. Hanko, M. G. Kanatzidis, *Chem. Mater.* **1998**, *10*, 1191–1199.

[68]   X. Jin, L. Zhang, G. Shu, R. Wang, H. Guo, *J. Alloys. Compd.* **2002**, *347*, 67–71.

[69]   K.-Y. Wang, D. Ye, L.-J. Zhou, M.-L. Feng, X.-Y. Huang, *Dalton Trans.* **2013**, *42*, 5454–5461.

[70]   M. Imafuku, I. Nakai, K. Nagashima, *Mater. Res. Bull.* **1986**, *21*, 493–501.

[71]   H. Li, M. G. Kanatzidis, C. D. Malliakas, Z. Liu, J. A. Peters, H. Jin, C. D. Morris, L. Zhao, B. W. Wessels, A. J. Freeman, *Chem. Mater.* **2012**, *24*, 4434–4441.

[72]   K. O. Klepp, *Z. Naturforsch. B* **1992**, *47*, 197–200.

[73]   M. G. Kanatzidis, A. C. Sutorik, *Prog. Inorg. Chem.* **1995**, *43*,151–265.

[74]   G. A. Marking, M. Evain, V. Petricek, M. G. Kanatzidis, *J. Solid State Chem.* **1998**, *141*, 17–28.

[75]   C. Zhang, M. Ji, S.-H. Ji, Y.-L. An, *Inorg. Chem.* **2014**, *53*, 4856–4860.

[76]   P. Feng, X. Bu, N. Zheng, *Acc. Chem. Res.* **2005**, *38*, 293–303.

[77]   J. Li, Z. Chen, R.-J. Wang, D. M. Proserpio, Coord. *Chem. Rev.* **1999**, *190–192*, 707–735.

[78]   a) W. S. Sheldrick, M. Wachhold, *Angew. Chem.* **1997**, *109*, 214–234; *Angew. Chem. Int. Ed. Engl.* **1997**, *36*, 206–224; b) A. Kromm, T. v. Almsick, W. S. Sheldrick, *Z. Naturforsch.* **2010**, *65b*, 918–936.

[79]   P. T. Wood, G. L. Schimek, J. W. Kolis, *Chem. Mater.* **1996**, *8*, 721–726.

[80]   T. Wu, X. Wang, X. Bu, X. Zhao, Le Wang, P. Feng, *Angew. Chem.* **2009**, *121*, 7340–7343; *Angew. Chem. Int. Ed.* **2009**, *48*, 7204–7207.

[81] T. Wu, X.Bu, X. Zhao, R.Khazhakyan, P. Feng, *J. Am. Chem. Soc.* **2011**, *133*, 9616–9625.

[82] X. Xu, W. Wang, D. Liu, D. Hu, T. Wu, X. Bu, P. Feng, *J. Am. Chem. Soc.* **2018**, *140*, 888–891.

[83] G. Thiele, T. Krüger, S. Dehnen, *Angew. Chem.* **2014**, *126*, 4787–4791; *Angew. Chem. Int. Ed.* **2014**, *53*, 4699–4703.

[84] N. Ding, D.-Y. Chung, M. G. Kanatzidis, *Chem. Commun.* **2004**, 1170–1171.

[85] C. Liu, Y. Shen, P. Hou, M. Zhi, C. Zhou, W. Chai, J.-W. Cheng, Y. Liu, *Inorg. Chem.* **2015**, *54*, 8931–8936.

[86] Y. Shen, C. Liu, P. Hou, M. Zhi, C. Zhou, W. Chai, J.-W. Cheng, Y. Liu, Q. Zhang, *Chem. Asian J.* **2015**, *10*, 2604.

[87] W.-W. Xiong, Q. Zhang, *Angew. Chem.* **2015**, *127*, 11780–11788; *Angew. Chem. Int. Ed.* **2015**, *54*, 11616–11623.

[88] W.-W. Xiong, E. U. Athresh, Y. Ting Ng, J. Ding, T. Wu, Q. Zhang, *J. Am Chem. Soc.* **2013**, *135*, 1256–1259.

[89] L. Nie, Y. Zhang, W.-W. Xiong, T.-T. Lim, Rong, Xu, Q. Yan, Q. Zhang, *Inorg. Chem. Front.* **2016**, *3*, 111–116.

[90] G. Zhang, P. Liu, J. Ding, Y. Liu, W.-W. Xiong, L. Nie, T. Wu, Y. Zhao, A. I. Y. Tok, Q. Zhang, *Inorg. Chem.* **2014**, 53, 10248–10256.

[91] D.-D. Yang, Y. Song, B. Zhang, N.-N. Shen, G.-L. Xu, W.-W. Xiong, X.-Y. Huang, *Cryst. Growth Des.* **2018**, *18*, 3255–3262.

[92] C. Zimmermann, C. E. Anson, F. Weigend, R. Clerac, S. Dehnen, *Inorg. Chem.* **2005**, *44*, 5686–5695.

[93] S. Dehnen, M. Melullis, *Coord. Chem. Rev.* **2007**, *251*, 1259–1280.

[94] T. P. Vaid, S. P. Kelley, R. D. Rogers, *IUCrJ* **2017**, *4*, 380–392.

[95] G. Thiele, S. Peter, M. Schwarzer, E. Ruzin, R. Clérac, H. Staesche, C. Rößer, B. Roling, S. Dehnen, *Inorg. Chem.* **2012**, *51*, 3349–3351.

[96] S. Haddadpour, M. Melullis, H. Staesche, C.R. Mariappan, B. Roling, R. Clérac, S. Dehnen, *Inorg. Chem.* **2009**, *48*, 1689–1698.

[97] a) E. R. Cooper, C. D. Andrews, P. S. Wheatley, P. B. Webb, P. Wormald, R. E. Morris, *Nature* **2004**, *430*, 1012–1016; b) R. E. Morris, *Chem. Commun.* **2009**, 2990–2998.

[98] P. Wasserscheid, T. Welton (Eds.) *Ionic liquids in synthesis*, Wiley-VCH, Weinheim, **2008**.

[99] Z. Ma, J. Yu, S. Dai, *Adv. Mater.* **2010**, *22*, 261–285.

[100] a) Y. Lin, D. Xie, W. Massa, L. Mayrhofer, S. Lippert, B. Ewers, A. Chernikov, M. Koch, S. Dehnen, *Chem. Eur. J.* **2013**, *19*, 8806–8813; b) Y. Lin, W. Massa, S. Dehnen, *Chem. Eur. J.* **2012**, *18*, 13427–13434.

[101] D. Freudenmann, S. Wolf, M. Wolff, C. Feldmann, *Angew. Chem.* **2011**, *123*, 11244–11255; *Angew. Chem. Int. Ed.* **2011**, *50*, 11050–11060.

[102] Y. Lin, S. Dehnen, *Inorg. Chem.* **2011**, *50*, 7913–7915.

[103] J.-R. Li, W.-W. Xiong, Z.-L. Xie, C.-F. Du, G.-D. Zou, X.-Y. Huang, *Chem. Commun.* **2013**, *49*, 181–183.

[104] J. A. Cody, K. B. Finch, G. J. 3. Reynders, G. C. B. Alexander, H. G. Lim, C. Nather, W. Bensch, *Inorg. Chem.* **2012**, *51*, 13357–13362.

[105] Y. Lin, W. Massa, S. Dehnen, *J. Am. Chem. Soc.* **2012**, *134*, 4497–4500.

[106] S. Santner, S. Yogendra, J. J. Weigand, S. Dehnen, *Chem. Eur. J.* **2017**, *23*, 1999–2004.

[107] Santner, J. Sprenger, M. Finze, S. Dehnen, *Chem. Eur. J.* **2018**, *24*, 3474–3480

[108] W.-W. Xiong, J.-R. Li, B. Hu, B. Tan, R.-F. Li, X.-Y. Huang, *Chem. Sci.* **2012**, *3*, 1200–1204.

[109] Q. Zhang, I. Chung, J. I. Jang, J. B. Ketterson, M. G. Kanatzidis, *J. Am. Chem. Soc.* **2009**, *131*, 9896–9897.

[110] E. Ahmed, A. Isaeva, A. Fiedler, M. Haft, M. Ruck, *Chem. Eur. J.* **2011**, *17*, 6847–6852.

[111] E. Ahmed, J. Breternitz, M. F. Groh, A. Isaeva, M. Ruck, *Eur. J. Inorg. Chem.* **2014**, *2014*, 3037–3042.

[112] M. F. Groh, J. Breternitz, E. Ahmed, A. Isaeva, A. Efimova, P. Schmidt, M. Ruck, *Z. Anorg. Allg. Chem.* **2015**, *641*, 388–393.

[113] K. Biswas, I. Chung, J.-H. Song, C. D. Malliakas, A. J. Freeman, M. G. Kanatzidis, *Inorg. Chem.* **2013**, *52*, 5657–5659.

[114] S. Santner, J. Heine, S. Dehnen, *Angew. Chem.* **2016**, *128*, 886–904; *Angew. Chem. Int. Ed.* **2016**, *54*, 876–893;.

[115] M. F. Groh, A. Wolff, M. A. Grasser, M. Ruck, *Int. J. Mol. Sci.* **2016**, *17*, 1452.

[116] S. Santner, A. Wolff, M. Ruck, S. Dehnen, *Chem. Eur. J.* **2018**, *24*, https://doi.org/10.1002/chem.201802199.

[117] A. L. Spek, *Acta Cryst.* **2015**, *C71*, 9-18.

[118] a) G. M. Sheldrick, *Acta Crystallogr., Sect. A* **2015**, *71*, 3–8; b) G. M. Sheldrick, *Acta Crystallogr., Sect. C* **2015**, *71*, 3–8; c) O. V. Dolomanov, L. J. Bourhis, R. J. Gildea, J. A. K. Howard, H. Puschmann, *J. Appl. Crystallogr.* **2009**, *42*, 339–341.